

# Material-Induced Platelet and Leukocyte Activation: A Systems Approach

by

Tidimogo Gaamangwe

A thesis  
presented to the University of Waterloo  
in fulfillment of the  
thesis requirement for the degree of  
Doctor of Philosophy  
in  
Systems Design Engineering

Waterloo, Ontario, Canada, 2014

©Tidimogo Gaamangwe 2014

## **AUTHOR'S DECLARATION**

I hereby declare that I am the sole author of this thesis. This is a true copy of the thesis, including any required final revisions, as accepted by my examiners.

I understand that my thesis may be made electronically available to the public.

## Abstract

A systems approach in the study of blood-biomaterial interactions (BBI) is likely to provide better insight into the transient behaviors of complex biological systems. Although some attempts have been made to apply a systems approach in blood-biomaterial studies, a good framework for applying a systems approach has not yet been achieved. In this thesis, the case for a systems approach is presented and a framework is proposed. As a demonstration, the systems approach is applied to the development of an *in vitro* model for BBI.

*In vitro* models play an important role in the initial investigation of BBI. Therefore, careful consideration of their parameters to mimic physiological parameters is crucial for results that can be translated to physiological conditions. The parameters of the *in vitro* model used in this thesis were determined using a systems approach method. The fluid dynamics of the model were characterized, to account for the model blood sample always including air, and an improved time-averaged wall shear stress was proposed. Since wall shear stress is an important parameter that determines cell activation and adhesion, *in vitro* studies were performed to investigate and validate the model with experiments. In line with a systems approach and clinical relevance, whole blood samples were used in the *in vitro* experiments.

Platelet activation was investigated, as characterized by platelet microparticle (PMP) formation and expression of both P-selectin and the integrin glycoprotein receptor GPIIb/IIIa. For whole blood, in the absence of model stents, there was no significant sample volume or shear effect on PMP formation for wall shear stress up to  $56 \text{ dyn/cm}^2$ . However, in the presence of model stents, combined volume and shear-dependent PMP formation was observed. While GPIIb/IIIa expression was reduced, P-selectin, on the other hand, did not generally show significant change after 2 hours of incubation.

Leukocyte activation was also investigated, as characterized by the expression of tissue factor (TF), Mac-1, C3aR and toll-like receptor 4 (TLR-4). In the absence of model stents, sample volume had minimal effect on leukocyte activation but in the presence of model stents, a sample volume effect was observed at high shear rates, especially on Mac-1 expression. The other markers, TF, C3aR and TLR-4 did not show sensitivity to the volume effect. However, under combined volume-stent-shear, all markers were down-regulated at high shear. Correspondingly, platelet-leukocyte aggregation was also generally reduced. Leukocytes, as well as platelets, were sensitive to surface-

area-to-volume ratio. The use of low surface area-to-volume ratio, below the ISO Standard recommended limit, resulted in reduced platelet and leukocyte sensitivity to shear and/or material. However, sensitivity to shear was still high on platelet-leukocyte aggregation. Also cell surface adhesion was shear-dependent but could not be linked to a sample volume effect.

Complement inhibitor FUT-175 reduced PMP formation but had less effect on GPIIb/IIIa expression. Complement inhibition also reduced leukocyte activation, especially under shear conditions. Considerable reduction in leukocyte activation was observed under shear in the presence of model stents. These conditions would normally be expected to produce high complement activation. Furthermore, the conditions with the most reduction in platelet and leukocyte activation corresponded with the most reduction in platelet-leukocyte aggregation in the fluid phase. On the stent surface, FUT-175 inhibited leukocyte adhesion but allowed some platelet adhesion. Thus, complement inhibition with FUT-175 has the potential to reduce thrombosis while possibly retaining platelet function in hemostasis.

The effect of surface roughness was investigated with inhomogeneous multiscale roughness surfaces. Although the unetched and acid-etched stent surfaces had similar average surface roughness values, the acid-etched surface resulted in increased platelet activation and platelet-leukocyte aggregation. In addition, platelet-leukocyte aggregates seemed to be more resistant to shear-induced disaggregation. However, when complement inhibitor FUT-175 was introduced, platelet and leukocyte activation and aggregation were reduced to similar levels as for unetched stents. This suggests that complement inhibition with FUT-175 has the potential to reduce material-induced thrombosis in the presence of nano/micro-structured stent surfaces such as those used for drug-eluting stents.

## Acknowledgements

I would like to sincerely express my gratitude to my supervisor, Professor Maud Gorbet, for her exceptional guidance and patience throughout my PhD research. I would like to particularly thank her for her understanding during the trying times and letting me develop my theories. I would also like to thank my co-supervisor Professor John Medley for his guidance and helpful suggestions.

I also would like to thank the members of my thesis committee, Professors Daniel Stashuk, Joe Quadrilatero, Sean Peterson, first for agreeing to be part of my experience at UW and for all their assistance. Thank you also to my external examiner Professor Richard Leask for his invaluable comments and assistance with the final leg of this journey.

I would like to thank the UW Machine Shop staff, especially Rick Forgett, for all the help with the mandrels. And of course a very big thank you to the phlebotomists, Elizabeth Martell (who has now gone on to do much more relaxed work) and Miriam Heynen, for all their help and going that extra mile to accommodate my requests. Thank you Sara Luck for your help with the reagent orders.

Thank you to all my MIBS lab colleagues, past (Laura, Xiaojian, Dan) and present (Sara, Rob, Cameron, Saman, Shahab) and to all the students who have gone through the lab during my time. Thank you to Jason Pye for his help with some of the experimental work during his co-op term. Though everyone was always busy, I always enjoyed the short chit chat and the coffee and lunches. Thank you for all the friendship and I wish everyone the best in all their endeavors.

A special thank you to my entire family for their unwavering encouragement and support and to all my friends for always being there. And thank you to everyone else who has contributed to my success in all the various ways. Last but not least, I would like to thank all the blood donors, without whom none of the experimental work would have been possible.

I gratefully acknowledge the financial support from NSERC, OGS and the University of Waterloo.

## **Dedication**

To my parents who have always supported my decisions from those humble beginnings

and

To my wife Louise and the children for all their love, support and encouragement through it all.

## Table of Contents

AUTHOR'S DECLARATION .....	ii
Abstract.....	iii
Acknowledgements .....	v
Dedication.....	vi
List of Figures.....	xiii
List of Tables .....	xvi
List of Abbreviations .....	xviii
Glossary of Terms .....	xix
Chapter 1 Thesis scope and hypotheses .....	1
1.1 Introduction .....	1
1.2 Thesis scope and format .....	4
1.3 Hypotheses and thesis objectives .....	5
Chapter 2 Blood-Biomaterial Interactions in Thrombogenicity and the Case for a Systems Approach	7
2.1 Introduction .....	7
2.2 The blood system.....	9
2.2.1 The immune system.....	12
2.2.2 Contact system.....	33
2.2.3 Hemostatic system.....	37
2.2.4 Fibrinolytic system .....	42
2.2.5 Summary.....	43
2.3 The fluidics system.....	45
2.3.1 Geometric parameters of the coronary system .....	46
2.3.2 Hemodynamic parameters of the coronary system .....	50
2.3.3 Summary.....	56
2.4 The biomaterial system.....	56
2.4.1 Surface roughness and topography.....	57
2.4.2 Surface chemistry .....	58
2.4.3 Surface charge .....	60
2.4.4 Surface energy .....	61
2.4.5 Electrochemistry.....	63
2.4.6 Summary.....	64

2.5 The case for a systems approach in blood-biomaterial studies .....	65
2.5.1 The biological tripartite .....	65
2.5.2 Blood-biomaterial interaction cube .....	66
2.5.3 The SAXSA sequence .....	68
2.5.4 Blood-biomaterial interactions and the broader picture .....	70
2.5.5 A systems approach framework .....	73
2.5.6 Summary .....	78
2.6 Conclusion .....	79
Chapter 3 A Systems Approach to <i>In Vitro</i> Model Design .....	80
3.1 Introduction .....	80
3.2 <i>In vitro</i> flow model selection .....	82
3.2.1 Materials and methods .....	82
3.2.2 Results and discussion .....	87
3.3 Determining model design parameters .....	89
3.3.1 Discussion .....	92
3.4 Fluid dynamics analysis of the model .....	93
3.4.1 Determination of sample volume .....	94
3.4.2 Analysis of the significance of volume .....	97
3.4.3 Frequency and volumetric flow rate analysis .....	100
3.4.4 Fluid friction factor analysis .....	102
3.4.5 Discussion .....	114
3.5 Implementing the model .....	117
3.6 Summary .....	118
3.7 Conclusion .....	119
Chapter 4 Model Stent Design, Fabrication and Characterization .....	120
4.1 Introduction .....	120
4.2 Model stent design and fabrication .....	121
4.2.1 Materials and methods .....	121
4.2.2 Results and discussion .....	124
4.3 Model stent surface characterization .....	126
4.3.1 Materials and methods .....	126
4.3.2 Results .....	129

4.4 Summary and conclusion .....	135
Chapter 5 Effect of Sample Volume on <i>In Vitro</i> Evaluation of Material-Induced Thrombogenicity	136
5.1 Introduction .....	136
5.2 Materials and methods.....	140
5.2.1 Flow model.....	140
5.2.2 Model stent design.....	140
5.2.3 Antibodies and reagents .....	141
5.2.4 Blood sample collection .....	141
5.2.5 Platelet and leukocyte activation and platelet-leukocyte aggregation.....	141
5.2.6 Immunolabelling and flow cytometry analysis .....	142
5.2.7 Scanning electron microscopy.....	143
5.2.8 Statistical analysis .....	144
5.3 Results .....	144
5.3.1 Effect of experimental groups and conditions on shear stress/rate .....	144
5.3.2 Effect of sample volume, shear stress and stent on platelet activation .....	145
5.3.3 Effect of sample volume, shear stress and stent on leukocyte activation.....	151
5.3.4 Effect of sample volume, shear and stent on platelet-leukocyte aggregation .....	165
5.3.5 Effect of sample volume and shear on surface adhesion.....	169
5.4 Discussion.....	171
5.4.1 Effect of experimental groups and conditions on shear stress/rate .....	171
5.4.2 Platelet activation .....	172
5.4.3 Leukocyte activation .....	174
5.4.4 Platelet-leukocyte aggregation .....	176
5.4.5 Surface adhesion.....	179
5.5 Conclusions .....	181
Chapter 6 Effect of Complement Inhibition on Platelet and Leukocyte Response to Shear and Biomaterials.....	183
6.1 Introduction .....	183
6.2 Materials and methods.....	185
6.2.1 Flow model.....	185
6.2.2 Model stents.....	186
6.2.3 Antibodies and reagents .....	186

6.2.4 Blood sample collection.....	186
6.2.5 Platelet and leukocyte activation and platelet-leukocyte aggregation .....	187
6.2.6 Immunolabelling and flow cytometry analysis.....	188
6.2.7 Scanning electron microscopy .....	189
6.2.8 Statistical analysis.....	189
6.3 Results.....	189
6.3.1 Effect of complement inhibition on platelet response to shear and model stents .....	189
6.3.2 Effect of complement inhibition on leukocyte response to shear and model stents .....	192
6.3.3 Effect of complement inhibition on platelet-leukocyte aggregation response to shear and model stents.....	199
6.3.4 Effect of complement inhibition on surface adhesion .....	201
6.4 Discussion .....	203
6.4.1 Platelet activation.....	203
6.4.2 Leukocyte activation .....	205
6.4.3 Platelet-leukocyte aggregation.....	207
6.4.4 Surface adhesion .....	208
6.5 Conclusion .....	209
Chapter 7 Effect of Surface Roughness on Blood Activation and Complement Inhibition .....	211
7.1 Introduction.....	211
7.2 Materials and methods .....	213
7.2.1 Flow model .....	213
7.2.2 Model stents surface treatment .....	214
7.2.3 Model stent surface characterization.....	214
7.2.4 Antibodies and reagents .....	214
7.2.5 Blood sample collection.....	214
7.2.6 Platelet, complement and leukocyte activation and aggregation .....	215
7.2.7 Immunolabelling and flow cytometry analysis.....	216
7.2.8 Surface adhesion characterization.....	216
7.2.9 Statistical analysis.....	217
7.3 Results.....	217
7.3.1 Lumen characterization.....	217
7.3.2 Model stent characterization .....	218

7.3.3 Effect of surface roughness on platelet activation.....	221
7.3.4 Effect of surface roughness on leukocyte activation.....	223
7.3.5 Effect of surface roughness on platelet-leukocyte aggregation.....	224
7.3.6 Effect of surface roughness on FUT-175 efficacy.....	226
7.3.7 Surface adhesion.....	229
7.4 Discussion.....	230
7.4.1 Surface roughness.....	231
7.4.2 Platelet activation.....	232
7.4.3 Leukocyte activation.....	233
7.4.4 Platelet-leukocyte aggregation.....	234
7.4.5 Surface adhesion.....	235
7.4.6 Complement inhibition effect.....	235
7.5 Conclusion.....	236
Chapter 8 Summary of Contributions and Future Work.....	238
8.1 Summary and perspectives.....	238
8.1.1 Significance of a systems approach.....	238
8.1.2 A systems approach to <i>in vitro</i> model design.....	238
8.1.3 Model stent design, fabrication and characterization.....	239
8.1.4 A method for determining appropriate blood sample volume.....	239
8.1.5 Fluid mechanics of the Chandler loop model.....	239
8.1.6 Effect of sample volume on platelet and leukocyte activation.....	240
8.1.7 Effect of complement inhibition on platelet and leukocyte activation.....	240
8.1.8 Effect of surface roughness.....	240
8.1.9 Perspectives on receptor expression and function.....	240
8.2 Major contributions.....	241
8.3 Future work.....	241
Chapter 9 Summary of Conclusions.....	247
References.....	249
Appendix A Material Composition and Properties.....	275
Appendix B Application of Blasius Correlation.....	276
Appendix C Determination of Density, Viscosity and Wall Shear Stress Effect of Humid Air.....	277
Appendix D Rotor Calibration.....	280

Appendix E Determining AFM Scanning Area.....	282
Appendix F Dynamic Contact Angle Analysis.....	284
Appendix G Physiological Solution Preparation .....	285

## List of Figures

Figure 2-1. Schematic of pattern recognition receptor types .....	14
Figure 2-2. Schematic of the conventional complement activation cascade.....	16
Figure 2-3. Detailed schematic of the conventional complement cascade.....	17
Figure 2-4. Schematic of the updated complement activation cascade.....	18
Figure 2-5. Schematic of the functions of complement and complement-mediated cell functions .....	19
Figure 2-6. Illustration of neutrophil functions .....	25
Figure 2-7. Illustration of monocyte functions.....	27
Figure 2-8. Block schematic of the coagulation cascade .....	28
Figure 2-9. Schematic of the coagulation cascade. ....	31
Figure 2-10. Schematic of the contact system pathway. ....	35
Figure 2-11. Contact system-biomaterial interaction schematic. ....	37
Figure 2-12. Illustration of platelet functions.....	40
Figure 2-13. Schematic of interactions in material-induced thrombosis.....	43
Figure 2-14. Cellular-based interaction and crosstalk triad between blood and other system. ....	45
Figure 2-15. Geometric and structural properties of the vascular system.....	46
Figure 2-16. Schematic representation of the blood-biomaterial interaction triads (BBITs).....	66
Figure 2-17. 3-dimensional representation of the blood-biomaterial interaction framework .....	67
Figure 2-18. Schematic of the mode of interaction, the SAXSA sequence .....	69
Figure 2-19. Schematic of systems approach based on immune system.....	72
Figure 2-20. Schematic of the systems approach framework.....	76
Figure 2-21. <i>In vitro</i> model design flowchart.....	77
Figure 3-1. Schematic of the cone-and-plate model.....	85
Figure 3-2. Schematic of the parallel plate chamber model.....	86
Figure 3-3. Schematic of the Chandler loop model.....	86
Figure 3-4. Representation of circulation loop with blood sample and model stent.....	90
Figure 3-5. Pulse wave representation of circulating blood sample flow for stationary observer .....	98
Figure 3-6. Comparison of friction factor equations for curved smooth tubes .....	104
Figure 3-7. Pulse wave representation of circulating blood sample with model stent.....	107
Figure 3-8. Time-averaged wall shear stress as a function of angular velocity. ....	111
Figure 3-9. Pulse wave representation of circulating blood sample with model stent, including effect of air.....	112

Figure 3-10. Combined time-averaged wall shear stress due to blood and air in the loop .....	114
Figure 3-11. Rotor with rotation disk and loops used as the <i>in vitro</i> flow model.....	117
Figure 4-1. Schematic of the longitudinal section view of the threaded rod with wire .....	122
Figure 4-2. Schematic of longitudinal section view of the mandrel with wire strip.....	122
Figure 4-3. Picture of mandrels with stents sealed in a quartz tube after heat treatment. ....	124
Figure 4-4. Typical model stent .....	125
Figure 4-5. Scanning electron micrograph of stent surface heat treated and quenched in air .....	125
Figure 4-6. Ti-6Al-4V SEM surface topography and roughness.....	129
Figure 4-7. TI-6AL-4V AFM surface topography and roughness.....	130
Figure 4-8. XPS survey spectra.....	133
Figure 4-9. Cyclic voltammetry curve for Ti-6Al-4V model stent.....	135
Figure 5-1. Characteristic flow cytometry analysis plots of platelet activation in whole blood.....	146
Figure 5-2. Effect of volume, shear and stent on platelet microparticle formation. ....	148
Figure 5-3. Effect of surface area-to-volume ratio on platelet microparticle formation.....	150
Figure 5-4. Effect of volume, shear and stent on percentage of monocytes expressing TF. ....	155
Figure 5-5. Effect of volume, shear and stent on TLR-4 expression. ....	158
Figure 5-6. Effect of surface area-to-volume ratio on Mac-1 expression.....	162
Figure 5-7. Effect of volume, shear and stent on platelet-leukocyte aggregation .....	168
Figure 5-8. Effect of surface area-to-volume ratio on platelet-leukocyte aggregation. ....	169
Figure 5-9. Scanning electron micrograph of cell adhesion pattern for 2 ml + 20 mm stent samples. .....	170
Figure 5-10. Scanning electron micrograph of cell adhesion pattern for 4 ml + 20 mm stent samples. .....	170
Figure 5-11. Scanning electron micrograph of cell adhesion pattern for 4 ml + 35 mm stent samples. .....	171
Figure 5-12. Schematic of shear stress sensitivity of platelet and leukocyte activation and platelet- leukocyte aggregation .....	179
Figure 6-1. Schematic of experimental conditions .....	188
Figure 6-2. Characteristic flow cytometry analysis dot plots for platelets .....	190
Figure 6-3. Effect of complement inhibition on platelet microparticle formation.....	191
Figure 6-4. Characteristic flow cytometry events histogram plots for CD11b on monocytes.....	193
Figure 6-5. Characteristic flow cytometry events histogram plots for CD11b on PMNs.....	193

Figure 6-6. Effect of complement inhibition on percentage of monocytes expressing TF. ....	194
Figure 6-7. Representative flow cytometry histogram plots showing FUT-175 effect on Mac-1 expression in stent samples .....	195
Figure 6-8. Effect of complement inhibition on Mac-1 expression on monocytes. ....	195
Figure 6-9. Effect of complement inhibition on Mac-1 expression on PMNs. ....	196
Figure 6-10. Effect of complement inhibition on platelet-monocyte aggregation. ....	200
Figure 6-11. Effect of complement inhibition on platelet-PMN aggregation. ....	201
Figure 6-12. SEM cell adhesion pattern for sample with and without inhibitor. ....	202
Figure 6-13. Magnified SEM cell adhesion pattern for sample with inhibitor. ....	203
Figure 7-1. Schematic of experimental conditions. ....	215
Figure 7-2. Schematic illustration of lumen and stent surface roughness .....	217
Figure 7-3. SEM micrograph comparison of unetched and acid-etched stent surfaces. ....	218
Figure 7-4. Atomic force micrograph of model stent surface topography and roughness. ....	219
Figure 7-5. Effect of surface roughness on PMP formation. ....	222
Figure 7-6. Effect of surface roughness on platelet-monocyte aggregation. ....	225
Figure 7-7. Effect of surface roughness on platelet-PMN aggregation. ....	226
Figure 7-8. SEM of cell adhesion pattern on acid-etched samples. ....	229
Figure 7-9. SEM of cell adhesion pattern on acid-etched sample, with inhibitor. ....	230
Figure 8-1. Schematics of events at a material surface and mediating factors. ....	242

## List of Tables

Table 2-1. Blood constituents. ....	10
Table 2-2. Physiological concentrations of the main complement proteins .....	15
Table 2-3. Diffusion coefficients of some major blood proteins. ....	20
Table 2-4. Neutrophil and monocyte characteristics. ....	22
Table 2-5. Some coagulation cascade proteins. ....	29
Table 2-6. Contact system proteins.....	34
Table 2-7. Selected platelet receptors .....	39
Table 2-8. Typical dimensions of coronary arteries. ....	47
Table 2-9. Typical surface tension values.....	62
Table 2-10. Surface characteristics and their broad implications .....	64
Table 2-11. Basic representation of systems and effect of interaction based on organizational level..	70
Table 2-12. Rationalization of <i>in vitro</i> model parameters .....	78
Table 3-1. Physiological parameters.....	83
Table 3-2. Model requirements and constraints.....	84
Table 3-3. Comparison of three <i>in vitro</i> flow models.....	88
Table 3-4. Fluid mechanics equations for the Chandler loop model .....	91
Table 3-5. Comparison of selected model parameters to average physiological LAD parameters .....	92
Table 3-6. Entrance length correlations. ....	94
Table 3-7. Model frequency and volumetric flow rate .....	102
Table 3-8. Typical friction factor equations for laminar flow .....	103
Table 3-9. Volume and stent ratio effect on friction factor weighting .....	109
Table 3-10. Time-averaged wall shear stress for selected sample volumes and stent samples .....	111
Table 4-1. Matching the tube to the rod.....	122
Table 4-2. Typical model stent parameters.....	126
Table 4-3. Ti-6Al-4V surface characteristics from AFM. ....	131
Table 4-4. Contact angle measurements .....	132
Table 4-5. Relative concentration (atomic %) of surface elements .....	134
Table 5-1. Experimental conditions .....	142
Table 5-2. Time-averaged wall shear stress/rate for the experimental groups and conditions .....	145
Table 5-3. Effect of sample volume and shear rate on platelet activation .....	147
Table 5-4. Effect of volume, shear and stent on CD61 and P-selectin expression .....	149

Table 5-5. Effect of surface area-to-volume ratio on CD61 and P-sel expression.....	151
Table 5-6. Effect of volume and shear on leukocyte activation .....	153
Table 5-7. Effect of volume and shear on TLR-4 expression on leukocytes .....	154
Table 5-8. Effect of volume in the presence of model stent on Mac-1 and C3aR expression on leukocytes.....	157
Table 5-9. Effect of volume, shear and stent on Mac-1 and C3aR expression on leukocytes .....	160
Table 5-10. Effect of surface area-to-volume ratio on C3aR and TLR-4 expression on leukocytes .	164
Table 5-11. Effect of volume and shear on platelet-leukocyte aggregation.....	166
Table 5-12. Summary of the effects of experimental conditions on platelets and leukocytes .....	181
Table 6-1. Effect of complement inhibition on CD61 and P-sel expression on platelets .....	192
Table 6-2. Effect of complement inhibition on C3aR and TLR4 expression.....	197
Table 6-3. Comparison of inhibitor effects on controls for Mac-1, C3aR and TLR-4.....	199
Table 6-4. Summary of inhibition effect. ....	209
Table 7-1. Surface roughness measurements .....	220
Table 7-2. The Z range and roughness ratio .....	220
Table 7-3. Contact angle measurements for unetched and acid-etched samples .....	221
Table 7-4. Effect of surface roughness on CD61 expression on platelets and PMPs .....	222
Table 7-5. Effect of surface roughness on leukocyte activation .....	224
Table 7-6. Effect of surface roughness on FUT-175 efficacy to reduce platelet activation.....	227
Table 7-7. Effect of surface roughness on FUT-175 efficacy to reduce leukocyte activation .....	228

## List of Abbreviations

AFM	Atomic force microscopy
BBI	Blood-biomaterial interaction
CD	Cluster of differentiation. CD antigen (CD and a number).
DES	Drug-eluting stents
FXIIa	Activated Factor XII
FITC	Fluorescein 5-isothiocynate, conjugated to antibody
FL	Fluorescence channels (FL-1 to FL-4)
fMLP	Formyl-methionyl-leucyl-phenylalanine
FSC-H	Forward scatter laser signal filter
GPIIb/IIIa	Surface glycoprotein receptor expressed on activated platelets
Ig	Immunoglobulin. Specific antibodies are designated a letter, e.g. IgG, IgM
IL	Interlukin is a type of cytokine. Usually it is followed by a number, e.g. IL-1
LAD	Left anterior descending
LMA	Left main artery
LCx	Left circumflex
Ligand	Molecule that binds to a specific target protein
Mac-1	Macrophage-1, member of integrin family of receptors
MIT	Material-induced thrombosis
mRNA	Messenger RNA (ribonucleic acid)
PE	Phycoerythrin, conjugated to antibody
PMPs	Platelet microparticles
PSGL-1	P-selectin glycoprotein ligand 1 (constitutively leukocyte receptor for selectins)
Ra	Average surface roughness: average mean of all the measured heights
RMS	Root-mean-square: quadratic mean of all the measured heights
RGD	Arginine-Glycine-Aspartic acid binding peptide. The R, G and D are letters designated to the respective amino acids.
Re	Reynold's number, which gives the ratio of inertial forces to the viscous forces.
SSC-H	Flow cytometer side scatter laser signal filter
THP-1	Human monocytic cell line
TNF	Tissue necrosis factor

## **Glossary of Terms**

Biocompatibility	The ability of a material to perform with an appropriate host response in a specific situation [1]
Complement system	A set of plasma proteins that act together to attack extracellular forms of pathogens [2]
Contact system	Group of coagulation proteins that require contact with negatively charged surface for enzyme activation
Surface area	Area of the 'real surface' defined by sample geometric boundaries. If measured by AFM, it is the area of the topographic surface defined by the scan boundary.
Surface area-to-volume ratio	Generally, it is the ratio of area of the 'real surface' that is immersed in a fluid to the volume of the fluid
System	A coordinated combination of elements or components working together to form a complex whole
Systems approach	A holistic and integrated problem solving method that entails both quantitative and qualitative decision-making processes to achieve a comprehensive solution for a variety of complex problems [3]
Thrombogenicity	The extent to which a device, when employed in its intended use configuration, induces adverse responses [4]



# Chapter 1

## Thesis scope and hypotheses

### 1.1 Introduction

Coronary stents are common cardiovascular intervention devices for arterial stenosis. However, one of the adverse outcomes of coronary stent implantation is material-induced thrombosis (MIT), which is normally prevented by anti-platelet, anti-coagulant and thrombolytic therapies. Despite years of research in biomaterials sciences and blood-biomaterial interactions, the holy grail of material-induced thrombosis (the formation of a blood clot) has not been found. Although considerable progress has been made, “the perfect material is yet to be identified” [5] and some researchers have suggested that “the perfect stent ... will probably never exist” [6]. The sentiments expressed in these statements in no way suggest that it is fruitless to continue research in these areas. To the contrary, they highlight the current dilemma and perhaps the need to rethink research methodologies. There are a variety of reasons for the continued search for the illusive holy grail of biocompatibility, none more important than the dynamic complexity and adaptability of the immune system. This results in complex blood-biomaterial interactions, which are not completely understood [7, 8]. For that reason, it has been suggested that the “true effect of a biomaterial surface on blood can only be identified when whole blood is used” [9]. Indeed a holistic approach has been previously undertaken to study blood interaction with polymeric materials [10]. Furthermore, a systems approach to blood-biomaterial studies has been suggested [11].

A **systems approach** is a problem solving method which “addresses the total problem-solving cycle” [3]. To that end, a systems approach can be defined as a holistic and integrated problem solving method that entails both quantitative and qualitative decision-making processes to achieve a comprehensive solution. Although a systems approach has increasingly been used to study biological systems such as coagulation [12, 13], an important system in thrombosis, there is generally limited application of systems methods in blood-biomaterial interaction studies. This could be due to a variety of reasons, such as lack of standardized tests and guiding principles for biocompatibility analysis [14]. Ideas for a framework for blood-biomaterial interaction assessment have been recently provided [4]. However, there is no framework for a systems approach in blood-biomaterial studies. Therefore, it is necessary to develop a systems approach framework for blood-biomaterial studies that also incorporates *in vitro* model design.

Various *in vitro* flow models [15-17] have been used to study blood-biomaterial interactions. Although there is rationale for each model, one of the key parameters that define each model is the ability to generate a wide range of shear rates. Shear rate is indeed one of the mechano-stimulators that has long been known to influence various aspects of cell interaction, activation and aggregation kinetics involved in hemostasis and thrombosis [18]. It also influences cell/protein-biomaterial interaction/adhesion [19]. Although these transient cell and protein behaviors have been observed from a variety of systems that can produce both constant or time-varying shear stress, there are other fundamental properties of flow that play equally important roles in influencing cell/protein behavior. These include the geometry of the model and the flow type and profile. Even though the response elicited by shear stress is generally known, the role of changes to the *in vitro* model design parameters, such as sample volume and flow type, and their influence on the rate, level and ultimate thrombotic behavior under flow conditions, are not well understood. As a result, there is no consistent and standardized set of *in vitro* model parameters, even for studying the same physiological location of interest such as coronary arteries. Hence, it is necessary to elucidate the role of other physiologically-based *in vitro* model design parameters and their possible impact on the interpretation of experimental results.

To understand material-induced thrombosis, much work has been done on polymeric materials. This is not surprising as they are used in a variety of medical applications, both short term and long term, such as catheters, dialysis tubing, blood warmers, stent coatings, etc. However, metallic biomaterials have continued to play an equally significant role in medical devices because of their unique properties and have found various applications in orthopedic, dental and cardiovascular implants [20]. Various metallic biomaterials have different levels of biocompatibility. The ones that are reasonably biocompatible and are used in cardiovascular devices include nitinol and Ti-6Al-4V [21]. These biomaterials still cause some level of blood activation, mostly because they are inorganic materials and will trigger an immune response [22, 23]. This results in the activation of leukocytes, which subsequently express cell surface markers such as Mac-1 and tissue factor (TF). The TF protein, which is expressed on monocytes and macrophages only after activation [24], is recognized as one of the key coagulation initiators. To understand the regulation of TF by biomaterials, it is necessary to understand the mechanism of leukocyte activation by biomaterials. Consequently, it would be informative to concurrently investigate other leukocyte receptors, which are related to recognition of foreign material, such as complement receptors. Complement proteins, which are one of the immune system surface recognition proteins, play an important role in biomaterial response

[22]. Since they also activate and recruit leukocytes, it is necessary to understand the regulation of their receptors on leukocytes. Understanding their regulation by biomaterial surface characteristics such as surface roughness and the impact of complement inhibition is also important in elucidating the pathways involved in material-induced TF expression and thrombosis since surface characteristics may influence the activation pathway [25]. In addition, platelets activation, which together with complement have been found to play an important role in material associated thrombosis [10], needs to be concurrently investigated in line with the need for a systems approach in blood-biomaterial interactions.

The adhesion of activated leukocytes to material surface depends on the material as well as the shear stress [26, 27]. Platelets similarly adhere in a shear and material-dependent manner. Since leukocyte surface adhesion is facilitated by complement fragments, as well as fibrinogen, and activated platelets and leukocytes form platelets-leukocyte aggregates which may localize on the surface, the effect of complement inhibition on leukocyte and platelet adhesion has been previously investigated [10]. While leukocyte adhesion was reduced, platelet adhesion was unaffected. This means the inhibition still left the problem of thrombogenicity. Because complement inhibition represents one of the important pathways to reduce material-induced thrombogenicity, it is necessary to investigate other methods of complement inhibition on platelet and leukocyte activation and surface adhesion. Since platelets mediate leukocyte TF expression [28], the link between TF expression and surface attachment or detachment has not been clearly studied. Therefore, there is need to elucidate the link between leukocyte and/or platelet adhesion and TF expression.

This thesis builds on the work started towards a systems approach in whole blood studies. The premise is that since a systems approach follows a methodology to establish the relationship between the emergent system behavior and the interactions of its elements, it facilitates tracing process pathway linkages and interactions that are important in blood-biomaterial studies. This will not only assist in interpreting experimental results, but will assist in activation measurements that are related to the physiological environment. A systems approach will also facilitate numerical simulations. Therefore, the objectives of this thesis are to:

- 1) Establish a systems approach framework and concepts in blood-biomaterial studies;
- 2) Select/design an appropriate *in vitro* model for coronary studies applying a systems approach method:
  - a. Develop a set of *in vitro* model parameters for coronary studies

- b. Establish an appropriate sample volume selection method
  - c. Characterize fluid flow and friction parameters
  - d. Establish the interaction relationships between volume, shear and a model stent;
- 3) Design, fabricate and characterize model stents for blood-biomaterial interaction studies;
- 4) Investigate the effect of volume and combined volume-shear-stent interactions on platelet and leukocyte activation and aggregation under flow conditions;
- 5) Investigate the effect of complement inhibition on platelet and leukocyte activation and surface adhesion with a selected volume-shear-stent combination;
- 6) Investigate the effect of model stent surface roughness on platelet and leukocyte activation and surface adhesion with a selected volume-shear-stent combination.

## 1.2 Thesis scope and format

Using a systems approach, *in vitro* model design requirements and constraints were developed based on the physiological location of interest. Three *in vitro* flow models were evaluated on the basis of their operation principles and one model with geometric and hemodynamic parameters that closely matched the design parameters was selected for modification, flow characterization and for use in this research. Since metallic biomaterials are extensively used as implants, metallic model stents were fabricated and used to investigate blood-biomaterial interactions under conditions mimicking coronary flow. The parameters of interest were expression of TF, Mac-1, complement fragment C3a receptor (C3aR) and toll-like receptor 4 (TLR-4) on leukocytes. Platelet microparticle formation was investigated to elucidate platelet activation. The interaction of platelets with leukocytes was investigated by platelet-leukocyte aggregation formation in the fluid phase as well as on a material surface. Since complement plays an important role in inflammation, particularly C3, which is a possible therapeutic target, the role of its fragment was investigated by expression of its receptor. Toll-like receptor 4 is an important recognition molecule in leukocyte inflammatory response and therefore was included in the investigation. More importantly, it is informative to profile other receptors in addition to the standard markers as receptors are often engaged in a specific combination for a specific immune response. Flow cytometry was used to study all blood activation/aggregation in the fluid phase and scanning electron microscopy was used to investigate material surface adhesion. All the investigations in this study were done with whole blood.

The thesis is comprised of independent but linked chapters. Chapter 2 presents an overview of the relationships and interactions of biological systems that play a role in blood-biomaterial interactions. An introduction of a systems approach framework and the use of a systems approach in these interactions and their role in thrombosis is also presented. Chapter 3 presents the selection of the *in vitro* flow model, analysis of model fluid mechanics characteristics and their significance in the interpretation of experimental results. In Chapter 4, model stents with specific characteristics are designed, fabricated and characterized. Chapter 5 examines the implications of model parameters, such as blood sample volume, on leukocyte and platelet activation and aggregation, with and without model stents. Some of the work in this chapter has been previously published [29]. Chapter 6 presents the effect of complement classical and alternative pathway inhibition on platelet and leukocyte activation, aggregation and adhesion. Chapter 7 presents the effect of model stent roughness on blood activation. Chapter 8 summarizes the contributions of this work and lessons learnt. Chapter 9 provides a summary of the conclusions.

### **1.3 Hypotheses and thesis objectives**

The overall goal of this thesis was to demonstrate that a systems approach provides an invaluable tool in the critical analysis of linkages and translation of a biological system to an *in vitro* model.

Hypotheses were formulated to assess mechanisms involved in material-induced platelet and leukocyte activation using a systems approach. These hypotheses are given below and associated with specific chapters of the thesis.

**Chapter 3** – Two hypotheses were formulated in this chapter; (i) *in vitro* flow model parameters mimicking physiological location of interest are better designed following a systems approach and (ii) blood sample volume influences flow dynamics and hence wall shear stress.

**Chapter 4** – The objectives of this chapter were to design and fabricate model stents with specific geometric and surface characteristics. An additional objective was to characterize the model stents and acquire essential information that would facilitate interpretation of investigation results of their influence on hemodynamics and blood activation.

**Chapter 5** – The hypothesis was that under shear and stent conditions, blood sample volume has different effects on blood cell activation and surface adhesion.

**Chapter 6** – The hypothesis was that under flow shear conditions, complement inhibition reduces leukocyte and platelet activation and surface adhesion.

**Chapter 7** – Two hypotheses were formulated in this chapter; (i) under flow shear conditions, multi-scale surface roughness influences leukocyte activation and (ii) surface roughness influences the effectiveness of complement inhibition.

## **Chapter 2**

# **Blood-Biomaterial Interactions in Thrombogenicity and the Case for a Systems Approach**

### **2.1 Introduction**

Cardiovascular diseases are the major cause of morbidity and mortality globally [30, 31]. While mortality is trending down, prevalence remains high. In the United States it is estimated that the prevalence of cardiovascular diseases (CVD) is greater than 1 in 3 adults (83.6 million) and coronary heart disease exists in 15.3 million (1 in 14 adults) [32]. The United States has seen a 28% increase in cardiovascular operations and procedures from 2000 to 2010. In 2009, the total inpatient hospitalizations from CVD was approximately 1 out of every 6 hospital stays, accounting for \$71.2 billion (approximately one fourth of the total inpatient care). The overall economic impact, i.e. direct and indirect cost, in 2010 was estimated at \$315.4 billion [32]. In Canada, it is estimated that heart diseases and stroke contribute 2.5 million hospitalizations per year [33] with an overall economic impact in 2009 estimated at \$22.2 billion CAD; direct costs (e.g. hospitalization) accounting for \$7.6 billion CAD and indirect cost (e.g. lost economic productivity) accounting for \$14.6 billion CAD [33]. These statistics illustrate not only the burden of disease, but the broader social, health and economic implications, both at personal and national levels. While there are great prevention methods at population, community and personal levels, there is great need for cost effective intervention methods.

The most common intervention method for the most prevalent cardiovascular disease, ischemic heart disease, which is caused by narrowing of coronary arteries (stenosis), is angioplasty followed by implantation of coronary stents. Angioplasty is a method of opening an occluded blood vessel with an inflatable balloon and the stent, which is a scaffold, keeps the blood vessel lumen patent. Although these devices have greatly improved patient outcomes, there has been a constant problem of in-stent thrombosis (formation of blood clots within a stent), for both first generation bare metal stents and drug-eluting stents [34-37]. First generation drug-eluting stents (DES) have reduced in-stent thrombosis to about 3% [38], but the risk of a late occurrence of material-induced in-stent thrombosis remains unabated. However, current studies show improvement with the use of second generation DES [39-41], although interestingly in terms of mortality, some studies suggest no significant difference between the first and second generation DES [39, 40]. Material-induced in-stent

thrombosis has been associated with a number of factors [42], more importantly delayed reendothelialization [43], which leaves stent struts exposed to blood for extended periods of time. Although this has also been improved by second generation DES [44], it has not been eliminated. The development of in-stent thrombosis can have several consequences. The blood clot (thrombus) may grow in situ and block blood flow, which would result in myocardial infarction and heart attack. The thrombus can also break off, flow with the blood and block blood supply to major organs such as the brain or lungs. Blockage of blood supply to the brain would result in a stroke, which is also a major cause of morbidity and mortality. Thus, in-stent thrombosis can cause serious complications, possibly resulting in debilitating permanent disability or death.

Several therapeutic interventions are available for preventing in-stent thrombosis [45]; anticoagulants, which block proteins that participate in coagulation pathways, antiplatelets [46], which block platelet receptors responsible for aggregation, and thrombolytic agents, which dissolve the thrombus. One common feature with these interventions is that they are curative and not preventive. In addition, they are usually prescribed for more than a year and thus do not only have systemic side effects, such as risk of developing bleeding complications [45], but also have economic implications for the patient. For that reason, there is need for better preventive solutions that stop or control the development of in-stent thrombosis in the first place. However, development of preventive interventions, whether device and/or pharmaceutical, requires better understanding of mechanisms involved in biomaterial-induced initiation and propagation of in-stent thrombosis.

Consequently, there has been extensive research in all areas of biomedical and biotechnology related to this problem; biomaterial sciences, blood-biomaterial interactions, devices and therapeutic interventions. Biomaterial sciences and blood-biomaterial interactions research areas particularly play a key role in this initiative, with the common objective of meeting the new functional biocompatibility requirements [47]. To that end, research and development in stent and other cardiovascular device materials has seen a great evolution in the last couple of years [47-49]. Despite the development of new materials, material-induced in-stent thrombosis remains a major concern. This is partly because in spite of years of research in blood-biomaterial interactions, “the fundamental principles of the causation of specific cellular responses as a result of the influence of materials are still not well known” [50]. Hence, there has been a call for a holistic approach to address not only the complexity of biocompatibility but also to include other aspects such as regulations [8]. Such an

approach requires systems thinking, which in turn requires clearly defining and understanding the various systems at play and their relationships.

There are three main systems involved in the development and propagation of in-stent thrombosis. These are (i) the blood (biochemical/cell-plasma) system, (ii) the fluidics system and (iii) the biomaterial system. The first two systems are intrinsic while the biomaterial system is extrinsic. Each of the systems has characteristic properties that define its role in the mechanism and level (spatial and time scales) of interaction. The blood system is really a system of systems, i.e. the system components are systems in their own right. These components or (sub)systems include the contact, the hemostatic and the immune systems. There is constant cross-talk between these systems in both health and disease states. The fluidics (transport) system is composed of the coronary arteries with their geometry and hemodynamics characteristics. The biomaterial system is characterized by the implant design structure, geometry and surface characteristics. The interactions between the systems elicit activation of complex pathways and biochemical networks that are involved in the initiation and propagation of in-stent thrombosis. The mechanisms involved in the interaction of these systems and the signal propagation pathways are not well understood. The key to understanding these mechanisms lies in understanding material-induced blood activation pathways and how these interactions propagate to produce thrombosis. Applying systems thinking to blood-biomaterial interactions would be invaluable in unraveling some of these complex interactions.

Therefore, this research presents the case for a systems approach for the study of blood-biomaterial interactions. In this chapter, a detailed literature review of each of the three systems and their interaction from a systems perspective will be discussed. The case for a systems approach is then presented and a framework for further development of this initiative is provided. In the subsequent chapters, the systems approach is applied in developing the *in vitro* model and in holistic laboratory experiments. The motivation for continued research in blood-biomaterial interaction is not only to address the continued risk of development of in-stent thrombosis in patients with coronary stents but also to contribute knowledge in biomaterial-induced thrombosis, especially with respect to the development of a systems approach framework.

## **2.2 The blood system**

The blood system is really a system of (biochemical) systems. Blood is an inhomogeneous colloidal fluid composed of relatively homogeneous plasma fluid (viscosity of 0.0012 Pa.s [51]) with

a suspension of particles (cells and proteins) of varying sizes, shapes and complexity (Table 2-1). The colloidal nature of blood gives it complex rheological properties. Its viscosity (0.003-0.004 Pa.s[52]) is influenced by a number of factors, including flow rate and hematocrit. Hematocrit, defined as volume ratio of red blood cells to the total blood sample volume, varies by individual but normal hematocrit level is about 45% [51]. Under isothermal conditions, blood has a relatively constant density, estimated at  $\rho \approx 1060 \text{ kg/m}^3$  [51], independent of pressure. Hence, it exhibits the properties of an incompressible fluid.

**Table 2-1. Blood constituents. Data adapted from [1, 53].**

Constituent	Size ( $\mu\text{m}$ )	Density (% by weight)	% of constituent	% of cell volume	% of blood volume
Plasma <ul style="list-style-type: none"> <li>○ Water</li> <li>○ Proteins <ul style="list-style-type: none"> <li>➤ Albumin</li> <li>➤ Immunoglobulins</li> <li>➤ Fibrinogen</li> </ul> </li> <li>○ Other solutes (salts, gases, nutrients, etc.)</li> </ul>	–	91g/ml (91%) 7g/ml (7%)  2g/ml (2%)	58% 38% 4%	–	55
Red blood cells (erythrocytes)	8-9	$4.2\text{-}5.8 \times 10^6 / \mu\text{L}$		95%	45
White blood cells (leukocytes)		$5\text{-}9 \times 10^3 / \mu\text{L}$		0.1%	
○ Neutrophils	10-15		60-70%		
○ Lymphocytes	7-18		20-25%		
○ Monocytes	12-20		3-8%		
○ Eosinophils	10-15		2-4%		
○ Basophils	10-15		0.5-1%		
Platelets	2-4	$250\text{-}400 \times 10^3 / \mu\text{L}$		4.9%	

The volume of blood in the human body is about 5L [54]. About 50% of the blood volume is composed of blood cells. Red blood cells, which have a lifespan of 120 days, form the most

constituent cell volume. They play an important role in metabolism while the other cells play a key role in defense. As discussed above, red blood cells also determine hematocrit, which has great influence on blood rheology and hemodynamics [55]. Thus, their influence on blood flow has mechanical implications on blood-biomaterial interaction as they influence flow segregation and particle dispersion [56, 57]. However, they can also have biochemical effects, such as in the event of hemolysis. Therefore, they cannot be ignored when performing *in vitro* flow studies.

Blood plasma, which constitutes a little over half of the blood volume, is mostly composed of water, about 90% by volume. The other 10% of the plasma volume is mostly occupied by proteins, which play a variety of roles including immune response. The fact that water constitutes close to 50% of the blood volume makes it an important constituent. It has both transport and regulatory roles. It is a solvent for a number of substances, such as proteins, gases and electrolytes. It also regulates osmotic pressure and tightly controlled blood acid-base balance; blood pH is maintained at a tight range of 7.35-7.45 [58]. More importantly, at material surfaces, water influences interfacial interactions and hence adsorption of molecules [59]. Consequently, it needs to be considered in blood-biomaterial interactions.

All the various components (sub-systems) of the blood are interlinked but have specialized broad functions, such as metabolism, regulation, transport and defense. While all the systems are important *in vivo* and in blood-biomaterial interactions, often they are not all investigated in *in vitro* studies based on their relative importance in influencing the results. Metabolism and regulation functions are often not investigated since their broader impact, such as change in blood pH and cell exhaustion, are minimized in the *in vitro* model by limiting the blood incubation time. Although in a comprehensive systems approach, it would be necessary to include all the systems, a systems approach can also be applied within defined system boundaries. Unlike standard modeling approach, which is not necessarily holistic, the systems approach is holistic by design, regardless of the extent of the defined system boundaries. For the purpose of this research, only the key systems generally related to blood-biomaterial interaction, i.e. systems responsible for transport and defense functions, are included.

The cardiovascular system defines the geometry and fluid dynamics parameters that characterize the coronary transport phenomenon. *In vivo*, these parameters modulate cellular and vascular functions, under both normal and disease conditions. They influence vessel wall intimal remodeling [60] and, development and localization of atherosclerotic lesions [61, 62]. Hemodynamics

can cause cell trauma in circulatory devices as well as cell activation. Similarly, the systems responsible for the defense (immune system) define parameters that characterize blood activation, coagulation and thrombosis. In both *in vivo* and *in vitro*, these parameters are influenced by hemodynamics as well as the “intruder system” (biomaterial) properties. There is a complex tripartite interaction between immune system, biomaterial and hemodynamics that often results in device related complications. Therefore, it is important for the transport phenomenon of *in vitro* model design to mimic physiological conditions. Similarly, for *in vitro* investigations to mimic physiological interactions with biomaterials *in vivo*, it is necessary to mimic the biochemical environment by using whole blood. Hence, the important parameters for each of these systems need to be clearly defined.

### **2.2.1 The immune system**

The immune system is a defense system protecting the host against microbial invasion or infection. It is composed of various elements at several levels of organizational complexity; from molecules to organs. The immune system is generally divided into three response mechanisms; the anatomical, innate and the adaptive response mechanisms or systems [63]. All the immune response mechanisms have their level of complexity and sophistication. The anatomical mechanism, which forms the body’s first line of defense, has some of the basic response mechanisms, which is simply to form a barrier. In medical device implant procedures, there are established methods to overcome or bypass this first line of defense. Therefore, this mechanism is not discussed in this work because this research deals with system responses after the medical device is implanted. In any case, complications that occur at this level of defense would trigger the subsequent levels of defense.

The innate and adaptive systems can in reality be regarded as a system of systems, but for simplicity, the word system will generally be used with understanding based on the context. Only where it is necessary to make a distinction will subsystem be used. There are similarities between the two systems in terms of functional purpose, i.e. recognition and elimination of infecting agents. However, there are distinct differences that are pertinent to their functional roles: the innate system has broad specificity in that it can immediately recognize self from non-self (‘what’) but has no memory of ‘who’ it encountered, and for that reason is sometimes thought to lack specificity [63, 64]. On the other hand, the adaptive system has fine antigen specificity for not only the ‘what’ but has memory of ‘who’ it encountered. It should be clarified here that as will be discussed in subsequent sections, the innate system does have some level of sophisticated specificity as well, albeit without memory, because of its receptor-ligand specificity. Hence the innate system responds rapidly during

the acute phase of injury or implanting of any foreign material and the adaptive is only activated in the chronic phase. Although the two mechanisms overlap through antigen-presenting cells such as dendritic cells and macrophages during the transition from acute to chronic phase, they can be compartmentalized and investigated independently. Therefore, only the innate system is relevant in the acute phase of blood-biomaterial studies.

At the core of the innate immune system is the ability to recognize foreign material, such as microbial agents. This is achieved through two recognition strategies; pattern recognition of conserved molecules on the microbial surface and the recognition of ‘missing’ molecules. Thus, molecules come in two forms; the conserved molecules are called pathogen-associated molecular patterns (PAMPs) and the missing molecules that are released from damaged or stressed cells, which are called danger/damage-associated molecular patterns (DAMPs). The recognition of pathogens, with or without conserved molecular patterns, is achieved through a variety of distinct host proteins called pattern recognition receptors (PRRs) [65, 66]. PRRs are distributed on the cell membrane surface as well as inside the cell, which enables targeting both extracellular (e.g. bacterial recognition) and intracellular pathogens (e.g. viral nucleic acids recognition) [2]. The main PRRs in innate immunity are the toll-like receptors (TLRs) [67]. TLRs occur on the cell surface as well as intracellular endosomes/lysosomes [66]. In general, microbial PRRs can be divided into three types; cytosolic/intracellular type, which include the retinoic acid-inducible gene I-like receptors (RLRs) and the nucleotide-binding oligomerization domain (NOD) and leucine-rich repeat-containing receptors (NLRs), soluble/secreted type, which include collectins and pentraxins, and transmembrane type (cell surface and endosomal/lysosomal), which include TLRs and C-type lectins [2, 68]. Figure 2-1 is a schematic depicting the PRRs and their effects.

Pattern recognition receptors that are of particular interest to this research are the pentraxins, collectins mannose binding lectins (MBL) and the TLRs because they form part of the innate immune system mechanisms. The MBL forms one of the plasma complement protein activation pathways, which are a component of the innate immune response called humoral response mechanism. TLRs occur on leukocytes, which form the second innate immune response called the cellular response mechanism. The humoral and cellular response mechanisms/system work in tandem with the hemostatic system in inflammation, coagulation and thrombosis, as described in subsequent sections. The interaction and crosstalk between these systems is well recognized. While inflammatory response prepares the stage for coagulation, they are intertwined processes as some of the inflammatory

response continues during coagulation, especially where there is infection. Hence, the two processes are discussed together, although the emphasis in this research is on coagulation and thrombogenicity, and any distinction should be understood from the text or specific sections.

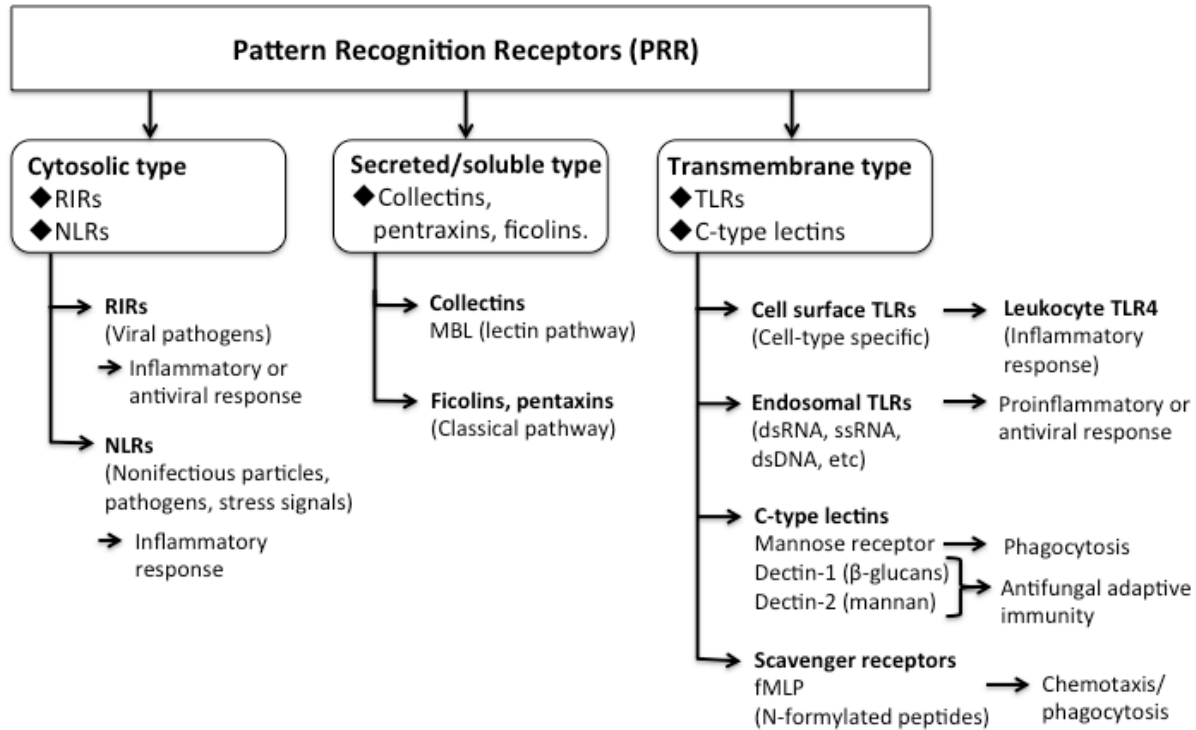


**Figure 2-1. Schematic of pattern recognition receptor types**

This section examines and further investigates some of the pertinent issues that arise from the crosstalk and interaction between elements of the immune system in the presence of metallic biomaterials, under flow conditions. Although it is known that the innate immune system response is based on the intensity of the intruder signal as well as the identity in some cases, where there is ligand-receptor specificity, the response is generally nonspecific, in the form of inflammatory mediators. There is an interesting question of whether the stimulus sensing mechanism has the ability to decompose the signal into other dimensions to facilitate response and determine the level of each inflammatory mediator. In this research, each system is examined and important questions that arise from a systems view are highlighted and where possible postulations are made.

### 2.2.1.1 Complement system

The complement system, which is made up of 32 proteins (plasma and membrane-bound) [2], is the backbone of the humoral innate system response mechanism, which plays an important role in health and disease states [69, 70]. It is always in an active surveillance state for any microorganism or foreign bodies. Consequently, complement proteins are immediately activated by the presence of microorganisms and/or implants through pattern recognition receptors, such as the mannose binding lectins or implant surface-bound proteins, such as immunoglobulin IgG. The complement system is composed of plasma proteins C1 up to C9 and regulatory proteins that mediate the various functions of activated complement fragments [2]. Complement system proteins occur at various physiological concentrations. The serum concentrations of the main proteins are presented in Table 2-2. The active enzymes are as described below in the system activation.

**Table 2-2. Physiological concentrations of the main complement proteins, adapted from [58].**

Protein	Serum concentration (mg/ml)	Estimated molecular weight (kDa)	Active enzyme
C1 (C1q, C1r, C1s)	(0.05-0.1, 0.035-0.04, 0.032-0.04)	(459, 83, 83)	C1r, C1s
C2	20-35	108	C2a
C3	1.5-1.7	185	C3bBb, C3b <sub>2</sub> Bb, C4b2a3b
C4	0.3-0.6	200	C4b2a
C5	0.12-0.18	185	

The complement system is activated through three main pathways: classical pathway (CP), lectin pathway (LP) and alternative pathway (AP), which all converge at a common point by formation of C3 convertase, which amplifies complement activation. The activation of fluid phase or surface-bound complement proteins occurs through a cascade of proteolytic cleavage of complement components and results in the generation of biochemically active complement fragments which

perform three main functions; inflammation (C3a, C4a and C5a anaphylatoxins), opsonization tagging (C4b and C3b opsonins) and membrane attack (terminal complement complex, MAC C5b-9), Figure 2-2.

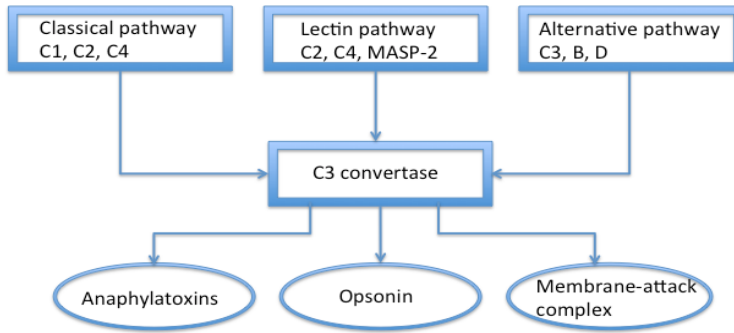


**Figure 2-2. Schematic of the conventional complement activation cascade, adapted from [2].**

The detailed conventional complement cascade is depicted in Figure 2-3. In the classical pathway (CP), complement C1 is activated by its component C1q directly binding to pathogen surface, e.g. CRP, apoptotic cells or indirectly binding to surface-bound antibodies, predominantly the immunoglobulins IgM and IgG [2]. This results in the activation of C1r, which activates C1s. Activated C1s then cleaves C4 to release anaphylatoxin C4a and surface bound C4b. C4b binds C2, which in turn is cleaved by C1s to release C2b and form the CP C3 convertase, C4b2a. In the lectin pathway, MBL is structurally similar to C1q and the mannose-binding-lectin-associated serine protease (MASP-2) enzyme plays the same activation pathway as the C1s in the classical pathway. Hence, the end result is the LP C3 convertase, C4b2a.

For the alternative pathway, which accounts for about 80-90% of complement activation [69], the key complement protein is C3. C3 is the most abundant as well as structurally and functionally diverse protein [2], which as described above, also plays a central role in all the three complement activation pathways. The spontaneously hydrolyzed complement component C3, C3(H<sub>2</sub>O), binds factor B, which is cleaved by the always active state factor D to form soluble C3 convertase, C3bBb. This then activates C3 into the soluble C3a and surface-bound C3b fragments. While C3a (9 kDa) is an anaphylatoxin that plays a role in leukocyte chemotaxis, C3b (176 kDa) is a short lived fragment with half-life ≈90-100 μs [71, 72] that has multiple binding sites [2, 71] and covalently binds to

surfaces [73]. Its half-life is increased 10-fold by binding to properdin [70]. It is then either inactivated by factor I to form the immobilized opsonin iC3b and other fragments (e.g. C3c, C3dg) or binds to factor B, subsequently cleaved by factor D, to form the potent surface bound C3 convertase.

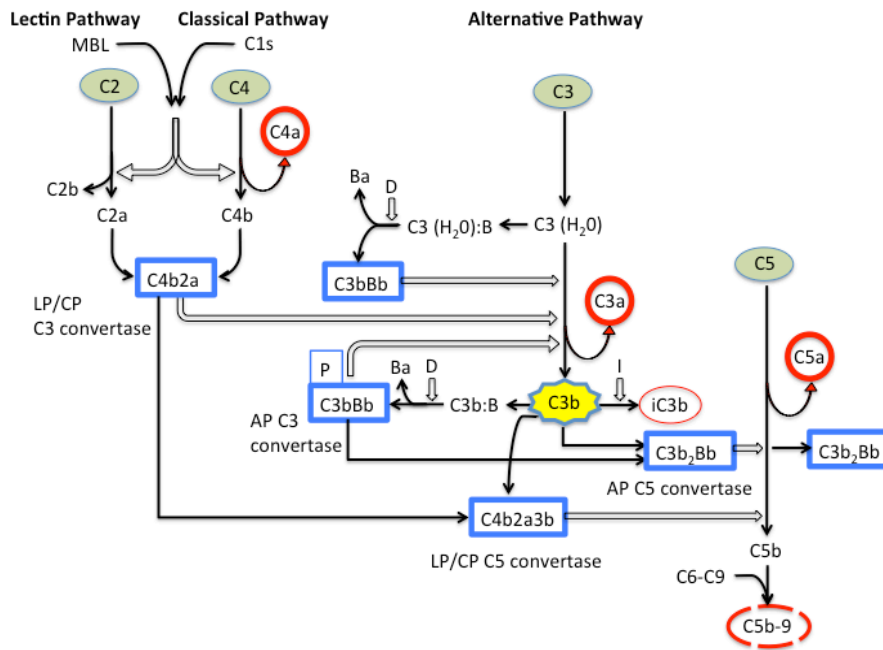


**Figure 2-3. Detailed schematic of the conventional complement cascade.** Rectangles indicate enzymes, red circles indicate anaphylatoxins, green ellipses indicate some of the main complement proteins, a red ellipse represents opsonin and a dashed red ellipse represents a membrane attach complex. The open arrows represent proteolytic activity.

The C3 convertase further cleaves C3 in a feedback loop, thus amplifying C3 activation. Additionally, C3 convertase also binds C3b to form C3b<sub>2</sub>Bb, C5 convertase. C5 convertase binds C5, which is then cleaved by the active site, Bb, to form the anaphylatoxin C5a and surface bound fragment C5b. C5b then binds C6 and other complement proteins C7, C8 and C9 bind to the C5b6 complex and go through conformational change that enables their hydrophobic sites to be inserted into the cell membrane, ending with the formation of a terminal complement complex (TCC), C5b-9, also called membrane attack complex (MAC). The end result of MAC is a 10 nm pore on the cell

surface [2], which compromises the cell membrane integrity. The MAC can also exist in a soluble form by binding of an S-protein through C5b-7 to form sC5b-9, which prevents surface binding.

While the above description forms the backbone of complement activation pathways, it only represents the classical or conventional view. Current knowledge suggests that the complement system is also activated through extrinsic pathways from the hemostatic as well the coagulation system. Platelets can activate the classical and alternative pathways [74] and thrombin and other factors of the coagulation cascade can cleave C3 and C5 [70, 75]. There is also evidence of other extrinsic pathways even in soft tissue [76]. Based on current knowledge, an updated representation of the complement cascade is presented on Figure 2-4.

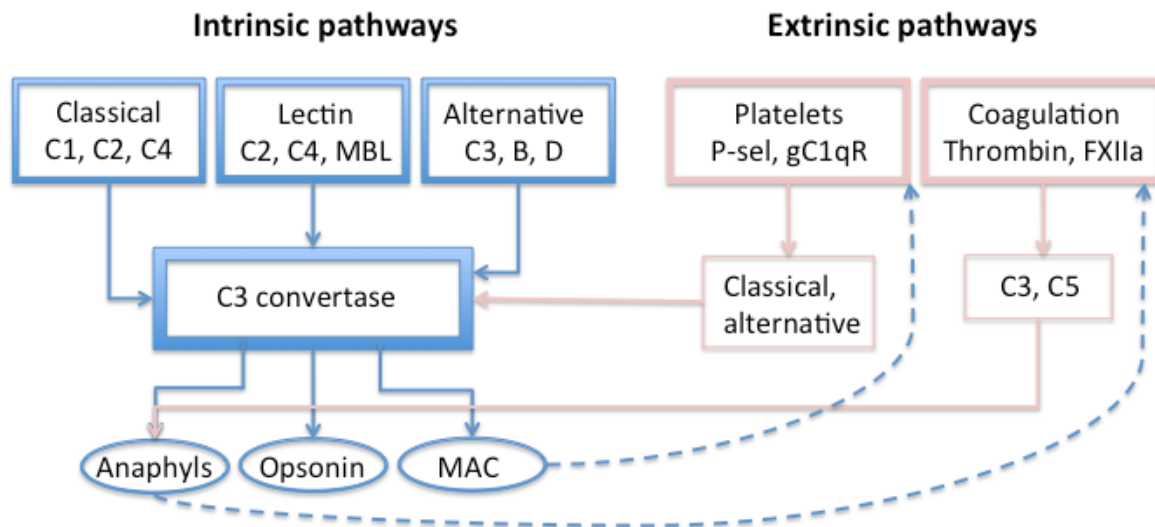


**Figure 2-4. Schematic of the updated complement activation cascade.** For simplicity no regulatory pathways are included; only the main activation feedback pathways (dashed lines) are shown. On the coagulation cascade there are many other factors involved, which include plasma kallikrein and factor Xa.

However, regardless of the activation pathway, there are three main functions that emanate from complement activation; inflammation, opsonization and cell lysis. In addition to these common functions, there has been evidence of a variety of other functions, including bridging the innate and adaptive immune systems [2], tissue remodeling and non-lytic complement C5b-9-mediated effects,

such as hemostasis (endothelial cell secretion of von Willebrand factor) [77] and platelet microparticle formation [78, 79]. Hence, complement proteins are an important component of the blood-biomaterial interaction system, *in vivo* and *in vitro*, and a complete investigation of MIT requires inclusion of complement activation. The broad variety of functions resulting from complement activation, as well as cell functions facilitated by complement fragments are depicted in a schematic in Figure 2-5.

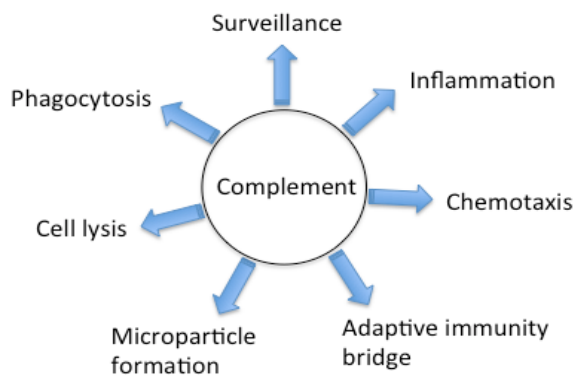


**Figure 2-5. Schematic of the functions of complement and complement-mediated cell functions**

#### 2.2.1.1.1 Complement-biomaterial interaction

In the presence of a biomaterial implant, the presence of water and other proteins in the plasma means complement competes with other proteins for specific interactions with cell receptors and non-specific interactions with a material surface. The arrival of proteins at the surface in a diffusion-limited case would depend on their diffusion coefficients and molecular weights. Some of the major proteins and their diffusion coefficients are listed on Table 2-3. Thus, based on simple diffusion-limited phenomenon, the arrival of the proteins at the implant surface will be in the order of first arrival; albumin>IgG>IgA>C3>fibrinogen [80]. In comparison, water has the highest diffusion coefficient at about  $4840 \times 10^{-7} \text{ cm}^2/\text{s}$ . Therefore, in reality water would appear ahead of albumin, giving the arrival sequence of water>albumin>IgG>IgA>C3>fibrinogen. However, under flow conditions, convective transport effects and lateral diffusion, influenced by the geometry of the conduit result in a much more complex phenomenon and these factors would have to be taken into account to develop a realistic interaction model. Due to water's volume effect, dynamic conditions

may have little influence on its arrival at the surface. More importantly, water molecules can easily dissociate into hydrogen and hydroxyl ions, which react with biomaterial surface molecules, raising important issues on surface hydration [81]. This makes water an important role player in blood-biomaterial interactions and therefore worthy of detailed investigation.

**Table 2-3. Diffusion coefficients of some major blood proteins.** Data adapted from [58, 80].

Protein	Concentration (mg/ml)	Molecular weight (kDa)	Diffusion coefficient ( $10^{-7}$ cm <sup>2</sup> /s)	Isoelectric point in neutral solution	Half-life (days)
Albumin	40-55	66-66.5	6.1	4.7-4.9	17-23
IgG	6.5-16.5	150	4.0	6.3-7.3	20-21
Fibrinogen	2.0-4.0	340	2	5.5-5.8	3.1-3.4
C3	1.5-1.7	180-185	4.5	6.1-6.8, 5.7 [71]	-
IgA	1.0-4.0	150-162	4	-	5.0-6.5

The arrival of proteins at the surface is not necessarily related to the participation of the protein in the formation of the biomaterial surface protein layer. The protein layer is determined predominantly by the protein and material characteristics, such as surface chemistry and surface charge. Hence, the isoelectric point has great significance because it is an indicator of the charge carried by the molecule in the blood. An isoelectric point is the pH at which the molecule carries no charge. At lower pH than its isoelectric point, the molecule becomes electropositive because of protonation (gain hydrogen atom) and at higher pH it becomes electronegative, because of deprotonation. Thus, at blood level pH ( $\approx 7.4$ ), the proteins will carry negative charge. This has great relevance to biochemical interactions of blood molecules with a biomaterial surface and hence will influence the protein function and participation in the formation of a protein layer on the biomaterial surface. Of particular interest are complement proteins, which although are influenced by a variety of material properties, have shown pH sensitive surface binding efficiency; increasing with decreasing pH [73] and C1 has affinity for negative surfaces [25].

At the biomaterial surface, complement is mostly activated through the alternative pathway although the other pathways also play an important role [7, 82, 83], such as the reported delay in the

alternative pathway related to lack of the classical pathway C4 [83]. When complement fragment C3b is bound to a foreign surface, it is stabilized by factor P (properdin) to ensure stability of C3 convertase [2, 71, 84]. The extent and pattern of complement activation is determined by biomaterial surface characteristics, such as size, chemistry and topography [25, 85]). The preference of C3 and C3b for hydroxylated surfaces [71], raise very interesting questions about complement interaction with TiO<sub>2</sub> since the presence of water forms hydroxyl groups on the titanium surface. Besides covalent bonding to hydroxyl groups, C3b can also form stable amide bonds with amino groups. Interestingly, C3b, which forms the basis for the alternative pathway C3 and C5 convertases, can adsorb on other surface bound proteins, except fibrinogen [83]. Although this suggests a competitive advantage in surface adsorption, some of the adsorbed proteins reduce complement activation [86]. Therefore, surface characteristics play an important role in influencing complement activation and adsorption.

The presence of surface-bound convertase facilitates localized amplification of complement activation, resulting in increased release of soluble leukocyte activating and recruiting anaphylatoxins C5a, C3a and C4a, in order of potency. Hence, C5a and C3a, which act through their specific G protein-coupled receptors, C5aR and C3aR, respectively, are the most important and the most investigated receptors [87]. They are of particular interest because of the linkage between inflammation and thrombosis. In addition, fragment iC3b acts as an opsonization agent, with the aid of antibody IgG binding to the FcγR (immunoglobulin receptor) on leukocytes. More importantly, in addition to leukocyte recruitment, biomaterial bound fragment iC3b is a ligand for leukocyte Mac-1 receptors, which facilitates leukocyte adhesion and possible localized oxidative stress, which can be detrimental to cell and tissue function. Indeed, fragments C3a and C5a have been associated with late lumen loss in drug-eluting stents [88]. Hence, complement inhibition has been investigated to reduce these effects and leukocyte activation.

It is important to note that the detrimental effects of activated complement are controlled by specific regulatory proteins that inhibit complement activation or formation of convertase. Complement C1 activation is inhibited by C1 inhibitor (C1INH), which binds C1r, C1s and activated MASP-2. Proteins that inhibit formation of C3 convertase include the decay-accelerating proteins (DAF) (displaces Bb or 2a from C3 convertase), factor H (displaces Bb) and complement receptor 1, CR1, (displaces 2a or C3b) [2]. There is also autologous cell protection from formation of MAP by

CD59 (protectin). Although these proteins are not discussed in this research, their role need to be recognized as they are equally important in regulating the cascade as well as the effector functions.

### 2.2.1.2 Leukocytes and the coagulation system

The leukocyte system is made up of a number of cell subpopulations; neutrophils, lymphocytes, monocytes, eosinophils and basophils. Leukocytes constitute only 0.1% of the blood cell volume, but they play various key roles in health and disease states. Leukocytes originate from the pluripotent hematopoietic stem cells of the bone marrow, with the common myeloid progenitor cell lineage [2]. They are already terminally differentiated when they are released into the peripheral blood circulation. Leukocytes have structural and biochemical similarities and differences. As a result they have some overlapping as well as specialized roles. Most of the leukocytes participate in the inflammatory response *in vivo* [54]. However, in subsequent coagulation and immune response to the presence of a biomaterial implant, monocytes and neutrophils are the main leukocytes known to play a significant role. Although eosinophils perform similar functions to neutrophils, they are small in number and so are not usually considered in blood-biomaterial studies. Hence, in this thesis, only neutrophils and monocytes are discussed. Some of the typical neutrophil and monocyte characteristics are depicted on Table 2-4. Although neutrophils and monocytes have some structural and biological similarities, they also have distinct differences, such as lifespan, both in circulation and in tissue, that are also reflected in their functions [67].

**Table 2-4. Neutrophil and monocyte characteristics.** Data adapted from [89].

	Geometry		Percentage of cell volume	
	Volume ( $\mu\text{m}^3$ )	Surface area ( $\mu\text{m}^2$ )	Granules	Mitochondria
<b>Neutrophils</b>	190	300	15.4%	0.6%
<b>Monocytes</b>	230	430	2.6%	3.5%

#### 2.2.1.2.1 Neutrophil structure and function

Neutrophils, also known as polymorphonuclear leukocytes (PMNs) because of their multilobe-shaped nuclei, are the most abundant cells of the leukocyte family, making up 60-70% of

the leukocyte population. They are formed in the bone marrow and released already terminally differentiated into peripheral blood circulation at a rate of about  $10^{11}$  cells per day [90], with a turnover of 6.6 days. Most of the produced neutrophils are held in the bone marrow and released into circulation on demand, such as during inflammation, but their homeostasis level is predominantly regulated by the granulocyte colony-stimulating factor (G-CSF) [91]. In mice only about 1% of PMNs are in circulation at any point in time [91]. Their lifespan *in vivo* is dependent on their location as well as the state of health and disease. In blood their lifespan is 4-8 hours and in tissue it is 4-5 days, but shorter in disease conditions [54]. However, it has been suggested that their lifespan may be extended by TLR4 stimulation and the presence of monocytes [92].

Under physiological conditions, quiescent circulating neutrophils are spherical with randomly shaped and distributed surface membrane folds and microvilli [93]. The height of the membrane folds is estimated at about 0.2  $\mu\text{m}$  [94]. The pleated membrane surface can unfold when the cell is stimulated to allow shape change and increase the surface area [93]. Leukocyte cell membranes constitutively express a variety of cell receptors that assist with the initial sensing of the environment and initial cell adhesion. P-selectin glycoprotein ligand 1 (PSGL-1) receptor, which is important for leukocyte arrest under shear [95-98], is expressed on the leukocyte microvilli at a density of  $10^4$  molecules/cell [99]. Also co-expressed on microvilli is L-selectin, which mediates surface scanning and secondary leukocyte arrest [97, 98, 100]. PMNs also express an integrin family of receptors, which stabilize adhesion interactions, such as the multifunctional Mac-1 [101]. Mac-1 is predominantly stored in the intracellular granules in quiescent PMNs and is translocated to the surface upon activation [102]. Other constitutively expressed receptors that assist with the initial cell response and function are called pattern recognition receptors. There are several pattern recognition receptors [65], but the most important receptors for this research are the toll-like-receptors (TLRs) and the complement receptors. TLRs, which are expressed predominantly on monocytes compared to neutrophils, are the main pattern recognition receptors in innate immunity [67]. There are nine human TLRs, but only TLR4 is of particular interest because in association with the co-receptor CD14, it is a receptor for the conserved bacterial gram-negative lipopolysaccharide (LPS), which is commonly encountered on biomaterial surfaces [103-105]. TLR-4 signals through the two independent TLR adaptor proteins, MyD88 (myeloid differentiation primary-response gene 88) and TRIF (Toll/IL-1R domain containing adapter protein-inducing interferon- $\beta$ ), with downstream activation of transcription factors NF- $\kappa$ B or the interferon response factors (IRFs) [2]. Activation of NF- $\kappa$ B

pathway results in an inflammatory response (production of pro-inflammatory cytokines) and can also activate adaptive immune responses [66]. On the other hand, activation of IRFs results in an antiviral response (production of interferon IFN  $\alpha/\beta$ ). Therefore, the NF- $\kappa$ B pathway is of particular interest in biomaterial studies because it is also the pathway for leukocyte tissue factor expression [106].

Besides pattern recognition, TLRs fall into a class of receptors called chemotactic receptors [92], together with receptors for platelet activating factor (PAF) and N-formyl peptide. The formyl peptide receptor (FPR), which has the tripeptide formyl-methionyl-leucyl-phenylalanine (fMLP) as its ligand, is one of the important leukocyte receptors because its intracellular signal is transduced through cytoskeletal actin microfilaments. fMLP is an effective chemotactic and greatly influences leukocyte function. There are also constitutively expressed complement receptors, C3aR, C4aR and C5aR, which are expressed on most leukocytes [107, 108]. Neutrophils express approximately 3100 C3aR and 63500 C5aR molecules/cell [108]. These receptors are signaling receptors, which induce a variety of functions other than inflammation, such as chemotaxis; an important leukocyte function that enables the cells to emigrate from circulation through the vascular wall into tissue (leukocyte extravasation) as a response to inflammation. Leukocyte extravasation predominantly occurs in venules [97], where shear stress is very low, although mechanisms that facilitate rolling and arrest at high shear have been recently highlighted [98]. After fulfilling their function in tissue, neutrophils are eliminated by apoptosis.

Neutrophil functional capabilities are also dictated by their intracellular biology. Inside the neutrophil cytoplasm, like all eukaryotic cells, is a cytoskeleton formed from abundant actin microfilaments, microtubules and intermediate elements [109, 110]. The cytoskeleton provides a signal transduction pathway for the chemical and shear sensitive G-protein-coupled receptor, FPR. Actin filaments and other cytoskeletal elements form an intracellular calcium dependent contractile mechanism that can be dynamically rearranged (expand and retract) in response to environmental chemical or mechanical (shear) conditions. The cytoskeletal rearrangement results in the rapid formation of pseudopods and lamellipods that induce change in morphology and confer leukocyte function to neutrophil [111]. Consequently, neutrophils have the capacity to rapidly respond and migrate to inflammatory sites where they can release inflammatory mediators, release oxygen radicals or engulf microorganisms (phagocytosis). Some of the important inflammatory mediators are the neutrophil extracellular trap (NETs) because of their possible role in mediating thrombosis [112, 113]. Phagocytosis is one of neutrophils main functions stimulated by chemotactic agents, such as

complement iC3b fragment. During chemotaxis, PMNs exhibit an asymmetric and directional cellular motility [114, 115], facilitated by intracellular calcium-dependent rearrangement of their abundant contractile proteins in the cytoskeleton [115]. Neutrophils also contain abundant granules in their cytoplasm, which contain lysozymes. During phagocytosis, neutrophils degranulate and release the enzymes to digest foreign materials, simultaneously releasing oxygen radicals through respiratory burst. This two-pronged process neutralizes any foreign material that cannot be digested by the lysozymes.

There are possible side effects that may occur while neutrophils perform their functions. Side effects include tissue damage from respiratory burst, which could trigger a further inflammatory response [116-118]. One mechanism of inflammation regulation by neutrophils is through production of anti-inflammatory cytokine, interleukin-10 (IL-10) [119, 120]. Another mechanism that controls inflammation is the PMN programmed cell death (apoptosis), which is followed by phagocytosis from macrophages, as cell membrane fragments could trigger coagulation [121]. The respiratory burst is also to some extent self-regulating because of the limited capacity of oxygen-dependent energy production. Neutrophils produce their energy primarily through anaerobic glycolysis [122] because they have few mitochondria compared to monocytes [93, 123] and hence the limited amount of oxygen used for respiratory burst. Their mitochondria seem to play a bigger role in apoptosis [123] and regulation of glycolysis. Thus, neutrophils have a broad range of functions, both at the biochemical as well as the cellular level. The broad range of functions are depicted on Figure 2-6.

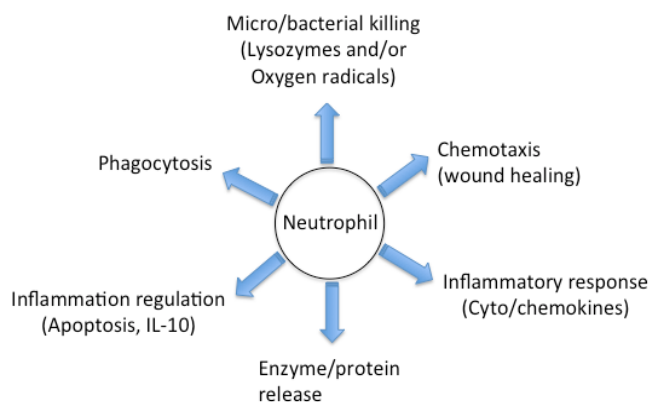


**Figure 2-6. Illustration of neutrophil functions**

#### 2.2.1.2.2 Monocyte structure and function

Monocytes are formed in the bone marrow, from the same myeloid progenitor lineage as neutrophils. Monocytes are larger than the other leukocytes. They constitute 3-8% of the leukocyte population and have a lifespan of 10-20 hours in blood [54]. Some of the monocytes in circulation extravasate through the vascular walls into tissue and become macrophages, which have a longer lifespan of several months. Macrophages may subsequently merge to form large and more aggressive foreign body giant cells, which have a lifespan of days [54].

Similar to PMNs, under quiescent physiological conditions, circulating monocytes are spherical with randomly shaped and distributed surface membrane folds and microvilli. Monocytes express the same family of selectins and integrin receptors. In monocytes, Mac-1 is translocated from intracellular vesicles to the surface upon activation [124]. Similarly, monocytes constitutively express the same pattern recognition receptors as PMNs although the surface expression density may vary. Monocytes express more TLR2 and TLR4 than PMNs [125]. Monocytes also express on average 2-fold more C3aR and 2-fold less C5aR than PMNs; 6000 C3aR and 34100 C5aR molecules/monocyte [108]. In the cytosol, monocytes have abundant intracellular cytoskeleton similar to PMNs, which facilitates similar functions as described for PMNs. However, unlike PMNs, they do not possess the same number of granules and hence do not possess the same phagocytotic capacity as PMNs. Their phagocytotic capacity is enhanced after they differentiate into macrophages.

Although some monocytes functions are generally similar to PMNs, such as production of pro/anti-inflammatory agents and physical participation in thrombus formation, one function where they play a distinct role is the tissue factor-dependent coagulation, especially LPS-induced tissue factor. Monocytes are recognized as the main leukocyte source of tissue factor (TF). It should however be noted that there is evidence that neutrophils are also indirectly involved in facilitating TF-dependent coagulation/thrombosis by cleaving tissue factor pathway inhibitor [126]. TF can be induced by a variety of stimulants under both *in vitro* and *in vivo* conditions [127-134]. One of the known TF regulating agonists is LPS, which has been shown to regulate TF expression at both the transcription and posttranscription levels on monocytes [135]. TF is induced through a number of pathways. LPS induces TF expression on monocytes through three MAPK pathways [24, 136], which can be inhibited by the PI3K/Akt signaling pathway [24, 136]. LPS is a ligand for TLR4 (and co-recognition of CD14), which signals through the NF- $\kappa$ B pathway [63]. This provides another TF expression mechanism as the NF- $\kappa$ B pathway has been implicated in TF expression. There has also been evidence of intracellular localization of TF in whole blood monocytes [137]. The significance of

this in biomaterial-induced thrombosis is not clear. The broad functions of monocytes are depicted on Figure 2-7. Since TF-dependent coagulation cascade is important in thrombosis, it is appropriate to discuss coagulation in more detail.

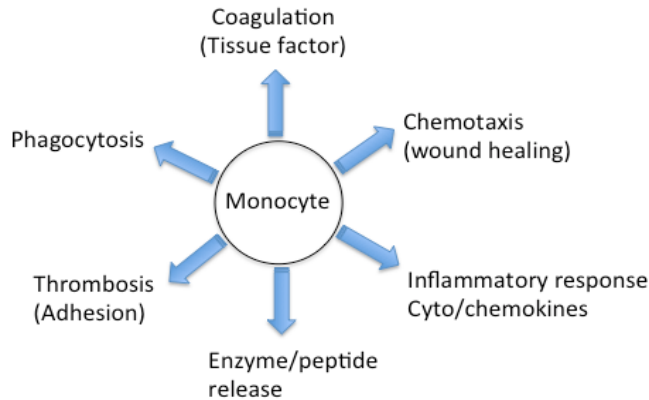


**Figure 2-7. Illustration of monocyte functions**

Coagulation is a complex biochemical process that involves cellular and plasma protein components to form a blood clot. It is characterized by a cascade of proteolytic activation of clotting factors, with amplifying pathways, which result in the formation of fibrin and activation of platelets. It is activated following an inflammatory response to vascular endothelial wall injury or response to a foreign body, such as an implant. In vascular wall injury, coagulation prevents blood loss by forming a hemostatic plug. In response to an implant, coagulation results in encapsulating the implant. However, if the implant is in a blood vessel lumen, such as a stent, blood coagulation may subsequently result in thrombosis, with undesirable consequences as discussed above. Regardless of the trigger mechanism, the coagulation cascade involves two pathways, the intrinsic and extrinsic pathways, Figure 2-8. As depicted in Figure 2-8, these pathways function in collaboration with other systems as previously described. The extent of involvement of each pathway in triggering coagulation may depend on the stimulus.

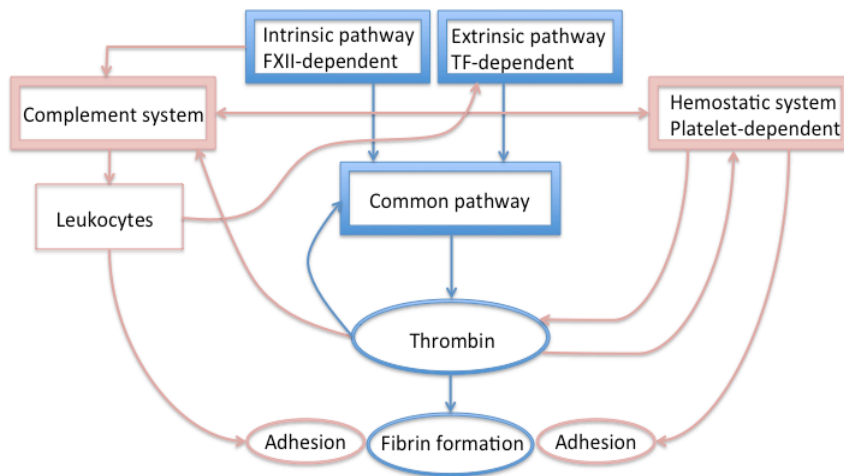


**Figure 2-8. Block schematic of the coagulation cascade.** The intrinsic and extrinsic pathways form the core of the classical coagulation system. Interaction with other systems is depicted but for simplicity the regulatory pathways are not included.

In the case of biomaterial implant, coagulation involves the two pathways. The intrinsic pathway, also called the contact activation pathway, forms the backbone of the contact system, section 2.2.2. The extrinsic pathway is composed of the tissue factor-dependent pathway. Tissue factor is a 45 kDa glycoprotein member of the class-2 cytokine family of receptors, well recognized as the blood coagulation initiator *in vivo* [24]. It is a transmembrane receptor, constitutively expressed in some cells, such as vascular smooth muscle cells and adventitial fibroblasts [24]. The constitutive expression of TF in the vascular adventitia facilitates its ability to initiate blood coagulation *in vivo* since it can be immediately exposed to blood proteins. In addition, in lung derived fibroblasts 75% of the synthesized TF is stored in Golgi and transported to the surface after surface TF complexes with FVIIa [138], suggesting that additional TF may be immediately sequestered in these cells.

Tissue factor is only expressed on endothelial cells, monocytes and macrophages [24], platelets [139] and PMNs [140, 141], when the cells are activated. It is also found in circulation on microparticles or as a soluble variant [142]. The issue of TF expression on platelets continues to be unresolved as some studies have shown platelet expression while others have shown surface expression after surface attachment of microparticles from other cells [143]. There has also been controversy on PMN TF expression [113]. The issue of TF expression on blood cells has been previously reviewed [144]. Thus, only monocytes and microparticle derived TF are undisputedly recognized as the main sources of TF in material-induced thrombosis. The TF-dependent cascade,

involves a number of proteins, Table 2-5. Most of the proteins form pathways common to the contact system, which is discussed in section 2.2.2.

**Table 2-5. Some coagulation cascade proteins.** Data adapted from [58, 145].

Protein	Plasma concentration	Estimated molecular weight (kDa)	Protein half-life (hours)	Active enzyme complex	Fold activity increase
Tissue factor	-	43-53	-	-	-
Prothrombin	1.1 $\mu$ M	72	48-72	-	-
Factor V	7 $\mu$ g/ml	>300	12-15	-	-
Factor VII	0.5 $\mu$ g/ml	50	2-5	TF.FVIIa.Ca <sup>2+</sup> .PL	57,000 [146]
Factor VIII	0.5 nM	>250	8-17	-	-
Factor IX	3-5 $\mu$ g/ml	55-57	24	FIXa.FVIIIa.Ca <sup>2+</sup> .PL	200,000 [147]
Factor X	10 $\mu$ g/ml	59 dimer	24-40	FXa.FVa.Ca <sup>2+</sup> .PL	500,000 [148]
Factor XIII	70 nM	320	216-240	FXIIIa.Ca <sup>2+</sup>	-
Fibrinogen	6-13 $\mu$ M	340	72-120	-	-

The detailed tissue factor dependent cascade is depicted on Figure 2-9. The intrinsic pathway is included for completeness as it is covered in section 2.2.2. Tissue factor has high Ca<sup>2+</sup>-dependent binding affinity to its cofactor, the vitamin K-dependent factor VII or its activated form (FVIIa), with dissociation constant  $K_d < 10$  pM [149]. Factor VII cleavage by FXa produces FVIIa, an enzyme with Ca<sup>2+</sup>-dependent affinity to phospholipids (PL). Upon binding to phospholipids, FVIIa goes through conformational change, which exposes epitopes that enable binding with TF [150]. The enzymatic function of FVIIa, a stable protein with half-life of 2.5 hours [151], has little dependence on phospholipid binding, but is activated by forming a complex with TF [152]. In the presence of calcium ions, the complex {TF.FVIIa.Ca<sup>2+</sup>.PL} has affinity for FIX, which when bound is cleaved to form FIXa. Cleavage of FIX to FIXa is also produced by FXIa from the contact system (section 2.2.2), from where the two systems have a common pathway. Factor IXa then forms a complex with FVIIIa (described below). In addition, the {TF.FVIIa.Ca<sup>2+</sup>.PL} complex also cleaves fluid FX to FXa. In this reaction, the phospholipid has an important role because it decreases the Michaelis constant

$K_m$  for FXa and thus increases the catalytic constant  $K_{cal}$  ( $K_{cal}=V_{max}/K_m$ ) [145]. FXa forms a prothrombinase complex with FVa, which rapidly activates prothrombin to thrombin.

Thrombin then cleaves fibrinogen to form fibrin, which forms the base membrane for thrombus formation. The developing thrombus is stabilized by the cross-linking of fibrin by FXIIIa. Therefore, FXIIIa may play a big role in thrombus growth [153], which may need closer examination. Thrombin is also a potent agonist for platelets. Hence it activates platelets and in a cyclic feedback amplifies some of the clotting factors. Activated platelets adhere to fibrin and conformational changed fibrinogen. Fibrinogen conformation change or structural unfolding occurs upon surface contact and adsorption [154-158], which results in the dissociation or opening of the  $\alpha C$  regions of its molecule [157], and subsequently exposes binding epitopes that are normally hidden [155, 156, 159]. Conformationally changed fibrinogen also offers similar binding epitopes to fibrin, which also bind leukocytes [160]. Hence, the TF expression initiates a TF-dependent blood clot formation, which without platelets will just be a fibrin mesh, with leukocytes and trapped RBC. Leukocytes have been found to form 16% of a blood clot [161]. Thus, they play an important role in initiation of TF-dependent thrombosis. In addition, monocyte-derived microparticles expressing TF seem to predominantly trigger thrombin formation in a TF-dependent pathway while platelet microparticles seem to trigger thrombin generation in a FXII-dependent pathway [162]. This may also provide a mechanism for propagation.

Besides extracellular effects of coagulation, the TF/FVIIa complex also possesses intracellular effects (signal transduction) through the G-protein coupled protease-activated receptor, PAR2 receptor [131]. This provides diverse roles, including inflammation, cancer progression and angiogenesis, which have been a subject of several reviews [163-165].

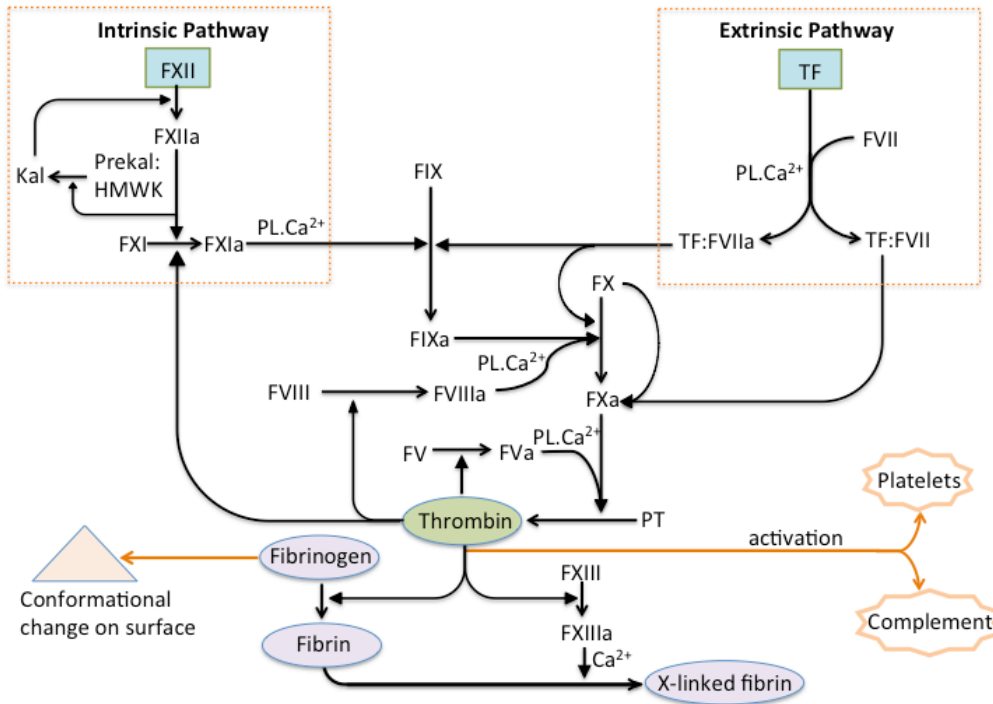


**Figure 2-9. Schematic of the coagulation cascade.** The pathways boxed with dashed lines represent the coagulation initiating process and the unboxed pathways are common pathways, which represent the propagation and amplification processes. For simplicity inhibitory pathways are not included. HMWK: high molecular weight kininogen, Prekal: pre-kallikrein, Kal: kallikrein, PL: phospholipid, PT: prothrombin.

While there are known inhibitory pathways, both at the cellular and molecular levels, to stop pathologic propagation of the clot, pathologic thrombotic conditions do occur in the presence of biomaterials. Mechanisms that regulate these pathways in the presence of biomaterials under flow conditions are not well understood. To develop intervention methods or novel biomaterials, it is necessary to understand the influence of biomaterial-blood-flow interactions on coagulation pathways.

#### 2.2.1.2.3 Effect of flow on leukocytes

Mechanical fluid shear stress/rate generally activates leukocytes resulting in the upregulation of surface receptors, such as Mac-1 and TF. However, there is evidence that at high shear rates leukocyte sensitivity to shear is reduced by internalization of the leukocyte mechanosensor, formyl

peptide receptor (FPR), and retraction of pseudopod [94, 166], which has also been shown in a rat model [167]. Shear stress has also been shown to inactivate the integrin  $\alpha_M\beta_2$  [166]. Recent studies have also shown Mac-1 down-regulation under high shear [168]. It is not clear what other factors influence the point at which leukocytes sensitivity to shear is reduced. Also the general implications of these observations are not clear on other receptors, such as TF, or on leukocyte material interaction under shear. As for leukocyte adhesion, generally high shear seems to reduce adhesion. However, there have also been conflicting reports, which may be partly attributed to experimental conditions, as highlighted by Gorbet, et al [169]. Further investigations are necessary to clarify the effect of shear rate on leukocyte activation.

#### 2.2.1.2.4 Leukocyte-biomaterial interaction

Biomaterial surface properties can activate leukocytes to express both TF [170] and Mac-1 [171], which are important receptors for coagulation and adhesion/aggregation [172], respectively. For that reason, they play an important role in material-induced thrombosis, as previously highlighted [7]. Material-dependent leukocyte activation is mediated by recognition molecules, such as complement proteins. The level of complement activation and hence, leukocyte recruitment and activation, depends on biomaterial surface characteristics. Complement anaphylatoxin C5a plays a double role in enhancing inflammatory response in a material-dependent manner. C5a induces both Mac-1 and TF expression on neutrophils [173], even though the two proteins are expressed through different mechanisms. While Mac-1 is translocated from cell vesicles, TF expression follows gene transcription and translation [135]. It is interesting to note that surface properties, such as chemistry, have been found to not only influence the overall cell receptor expression, but also influenced specific coagulation pathways such as the preference of the intrinsic (FXIIa-dependent contact system) over the extrinsic (TF/FVIIa-dependent) pathway [170]. Thus, in investigating leukocyte activation, it is important to note that the coagulation initiating pathway may not be reflected merely from the cell receptor expression.

Activated leukocytes physically interact with a biomaterial surface through surface adsorbed proteins, predominantly complement fragment iC3b and fibrinogen. As previously described, complement fragment iC3b is a surface-bound ligand for Mac-1 receptors and therefore facilitates leukocyte adhesion. Similarly, surface adsorbed fibrinogen conformational change exposes its hydrophobic D domain binding peptide sequences P1 ( $\gamma$ 190-202) and P2 ( $\gamma$ 377-395) [160], which have affinity for integrins, such as Mac-1 receptors. The P1 and P2 peptide sequences also exist on

fibrin, facilitating leukocyte adhesion to fibrin. The ability of proteins to adsorb varies, not only with the biomaterial, but with each protein's intrinsic and extrinsic properties, bulk concentration [174], molecular weight, structure and conformational stability [174, 175].

The primary material characteristics that influence protein conformational change and adsorption are surface chemistry [174], surface energy and surface electrostatics/charge [176]. The secondary material properties are roughness and topography, and geometry. Thus, material characteristics influence the pattern or selective expression of absorbed protein epitopes, e.g. RGDS sequence on fibrinogen [155], the rate of structural transition, e.g. different polymeric materials induce different structural transition rates [177] and the extent of binding sequence exposure [160]. Both the rate of protein structural transition and the extent of binding sequence exposure have implications for the accumulation of leukocytes, which have an equally important role as platelets in material-induced thrombosis [178]. While the extent of sequence exposure will influence the extent of aggregation and thrombus formation, the rate of leukocyte accumulation may be particularly important in determining the fate of the thrombus. It remains unclear whether the accumulation rate has any effect on the stability of the thrombus or on the localized detrimental effects of oxidative stress.

Therefore, the effect of material characteristics on the rate of protein structural transition – leukocyte accumulation rate – may need closer scrutiny. This is important not only for *in vivo*, but also for *in vitro* conditions. Besides the need to understand its effect on thrombus, the effect on *in vitro* investigation results are crucial. If the investigation is terminated before transition is complete, the rate will influence the interpretation and extrapolation of experiment results. Hence, this is a critical issue that needs to be determined for *in vitro* models.

### **2.2.2 Contact system**

The contact system is a component of the coagulation system and is composed of four main proteins; factor XI (FXI), factor XII (FXII), plasma pre-kallikrein and high molecular weight kininogen (HMW kininogen or HMWK), Table 2-6. While the rest of the proteins are zymogens (inactive form of enzymes) for active enzymes, only HMWK is a non-zymogen. HMWK is a co-factor for pre-kallikrein and FXI zymogens and their respective enzymes, with dissociation constants of  $K_d=15\text{nM}$  [179] and  $K_d=32\text{nM}$  [180], respectively. Besides existing as a co-factor, HMWK facilitates binding of the complex to negatively charged surfaces, such as phospholipids. Factor XII/XIIa on the other hand can bind directly to negatively charged surfaces. The binding of the

proteins to the surface facilitates the surface-initiated and propagated coagulation process. Thus, limiting coagulation in the fluid phase.

**Table 2-6. Contact system proteins, adapted from [58, 145].**

Protein	Plasma concentration	Estimated molecular weight (kDa)	Active enzyme	Protein half-life (hours)
Factor XI	6µg/ml (≈35 nM)	150 dimer	FXIa (SP)	48-84
Factor XII	40µg/ml (≈500 nM)	80	FXIIa (SP)	50-60
Pre-kallikrein	40µg/ml (≈500 nM)	85-88	Kallikrein (SP)	-
HMW-kininogen	70-90µg/ml (≈1 µM)	110	Co-factor	-

SP: serine protease

The contact system interaction and activation pathways are depicted on Figure 2-10. Generally it is accepted that FXII plays a central role in the contact system. When FXII is activated, either auto-catalytically or through conformational changes after surface binding, it forms the  $\alpha$ FXIIa (80 kDa) and  $\beta$ FXIIa (28 kDa) isoforms. The  $\alpha$ FXIIa, which consists of disulfide-linked light and heavy chains, remains surface bound because of the heavy chain affinity to negatively charged surfaces.  $\alpha$ FXIIa then acts through two main pathways; the pre-kallikrein and the FXI pathways. In the former pathway,  $\alpha$ FXIIa cleaves plasma pre-kallikrein to plasma kallikrein, which in turn amplifies FXIIa by cleaving FXII or converts  $\alpha$ FXIIa to  $\beta$ FXIIa. Kallikrein also cleaves HMWK to release bradykinin (an inflammatory mediator) and reorganizes HMWK, which has higher affinity for negatively charged surfaces. In the FXI pathway,  $\alpha$ FXIIa cleaves FXI to FXIa, the main effecting enzyme in coagulation, which activates factor IX of the common pathway with TF-FVIIa, resulting in the production of prothrombinase and subsequently thrombin. The contact system is regulated in part by C1-inhibitor, which inhibits FXIIa.

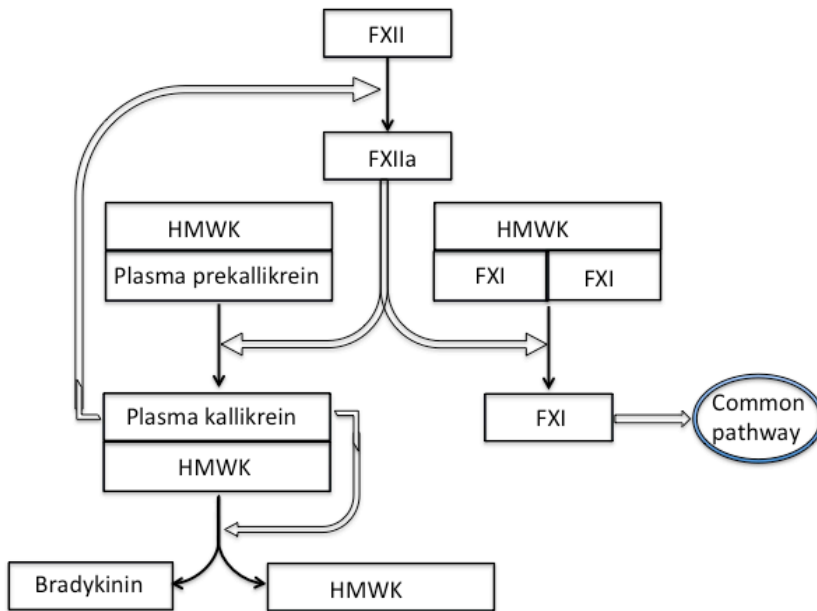


**Figure 2-10. Schematic of the contact system pathway.** Open arrows represent catalytic activity.

### 2.2.2.1 The common pathway

Although the released FXIa is an enzyme, in the presence of  $\text{Ca}^{2+}$ , its catalytic activity increases 2000-fold [145]. The  $\{\text{FXI}.\text{Ca}^{2+}\}$  enzyme cleaves FIX (the same bonds as TF-dependent enzyme) to FIXa. FIX and FIXa have  $\text{Ca}^{2+}$ -dependent affinity to negatively charged phospholipid (PL). The surface-bound FIXa, binds to FVIIIa, which is also surface bound and in the presence of calcium ions, the  $\{\text{FIXa}.\text{FVIIIa}.\text{Ca}^{2+}.\text{PL}\}$  complex cleaves vitamin K-dependent fluid phase FX zymogen to FXa. The FVIIIa comes from cleaving of FVIII which circulates bound to co-factor vWF. Thrombin separates FVIII into fragments; one fragment which remains bound to vWF and another procoagulant heterodimer which has surface affinity, independent of calcium. The produced FXa heterodimer has  $\text{Ca}^{2+}$ -dependent affinity for acidic phospholipids. FXa activity is increased by non-enzymatic FVa, which is also surface-bound. FVa comes from cleavage of fluid phase FV by thrombin. In the presence of calcium, the surface bound prothrombinase complex  $\{\text{FXa}.\text{FVa}.\text{Ca}^{2+}.\text{PL}\}$  binds circulating vitamin K-dependent prothrombin, through FVa, and cleaves it to release thrombin into circulation. The prothrombinase complex plays a crucial role in rapid thrombin production because of its very high catalytic activity, which is 500,000-fold compared to FXa alone [148]. As noted above, thrombin amplifies the reactions by cyclically activating some of the co-factors. It is

worth mentioning that a recent study has found that some of the coagulation factors are expressed by cells such as monocytes, suggesting the possibility of much more involvement of these cells in coagulation than merely providing surface or expressing receptors [181].

#### 2.2.2.2 Flow effect on the contact system

Blood flow influences the contact system reaction kinetics by transporting liquid phase zymogens and enzyme molecules to wall/surface bound activated or activating sites. More importantly, flow is known to induce formation of monocyte and platelet microparticles as discussed in sections 2.2.1.2.3 and 2.2.3.1.1, respectively. While all cell derived microparticles expose abundant phospholipids, specifically phosphatidylserine, which are binding sites for FXII activation, platelet microparticles seem to be dominant in generating thrombin in a FXII-dependent pathway [162]. Thus, the effect of flow on the contact system seems to be through kinetics and indirect activation through other systems.

#### 2.2.2.3 Contact system-biomaterial interaction

The contact system proteins interact with a material surface [182] in a matter of seconds after implantation. In the presence of a negatively charged material, the proteins may activate each other but the most likely initiator of contact system activation could be FXII since its sensitivity to kallikrein increases 500-fold after surface adsorption [183]. The presence of a biomaterial is also known to induce formation of platelet microparticles, which as discussed above activate the contact system. Figure 2-11 is a representation of the surface-mediated activation of the contact system. In the presence of a biomaterial, it is possible that conformationally changed fibrinogen could directly activate FXII and contribute to polymerization since there is evidence of direct FXIIa interaction with fibrin to influence the clot structure [184]. Adherent and activated platelets also expose phospholipids, which provide a localized activation surface for contact system proteins. In addition, activated platelets may enhance contact system activation by releasing polyphosphates from their dense granules, which have been shown to activate FXII *in vivo* [185]. Certainly, a variety of mechanisms may contribute to the activation of the contact system in the presence of biomaterials. While some kinetics of the process have been described [186, 187], there is limited detailed *in vitro* kinetic parameters for biomaterial studies simulating a stented coronary artery.

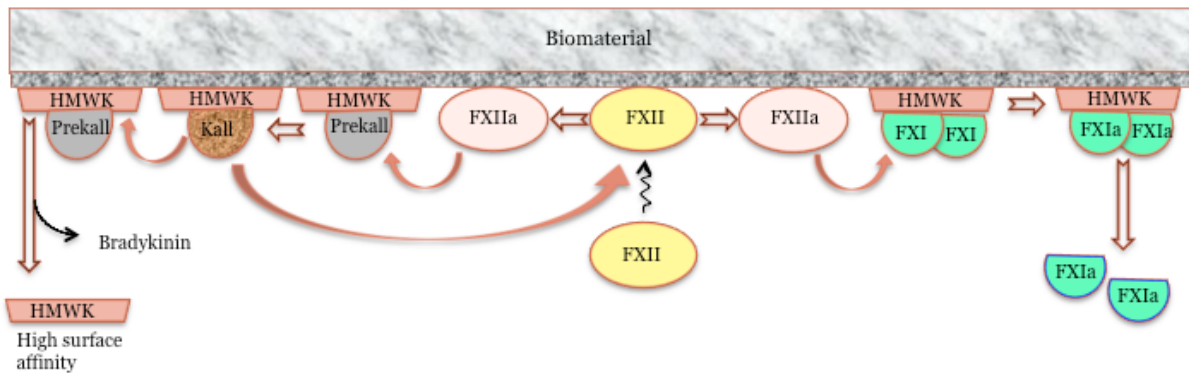


**Figure 2-11. Contact system-biomaterial interaction schematic.** Prekall: plasma prekallikrein, Kall: plasma kallikrein. Curved arrow: proteolytic cleavage, open arrow: consequences. Adapted from [145].

Under flow conditions, the reaction kinetics will increase due to the transport dispersion effect. The strength of protein adsorption would depend on the surface characteristics of the material. Since surface adsorption is a critical factor in initiating and facilitating activation of the contact system, it is not clear if the system proteins have higher adhesion force than other proteins. It is also not clear if there is a shear stress at which the contact system is inhibited, such as by dislodging the proteins or reducing enzyme-substrate contact time.

### 2.2.3 Hemostatic system

The hemostatic system is responsible for the formation of a hemostatic plug in the event of vascular wall injury and plays a role in wound healing *in vivo*. It is composed of the vascular endothelium and platelets, which are the key components. The hemostatic system collaborates with other systems; coagulation and fibrinolytic systems. The coagulation system collaborates in several processes, including the polymerization of fibrinogen to form fibrin, while platelets are the ones responsible for the hemostatic plug. The fibrinolytic system plays a regulatory role.

In blood-biomaterial studies, platelets are still the key component of the hemostatic system. However, there are also important plasma proteins that play a vital role in the hemostatic system. These include von Willebrand factor (vWF), fibrinogen and fibronectin. vWF is an effective protein in mediating adhesion of activated platelets at high shear stress. Fibrinogen, which is polymerized into fibrin by thrombin, also mediates platelet adhesion and platelet aggregation. Since platelets play

a central role in hemostasis and thrombosis, they have developed structural and biological capabilities that enable them to play divergent roles.

### 2.2.3.1 Platelet structure and function

Platelets are minute anuclear plate-shaped blood cells produced by fragmentation of large bone marrow cells called megakaryocytes, which are a sub-lineage of myeloid progenitor cells. About  $30 \times 10^3$  platelets are produced per day per microliter, with a turnover of 10 days [54]. They are about 2-4  $\mu\text{m}$  in size and number  $250\text{-}400 \times 10^3$  per microliter of blood. Despite the lack of a nucleus, platelets possess very complex biological mechanisms. In the cytosol, platelets contain messenger-RNA and abundant translation regulators, micro-RNAs, enabling platelets to synthesize a variety of proteins [188]. Splicing of mRNAs has been implicated in the existence of TF mRNA in platelets and hence expression of functional TF on platelets [139]. Although TF expression on platelets is still a topical issue of debate, the splicing of mRNAs in platelets sheds some light on their complexity. In addition, platelet cytosol uniquely contains  $\alpha$  and dense granules which release adhesive proteins and activation mediators upon platelet activation [189].

The platelet membrane structure, like other cell membranes, is composed of phospholipids whose proportion distribution between the extracellular and intracellular space depend on the state of the cell. On the surface of quiescent platelet the proportional distribution of the phospholipids results in a neutral charge on the surface because the negatively charged phospholipids, phosphatidylserine (PS) and phosphatidylinositol (PI) are in the cytosol. Upon activation, the phospholipids flip inside out and hence the majority of the PS and PI are on the surface, effectively dictating the surface charge, which becomes negative. This facilitates binding of proteins and enzymes with affinity for negatively charged phospholipids.

Platelets express a variety of receptor molecules for adhesion and/or transmembrane signaling; some constitutively and some upon activation. These include the glycoprotein GPIIb/IIIa for fibrinogen, GPIb/V/IX for VWF, protease activated receptor (PAR1/4) for thrombin and  $\text{P2Y}_1/\text{P2Y}_{12}$  for adenosine 5'-diphosphate (ADP) [189]. Some selected key receptors and their densities are presented on Table 2-7. Constitutive receptors include TLR4 and integrin  $\alpha_{\text{IIb}}\beta_3$  (GPIIb/IIIa). Although platelets express TLR4, in general it is believed that they do not express the associated CD14 for LPS recognition and hence LPS does not effectively stimulate some of the platelet functions, such as formation of microparticles. However, there has also been evidence to suggest that platelets express CD14 and hence LPS can stimulate platelet secretion and potentiates

aggregation through TLR4 [190]. One wonders also whether platelet TLR4 may play an important part in biomaterial-platelet-leukocyte interaction and TF expression.

**Table 2-7. Selected platelet receptors, adapted from [191].**

<b>Receptor</b>	<b>Density (No. receptors/platelet)</b>	<b>Ligand</b>
GPIIb/IIIa	60,000-100,000	Fibrinogen, vWF,
GPIb/V/IX	25,000	vWF
GPVI	15,000-25,000	Collagen
P-selectin	12,000	PSGL-1

Platelets can be activated by a variety of biochemical agonists as well as mechanical stimulus. The biochemical agonists include thrombin, thromboxane A<sub>2</sub>, adenosine 5'-diphosphate (ADP) and platelet activating factor (PAF). Activated platelets express receptors, such as glycoprotein GPIIb/IIIa and P-selectin, and release a number of byproducts, some of which promote further activation and aggregation, and some inhibit platelet aggregation [192]. Byproducts such as ADP, Ca<sup>2+</sup>, serotonin and thromboxane A<sub>2</sub> activate more platelets through positive feedback loops. The result of ADP feedback through P<sub>2</sub>Y receptors on platelets is rapid mobilization of platelet cytosolic Ca<sup>2+</sup>, in the order of 20 ms, which is estimated to be 10 times faster than thrombin and thromboxane A<sub>2</sub> [193]. ADP also induces integrin  $\alpha_{Ib}\beta_3$  (GPIIb/IIIa) expression, which has affinity for fibrinogen. Therefore, the consequence of the ADP effect on both platelets (GPIIb/IIIa expression) and monocytes (increased Mac-1 affinity to fibrinogen and FX [194]) is promotion of platelet-leukocyte aggregation. Platelet-leukocyte aggregation is also initiated by the P-selectin-PSGL-1 interaction.

In addition, the effect of increased Mac-1 affinity to FX results in promotion of coagulation within and/or on the aggregate as Mac-1 can also coordinate FX activation [195]. It is interesting to note that besides enhancing Mac-1 expression and affinity, activated platelets also release soluble CD40 ligand (sCD40L), which binds to Mac-1 and induces TF expression, thus amplifying the coagulation cascade. Blood flow may help promote coagulation because there is constant transport of reactants to the immobilized substrate. These mechanisms have the potential to promote thrombus propagation.

Besides receptor expression and protein release, activated platelets are characterized by shape change. Activated platelets become round and form long filaments that allow them to increase their surface area and adhere to fibrin mesh, thereby blocking larger cells and stopping bleeding. In addition, they degranulate and form microparticles, about 0.1  $\mu\text{m}$  in size [196], carry surface binding proteins [196, 197] and hence amplify the hemostatic interaction with other clotting systems, such as the intrinsic coagulation system. Therefore, activated platelets facilitate their functions by expressing surface receptors, releasing proteins, forming microparticles and changing their shape. The properties of each of these transformations allow them to contribute in various biological processes. Thus, platelets play a variety of roles in inflammation [198], coagulation, thrombosis and hemostasis [199]. A recent review suggests that they may be playing much more diverse roles than the classical ones (e.g. hemostasis and coagulation) [192]. The main platelet functions are summarized on Figure 2-12.

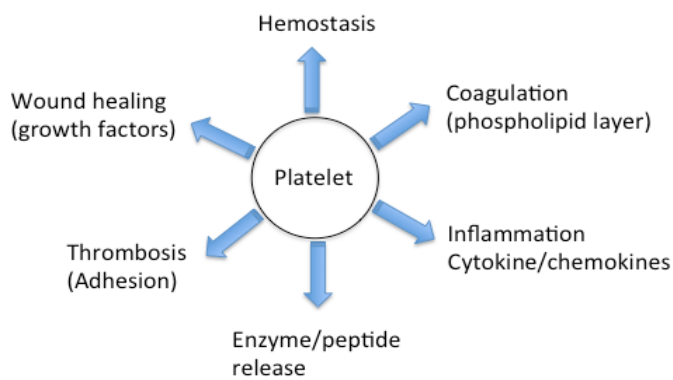


**Figure 2-12. Illustration of platelet functions**

#### 2.2.3.1.1 Flow effect on platelets

Mechanical stress, such as shear stress is known to mediate platelet activation and aggregation both *in vivo* and *in vitro*. The molecular basis of flow effects have been reviewed elsewhere [200, 201]. Blood flow influences platelet activation and aggregation through two main mechanisms – fluid forces and transport phenomenon [202]. In whole blood, these mechanisms are always augmented by biochemical agonists. Fluid shear stress type (e.g. pulsatile vs continuous) [203], level [204] and exposure time [204] predominantly influence platelet activation. The relationship between shear type, level and time is not clear. However, to predict the effect of shear and exposure time, various platelet activation models have been previously proposed [199, 202, 204,

205]. There are also more elaborate models that have taken into account some biochemical aspects [206].

The other important flow parameter that influences platelet activation and aggregation is transport phenomena, which influences particle distribution, hence affects cell-cell or cell-wall interaction and subsequent aggregation. A parameter that is a function of the transport phenomenon is the cell collision efficiency, previously described [199]. Thus, platelet activation and aggregation may be defined as a much more complex function besides shear magnitude or time-averaged shear stress. The existence of biochemical kinetics inherently complicates the relationship between platelet activation/aggregation and the various parameters. At what point one parameter overrides the others, e.g. shear over collision efficiency, is not clear, granted that these are intertwined.

Generally high shear stress increases platelet receptor expression as well as protein release from dense granules. High shear stress also correlates with one other key property of activated platelets; the formation of microparticles [207, 208]. Microparticles, which are a common feature of cardiovascular diseases, from both activated leukocytes and platelets [209], are formed through cell degranulation. MPs express their parent cell proteins and bioactive molecules, which can have both pro-inflammatory and anti-inflammatory effect [210]. MPs carry TF, which plays an important role in thrombosis [163, 211]. Platelet microparticles (PMPs) express abundant factor V (FVa) receptor [197], which is a catalyst in the coagulation cascade, and PMPs from high shear activated platelets have been shown to enhance time-dependent cytokine production and Mac-1 expression on monocytic THP-1 cells [212]. In addition, activated platelets and PMPs have been shown to express procoagulant TF [139]. More importantly, PMPs and TF expression have been implicated in thrombosis. Thus, microparticles are an important feature in *in vitro* investigations.

Besides, influencing platelet activation, shear stress also influences platelet adhesion and shape change [213]. Platelets have developed adhesion mechanisms under different shear rates [214]. *In vivo*, low physiological shear rates do not significantly activate platelets, but can sensitize platelets for high shear activation. On the other hand, high shear rates activate platelets and increases affinity of immobilized vWF, which enables platelets to still adhere at high shear rates, above  $1000 \text{ s}^{-1}$ . However, under *in vitro* conditions, high shear stress may produce contrary results, such as decreased platelet adhesion, depending on the type of flow, even though platelet activation is still high [215]. This is an important difference to note in *in vitro* investigations. The threshold of activation may vary according to the type of flow as well as on whether PRP or whole blood is used.

#### 2.2.3.1.2 Biomaterial-platelet interaction

In addition to shear and biochemical agonists, platelets can be activated by biomaterial surfaces [7, 216-218], mediated by adsorbed proteins, which form a surface layer of about 0.1-0.5  $\mu\text{g}/\text{cm}^2$  [174], depending on material surface properties as well as the size and orientation of the adsorbed proteins. Fibrinogen is particularly an important protein in platelet adhesion [219]. Fibrinogen interaction with biomaterial surface results in material-dependent conformation change and surface absorption [220, 221], which results in selective expression of adsorbed protein epitopes, such as the RGDS sequence [155]. The exposure of epitopes that have affinity for platelet integrin GPIIb/IIIa greatly influences platelet adhesion and activation. As previously discussed, material properties do not only influence the extent of binding sequence exposure, but more importantly can influence structural transition rates [177]. The issue of structural transition rates is important because that may relate to thrombin production rate, which as highlighted by Gorbet et. al [169] may be one of the better indicators of thrombogenicity. This begs the question what epitopes are expressed, and at what rate, in the case of specific biomaterial surfaces such as  $\text{TiO}_2$ , which is found on some of the common metallic biomaterials such as titanium and its alloys? Which material property plays what role in the rate, pattern and extent of structural change? Fundamental understanding of these mechanisms is necessary in order to derive relationships between these interfacial phenomenon and platelet activation and adhesion and hence thrombin generation and thrombogenicity.

#### 2.2.4 Fibrinolytic system

There are three main subsystem levels of control in this system. The main function of the fibrinolytic system is to degrade fibrin and thus dissolve unwanted blood clots, such as to control the growth of a clot after successful wound healing. A fine balancing interplay between fibrinolytic and coagulation systems is necessary because any imbalance can be detrimental. Imbalance towards fibrinolysis would result in bleeding and towards coagulation would result in excessive thrombus, which in blood vessels would occlude blood flow. Fibrinolytic system proteins cross-talk with proteins and inhibitors from other systems involved in coagulation [75]. Therefore, it has a role in material-induced thrombosis. While this is recognized, fibrinolytic system proteins are not investigated in this thesis and therefore, the relevance of the system is only mentioned for completeness and is not discussed any further.

## 2.2.5 Summary

The immune system response to the presence of a biomaterial is a very complex process, which is influenced by material characteristics as well as blood flow. It involves various biochemical cascades and feedback loops that amplify as well as regulate the response. A simplified schematic of the system interactions is presented on Figure 2-13. While there is a lot of knowledge on the various pathways and material-induced thrombosis, the mechanisms involved in the regulation of some of the key pathways, such as the tissue factor pathways, in the presence of biomaterials are not completely understood. Hence, further investigations into the roles of the various pathways in material-induced thrombosis are necessary.

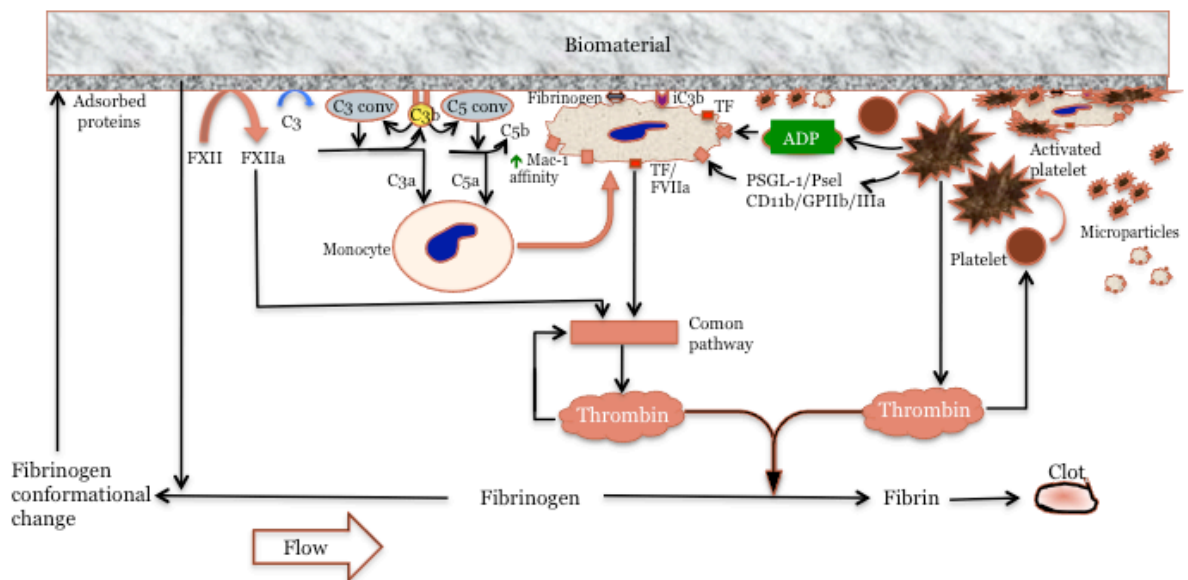


**Figure 2-13. Schematic of interactions in material-induced thrombosis.** Adapted from [169].

Material characteristics are often investigated for adsorption of major proteins like fibrinogen and cell activation and adhesion. However, since phospholipids influence coagulation factor adsorption and reaction kinetics such as {FXa.FVa.Ca<sup>2+</sup>.PL} complex, the question that remains is what are the effects of material characteristics, e.g. TiO<sub>2</sub> on coagulation proteins and reaction kinetics. This question is valid even for the {TF.FVIIa.Ca<sup>2+</sup>.PL} complex, which seems to have less dependence on phospholipids [222]. Although TF is not an active enzyme, discussions on its function/activity seem to treat it as if it is an active enzyme. To that end, there is need to pay more

attention to the link between TF and the co-factor FVIIa, especially because there is evidence that recombinant FVIIa can activate FX by itself [223], tissue factor accumulates in thrombus and not hemostatic plugs [224] and tissue factor has been shown to disappear from wound sites [225]. This raises the question whether this also occurs with physiological FVIIa and if there are specific circumstances under which FVIIa may preferentially act on its own.

With regards to the contact system, its role in thrombosis is predominantly linked to the generation of thrombin. However, there is evidence that FXIIa also interacts directly with fibrin, to influence the clot structure, in a dose dependent manner [184]. This raises the question of whether, in the presence of biomaterials, which could localize FXIIa activity, FXII does not also interact directly with fibrinogen after conformational change and polymerized fibrin to influence material-induced thrombogenicity. This may suggest that the contact system may be playing a wider role in thrombosis development and propagation than initially thought. Further investigations are necessary to elucidate this fact.

Clearly a holistic approach, at various complexity levels, is necessary to investigate the interaction between the various systems. Various high level representations of the system interactions have been previously presented. Since cells play an important role in expressing receptors, providing a surface for enzymes or substrate and physical aggregation, it is possible to represent them as the pillars of the interactions. Others have also noted the importance of including cells in relation to coagulation [226]. Therefore, from a cellular response point of view, the interaction of blood with other systems can be represented by a cellular-based triad, Figure 2-14. This representation emphasizes the already known fact that water and plasma proteins play a central role in the initial interaction with a biomaterial surface. Hence, after interrogation, the pattern of response and the 'decision' to involve cellular components lies with this milieu. Proteins provide the initial and subsequent hidden reaction permutations. How these permutations are controlled by material characteristic remains largely unclear. Cells predominantly respond according to information from proteins. They complement the proteins by recruiting more and controlling the termination of the response. Therefore, closer attention needs to be paid to the material and shear-dependent protein dynamics as well.

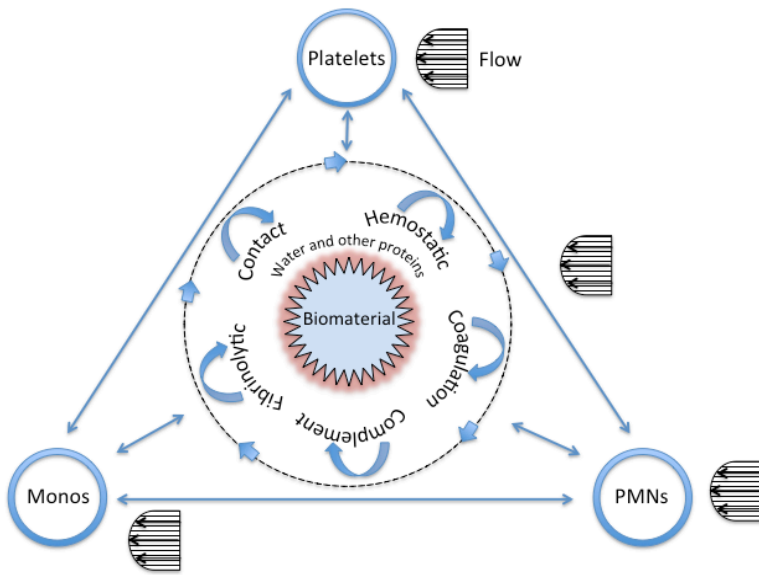


**Figure 2-14. Cellular-based interaction and crosstalk triad between blood and other system.** The arrows depict communication in both directions. The big circle represents the milieu of interactions around the biomaterial, driven by several systems/cascades. Interactions within the triad occur regardless of flow, but with different dynamics. Adapted from [7].

Figure 2-14 can be examined at the system level in terms of the systems involved. These are; (i) the fluidics (dynamics) system, (ii) the blood/biochemical system and (ii) the biomaterial system. All these systems have essential characteristic parameters that allow them to interact with each other at different spatial and time scales. Similar to the blood system discussed above, the other two systems and their characteristics are discussed in the next sections.

### 2.3 The fluidics system

The fluidics system is defined by the cardiovascular system geometry and hemodynamics. The vascular system is composed of blood vessels of various geometric and structural differences, Figure 2-15. The blood vessels are also characterized by numerous curvatures and bifurcations, which facilitate blood distribution throughout the body. These physical characteristics of the vascular tree influence hemodynamic parameters, such as flow velocity, blood pressure, type of flow and vessel wall shear stress (WSS).

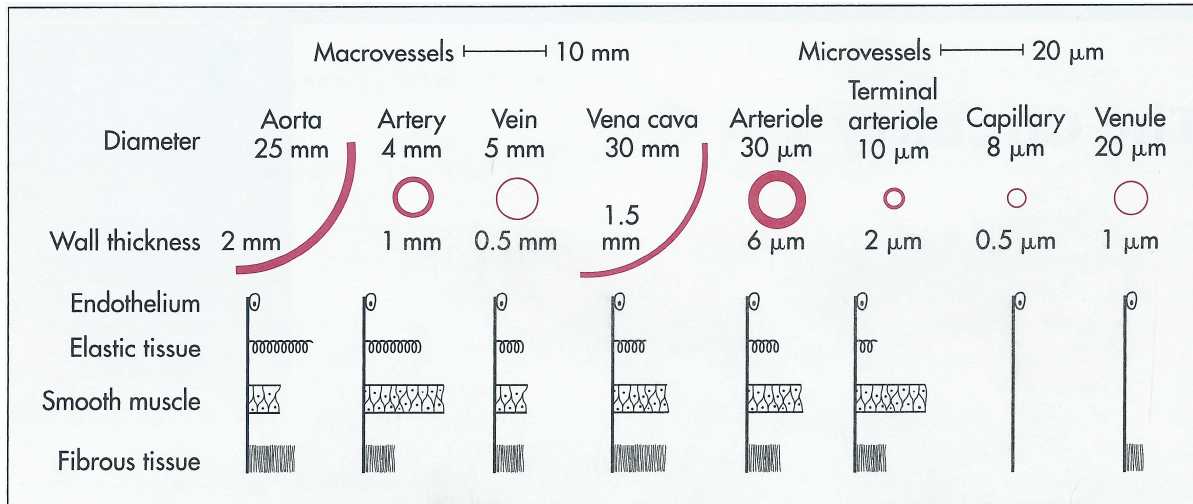


**Figure 2-15. Geometric and structural properties of the vascular system. Not drawn to scale. Used with permission from Elsevier. Source: Berne, R.M. and M.N. Levy, *Cardiovascular physiology*. 7th ed. 1997, St. Louis: Mosby, xi, 324 p.**

Perhaps the prominent influence of vascular geometry and hemodynamics is in development and localization of atherosclerotic plaques, which preferentially develop in the distal aorta, carotid artery, lower extremity arteries and coronary arteries [61]. Atherosclerotic plaque is a major risk factor for arterial lesions, such as thrombosis or stenosis, which are the major causes of cardiovascular diseases and some of the leading causes of mortality and morbidity. Due to the significance of the geometric and hemodynamic characteristics in atherosclerosis, and in this research, a review of these parameters in the coronary systems is appropriate. This section examines the geometric parameters of the cardiovascular system and their relevance to the design of *in vitro* flow models and to the function and distribution of immune system components.

### 2.3.1 Geometric parameters of the coronary system

The coronary system supplies blood to the myocardium (heart muscle), with two main coronary arteries emanating from the aorta. These are the left main coronary artery (LMA) and the right coronary artery (RCA). The LMA, with typically internal diameter of  $4.5 \pm 0.5$  mm [227], supplies blood to the left ventricle. It branches into the circumflex (LCx) and the left anterior descending (LAD). The significance of the LAD is that it supplies blood to the left ventricle; the main

heart chamber for pumping blood into circulation. Hence occlusion of the LAD has immediate impact on cardiac function. The RCA is also susceptible to stenosis but its occlusion is often survivable because it supplies blood to the right ventricle. Thus, any consideration for geometric and hemodynamic parameters in this research will be with particular reference to the LAD. However, the LAD and RCA are relatively similar in size, Table 2-8. They also have similar curvature [228], although there can be some differences in tortuosity [228]. Therefore, any discussion on LAD is in many cases applicable to the RCA.

**Table 2-8. Typical dimensions of coronary arteries. Values are mean±SD. Adapted from [229].**

Vessel	Internal diameter (mm)	Area (mm <sup>2</sup> )	Area taper (% per cm)
LAD	3.7±0.5	11.1±2.8	9.8±3.3
RCA	3.6±0.5	10.2±2.8	6.8±2.3

The basic physical parameters that define the arterial blood vessels are diameter, wall thickness, surface topography, modulus of elasticity, cross-sectional profile, length, branching angle and tortuosity. Only parameters pertinent to this research are discussed.

### 2.3.1.1 Diameter

The blood vessel diameter is controlled by smooth muscle cells (vasoconstriction and vasodilation), which form the major constituent of the arterial wall, Figure 2-15. Coronary arteries do not have constant diameter, but taper off with each bifurcation [230]. As a result, the diameters of the coronary arteries are often measured at midpoints of defined segments: proximal segment, mid-segment and distal segment. Some typical diameters are 4.5±0.5 mm for LMA, and 3.7±0.4 mm and 1.9±0.4 mm for LAD proximal and distal segments, respectively [227]. Taking average diameter and applying Poiseuille and Navier-Stokes equations to flow in arteries, the flow resistance is inversely proportional to the fourth power of vessel diameter and the shear stress is inversely proportional to the third power of the diameter [231]. In addition, the diameter also affects viscosity due to the colloidal nature of blood – Newtonian in arteries and non-Newtonian in capillaries [52]. Therefore, the vessel internal diameter is an important physiological parameter to mimic in developing *in vitro* models because of its implications on fundamental hemodynamic parameters.

### 2.3.1.2 Elasticity

Blood vessels show viscoelastic properties, which gives them compliance. As a result, the diameter of coronary arteries varies intermittently with the pulsatile cardiac cycle. At a nominal physiological heart rate of 60-70 beats per minute, the main frequency of pulsatility is  $F=1.0-1.2$  Hz (cycle period  $T=0.8-1.0$  s). This frequency relates more to the curvature variation than the diameter variation as there has been evidence of harmonics in arterial flow. Although it has been suggested that collision of a particle with an elastic wall may reduce shear stress by about 25% [232], in general when performing blood flow analysis, elastic effects can be ignored because they have been found to introduce very little error [60]. Hence, flow equations for rigid tube analysis, with mean pressure and volume, can be applied without loss of generality. Thus, unless the study is investigating the physics of pulsatile flow, a rigid vessel is reasonably appropriate for most *in vitro* flow models.

### 2.3.1.3 Surface topography

One common feature of the cardiovascular system is the existence of endothelial cell lining in all blood vessels Figure 2-15, which forms a barrier between the blood and the sub-endothelial milieu. The endothelial cell lining provides a smooth and non-thrombogenic surface. The smooth surface ensures efficient flow with little friction resistance. This topography may change with the introduction of a vascular device such as a stent. If the stent strut size is too large, the struts may introduce turbulence in regions that originally had laminar flow. The strut size and shape lower the critical Reynold's number at which flow transitions from laminar to turbulent flow [233]. The relevance of topography in *in vitro* models incorporating stents is that it introduces roughness and therefore additional friction in the model vessel. This factor needs to be considered in fluid mechanics analysis of the model. While it is recognized that fluid dynamic changes *in vivo* will affect endothelial cells lining the vasculature, e.g. remodeling and expression of adhesion molecules, the focus of this thesis is on the interaction of blood with biomaterials and thus endothelial cells are not investigated.

### 2.3.1.4 Cross-sectional area

The cross-sectional profile of normal vascular arteries is generally circular, Figure 2-15. The circular approximation has been significantly used in developing engineering analysis of the arterial wall dynamics as well as developing blood flow equations. In diseased vessels, e.g. due to atherosclerotic plaque lesions, the cross-sectional profile can be quite different. The existence of a lesion will also affect flow parameters and any analysis would need to take this into account. This

type of analysis is beyond the scope of this research and therefore a circular geometry is assumed for the purpose of this research.

### 2.3.1.5 Curvature and tortuosity

Coronary arterial curvature emanates from a number of geometric factors. These include heart curvature, arterial tortuosity and bifurcation. Curvature introduces several velocity components and dispersion of colloid suspensions which can result in wall adaptations, correlating with atherosclerotic lesions in arteries [234] and arterioles [235]. More importantly, curvature and tortuosity, as well as torsion, have been shown to have considerable individual variability, which may account for variation in parameters that mediate development of atherosclerosis among individuals [228]. *In vivo*, curvature varies with cardiac pulsatility, both spatially and in time.

Tortuosity, the degree of winding and meandering along the length of a vessel, exists to varying degrees throughout the circulatory network. The LMA is generally straight, but the other main coronary vessels (RCA, LAD and LCx) have varying degrees of tortuosity. Blood vessel tortuosity affects flow dynamics; WSS on the outer wall is higher than on the inner wall of the curvature. Representative *in vitro* models have shown its effect on flow parameters [236]. It is also an important factor to consider in device design and implantation. A tortuous vessel can increase the possibility of perforation. In addition, the location of an implant relative to the sharp curvature also affects flow, as demonstrated by the effect of stent position in studies with 90° bends. Thus, curvature and tortuosity are important to take into account in understanding flow-mediated phenomenon.

### 2.3.1.6 Bifurcation

Bifurcation is a flow divider and as a result it introduces change in flow dynamics, which can result in complex fluid velocity distribution and shear stress patterns. Wall shear stress on the inner wall of the bifurcating branch is higher than WSS on the outer wall of the branch [61, 234], which mimics flow at a curvature of a tortuous vessel. Bifurcation influences WSS distribution both in steady and pulsatile flow [237]. Simulation studies of the coronary artery have also shown that the velocity profile is skewed toward the inner wall of the bifurcating branch during diastole [238]. The region of low shear stress and complex flow has been found to be a preferential location for atherosclerotic lesions [61, 234]. Thus, bifurcation is one of the important geometric parameters that have great influence on blood flow patterns.

The role of red blood cells (RBC) cannot be ignored in flow geometries. In a straight tube at low shear rate  $<100 \text{ s}^{-1}$ , they behave like ordinary particles. At high shear rates, they are deformed into elliptic shape aligned with the direction of flow [239]. In curved flow, these ellipses cannot be expected to remain in the center of the flow because of the secondary flow vortices. This is important because in different simulation studies, RBC collisions have been shown to influence leukocyte [240] and platelet [241] wall interactions. The relevance of curvature and its influence on hemodynamics is discussed in section 2.3.2.4. Some positive aspects of the influence of this geometry on fluid flow are exploited for various industrial and biomedical engineering applications [242-244].

### **2.3.2 Hemodynamic parameters of the coronary system**

The geometric characteristics of the vascular system and the blood fluid properties influence the blood flow (hemodynamic) parameters. The important hemodynamic properties that influence the fluid dynamics as applied to blood are blood rheology, velocity and wall shear stress/rate. The specific fluid mechanics parameters that define these hemodynamic properties may vary according to the physiological location of interest (PLOI).

Fluid dynamics equations to describe blood flow are derived on the basis of continuum mechanics, i.e. fluid motion can be described in terms of the laws of classical continuum physics (conservation of mass, conservation of momentum and conservation of energy). It should be noted that while blood flow is pulsatile, generally steady state solutions for a rigid tube are used in flow analysis. Pulsatile flow and wall compliance add considerable complexity and exclusion of the pulsatile component has been shown to have little effect on the accuracy of the analysis. Thus, unless otherwise stated, the flow is assumed to be steady, laminar and fully developed.

#### **2.3.2.1 Blood rheology**

As discussed in section 2.2, blood is an incompressible and colloidal non-homogeneous fluid, with complex rheological properties. Due to the complex rheological properties of blood, its viscosity is influenced by a number of factors, including hematocrit and strain rate. At high shear rates, such as in the microcirculation, blood displays non-Newtonian fluid behavior, with non-constant viscosity – decreasing non-linearly with decreasing flow rate or increasing shear rate. This is because particle interactions increase at low flow rates. Thus, blood rheology in capillaries is often modeled as a non-Newtonian power law fluid, with the shear stress,  $\tau$ , given by the equation,

$$\tau = K\gamma^n \quad (1)$$

where, K is the consistency coefficient (Pa.s), n (<1 for pseudoplastic or shear-thinning fluids) is a dimensionless power law index and  $\gamma$  is shear rate. However, in larger blood vessels with high shear rates, such as arteries, blood behaves like a Newtonian fluid with relatively constant dynamic viscosity, estimated at 0.003-0.004 Pa.s [52].

### 2.3.2.2 Blood velocity

Blood flow velocity is important for transportation of metabolic products, immune system agents and other biochemical agents to regulate physiological processes. It also plays a significant role in enzyme-substrate interaction kinetics [149]. Hence, the velocity distribution in vascular systems is related to function. Fluid dynamic equations to describe blood flow are derived from basic fluid mechanics principles.

Assuming a rigid horizontal cylindrical tube of constant cross-sectional area, the blood flow velocity can be derived based on the following fluid assumption; Newtonian incompressible fluid (constant density), steady state (flow independent of time), fully developed flow and laminar. The derived velocity is described by a parabolic profile (based on the Poiseuille equation) with the axial component, expressed as,

$$v(r) = \frac{(\Delta P)R^2}{4\mu L} \left[ 1 - \left( \frac{r}{R} \right)^2 \right] \quad (2)$$

where  $\Delta P$  is the pressure gradient across a fluid element, L is the length of the element, r is the radial coordinate, R is the radius of the tube and  $\mu$  is the fluid viscosity. Since this is a pressure driven flow, the axial pressure gradient drives the flow velocity while the radial pressure gradient results in the circumferential wall stress. In blood flow in arteries, the tensile stress, which can be approximated by Laplace's Law [61], will change with arterial geometry as well as cardiac cycle. In this research, the geometry is considered constant.

The general velocity profile, equation (2), predicts that the velocity is zero at the wall, assuming no slippage. This means transport of molecules near the wall is aided by diffusion forces, whereas the axial transport of the bulk of the blood components is predominantly driven by

convective forces. However, it has been shown that the presence of red blood cells enhances platelets dispersion and interaction with the vessel wall so that diffusion alone is not sufficient for particle interaction with the wall [149]. Equation (2) can also be written in terms of volumetric flow rate ( $Q$ ) as,

$$v(r) = v_{\max} \left[ 1 - \left( \frac{r}{R} \right)^2 \right] \quad (3)$$

Hence the average velocity is expressed as,

$$v = \frac{v_{\max}}{2} = \frac{Q}{\pi R^2} \quad (4)$$

These equations are used in arterial blood flow analysis since arterial elastic effects can be ignored [60] and because blood behaves like a Newtonian fluid in the arteries. Using the physiological stroke volume  $V_s$  and heart rate frequency  $F$ , the cardiac output is defined as  $Q = FV_s$ . With a nominal heart rate of 60 to 70 beats per minute, giving a frequency  $F = 1.0$ - $1.2$  Hz, and a stroke volume of approximately 80 ml per contraction cycle, the cardiac output is about 4.8 L/min [51].

The assumption of laminar flow in deriving the velocity equation is characterized as a dimensionless ratio of inertial forces to the viscous forces, called the Reynolds number. It is defined by the equation

$$R_e = \frac{\rho v D}{\mu} \quad (5)$$

where  $\rho$  is fluid density,  $v$  is mean velocity,  $D$  is vessel diameter and  $\mu$  is dynamic viscosity (Pa.s). For Poiseuille flow, laminar flow in a tube occurs for  $Re < 2100$  [245]. When fluid is flowing in a tube, the tube wall resistance to flow results in wall shear stress, an important parameter that influences cell activation and adhesion.

### 2.3.2.3 Shear stress/rate

Wall shear stress is a measure of wall viscous frictional force per unit area. Related to shear stress is the rate of shear, which is used to characterize local flow conditions in relation to local shear forces. The rate of shear or shear rate, for pipe flow with only axial velocity component, is defined as the rate of axial velocity increase with distance away from the vessel wall to the vessel centre. The WSS for a rigid circular straight tube with fully developed Newtonian fluid flow is defined as the derivative of equation (3) with respect to the radius. At the wall where  $r=R$ , the wall shear rate is expressed as,

$$\gamma_w = \frac{4Q}{\pi R^3} \quad (6)$$

where Q and R are as previously defined.

Shear rate influences phase separation in multi-phase flows [244]. The significance of this effect on blood is that blood experiences shear thinning at high shear rates [57], meaning the red blood cells migrate to the center of the flow, and plasma, which contains more platelets than the center [149], forms the boundary layer between the thick center and the vessel wall. Shear rate does not only affect particle dispersion in flowing blood, but also activates immune system cells. Shear rate has been shown to influence platelet adhesion [60, 246, 247], platelet interaction with immobilized tissue factor [248] and tissue factor initiated coagulation [249]. Thus, shear rate influences a variety of cell functions.

Shear rate is related to shear stress by equation (1). For a Newtonian fluid, as it applies to blood in large arteries, the constants are  $n=1$  and  $K=\mu$ , the dynamic viscosity. Therefore, the wall shear stress is expressed as,

$$\tau_w = \frac{4\mu Q}{\pi R^3} \quad (7)$$

This equation has been used to estimate the physiological vascular WSS magnitude [250] and mean-average WSS [251]. Vascular shear stress is particularly important because it has been found to modulate a number of vascular physiological responses and adaptation mechanisms [252]. Physiological shear stress in the arteries is estimated at 10 to 70 dyn/cm<sup>2</sup> [250], with the nominal

value taken as 15 dyn/cm<sup>2</sup>. Deviation from this range has pathologic consequences. Endothelial cells have been reported to lose structural integrity at wall shear stresses above 420 dyn/cm<sup>2</sup> [253]. At molecular level, low shear stress (<4 dyn/cm<sup>2</sup>), which may occur at bifurcations, is associated with expression of the transcription factor nuclear factor-κB (NF-κB) in endothelial cells [149], with consequential vascular remodeling and expression of inflammatory proteins, such as monocyte chemoattractant protein (MCP-1) and intercellular adhesion molecule (ICAM-1). MCP-1 and ICAM-1 are responsible for leukocyte recruitment and adhesion to the endothelial cells. At functional level, low shear stress has been shown to induce intimal thickening [60].

Besides modulating endothelial cell function, shear stress also modulates function in plasma proteins and blood cells. Blood from hypertensive individuals with intimal thickening has elevated levels of C-reative protein (CRP), an inflammatory response protein [254]. High shear stress also modulates platelet activation and adhesion through activation of calcium channels – up-regulating cytosolic Ca<sup>2+</sup> concentration [255]. Wall shear stress greater than 50 dyn/cm<sup>2</sup> has been shown to activate plate rich plasma (PRP) [149]. It is also suggested that periodic high shear stress, as may occur due to stenosis or heart valves, sensitizes platelets to activation at low shear stress [256]. More importantly, shear stress has been shown to have some correlation with in-stent thrombosis [257].

Thus, hemodynamic parameters are important in examining blood-biomaterial interactions as they modulate cellular and vascular functions, both under normal and disease conditions. While the role of endothelial cells in vascular function is important to consider in the development of stenosis, their role in thrombosis is not investigated in this research because the emphasis is on blood-biomaterial interactions.

#### 2.3.2.4 Flow in a curved tube

Physiological curvature, due to heart curvature, tortuosity or bifurcation, defines geometric parameters that influence curved tube flow dynamics. One of the important parameters that is used to characterize curved tube geometry, and hence curved tube flow, is the non-dimensional curvature ratio, which can be defined as the ratio of the internal tube radius to curvature radius or vice versa, equation (8),

$$\kappa = \frac{R}{R_0} \tag{8}$$

where  $R$  is mean internal vessel radius and  $R_0$  is mean radius of curvature. Curvature ratio influences some of the key fluid mechanics parameters that characterize curved tube flow [242, 258-260]. The physiological curvature ratio for the left coronary arterial tree varies from 0.02 to 0.5 [261]. It is influenced by the spatial location of the observation point as well as the cardiac cycle.

An additional parameter that characterizes flow in a curved tube, besides curvature ratio ( $\kappa$ ), is the Dean number ( $D_n$ ) and its related Reynolds number (Re). Although the Dean number is related to the Reynolds number, which is used to characterize both straight and curved flows, it is important to recognize their differences. In a straight tube flow the Dean number is zero even though the Reynolds number can still be defined. The Dean number is defined as,

$$D_n = R_e \sqrt{\kappa} \quad (9)$$

One of the interesting influences of curvature on Re is that it increases the transition point to turbulent flow slightly above the 2100 for the straight tube flow. For curved flow, the critical Reynolds number for transition to turbulent flow is expressed as [262],

$$R_e = 2100(1 + 12\sqrt{\kappa}) \quad (10)$$

The significance of the Dean number is its influence on the development of secondary flow vortices, which were first described by Dean as early as 1927 and 1928 [263]. The overall effect of additional velocity vector components in curved tube flow is increasing radial mixing and mass transfer [264]. This has been demonstrated numerically [264] as well as experimentally in whole blood [56]. The increased radial and reduced axial dispersion results in reduced residence time distribution, which can make the flow approach plug flow and the velocity showing an ‘M’ profile [262]. Particle dispersion has direct impact on cell-wall interactions *in vivo* [61], and hence is very relevant for *in vitro* blood-biomaterial interaction studies under flow conditions and interpretation of results. For that reason, all the flow parameters such as velocity and shear rate/stress need to be appropriately defined in terms of curvature parameters.

### 2.3.3 Summary

The coronary geometry and hemodynamics define the fluidics system. The geometry defines some of the boundary parameters of the fluid flow. These parameters are important *in vivo* as they relate to some of the pathologic conditions in the coronary system. Flow is equally important *in vitro* as it influences cell-cell or cell-material interaction and adhesion. Hence, close attention to the design of the *in vitro* model is necessary. In this research, the governing conditions for the transport phenomena, such as the geometry and hemodynamics of the location of interest, are closely examined in order to relate them to the *in vitro* model design. One of the key parameters that characterizes flow in coronary arteries is curvature ratio. However, it is important to note that the dimensional parameters of the ratio are equally important. This is because similar curvature ratios can be obtained with vastly different curvature and tube radii, yielding fluid dynamics results that may not be comparable. Therefore, if an *in vitro* model is designed with a similar dimensionless ratio to the physiological location of interest (PLOI), the results may not be relevant if the curvature radius and vessel radius are not comparable. For that reason, this is an important aspect of the *in vitro* model design.

A systems approach is adopted because there are several systems that are involved *in vivo* in the physiological system response to biomaterials. The effect of the *in vitro* model parameters can then be investigated in the attempt to unravel the pathways involved in blood-biomaterial interactions under the *in vivo* conditions, for the selected location of interest. Thus, the motivation for this research is the application of a systems approach for investigating mechanisms involved in *in vitro* conditions mimicking coronary in-stent thrombosis. Hence the coronary system is of particular interest in understanding transport phenomenon and translating parameters to *in vitro* model design.

## 2.4 The biomaterial system

The selection of biomaterials for various biomedical applications is based on a variety of mechanical and chemical properties, such as material tensile strength, corrosion resistance and biocompatibility [20]. Biocompatibility determines the suitability of a biomaterial for biomedical applications. It has been defined as the ability of a biomaterial to positively interact with the biological system in a specific application [1]. It is of particular significance because it is a function of material surface characteristics, which are the main determinants of the initial implant interactions with the biological system.

There are a variety of reasonably biocompatible polymeric, ceramic and metallic biomaterials available for biomedical applications [265]. Some of the relatively biocompatible and commonly used metallic biomaterials in orthopedic, dental and cardiovascular implants are made from titanium and its alloys, e.g. Nitinol® and Ti-6Al-4V [20]. These are used because of their chemical and mechanical characteristics. Both are reasonably biocompatible, corrosion resistant and have high tensile strength. Nitinol is an alloy made from approximately equal amounts of nickel and titanium. Ti-6Al-4V is made by replacing some of the Ti atoms with aluminum (Al) and vanadium (V) to increase its strength, see Appendix A for detailed material composition and characteristics. Thus, Ti-6Al-4V has both alpha (Al) and beta (V) phases. The alpha phase has hexagonal structure, is soft and ductile whereas the beta phase has cubic structure and is harder and stronger. Because Ti-6Al-4V has both alpha and beta phases, it can be heat treated to stabilize at desired phase proportions. For example, at high temperatures, it exists predominately in the beta phase. The rate of heating and cooling cycles determines the transformation dynamics. This property is exploited in making model stents for this research.

While material bulk properties are important, the surface characteristics are of particular significance in blood-biomaterial interactions because they influence protein adsorption and cell adhesion and proliferation, just as much as mechanical cues imposed by hemodynamics. Numerous studies have been done to investigate the effect of material properties on protein and cell adhesion [266, 267]. Both nitinol and Ti-6Al-4V can be subjected to various surface treatment methods, such as mechanical polishing, chemical etching and heat treatment, during or after the manufacturing processes, in order to produce desirable surface characteristics. The effects of some of these methods on nitinol have been reported [268]. Of particular interest is the heat treatment method, which can be used during manufacturing and device shape setting. Studies have shown that heat treatment alters surface oxide layer nanostructure by increasing its thickness and roughness, on both nitinol [269] and Ti-6Al-4V [267]. Increased roughness may be desirable where there is need for adhesion as it increases surface energy, such as orthopedic or dental implants. Biomaterial surface properties that are of interest are surface topography/roughness, surface chemical composition, surface energy and wettability.

#### **2.4.1 Surface roughness and topography**

Topography and roughness are sometimes used interchangeably. While they both describe texture, they are two different concepts. Topography is usually qualitative while roughness is

quantitative. While topography can be defined in terms of form, waviness and roughness [270], which is equivalent to texture, in this research it is generally used to describe the qualitative surface morphology or form and roughness is generally used for quantitative description. Two surfaces can have comparable roughness values but vastly different topography, e.g. one with spiky ridges and the other with square ridges [271].

Biomaterial surface topography and roughness influence cell adhesion and proliferation, depending on the range and scale of roughness as well as on the cell type [266, 272]. For example, fibroblasts and osteoblasts have been shown to respond differently to the same roughness, for both nitinol [273] and Ti-6Al-4V [274]. Surface topography and roughness parameters are both equally important as materials of the same roughness but different topographies can produce very different cell responses [272]. However, roughness may have limited effect on adsorption of proteins, such as albumin [275] and fibrinogen [220]. When considering protein adsorption, it may be necessary to consider the scale of roughness (micro or nano) as nanopores have been shown to affect complement activation and adsorption [85]. Furthermore, molecular level surface roughness is important because it has implications on surface energy, due to the fact that when atoms are closer together, there is stronger interactions, which reduces surface energy [276]. Increase in surface roughness can have the effect of increasing surface energy. Thus, it is important to determine the surface topography and roughness in blood-biomaterial interaction studies in order to relate them to observed biological effects.

#### **2.4.2 Surface chemistry**

Although the bulk chemical composition of the biomaterial is important for the overall chemical and mechanical characteristics of the material, the surface elemental composition is even more important in cardiovascular devices because it determines initial release or non-release of ions and subsequent electrostatic material-blood interaction, regardless of the roughness and topography length scales. Surface chemistry is probably the most fundamental characteristic of the material. It determines both surface charge and energy. Consequently surface chemistry influences interfacial water properties [277], protein-biomaterial interaction dynamics and subsequent adsorption [170, 220, 275, 278]. Conformational change and adsorption of fibrinogen, one of the important proteins that mediate material-blood interaction, is dependent on surface chemistry [160]. Platelet microparticle formation has also been shown to exhibit surface chemistry sensitivity compared to leukocytes in a polymeric bead model [178].

One of the most important surface chemistries in metallic biomaterials is the oxide layer, particularly the titanium oxide surface layer, which forms spontaneously on titanium alloys because of titanium's thermodynamically driven affinity to oxygen. Titanium oxide surfaces react with a number of substances, including metals and inorganic and organic substances, which has made them suitable for a variety of applications [279].

#### 2.4.2.1 Fundamentals of titanium oxide

Atomic elements are composed of electrons spinning around the nucleus of an atom in different configuration states and energy levels. The electron spin configuration states are described by probability functions; orbitals. Orbitals describe the spin state and specific energy levels of electrons and thus describe the basic chemistry of each atomic element. They are labeled as  $1s^2$ ,  $2s^2$ ,  $2p^6$ ,  $3s^2$ ,  $3p^6$ ,  $3d^{10}$ ,  $4s^2$ ,  $4p^6$ ,  $4d^{10}$ , etc., where the numbers indicate the energy level and superscripts indicate the maximum number of possible electrons. Electrons fill the lower energy states first, but  $4s$  is slightly lower than  $3d$  and thus will be filled first before  $3d$  in most atoms.

Titanium is a transition metal with 22 electrons arranged in orbitals as follows:  $1s^2$ ,  $2s^2$ ,  $2p^6$ ,  $3s^2$ ,  $3p^6$ ,  $4s^2$ ,  $3d^2$ . Thus, it has four incomplete  $3d$  orbitals. On the other hand, oxygen has 8 electrons arranged in orbitals as follows:  $1s^2$ ,  $2s^2$ ,  $2p^4$ , resulting in one incomplete  $2p$  orbital. When titanium oxide ( $TiO_2$ ) is formed, the compound has  $3d^0$  because the electrons fill the  $2p$  orbitals first as they are at a lower energy level than the  $3d$  orbitals, which explains the titanium affinity to oxygen. The  $d$  orbitals, unlike the  $s$  and  $p$  orbitals can have complicated shapes. As a result  $TiO_2$  can have several phases and exhibit complex interaction mechanisms. There are three forms of  $TiO_2$  layers; rutile, anatase and brookite [279]. The rutile  $TiO_2$  layer is the strongest and most stable layer, and hence the predominant layer on titanium alloy biomaterials. The rutile layer has three forms, designated as (110), (100) and (001) [279, 280]; determined by their atomic surface termination structure. The basic structural element of  $TiO_2$  (110) is composed of one titanium atom surrounded by six oxygen atoms in an octahedral coordination [281].  $TiO_2$  (110) surface is composed of alternating rows of oxygen atoms and 5-fold coordinated titanium atoms. The oxygen atoms protrude above the surface because the surface termination is similar to the bulk structure. Because of the similarity between termination and bulk geometry,  $TiO_2$  (110) has been found to have the lowest surface energy, and thus better thermodynamic stability compared to  $TiO_2$  (100) and  $TiO_2$  (001). Therefore, any discussion on  $TiO_2$  will be based on the strongest rutile  $TiO_2$  (110) form unless stated otherwise.

The spontaneously formed titanium oxide layer on Ti-6Al-4V has a thickness of 3-10 nm [274]. Surface TiO<sub>2</sub> layer forms on both nitinol and Ti-6Al-4V [282]. Despite formation of TiO<sub>2</sub> layer on nitinol, nickel ion (Ni) can still be released from the surface, depending on nitinol treatment method [283]. However, the Ni release rate diminishes over time *in vitro* [282]. Several nitinol treatment methods, have been used to reduce surface Ni [268]. Nitinol heat treatment in air and annealing in argon at 500 °C for 20 minutes can reduce surface Ni content [284], and higher temperature increases surface Ti, which would promote formation of TiO<sub>2</sub> layer. The formation of a surface hydrophilic TiO<sub>2</sub> layer has significance in biomaterials because it facilitates biological integration of the biomaterial. In orthopedic implants, the integration is through formation of a calcium-phosphate layer. In blood, the TiO<sub>2</sub> layer promotes blood plasma protein adsorption, mostly through the RGD sequence. The charge on the oxide surface is a function of the surface treatment method.

### **2.4.3 Surface charge**

The predominant TiO<sub>2</sub> layer on titanium alloy biomaterials has an isoelectric point at pH ≈ 5 [285]. As previously described, the isoelectric point is the pH at which a molecule carries no net charge. At higher pH it becomes electronegative, which means at the blood pH level (≈7.4), the TiO<sub>2</sub> layer is negatively charged. The strength of charge on the oxide layer may be influenced by the material treatment method [286]. This is important to note because the surface interaction with blood proteins depends on its charge and chemistry. Surface charge has been shown to have a differential effect on contact pathway and platelet activation [176]. Current data suggests that even though steady state adsorption is influenced by other factors such as competitive adsorption, surface chemistry seems to play a key role in initiating contact system adsorption and activation. For example, complement proteins have been shown to be activated by negatively charged surfaces. With regards to protein adsorption, it has been reported that in the presence of low molecular weight ions that can be co-adsorbed, electrostatic repulsion between a biomaterial surface and proteins is not sufficient to prevent adsorption [175].

When TiO<sub>2</sub> is in an electrolyte solution, complex interactions, which are pH dependent, occur at the titanium oxide-fluid interface. There is initial preferential adsorption of water through the hydroxylation of the Ti ion (TiOH), followed by some cations replacing some of the water molecules by interacting with surface oxygen [287]. Experimental studies have suggested that peptide binding to the TiO<sub>2</sub> layer is facilitated by pH dependent electrostatic bonding through the carboxyl group [288],

although conformational change may also involve an amide group. A study on fibrinogen adsorption on TiO<sub>2</sub> at pH 7.4 suggests involvement of hydrogen bonding (TiO<sub>2</sub> - H<sub>2</sub>O) and electrostatic interactions through the amide groups [289]. Different surfaces may involve different binding groups, which would influence protein adsorption and subsequent cell adhesion. The hydroxyl binding group which favors complement activation and adsorption, has also been shown to favor leukocyte adhesion [278].

Molecular dynamics simulation of the interaction between the TiO<sub>2</sub> atoms and RGD sequence groups, using fibronectin, has confirmed the involvement of the carboxyl group, both under different surface topographies [290] and different water solutions [291]. The bonding happens through replacement of water molecules from the TiO<sub>2</sub> layer [290]. Interestingly, once the peptide is adsorbed, the spatial orientation is influenced by the topography of the TiO<sub>2</sub> surface [290] and the solvent [291]. The peptide-TiO<sub>2</sub> bonds were found to be stronger on grooved surfaces [290], possibly due to the increase in surface energy and surface area with increased roughness of the TiO<sub>2</sub> layer [276]. This particular RGD binding with the TiO<sub>2</sub> layer is important because it suggests that the amide groups are the ones available to interact with the cell membrane.

#### **2.4.4 Surface energy**

Besides electrostatic material-blood interactions, there are also hydrophilic/hydrophobic interactions that are determined by thermodynamic factors; material surface energy. A hydrophilic surface possesses relatively high surface free energy while a hydrophobic surface possesses low surface free energy and the limits are generally 72.8 mJ/m<sup>2</sup> and ≈36 mJ/m<sup>2</sup>, respectively [292]. Thus, the material surface energy determines the ability of water to wet the surface. Titanium surface hydrophilicity and hydrophobicity have been shown to influence the expression and recognition of cell activation markers [293]. Material hydrophilicity/hydrophobicity is used to indicate general material-solution interaction tendencies and thus provides a general measure of surface wettability, which depends on material chemistry and surface roughness.

The fundamental basis of wettability is that a water droplet will tend to spread on a hydrophilic surface more than on a hydrophobic surface. Hence, one of the common methods used to determine wettability is the contact angle method, which assesses the ability of a liquid to spread on a surface. A small droplet of a selected fluid, such as water, with size in the capillary length range (<=1mm radius), is placed on the material surface and the internal droplet contact angle at the liquid/vapor/material interface is measured. When a liquid droplet is placed on a surface, it will

spread according to interfacial surface tension. The sum of the interfacial tensions for a perfectly smooth surface is given by Young's equation [294],

$$\gamma_{sv} - \gamma_{sl} - \gamma_{lv} \cos\theta = 0 \quad (11)$$

where  $\gamma_{sv}$ ,  $\gamma_{sl}$  and  $\gamma_{lv}$  represent surface free energy at solid-vapor, solid-liquid and liquid-vapor interfaces, respectively. Another method that is used to determine surface energy is the Wilhelmy method, discussed in Chapter 4. Equation (11) can also be written in terms of the dispersive and polar intermolecular components of the surface free energy [295],

$$\gamma_l(1 + \cos\theta) = 2\left(\sqrt{\gamma_l^d \gamma_s^d} + \sqrt{\gamma_l^p \gamma_s^p}\right) \quad (12)$$

where  $\gamma_l$  and  $\gamma_s$  represent liquid and solid surface free energy. The effect of the dispersive (van der Waals) and polar (acid-base) interactions depend on the wettability of the surface, with hydrophobic predominately dispersive and hydrophilic predominantly polar [292]. Ultrapure water with free surface energy of 72.8 mJ/m<sup>2</sup> has a dispersive component of 21.8 mJ/m<sup>2</sup> and a polar component of 51.0 mJ/m<sup>2</sup> [295, 296]. Experiments have suggested that molecular interactions are dictated by the dispersive component of the surface energy [295] and the polar component plays a role in cell adhesion [50]. For liquids, this energy takes the form of surface tension. Typical surface tension values for water and blood are presented on Table 2-9. It is interesting to note the low sensitivity of water surface tension to temperature. Even at 60°C it only drops to 66.2 dyn/cm [51]. Since water makes approximately 50% of blood, it can be expected that the surface tension for the plasma and whole blood at 37°C will not be significantly different from that at 20°C.

**Table 2-9. Typical surface tension values. Adapted from [51, 58, 297].**

Liquid	Surface tension, $\gamma$ (dyn/cm)
Water	72.8 (20°C), 70 (37°C)
Blood plasma	50.0-56.2 (20°C)
Whole blood	55.5-61.2 (20°C)

1 dyn/cm = 1 mN/m = 1 mJ/m<sup>2</sup>

Materials with low surface energy or that result in a negative Gibbs free energy at the solid-fluid interface, thermodynamically favor protein adsorption [175]. Thus, it has long been established that in general increasing hydrophobicity on polymeric surfaces increases protein adsorption but minimizes blood activation, while increasing hydrophilicity has the opposite effect [292]. Some of the most common polymers such as poly-tetra-fluoro-ethylene [298] and coatings such as diamond-like coatings [299] are based on this principle. Although it is generally true that materials with the lowest critical surface energy reduce adhesion and platelet shape change [300], the interactions are much more complex and hence results can be contradictory. Equilibrium between hydrophobic and hydrophilic properties is usually desirable. However, the right combination is still illusive. Simulation studies have suggested that even hydrophilic surfaces can show properties generally associated with hydrophobic surfaces [301].

When the surface is rough, a roughness factor can be incorporated into the above equations as roughness influences contact angle [302]. Taking the roughness factor into account suggests that roughness enhances hydrophobicity [303, 304]. However, it has also been suggested that based on the equation, roughness enhances hydrophobicity only if the initial contact angle of the material is above  $90^\circ$  ( $\theta > 90^\circ$ ) but otherwise it enhances hydrophilicity [305]. This may depend on the material as it has also been found that commercially pure titanium contact angles increased with roughness for  $\theta > 45^\circ$  and decreased with roughness for  $\theta < 45^\circ$  [306]. While Ti-6Al-4V followed similar contact angle increases with roughness for  $\theta > 45^\circ$ , it did not show sensitivity to roughness change for  $\theta < 45^\circ$  [306]. An increase in hydrophobicity and decreased cell adhesion was previously observed with patterned titanium surfaces [50]. It should be noted that although wettability is generally accepted as an indicator of surface adhesion tendencies, it lacks details on the microscale solid-liquid interfacial interactions [307] and hence some of the difficulty remains in using it to accurately predict surface adhesion.

#### **2.4.5 Electrochemistry**

Biomaterial electrochemical properties are important parameters that influence material biocompatibility. The electrochemical nature of the biomaterial determines the chemical stability of the material surface and hence its susceptibility to react with an electrolytic fluid, such as blood. The susceptibility to reaction is related to susceptibility to corrosion. Previous studies, using cyclic voltammetry [308] and anodic polarization of nitinol and Ti-6Al-4V [282], have shown that Ti-6Al-

4V has better corrosion resistance than nitinol. Electrochemical properties have been shown to influence cytokine production in soft tissue [309], platelet and thrombus formation on stent surfaces of other types of biomaterials [310]. For investigation of acute blood-biomaterial interactions, this test can be used to determine the stability of the TiO<sub>2</sub> surface layer on the material samples.

#### 2.4.6 Summary

The interaction of biomaterial surfaces with proteins results in conformational change, adsorption and binding sequence exposure on proteins such as complement and fibrinogen. While this fact is known, it remains unclear whether specific biomaterial characteristics induce specific spatial orientation on binding sequences that in turn influence cell adhesion patterns. It is also not clear if flow conditions induce different conformational change or enhance binding sequence exposure. The dynamics of protein conformational change and cell activation and adhesion need further investigation. Material characteristics and their broad implications in blood-biomaterial interaction can be summarized as in Table 2-10. Their subtle synergistic influence on thrombogenicity is not well understood.

Clearly biomaterial characteristics augmented by flow influence blood activation and function at macro as well as molecular and cellular levels. The multiscale interactions between these complex systems compound the problem of discerning the mechanism of influence between the countless variables. Therefore, the fundamentals of blood-biomaterial interaction under flow conditions needs further scrutiny. Perhaps a different approach may be necessary at this point.

**Table 2-10. Surface characteristics and their broad implications**

<b>Surface property</b>	<b>Implications</b>
Surface chemistry	Influences surface water structure and protein conformational change
Surface charge	Attraction or repulsion. Facilitates enzyme activity
Surface energy	Influences surface water structure, protein adsorption, cell adhesion
Surface morphology	Influences surface energy, adsorption/adhesion strength Can influence fluid retention and flow at surface

## **2.5 The case for a systems approach in blood-biomaterial studies**

A variety of organizational and physical constructs, whether natural or engineered, form systems and in some cases a system of systems. These include social systems, engineering systems, as well as biological systems. Examples of these systems include healthcare systems, defense systems and the human body. One common feature between these systems is that they are complex. They embody characteristics that define complex systems; i.e. nonlinear, adaptive, dynamic, compensatory and where small perturbations can have large consequences. For the systems to achieve their goal, there are underlying functional characteristics/properties, such as collaboration, cooperation, etc. that determine the interaction between the system elements. To understand the driving force behind a particular system's behavior requires a systems approach. The fundamental thinking behind a systems approach is to understand how the behavior or properties of a complex system emanates from the interactions of the fundamental components of the system or system of systems. While engineering systems have often applied a systems approach in analyzing system input, control and output parameters, biological systems operate under similar principles and hence a systems thinking is equally applicable. The human body, which can be viewed as a system of systems, is composed of some of the systems that are of particular interest in this research, specifically the coronary systems, as previously discussed.

The purpose of this section is to examine the relevance of systems approach in blood-biomaterial interaction studies, with particular emphasis on the coronary system and the use of a systems approach in designing an *in vitro* model. General representations of the system interactions are proposed and form the basis of a systems approach framework proposal.

### **2.5.1 The biological tripartite**

The tripartite interaction between blood components, flow and blood vessel endothelial cell walls has long been represented by the Virchow's triad [311]. In view of the role played by medical devices, the triad has also been adapted to reflect this fact by including biomaterials [4]. The broad description of a systems perspective in sections 2.2 through 2.4 highlights the key roles played by the major system of systems pillars – blood system, fluidics system and biomaterials system. This two-dimensional tripartite interaction can be referred to as the blood-biomaterial interaction triad (BBIT). However, with the introduction of biomaterials, the BBIT may not sufficiently represent the interactions *in vivo*. A more general representation of the interactions between all the systems would be a blood-biomaterial interaction pyramid (BBIP) or more appropriately the blood-biomaterial

interaction triad of triads (BBITT or BBIT<sup>2</sup>), Figure 2-16. The acronym for this interaction could also be based on the four vertices of the blood-biomaterial-flow-geometry (BBFG) pyramid.

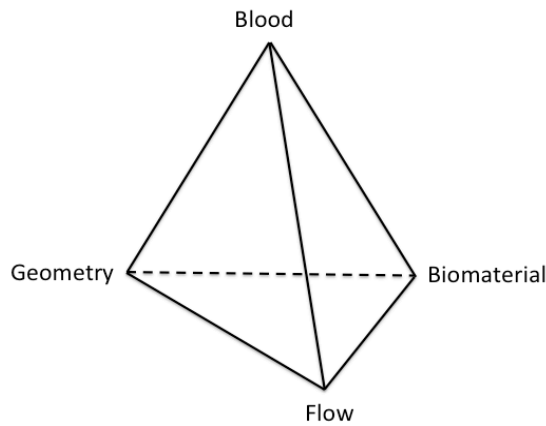


**Figure 2-16. Schematic representation of the blood-biomaterial interaction triads (BBITs)**

The BBITs or BBFG representation emphasizes the fact that even in the case of *in vitro* investigations where the interest is in the blood-biomaterial-flow triad, geometry still plays an important role. In vascular geometry, there are some differences in arterial, venous and microcirculation, which influence subsequent mechanisms involved in the development of thrombosis. Hence, there is a need to distinctly identify the role of geometry. Moreover, even for a biomaterial, the geometry of the device plays a distinct role compared to the surface characteristics. For that reason, the BBITs representation remains valid for *in vitro* investigations. It is inherently understood that all the interactions will vary with time and therefore the time dimension has not been included in the BBITs representation. Thus, the proposed BBITs should provide an improved high-level representation of the interactions between the various systems, without including the embodied complexities.

### **2.5.2 Blood-biomaterial interaction cube**

The interaction of blood with biomaterials occurs at various multiscale levels, both organizational/dimensional as well as time scales. The purpose of the proposed blood-biomaterial interaction triads (BBITs) is to provide a high level understanding of the interactions between various systems. However, it is also necessary to understand the system interaction mechanisms at various length-scale or organizational complexity levels of the system. The length-scale levels can usually be

broken down from the organism down to the basic atom. For the purpose of this research, the basic level of the atom is understood and the levels are grouped into molecular, cellular, tissue, organ and organism level. The organ and organism levels are listed for completeness, but are assumed to exist for the other levels to exist and therefore are not specifically discussed. Therefore, only the molecular, cellular and tissue levels are relevant for blood-biomaterial interactions. In addition, the interaction time-scales between parameters are not specifically discussed but need to be considered and understood as they depend on the organizational level as well as the specific system.

A representation that includes the first level complexities of the system, i.e. depicting primary level characteristics of each system that facilitate the various interactions is necessary. To do that, the BBITs is represented in a different form applicable to *in vitro* models. First the flow and geometry are combined to form the fluidics system. The BBITs representation is then extended to a 3-dimensional cube, similar to the Rubik's cube, to conjure the complex interactions between system components/elements, Figure 2-17. It is important to highlight the fact that using a systems approach, some of the fundamental components, such as the role of water, can be included. Water plays a vital role in blood-biomaterial interaction and without this understanding a big piece of the biocompatibility puzzle is missing [292].

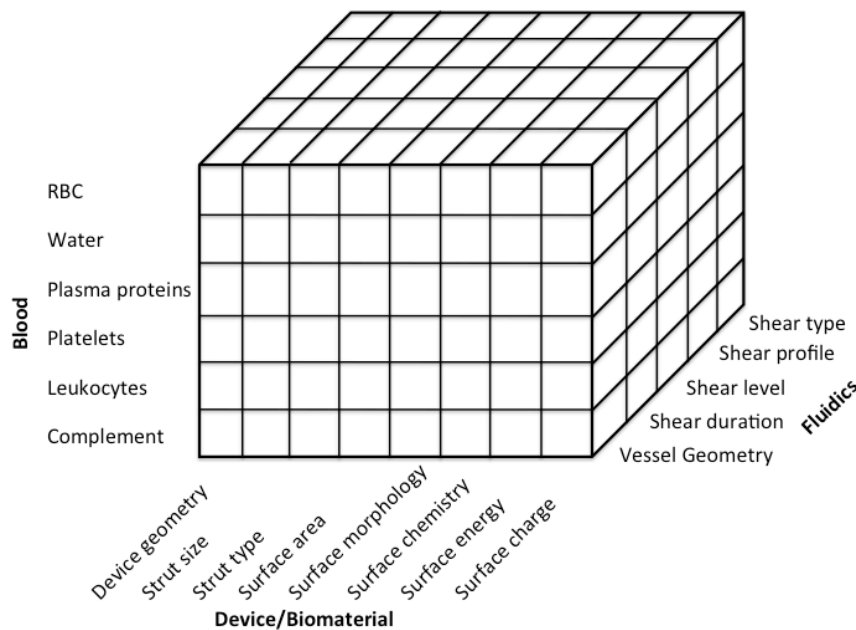


**Figure 2-17. 3-dimensional representation of the blood-biomaterial interaction framework**

Clearly the cube representation brings to the fore the complexity embodied in blood-biomaterial interactions and the fact that the solution for the key to the holy grail is buried in the vast number of combinations. It also gives a much better visual representation that immediately shows the possible system permutations. In a fully developed framework, the interaction permutations would have weighting functions that can be used to indicate the relevance of each element in a particular investigation. For the purpose of this work, it is sufficient to show only the permutations. Since currently there is no consistent framework to apply a systems approach, the proposed blood-biomaterial interaction cube (BBIC) provides the initial work towards developing such a framework. Furthermore, the modes of interactions need to be understood.

### **2.5.3 The SAXSA sequence**

Since the broad relationship between the various systems as represented by the BBITs and the framework parameters that facilitate interactions as represented by the BBIC are understood, it is now important to understand the mode of interaction. Thus, it is necessary to develop another framework representation level that deals with the interactions between the various systems. For the interactions to occur, one or more of the interactions has to initiate the process, i.e. act as the stimulus. The purpose of the stimulus is to activate the system, i.e. to initiate a system response, regardless of whether it is intentional. The activated system subsequently expresses specific proteins for specific activity or function. For the proteins to carry out the intended activity, there has to be an element of stability built in or facilitated by co-factors. The above description can be presented in a simplified framework in the form of a sequence, Figure 2-18. It should be understood that the sequence is merely a representation as the interactions are not linear. The sequence can be applied to one system or to a system of systems, where the expression or the activity could be inputs to other systems or feedback to the system itself. From the Stimulus, Activation, eXpression, Stability and Activity sequence, the acronym SAXSA is proposed.

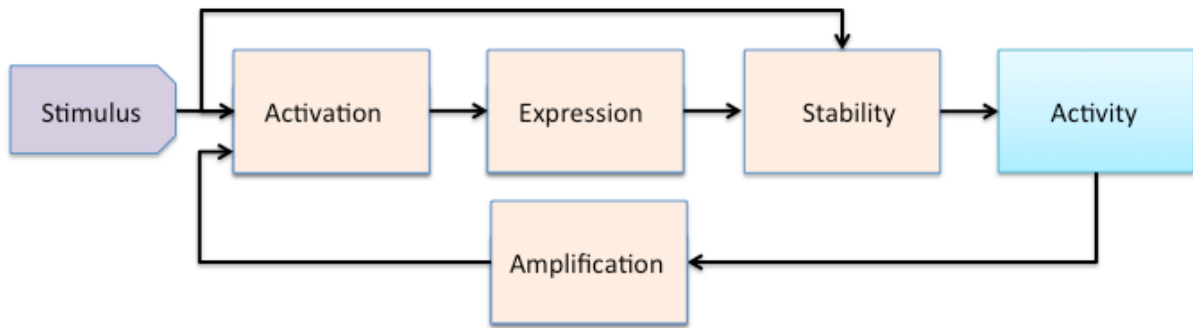


**Figure 2-18. Schematic of the mode of interaction, the SAXSA sequence**

While the broad idea of initiation, propagation and amplification is well known, e.g. in coagulation [148, 226], the SAXSA sequence incorporates important mechanistic information. Hence a closer look at the cube framework and the SAXSA sequence reveals that in order to understand the implications of the interactions, it is necessary to clearly characterize the system, particularly the stimulus, whether it is mechanical shear or biological agonist. This is because the cause and effect relationship is stimulus-dependent. Some stimuli may only effect specific aspects, such as expression, activity or stability. Examples include activation of platelets, leukocytes and complement. As previously described, material bound C3b, which has a short half-life, is stabilized by factor P in order to maintain activity. On leukocytes, the chemoattractant fMLP increases Mac-1 expression without increasing affinity [312] while on the other hand ADP increases Mac-1 affinity without increasing expression [194]. Interestingly, expression with or without function is also observed with platelet microparticle formation. In some cases, there are clear biological reasons for these interactions but in some cases the rationale is unclear or has not been investigated because there is no overall view on the mode of interactions. Therefore, the SAXSA framework is proposed to facilitate characterization of different aspects of the system in order to develop a mechanism for investigating cause and effect in blood-biomaterial interactions.

Further to the SAXSA sequence, system characteristics can be defined in terms of functions at various levels – main and sub functions. Due to the complex interactions, there can be both specific and non-specific effects from each on the overall system behavior. Each function level can then be broken down further into tasks and sub-tasks. The same should be done with interconnections. This way a protein can be mapped out as to what role and pattern it plays in achieving a goal, e.g. coagulation. As an illustration, very rudimentary system properties and the basic effect of their

interactions based on organizational levels are presented on Table 2-11. Thus, each level of the system interactions can be represented by an appropriate framework to facilitate investigations.

**Table 2-11. Basic representation of systems and effect of interaction based on organizational level**

	<b>Property and effect</b>			
<b>Level</b>	<b>Blood system</b>	<b>Biomaterial</b>	<b>Hemodynamics</b>	<b>Geometry</b>
<b>Molecule/ protein</b>	Recognition molecules (e.g. complement, TLR4) <i>(signal transduction, defense, activation, chemotaxis)</i>	Surface chemistry, energy, charge <i>(surface water structure, protein epitope exposure, adsorption)</i>	Microdynamics <i>(interaction, bond mechanics, epitope exposure, act/deactivation)</i>	Adhesion surface
<b>Cell</b>	Leukocytes, platelets <i>(mechano-transduction, adhesion, aggregation, defense)</i>	Surface morphology, surface area <i>(activation, adsorption)</i>	Shear <i>(shear-induced dispersion, activation, lysis)</i>	Cell-surface interaction <i>(flow profile, wall interaction)</i>
<b>Tissue</b>	Rheology <i>(transport medium)</i>	Surface area, device design geometry <i>(aggregation pattern)</i>	Shear (Newtonian vs non-Newtonian) <i>(mass transport, phase separation, wall shear stress)</i>	Flow type <i>(flow profile)</i>

### 2.5.4 Blood-biomaterial interactions and the broader picture

The motivation for the previous discussions was to understand systems relationships, parameters and the modes of interaction that occur in various health and disease states. In disease states, the subsequent motivation is to develop appropriate intervention methods. Therefore, understanding of the system interactions at various complexity levels forms the basis for the

development of mechanism-based clinical intervention methods. They form part of a much bigger picture beyond investigations, which warrants a systems view.

Based on the previous discussions, it is possible to build a typical model of interactions in line with a systems approach, Figure 2-19. The system and its functions are first identified, from which the interactions, can be represented in a schematic; in this case the example is the complement and leukocyte collaboration in identifying and responding to the presence of a foreign body. From this schematic, a typical flow chart type representation can be drawn to show the flow of information or influence. Once this is completed, with additional existing information on kinetics, experimental or mathematical models can be built for further investigation of the interactions. The end result should be understanding of the interactions from an input, control and output point of view as well as the development of intervention methods, such as device or drug delivery. The intervention methods are meant to influence the identified pathway(s) and therefore, they also provide additional input to the system. Hence, analysis of the effect of the intervention methods would also be necessary.

In the simplified representation of the foreign body response to a biomaterial in Figure 2-19, a collaborative and cooperative system approach is assumed. For the most part, this is valid in blood. It is important to establish the type of system because this influences the emergent behavior and the way the system is analyzed. In a collaborative system, one may ignore (without excluding it in the analysis) the conflict parameters, for the most part. In homogenous systems, such as the case of bees, the collaboration/cooperation system behavior can easily be deduced. However, in the case of bacterial quorum-sensing to influence group behavior, complex communication issues can arise [313, 314]. The situation is even much more complex in an inhomogeneous environment of cells and proteins, such as in blood. Sequential decision making to enhance value is no longer straight forward. Although generally collaboration and cooperation are the norm, conflict may arise from self-preservation or opposing goals. How the conflict is resolved remains unclear. What is known is that the desire to preserve the tissue and hence the organism does not always win. This is a systems approach problem since its fundamental premise is that interactions between components determine the system behavior or properties.

While a representation such as this is possible to develop, there still remains the actual work required to understand the fundamental interactions and the kinetics to build a systems approach model. Individual attempts have been made to use a systems approach, but there is no defined framework that provides guidance and building block for all researchers.

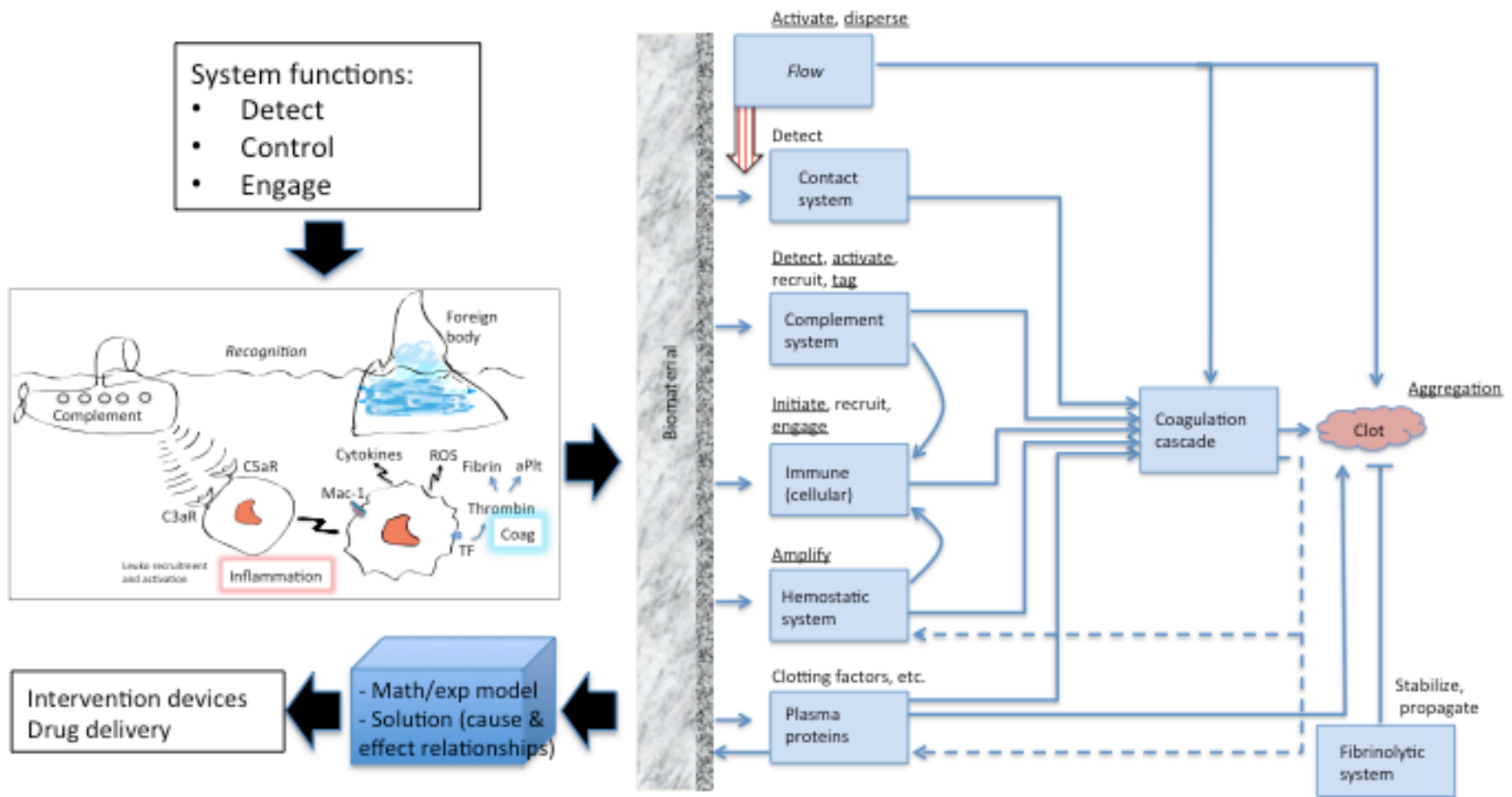


Figure 2-19. Schematic of systems approach based on immune system

### 2.5.5 A systems approach framework

As previously discussed and illustrated, the interaction of biological systems with implants involves a combination of complex interconnected and overlapping pathways. To understand such complex systems, it is often necessary to apply a holistic or systems approach. While systems approach methods have been previously applied to the blood coagulation system, there has been limited discussion in the context of biomaterial interactions. A systems approach compels researchers to appropriately characterize the system or subsystem of interest, their mode of control and input and output parameters. This provides a structured framework, which facilitates application of simulation methods used in complex systems. It also facilitates design of *in vitro* experiments in the context of their relevance for evaluating specific system functions or tasks. Therefore, building on previous work, a high-level breakdown of the blood-biomaterial interaction system into subsystems that are relevant for *in vitro* studies is examined. It should be noted that this approach is also applicable for numerical models. The use of systems methods in blood-biomaterial studies is proposed not only to facilitate understanding of subsystem interactions but to also assist in examining subtle system factors that may not be obvious when looking at bulk measurements.

In cell biology, intracellular pathways have been extensively studied in various specializations such as pharmacology, molecular cell biology and biochemistry. In recent years, there have been numerous initiatives to apply systems thinking to understand and characterize these biochemical networks and their interactions [315, 316]. Due to the complexity of the systems (multiscale organization, network interconnections, spatial and time dimensions), qualitative descriptions are not sufficient to explain the interaction kinetics. Therefore, quantitative analysis and description of these interaction kinetics have applied engineering and mathematical principles, such as network analysis and differential equations. These in turn are amenable to the application of computer simulations, which are excellent research tools to validate experiments but can also be used for deciding specific interventional tools, such as drug delivery and kinetics of control. From these initiatives has emerged the field of systems biology, which deals with how molecular interactions form building blocks for cellular operation that form physiological function. Blood-biomaterial interactions involve the same biochemical networks, except with an added level of complexity due to the presence of biomaterials. Therefore, this provides the impetus for a case for a systems approach in blood-biomaterial interaction studies.

The need for systems approach in blood-biomaterial studies due to the complex nature of the interactions has previously been identified [11] and the complexity of blood-biomaterial interactions has been previously highlighted by other researchers [7, 14]. A schematic representation of extracellular signals and interactions between cell-cell, cell-shear and between cells-milieu of cascades around the biomaterial was presented on Figure 2-14. Numerous experiments have investigated the co-relation between biomaterial characteristics and blood activation parameters. While these are invaluable in establishing the network pathways, they cannot provide sufficient information that describes the true interactions in whole blood. To that end, there has been use of a holistic approach by using whole blood and investigating several parameters simultaneously [317] and cytokine profiling *in vivo* [309, 318]. The number of dynamic variables in such holistic approach studies makes it difficult to analyze and understand without systems analysis, especially if they are coupled with intracellular interactions.

There have already been studies that employed a systems approach to understand the coagulation system [12, 13, 319]. Since the coagulation system plays a central role in thrombosis, these studies provide an invaluable stepping stone for the adoption and application of a systems approach in blood-biomaterial studies. What is required is a methodology framework that through consensus can be adopted and refined with time, as guidance for blood biomaterial studies. The fundamental principles of a systems approach as it applies to blood-biomaterial studies needs to be defined. To start the work towards this initiative, a systems approach illustration is proposed. An example with the design of an *in vitro* model is provided.

Based on the above discussions and previous subsections, the overall systems approach framework is presented as a flowchart representation where all the data is integrated to design an appropriate model. This is because one of the features of this framework is the requirement to mimic the physiological location of interest. The framework is depicted in Figure 2-20. For the framework to be useful, there is need for reference simulation models and data that has been validated so that other researchers do not have to reinvent the wheel. The development of reference data requires concerted efforts in standardization of protocols [320]. For simulation models, the Cardiac Physiome Project, whose progress and challenges are reviewed elsewhere [321], provides an excellent example. The development of a data repository provides a mechanism for data improvement through constant update. It also provides an invaluable tool for data mining research. There are also several online databases and some of the well known examples of the reference data that are useful to other

researches are the genome and proteomics databases. The development of a database on material treatment methods and characteristics is crucial for the framework.

The other important aspect of the framework is the need for comprehensive indicators for specific investigations under specific conditions. Generally known indicators are used for most investigations but there has been evidence that some markers vary with physiological conditions. For example, although C-reactive protein (CRP) levels after stent implantation have been reported to be higher for bare-metal stents compared to drug-eluting stents [322], CRP has also been found to be a predictor of in-stent thrombosis for drug-eluting stents [323]. Also the case of only C5a correlating with implantation of drug-eluting stents, and C3a correlated with development of in-stent thrombosis, while both correlated with late lumen loss [88]. In addition, to facilitate translation of results, it is important to include clinical biomarkers such as cell count and hematocrit. Review of current evidence suggests they are risk factors for coronary heart diseases [324]. Leukocyte cell count in particular has been shown to be independently associated with mortality [325, 326]. Therefore, how they correlate with biomaterial response would be informative. In particular, profiling cell sub-populations as opposed to bulk investigation would be beneficial. These issues point to the need to develop methods-based biomarkers. Thus, the use of a systems approach framework will go a long way in not only unraveling the much sought after causation relationship between material properties and biochemical pathways, but in standardizing investigations and comparison of results.

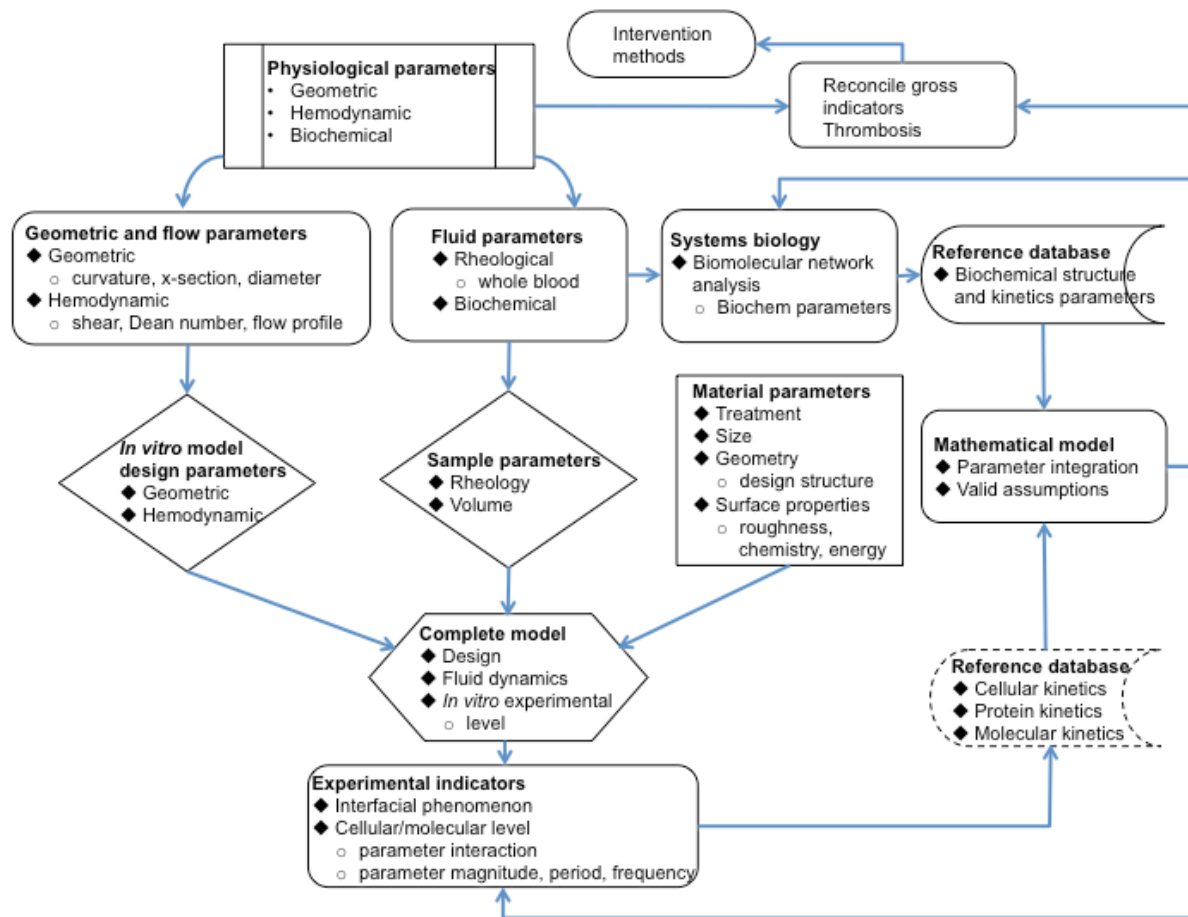


**Figure 2-20. Schematic of the systems approach framework**

### 2.5.5.1 Applying the framework principles to *in vitro* model design parameters

*In vitro* models form the cornerstone of investigations for research and development. Therefore, in designing an *in vitro* model, the aim is to mimic the physiological location of interest and the intended implant application. Hence, the design of an *in vitro* model, by its very nature requires a reductionism approach since the *in vivo* system cannot be duplicated. The problem then becomes how does one identify the key systems or components to preserve for experimental or mathematical modeling. Based on the previous discussion and the framework, the following general design methodology can be applied, Figure 2-21.

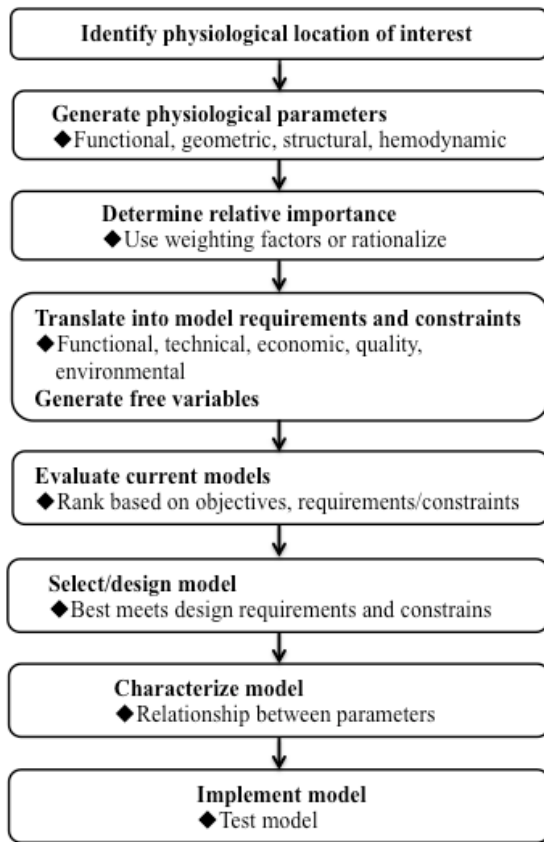


**Figure 2-21. *In vitro* model design flowchart**

The general methodology can be applied for model stent design as well. Ideally the minimum physiological parameters and key end-use implant characteristics, in the case of model stents, would be standardized on a reference database. Based on the above procedure, the initial rationalization of parameters is developed, as presented on Table 2-12. It should be noted that the multiscale interaction levels as discussed before are understood and taken into account in detailed design. Where there are no weighting functions to provide a quantitative mechanism to validate the rationalization decision, the overriding factor to mimic the PLOI is used. This rationalization of parameters forms the basis for subsequent development of detailed design parameters. One of the essential applications of a systems approach as discussed under the SAXSA sequence is appropriate characterization of the stimulus as this forms the input to the system. The system input is one of the key determinants of the system output. Hence, understanding its characteristics is vital. In the case of an *in vitro* model, the stimulus is the flow shear and the biomaterial under study. This is applied in the detailed design of the model

as discussed in Chapter 3. Even though the information below indicates all material and flow parameters are included, the cellular transport dynamics at the material surface is not addressed thoroughly by the bulk flow model. Only multiscale modeling would address that level of interaction.

**Table 2-12. Rationalization of *in vitro* model parameters**

<b>Property</b>	<b>Parameters</b>	<b><i>In vitro</i> parameters</b>	<b>Rationale</b>
<b>Geometry</b>	Curved -curvature ratio, Dean number Diameter	Curved tube and diameter mimic physiology	Curvature and diameter influence flow characteristics
<b>Flow</b>	Shear stress -duration, level, frequency, pulse width, time-averaged	All included under steady flow	All important <i>in vivo</i> , not only duration and level. Mimic <i>in vivo</i> as close as possible
<b>Material surface</b>	Surface morphology -indent vs protrusion -multiscale vs homogeneous Surface chemistry, energy, electrostatics	All considered	Important in blood activation
<b>Stent</b>	Length Diameter Surface area Structural design	All included + surface area-to-volume ratio	All influence flow, e.g. friction, and blood activation
<b>Rheology</b>	Whole blood vs plasma Newtonian vs non-Newtonian	Whole blood, Newtonian	Holistic approach, Newtonian acceptable in arteries

### 2.5.6 Summary

In this section, the case for applying a systems approach in blood-biomaterial interaction studies was presented. Some of the important aspect of a systems approach such as methods-based

indicators, standardized tests and rationalization of parameters [14], multi-parameter profiling [327] and a repository database for blood-biomaterial interaction studies were highlighted. More importantly, representative models of system interactions and the systems approach framework were proposed. However, there is still work to be done.

To develop a comprehensive systems approach framework, it is also necessary to incorporate a number of disciplines such as chaos theory. Although chaos theory stems from mathematics, its concept of the “butterfly effect” is relevant to biological systems. A small perturbation can result in large system changes over time as it propagates through the system. There is already some evidence of this in the feedback loops in some of the biochemical pathways, which are triggered by low levels of substrate-enzyme but amplified through cyclic positive feedback loops. Also the issues raised in bacterial quorum-sensing studies and reviews [313, 314], such as system noise and the integration of signals, raise some interesting questions that are relevant to blood-biomaterial interactions. Is there any prioritization to signal response and does it have effect on outcome? Are certain stimuli more likely to cause noise? Similar studies may be necessary in blood-biomaterial studies to elucidate cell communication strategies.

Clearly a concerted effort is necessary [320], such as the one that has seen the development of systems biology. At the organizational level, there is need to develop a collaboration model for the various disciplines involved in this problem. The current model of learning from each other without a defined collaboration model is not feasible to produce a holistic approach to this problem.

## **2.6 Conclusion**

In this chapter, the relationships between the various systems involved in blood-biomaterial interactions were presented. Some literature review was presented and pertinent issues related to a continued search to resolve the issue of material-induced thrombogenicity were highlighted. The case for a systems approach was presented and a systems approach framework was proposed. Subsequently, an illustration to apply the systems methodology to determine design parameters for an *in vitro* model was presented. A comprehensive systems approach will require concerted effort and therefore a collaboration model is also necessary. This chapter has presented information to support and demonstrate the significance of a systems approach in blood-biomaterial studies. A thorough development of this concept is necessary.

## Chapter 3

### A Systems Approach to *In Vitro* Model Design

#### 3.1 Introduction

*In vitro* models are mockup devices used to study complex biological systems. They play an important role in the investigation of complex biological systems because they are cheaper, easily controllable and provide more reproducible results compared to clinical and animal studies. Over the years, numerous static and flow models have been developed and used to investigate a variety of biological system interactions such as cell-cell/molecule interactions, blood-biomaterial interactions or the effect of flow shear stress on blood activation [15-17, 272, 328-330]. While static models are used to investigate material-induced biochemical processes, flow models, which are more physiologically relevant, incorporate the effect of flow in addition to biomaterials. Hence, their design is more elaborate since the incorporation of flow requires consideration of geometry and other factors. Geometry is particularly important because it affects flow parameters. A typical illustrative example of the effect of geometry on flow is the comparison of the average velocity between a cylindrical tube and a rectangular tube, which is half of the maximum velocity and two-thirds of the maximum velocity, respectively [331]. A relevant physiological example is the evidence of complex flow and low shear stress at curvatures and bifurcations [61, 234]. Nonetheless, *in vitro* models simulating flow in blood vessels have come in various configurations, such as straight circular tube flow [332], curved circular tube [15, 333], idealized stenotic coronary artery [334], rotating disc [17], cone and disc [329] and rectangular channel [335]. While some of the configurations may be useful in investigating specific fluid dynamics aspects, translation of the results to physiological relevance encounters some difficulties.

However, there are also models that have taken into consideration some of the geometrical parameters of the physiological location of interest they are designed to mimic. These include the orifice plate and chamber which mimics the heart valve flow [336] and the Chandler loop which mimics blood flow in curved arteries [15]. While *in vitro* models, regardless of the design geometry, have known limitations [337], they have contributed and continue to contribute tremendous knowledge to the understanding of blood rheology, blood interaction with biomaterials or immobilized molecules and biomaterial interaction with tissue. They also provide an invaluable tool for validating computer simulation models. The existence of limitations means that closer attention

needs to be paid to the models design, starting with the fundamental properties and not merely the gross requirement for flow. Hence, it is necessary to apply a systems approach when designing *in vitro* flow models.

From a systems perspective, the *in vitro* model is equivalent to the fluidics system discussed in Chapter 2 and therefore should ideally mimic this complex physiological system. For that reason, it is important that the model geometric and hemodynamic design parameters closely mimic the physiological location of interest (PLOI). Geometric characteristics, in particular, have a major impact on hemodynamics and localization of atherosclerotic lesions *in vivo* [61, 62, 250, 338], regardless of whether the influencing mechanism is from other cardiac pathologies or within the coronary arteries [237]. One of the key geometric features that influence a variety of flow parameters is curvature and/or curvature ratio. Curvature influences the skewing of the axial velocity profile [258], induction of centrifugal force-driven secondary flow vortices [258], the pressure gradient across the tube diameter and hence fluid friction [258] and axial pressure loss [260]. While other flow parameters are equally important, the dimensionless Dean number is often used to characterize the effect of curvature on hemodynamics [259]. Therefore, one cannot describe the fluid mechanics of coronary studies without including or recognizing the effect of the Dean number.

The key hemodynamic parameter that is linked to the *in vivo* localization of lesions as well as *in vitro* cell-wall interactions is wall shear stress (WSS). Fluid shear stress influences near wall transport phenomenon [56, 57] and consequently influences platelet dispersion [149, 339] and adhesion [247], platelet interaction with tissue factor [249], as well as monocytic cell [332] and neutrophil [334] adhesion. More importantly, shear stress has been shown to have some correlation with in-stent thrombosis [257]. Hence, it is an important parameter in blood-biomaterial interaction studies. While shear stress/rate can be produced with various geometries, other hemodynamic parameters such as the flow pattern or velocity profile depend on the geometry. Hence, the geometric and hemodynamic factors need to be taken into account in determining the appropriate *in vitro* model for this research.

Therefore, the objective of this work was to design or select an appropriate *in vitro* blood flow model that mimicked the physiological location of interest for this research using a system approach. It was hypothesized that *in vitro* flow model parameters mimicking physiological location of interest are better designed following a system approach and that blood sample volume influences flow dynamics and hence wall shear stress. Hence, specifically, this chapter describes the process that

was followed to, (a) evaluate existing *in vitro* flow models and select the appropriate model, (b) determine model design parameters, (c) analyze the model fluid mechanics and (d) implement the model.

### **3.2 *In vitro* flow model selection**

As highlighted above, the design or selection of a model needs closer attention as it already provides a limited representation of a biological system. Hence, it is necessary to follow a systematic procedure as highlighted on Figure 2-21, Chapter 2.

#### **3.2.1 Materials and methods**

##### **3.2.1.1 Physiological location of interest (PLOI) and parameters**

The main question was how to establishing the design requirements for *in vitro* model that mimics the PLOI for systems approach experimental investigations. The PLOI for this research was the coronary arteries, more precisely the left anterior descending (LAD). Some details of coronary arterial system were discussed in Chapter 2. In this section, the main physiological parameters are summarized, Table 3-1. The relative importance of each parameter in *in vitro* model design varies with the objective of the design or the specific study. For this work, the objective was to design or select an *in vitro* flow model appropriate for coronary flow studies. The functional parameters were considered in terms of the need for flow. Here they are stated in terms of the systolic pressure, which drives flow in the coronary arteries, and the heart rate. While flow requires pressure, the specific driving pressure was considered less important as different mechanisms could be used to generate flow. Regarding the structural parameters, it has been previously suggested that the error in using fixed geometry is reasonably small, comparable to the assumption of rigid vessel wall and Newtonian rheology [261]. This suggests fixed geometry could be used within reasonable error. Hence, the structural parameters were not considered important for this research. On the other hand, both the geometric and hemodynamics parameters are considered very important as previously discussed in Chapter 2, and therefore critical in determining model parameters.

Some of the important geometric parameters for the coronary system are the heart curvature and vessel tortuosity [228, 237], and vessel bifurcation and diameter [229, 340]. Hence, curvature, vessel radius and lumen cross-sectional shape are key physiological geometric parameters. Since curvature is a critical property of the coronary arteries, the corresponding curved flow is equally

important. The effect of curvature on hemodynamics is predominantly characterizes by the Dean number [259]. The other important hemodynamic parameters of interest included the velocity profile, Reynolds number and shear stress. Shear stress is particularly a critical parameter because of its role in atherosclerosis and thrombosis [250, 338, 341], blood coagulation [149] and material induced thrombosis [257]. *In vitro* models used to study coronary flow should ideally take into account the parameters listed on Table 3-1. Although both the geometric and hemodynamic parameters vary dynamically (spatial and time) due to the pulsatile nature of myocardial contraction, nominal values can be adopted as previously discussed.

**Table 3-1. Physiological parameters. NB: ranges of physiological parameters may vary slightly, depending on the quoted study.**

Parameter type	PLOI	Parameter
<b>Functional</b>	Coronary arteries	Maintain flow at 80 mmHg, 1 Hz
<b>Structural</b>	Coronary arteries <ul style="list-style-type: none"> <li>• Elastin</li> <li>• Collagen</li> <li>• Smooth muscle</li> </ul>	E = 0.1 MPa, viscoelastic, anisotropic [51] E = 0.3 MPa [51] E = 100 MPa [51] E = 0.1-0.2 MPa [51]
<b>Geometric</b>	Heart  LAD	Radius of curvature = 42.8 mm [238], 56.3 mm [237]  Diameter = 3.7±0.5 mm [229]  Curvature ratio = 0.02-0.5 [261]  Lumen X-section: circular [342]
<b>Hemodynamic</b>	LAD	Velocity = 10.6-43.0 cm/s [229]  Dean number = 22.9 [331]  Reynolds No. =100-217 [229]  Shear rate = 100-1000 s <sup>-1</sup> [52]

E: Young's modulus

### 3.2.1.2 Model requirements and constraints

Based on the above discussion, the *in vitro* model requirements and constraints are as listed in Table 3-2. The flow and geometric parameters are important in the design of *in vitro* models design [320]. The functional need for whole blood is in line with the systems approach. The free variable was the operating temperature.

**Table 3-2. Model requirements and constraints**

Requirement/constraint	Parameter/property
Functional	Must have curved flow and use whole blood
Technical	Shear rate = 100-1200 s <sup>-1</sup> Velocity = 10-43 cm/s Flow tube diameter < 5 mm Curvature radius 40-60 mm Circular x-section flow tube Blood sample < 10 ml
Quality	Flow tube must be medical grade
Economic	Low operating cost

### 3.2.1.3 Model analysis/evaluation

Although a number of flow models have been used for coronary flow studies, some of them are variations of the three commonly used models; cone and plate, parallel plate flow chamber and Chandler loop model. Hence, the evaluation to select an appropriate model for this research was based on these three models. The evaluation was based on information from section 3.2.1.2 and the models' theoretical operating principles. The selection was based on meeting the

stated design requirements/constraints and the ability to mimic PLOI parameters. Because of the manageable number of parameters, it was not necessary to develop extensive ranking criteria.

#### 3.2.1.3.1 Cone-and-plate model

This model is used to apply shear by a circulating cone on a flat plate [329]. A schematic of the cone-and-plate model is depicted on Figure 3-1. This model and modified versions [343, 344] are often used to investigate the effect of shear on platelets or immobilized proteins/molecules or cells [343, 344]. While this model is useful for isolating the effect of shear and can generate a wide range of shear rates, it does not mimic physiological geometry and hemodynamic flow conditions. The parameters that influence shear rate are the cone angle and its rotational speed [329]. One interesting feature of this model is its standardized geometry.

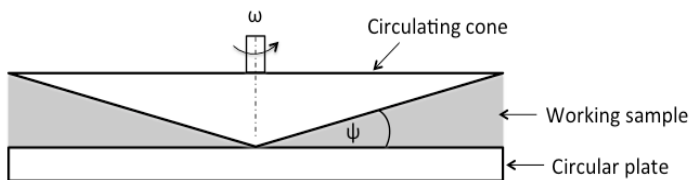


**Figure 3-1. Schematic of the cone-and-plate model**

#### 3.2.1.3.2 Parallel plate flow chamber model

This model is composed of a perfusion pump, flow tube and sample chamber [16]. A schematic of the parallel plate flow chamber model is depicted on Figure 3-2. It has been mostly used to study blood interactions with immobilized proteins or cells [16, 248]. This model uses a tube flow but the sample under study is subjected to plate flow. The model parameters that influence shear rate are the plate separation distance, plate width and flow rate [16].

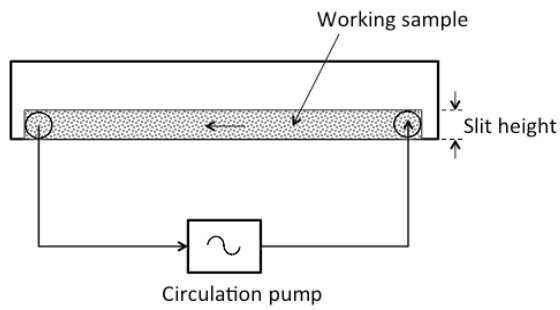


**Figure 3-2. Schematic of the parallel plate chamber model**

### 3.2.1.3.3 Chandler loop model

The Chandler loop model is based on a circular loop configuration. It is composed of a tubing loop on a rotating turntable [15]. A schematic of the Chandler loop model is depicted on Figure 3-3. The circular loop provides curved flow, with a skewed velocity profile and secondary flow pattern [345], similar to that observed at physiological curvatures and bifurcations [331, 346]. This model has been used to study whole blood thrombus formation and blood interaction with immobilized molecules [15, 347-349] as well as stents [26, 27, 350]. Model parameters that influence shear are the loop curvature and tube radius.

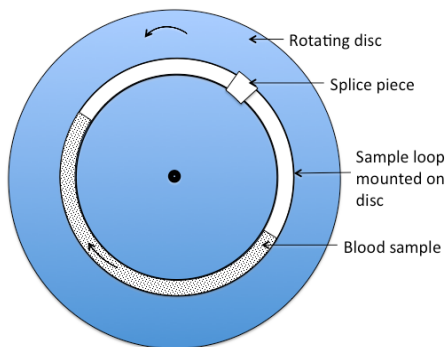


**Figure 3-3. Schematic of the Chandler loop model**

### 3.2.2 Results and discussion

Comparison of the three *in vitro* flow models on the basis of their operating principle shows that they can be used to generate a wide range of shear rates within physiological range, Table 3-3. However, their appropriateness for coronary flow studies is quite diverse. The cone-and-plate model can easily isolate the effect of shear stress and can be used to generate pathologic shear conditions. However, when the model geometry and other hemodynamic factors such as the flow pattern are considered, the model turns out to be inappropriate for this research because it does not meet some of the model requirements/constraints and does not mimic physiological geometry and hemodynamic flow conditions.

For the parallel plate chamber flow model, the use of a plate chamber makes it unsuitable for this research because there is a difference between plate flow and tube flow dynamics, which would influence material deposition kinetics on the surface. Although the plate chamber is commonly used, this model can be adapted by replacing the chamber plate with a rectangular or circular tube. Since it uses a pump, the tube could also be configured to form a loop or curve. Other chamber modifications such as introducing vertical-steps have been used to study the effect of disturbed flow on monocyte dispersion and adhesion [335], neutrophils [351] and whole blood leukocytes [352]. A modified version of the perfusion system can also be used to perform parallel studies and provide pulsatility [353]. The limitation with parallel investigations is that the investigations have to be identical as there is one common pump. This model may offer versatility where the geometry of the chamber or tube needs to be adapted for specific studies. However, it was not selected because of the possibility of platelet activation or sensitization from the perfusion pump, which could affect experimental results. The effect of pumping on platelet activation and hemolysis has also been demonstrated with a roller pump loop model when compared to the Chandler loop [333]. For that reason, it was not considered appropriate for this research.

**Table 3-3. Comparison of three *in vitro* flow models.**

Flow model	Wall shear rate (s <sup>-1</sup> )	Ref	Relevance to physiological conditions
Cone and plate	$\gamma = \frac{\pi\omega}{30\psi}$	[329]	<ul style="list-style-type: none"> <li>• Good for isolating effect of shear on sample</li> <li>• Generates wide range of shear rates, including pathologic</li> <li>• Does not mimic physiological geometry and hemodynamic flow conditions.</li> </ul>
Parallel plate flow chamber	$\gamma = 1.03 \frac{6Q}{ab^2}$	[16]	<ul style="list-style-type: none"> <li>• Active sample pumping makes it possible to study the effect of channel geometry changes, such as stenosis</li> <li>• Generates wide range of shear rates</li> <li>• Plate flow does not mimic physiological geometry and hemodynamic flow conditions</li> </ul>
Chandler loop	$\gamma = \frac{2\pi R_0\omega}{15R}$	[354]	<ul style="list-style-type: none"> <li>• Passive flow makes it difficult to simulate effect of channel geometric changes, such as stenosis</li> <li>• Generates wide range of shear rates within physiological ranges</li> <li>• Curved tube flow mimics physiological coronary flow.</li> </ul>

$\gamma$ =wall shear rate (sec<sup>-1</sup>),  $\omega$ =angular velocity in revolutions per minute (RPM),  $\psi$ =cone angle (radians), Q=volumetric flow rate (ml/sec), a=slit width (cm), b=slit height (cm), R<sub>0</sub>=loop radius, R=tube radius.

The circular loop configuration of the Chandler loop configuration mimics physiological curvature and meets the requirements/constraints. It produces curved flow, with a skewed velocity profile and secondary flow pattern similar to that observed at physiological curvatures, such as coronary vessel curvature resulting from heart curvature, and bifurcations [61, 331]. Hence, it is fitting for *in vitro* coronary blood flow studies. An additional benefit of this model is the ability to study several biomaterials simultaneously [350]. This model has the advantages of simplicity, clinical relevance and ease of modification to mimic desired physiological conditions. It is also referenced in ISO 10993-4 Standard [355]. It may have limitations where pathologically high shear rates are necessary. However, it is suitable for physiological hemodynamic conditions and modified versions have been used to mimic pulsatile flow [333] and coronary pulsatility [356]. For this research, vessel pulsatility is not included as it has been shown to have limited error implications on the wall shear stress [261]. Therefore, the Chandler loop model was considered appropriate for this research. The

determination of specific model parameters and issues regarding their implications on fluid dynamics are discussed in the subsequent sections.

### 3.3 Determining model design parameters

To determine the specific model parameters, previous experiments using the Chandler loop model were reviewed. A great diversity was observed in the range of parameters selected by the investigators [15, 26, 27, 347, 349, 354], but with little guidance on the method used to select the parameters. Therefore, the model requirements and constraints together with parameters of the PLOI were used as a guide to generate the specific model parameters. Thus, in this section, the key physiological parameters considered relevant for any investigation mimicking coronary flow and hence relevant to this research, are determined.

Figure 3-4 a schematic representation of the circulating loop model with model stent. The parameter  $R_0$  is the mean loop radius or radius of curvature,  $2R$  is the tube internal diameter (radius  $R$ ) and  $\omega$  is the loop rotational speed (RPM). Since the error in using a fixed geometry is considered reasonably small [261], the tube and loop radii were held constant in this research. To mimic coronary arteries, a commercially available Silastic silicone circular tube #62999-874 (VWR, PA, USA) with internal diameter of 0.188" (4.775 mm) and external diameter of 0.313" (7.950 mm) was selected. The length of the sample tubes (371 mm) was selected to give a radius of curvature of about 59 mm. One of the consequences of the presence of curvature on flow is the development of centripetal force due to the change in momentum of the flowing liquid. As a result, there exists a centripetal pressure on the outer wall given by equation [51],

$$P = 2\rho v^2 \frac{R}{R_0} \quad (13)$$

where  $\rho$  is fluid density and  $v$  is average flow velocity. Thus, there exists a pressure gradient across the tube. To assess the effect of curvature on the pressure gradient, it has previously been proposed that the design Reynolds number should meet the condition  $R_e < 40\sqrt{R_0/R}$  [357]. This condition may or may not be desired, depending on the experiment. Thus, loop curvature has major implications on the fluid mechanics of the model. In this research, curvature radius is held constant both in space and time while flow is varied.

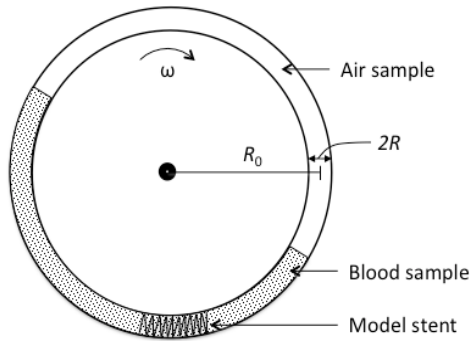


**Figure 3-4. Representation of circulation loop with blood sample and model stent**

Fluid mechanics of the Chandler loop model with fixed curvature have been previously described by Gardner [354]. The model wall shear rate from Gardner's analysis is given by the equation,

$$\gamma_w = \frac{2\pi R_0 \omega}{15R} \quad (14)$$

Besides shear rate, some of the key parameters characterizing steady state flow in a curved circular tube are the curvature ratio, Dean number ( $D_n$ ) and/or Reynolds number [259]. They influence skewing of axial velocity profile, pressure loss and fluid friction [258, 259]. Therefore, these parameters were included to characterize the circulation loop fluid mechanics. Defining the average axial velocity in terms of the angular velocity gives the expression,

$$v = 2\pi\omega R_0 \quad (15)$$

Using previous definitions from Chapter 2, a summary of the important fluid mechanics parameters of the Chandler loop model is presented on Table 3-4.

**Table 3-4. Fluid mechanics equations for the Chandler loop model**

Average velocity	Curvature ratio	Reynolds number	Dean number	Wall shear rate
$v = \frac{\pi R_0 \omega}{30}$	$\kappa = \frac{R}{R_0}$	$R_e = \frac{\pi \rho \omega R_0 R}{15 \mu}$	$D_n = R_e \sqrt{\kappa}$	$\gamma_w = \frac{2 \pi R_0 \omega}{15 R}$

$\rho$  is fluid density,  $R_0$  is loop radius (curvature radius),  $R$  is tube internal radius,  $\mu$  is fluid dynamic viscosity and time is defined in seconds.

Based on the shear rate equation and the selected model geometry, the range of rotational speeds necessary to give the shear rate corresponding to a physiological range is approximately 10-100 RPM. As an example, two rotational speeds (24 and 45 RPM) were selected for comparison purposes, Table 3-5. Unless quoted directly from a reference, some of the data are calculated based on equations in Table 3-4. Considering the rheological properties of blood at the selected shear rates and the model tube size, the blood sample can be assumed to behave as a Newtonian fluid [52]. While this assumption simplifies fluid mechanics and holds the viscosity constant, it does not take away the particle dynamics that occur under shear and hence the need for consideration in analyzing experimental results. Comparison of the model parameters with some of the physiological parameters shows that the choice of experimental parameters was close to the physiological parameters, suggesting that the selected model is reasonably appropriate for LAD flow studies.

**Table 3-5. Comparison of selected model parameters to average physiological LAD parameters**

Parameters		Physiological	Model	
<b>Geometry</b>	Diameter	3.2-4.2 mm [229]	4.78 mm	
	Surface topography	Smooth	Smooth	
	X-sectional profile	Circular	Circular	
	Heart radius of curvature	42.8 mm [238]	59 mm	
	Curvature ratio	0.04-0.05	0.04	
<b>Flow dynamics</b>	Bifurcation/Curvature	Curved tube flow	Curved tube flow	
	Rheology	$\rho=1060 \text{ kgm}^{-3}$ , $\mu=0.003\text{-}0.004 \text{ Pa.s}$ [52]	$\rho=1060 \text{ kgm}^{-3}$ , $\mu=0.0035 \text{ Pa.s}$	
	Velocity: Inlet	10.6-16.6 $\text{cms}^{-1}$ [229]	24 RPM	45 RPM
	Downstream	13.0-43.0 $\text{cms}^{-1}$ [229]	15.5 $\text{cms}^{-1}$	29 $\text{cms}^{-1}$
	Reynolds number (Re)	100-217 [229]	215	402
	Dean number ( $D_n$ )	19-48 *	43	81
	Wall shear rate	100-1000 $\text{s}^{-1}$ [52] (350-1200 $\text{s}^{-1}$ ) [229]	250 $\text{s}^{-1}$	470 $\text{s}^{-1}$
<b>Biochemical</b>		Physiological thrombi	Similar thrombi [347]	

\*Calculated based on other physiological parameters in the table.

### 3.3.1 Discussion

In this section, relevant *in vitro* model parameters were determined based on the physiological location of interest. However, one physiological parameter that is not included above is the dynamic cardiac cycle and pressure pulsatility. As discussed in Chapter 2, cardiac cycle does not only influence the dynamic variation of curvature, but also determines the flow frequency and the vessel diameter. Although the importance of geometric variation with pulsatility on flow has been demonstrated [261, 358], it is important to note that the difference in wall shear stress (WSS) between dynamic and static conditions is heavily dependent on the selected curvature ratio as well as the assumed amplitude of the change of radius of curvature [261]. The difference is small for low curvature ratio and small deformation amplitude change. Hence, it has been suggested that the error in using fixed geometry is reasonably small [261].

Therefore, besides the fact that it is also important to understand flow dynamics at specific geometries, such as at mean geometric values, based on Table 3-5, the effect of curvature variation can be considered small. Hence, fixed geometry was adopted in this research. Model parameters, such as the curvature ratio, were based on mean physiological values. Comparison of the selected model parameters and LAD suggest that model parameters reasonably mimic the physiological location of interest.

Flow pulsatility or frequency on the other hand remains relevant for *in vitro* models because it influences flow parameters even in the absence of vessel geometric variations [359]. For the selected model, the fact that flow is induced by rotation at various angular velocities means some aspect of flow frequency can be mimicked, which raises the question of relevant frequency and volumetric flow rate. Furthermore, the fact that sample volume occupies a portion of the circulation loop raises the question of the appropriateness of the sample volume and its implications on fluid dynamics. Therefore, while the main parameters are as listed on Table 3-5, the issues of frequency and sample volume are important aspects of the model's relevance to physiological flow parameters. The issues concerning fluid dynamics are analyzed further in section 3.4.

### **3.4 Fluid dynamics analysis of the model**

Fluid dynamics influences both vascular response and blood activation kinetics under different *in vitro* and *in vivo* conditions [149, 360, 361]. Understanding flow characteristics is also important in coagulation diagnostic instruments [362]. For that reason, it is essential to appropriately characterize flow for the evaluation of blood-biomaterial interaction in order to enhance interpretation of results. Since the sample volume for the selected model occupies a portion of the circulation loop, it was hypothesized that sample volume has an effect on fluid dynamics and hence blood activation. If that is the case, then the question of what is the appropriate sample volume arises. In addition, how is this volume determined? Review and comparison of previous studies [15, 26, 27, 333, 347, 349, 354] revealed variability in sample volume selection with no guidance on how the sample volumes were selected. Therefore, there was a need to develop a method to determine the appropriate blood sample volume for this model and determine its influence, if any, on the model fluid dynamics.

### 3.4.1 Determination of sample volume

In determining the model hemodynamic parameters, Gardner [354] used a 50% volume fraction and an implicit assumption of sufficient sample volume and fully developed flow was used. Since then, the shear rate equation has been used with different volume fractions under the assumption of fully developed flow but with little validation as to whether this is met. Hence, there has been no guidance on the minimum volume required for this model. Furthermore, the use of this model in the presence of stents has not been accompanied by justification of the selected volume and stent size to meet the ISO 1993 standard for the ratio of material surface area to blood sample volume. This means, such studies may inadvertently violate the standard and hence produce erroneous results. Therefore, there is need to develop a method for determining the minimum sample volume required for *in vitro* experiments, taking into account the entrance length and the surface area-to-volume ratio.

In order to assume fully developed flow, the sample volume must be generally greater than the entrance length, the flow adjustment region where the velocity profile is dependent on both the radial and axial directions and is characterized by high friction [331, 346]. Hence, to perform fluid mechanics analysis of the *in vitro* model under the assumption of fully developed flow conditions, the sample volume must greatly exceed the minimum entrance length requirement. A number of equations have been developed to describe entrance length for laminar and turbulent flow, Table 3-6. Since entrance length is related to the characteristics of the flow, all entrance length correlations depend on the Reynolds number. The extent of the Reynolds number dependence is influenced by the geometry and the type of flow. For example, in a smooth straight tube, the entrance length for steady laminar flow is longer and has high dependence on Re compared to turbulent flow. Similarly, in curved tubes steady flow has longer entrance length than pulsatile flow [363]. The entrance length equation relevant to the *in vitro* model selected for this study is the one for curved flow [364].

**Table 3-6. Entrance length correlations.**  $\chi_{e\theta}$  is in degrees of axial curvature.

Flow type	Tube type	Entrance length	Ref
Steady laminar	Straight	$\chi_e = 0.057R_e D$	[331]
	Curved	$\chi_{e\theta} = 49R_e^{1/3} \sqrt{\frac{R}{R_0}}$	[364]
Steady turbulent	Straight	$\chi_e = 0.693R_e^{1/4} D$	[365]

As stated above, in experiments where biomaterial samples such as model stents are included, the flow model should also satisfy biochemical requirements, in addition to geometric and hemodynamic requirements. To determine the appropriate sample volume for an *in vitro* flow model with a biomaterial sample, a theoretical analysis was performed based on minimum volume requirements. It is necessary for the sample volume to meet two conditions:

- (i) To greatly exceed the fluid flow entrance length
- (ii) To meet the ISO 10993 Standard on the ratio of material surface area-to-volume ratio (0.5-6.0 cm<sup>2</sup>/ml)

To perform analysis for the entrance length condition, assuming Newtonian fluid and a rigid tube wall, the entrance length volume element can be defined in terms of tube diameter as,

$$V_e = \pi \left( \frac{D}{2} \right)^2 \chi D \quad (16)$$

where  $\chi$ , which has been estimated as 3 from previous studies [364], is a multiple of tube diameter,  $D$ . This approximation is valid for nominal  $Re$  in coronary arteries. As observed from Table 3-6, the entrance length for curved tube flow is less dependent on  $Re$  compared to straight tube flow. It is interesting to note that based on a straight tube approximation, the entrance length for the LAD has been estimated as  $3.8 \pm 0.8$  diameters [229].

If the tube volume fraction occupied by the sample is defined by a parameter  $\lambda$  ( $0 < \lambda < 1$ ) as  $\lambda = V/V_0$ , where  $V$  is blood sample volume and  $V_0$  is tube volume, then the entrance length volume fraction condition becomes  $\lambda \gg V_e/V_0$ . To avoid solid body rotation, the tube cannot be full and thus the volume fraction constraint can be expressed as,

$$\delta(V_e/V_0) \leq \lambda \leq C \quad (17)$$

where  $\delta > 1$  is a selected weight factor and  $C$  is less than one and is a function of the angular velocity.

To meet the ISO limits, which require the surface area-to-volume ratio of 0.5-6.0 cm<sup>2</sup>/ml, the volume constraint becomes  $A/6 \leq V \leq 2A$ , where  $A$  is a known model stent surface area in cm<sup>2</sup> and 6 and 2 have units of cm<sup>2</sup>/ml and ml/cm<sup>2</sup>, respectively. Using the  $\lambda$  definition, the ISO constraint can be written as  $A/(6V_0) \leq \lambda \leq 2A/V_0$ . Based upon the above requirements and volume fraction constraints a Chandler loop sample volume fraction (CLSVF) criterion was developed, equation (18),

$$\max\left(\delta \frac{V_e}{V_0}, \frac{A}{6V_0}\right) \leq \lambda \leq \min\left(\frac{2A}{V_0}, C\right) \quad (18)$$

If high angular velocities are used, the limiting value of  $C$  can be evaluated from the meniscus relationship from Gardner [354]. For this research, the limiting value was not evaluated because of the selected angular velocities. To calculate the volume fraction using the CLSVF equation (18), it is necessary to determine  $\delta$ . The other variables can be determined from the model specifications. From Table 3-5,  $V_0=6.64$  ml,  $V_e=0.26$  ml and  $A$  is determined from Table 4-2, depending on the stent size. If  $\delta$  is defined in terms of the stent length normalized by its diameter or radius, this gives a range of  $\lambda$  values. Hence, for the 20 mm and 35 mm stents  $\lambda=0.3$  and 0.6 were selected, respectively. This gives 2 ml and 4 ml as two sample volumes for the blood activation experiments.

Because of the sample surface area and volume relationship, a given surface area will impose a limit on the minimum loop size. Similarly, a given loop tubing size will impose a limit on the maximum sample surface area under study. With regards to the maximum sample volume, there is another factor that needs to be considered – the rotational speed. Once the maximum sample volume is selected accordingly, it will impose limits on the maximum rotational speed to avoid the leading end of the sample spilling over at high rotation. If the maximum rotational speed has been selected as a fixed variable then the volume would be restricted accordingly by the speed.

Thus, the CLSV equation provides a reasonable method for determining blood sample volume for the Chandler loop model, which was not previously addressed in the literature. The other aspect of sample volume that required further investigation was to determine if it had any implications on model flow characteristics.

### 3.4.2 Analysis of the significance of volume

Besides blood sample volume size, the effect of the sample volume on fluid mechanics and blood activation has not been discussed in previous studies. Since the effect is not intuitively clear, further analysis was necessary to elucidate the effect of sample volume in this model.

In the previous section, the appropriateness of the sample volume was addressed by developing the CLSV equation. However, even when the conditions for the appropriate sample volume are met, it still raised the question of whether varying the sample volume within the appropriately defined limits has any significance on the experimental results. Sample volume in previous studies showed variations, but very little discussion on its possible effects on some of the key hemodynamic factors, such as the continuum effect and shear stress, and consequently on blood activation. It is possible that this may have been due to the fact that according to the simplified approximation equation developed by Gardner [354], shear rate does not depend on sample volume. The level of accuracy of this equation has not been evaluated, but the fact that second-order effects have been ignored may introduce some error. More importantly, the shear equation has no dependence on the Dean number, one of the key parameters that characterize curved tube flow. This is particularly important because although the analysis is for a rotating curved tube, only curvature conditions related to centripetal force are included and not rotation conditions related to the Coriolis force. For consistency, analysis and derivation of shear stress approximation in this research are based only on curvature conditions.

To address the question of sample volume effect, a stationary observer, equivalent to an adherent particle or thrombus, in the tube wall will be assumed. For this observer, strictly speaking flow in this model is intermittent since the blood sample occupies only a fraction of the loop. If the characteristic circulation period is  $T = 30/\pi\omega$  seconds, then the fraction of time that the fluid flows over the observer can be represented approximately by a square wave with pulse width  $\lambda T$ , where  $\lambda$  is as previous defined. Since the internal diameter of the tubes falls within the definition of large arteries, Newtonian rheology can be assumed for this model [52]. Hence, the wall shear rate equation (14) can be converted to WSS by using the Newtonian relation  $\tau = \mu\gamma$ , where  $\tau$  is the fluid shear stress,  $\gamma$  is the shear rate of the fluid, and  $\mu$  is blood dynamic viscosity, which gives the shear stress equation,

$$\tau_w = \frac{2\pi R_0 \omega \mu}{15R} \quad (19)$$

This WSS is predominantly on the outer walls of the curved tube. Thus, the square wave is represented on Figure 3-5.

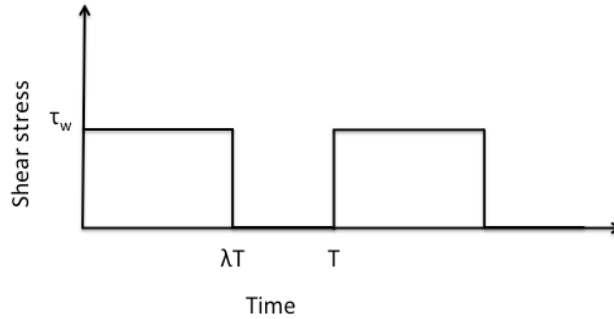


**Figure 3-5. Pulse wave representation of circulating blood sample flow for stationary observer**

From this point of view, it can be seen that the flow can be characterized as unidirectional and cyclical. For simplicity, the pulses are represented with instantaneous rise and fall. In reality, there would be a trailing edge transition. Although periodic shear change as represented on Figure 3-5 is appropriate for flow in coronary arteries, the change *in vivo* is not instantaneous. However, the model remains a useful representation as it incorporates the main feature of periodicity. It is important to note that depending on the investigation, the model may not always have to be completely realistic to be useful; given the objectives of this thesis the step change approximation used in this model is acceptable.

Since the experienced shear stress would be time variant, it is appropriate to express it as time-averaged wall shear stress. Shear stress *in vivo* is also expressed as time-averaged because of the pulsatile nature of the cardiac cycle. Time-averaged shear stress is expressed as,

$$\tau = \frac{1}{T} \int_0^{\lambda T} |\vec{\tau}| dt \quad (20)$$

where T is the period,  $|\vec{\tau}|$  is the magnitude of the axial wall shear stress vector. Hence, the time-averaged shear experienced by the adherent particle would be,

$$\tau = \tau_w \lambda \quad (21)$$

Thus, the effect of sample volume is scaling the shear magnitude by the volume fraction  $\lambda$ .

If the observer now is in a small volume element, it experiences shear rate almost for the whole period T. However, there are intermittent disruptions each time the element reaches the proximal or distal end of the flowing sample due to the fluid-air interface. Rigorous analysis can estimate the fraction of time that the volume element takes at the interface and the radial velocity component due to secondary flow, but for the purpose of this study, it can be assumed that the fraction of time at the air interface and the radial velocity gradient are negligible. Since the volume element also follows a helical path due to the secondary flow vortex, it has the axial component of the secondary vortex. It is possible to calculate the vortex axial component numerically [259], but for the purpose of this work, simplifying assumption can be made.

If the internal diameter of the tube is taken as the maximum characteristic distance that the cell travels before it experiences shear again (after fluid-air interface), then the average characteristic distance can be taken as the tube radius. For simplicity a straight travel is assumed since the distance is a short arc, especially if the flow approaches plug flow. Since the intensity of the secondary flow vortex cannot be determined, for simplicity it can be assumed to be approximately 50% of the axial velocity as previously reported [366]. Hence, the time to travel the fluid-air interface can be expressed as,

$$t_\sigma = \frac{60R}{\pi\omega R_0} \quad (22)$$

As a function of T for this model,  $t_\sigma = \zeta T$ , where  $\zeta=80.9 \times 10^{-3}$ . This small time difference can be visualized on Figure 3-5 (above) as the difference between  $\lambda T$  and T. As  $\lambda T$  approaches T, the pulse is almost continuous for the whole period. It is difficult to determine the shear stress during the fluid-

air interface transition. If it is assumed its magnitude is a fraction of the wall shear stress, given by  $\tau_w' = \sigma\tau_w$ , then the time-averaged shear stress can be expressed as,

$$\tau = \frac{1}{\lambda T + t_\sigma} \left[ \int_0^{\lambda T} |\tau_w| dt + \int_{\lambda T}^{\lambda T + t_\sigma} |\tau_w'| dt \right] \quad (23)$$

which becomes,

$$\tau = \tau_w \left( \frac{\lambda + \sigma\xi}{\lambda + \xi} \right) \quad (24)$$

where, based on the previous velocity estimation,  $\sigma$  can be estimated as 50%. Hence, the time-averaged wall shear stress is a fraction of the original wall shear magnitude. The difference is reduced by small tube diameter or increasing volume fraction,  $\lambda$ . When  $\lambda$  is doubled, i.e. increased from 0.3 to 0.6, the bracket term increases from 0.89 to 0.94. This means that in the absence of stents, the volume effect on wall shear stress is minimal.

While the analysis assumed small parabolic flow, the presence of red blood cells and the existence of secondary flow vortices would make the flow approach plug flow, as previously highlighted. That means the velocity gradient along the radial direction is almost zero ( $dv/dr \approx 0$ ). For this condition,  $t_\sigma \approx 0$ , which supports the above analysis. Thus, this work has shown through mathematical analysis that the time-averaged fluid shear in the absence of a stent is very close to the shear magnitude, regardless of the volume. However, this does not preclude a small volume effect on blood activation as biochemical activity is not dependent on shear alone.

### 3.4.3 Frequency and volumetric flow rate analysis

Besides curvature ratio and Dean number, volumetric flow rate is one of the parameters that characterizes pulsatile flow in curved tubes [363]. The frequency and volumetric flow rate from the left ventricle or cardiac output have been previously discussed in Chapter 2. At a nominal physiological heart rate of 60 beats/minutes (fundamental frequency  $F \approx 1.0$  Hz), the cardiac output is approximately 4.8 L/min [51]. However, this is not the volumetric flow rate for the coronary arteries

because the cardiac output occurs during systole while flow in the coronary arterial tree peaks during diastole, which has lower pressure than systole, but occupies two-thirds of the cardiac cycle.

The total volumetric flow rate for the coronary arteries is approximately 0.25 L/min and for the left coronary arteries has been estimated at 0.15 L/min [229]. The volumetric flow rate can also be calculated from  $Q = A_x v$ , where  $A_x$  is the vessel cross-sectional area and  $v$  is the average blood velocity. Using the physiological average LAD radius  $R=1.9$  mm and velocity range  $v=10.6-43.0$  cm/s from Table 3-5, gives estimated LAD volumetric flow rates  $Q=0.07$  L/min to 0.29 L/min. Just as the cardiac output is necessary for physiological functions, the volumetric flow rate for the coronary arteries is critical for proper metabolic exchange in the myocardium and cardiac function. Thus, the volumetric flow rate is relevant for an *in vitro* model because of its importance in the rate of exchange of biochemical agents.

*In vivo* pulsatile flow is induced by variation of the heart geometry, which also deforms the coronary arteries. As a result, there are complex spatial, phase and time interactions between geometric and hemodynamic parameters in the coronary arteries, especially at bifurcations [237]. For *in vitro* modeling, if the mean coronary arterial geometry is adopted, pulsatile frequency can be simulated by intermittently varying the fluid flow. This method of fixing the geometry and varying the flow is adopted in this research. The flow frequency for the model is given by the expression  $F = \pi\omega/30$ . Therefore, for any sample volume  $V$  and loop volume  $V_0$ , the volumetric flow rate can be defined as  $Q = FV_0\lambda$ , where  $\lambda$  is the volume fraction as previously defined. Using the selected experimental volumes and angular velocities, the model frequencies and volumetric flow rates can be determined, Table 3-7. The volumetric flow rate for 2 ml at 2.5 Hz was similar to the calculated LAD flow rate. Although the frequency is up to 4.7 Hz and volumetric flow rates are high, thus producing high shear stress, it is interesting to note that cardiac cycle harmonics of up to 5 Hz have been reported and therefore used in investigating the effect of dynamic curvature on wall shear stress in coronary arteries [358]. Therefore, the use of frequencies other than 1 Hz is reasonable with this consideration.

**Table 3-7. Model frequency and volumetric flow rate**

Angular velocity $\omega$ (RPM)	Frequency $F$ (Hz)	Period $T$ (s)	Volumetric flow rate	
			2 ml sample	4 ml sample
			Q (L/min)	Q (L/min)
24	2.5	0.4	0.3	0.6
45	4.7	0.2	0.6	1.1

### 3.4.4 Fluid friction factor analysis

Fluid flow is characterized by a number of parameters, such as flow type (laminar or turbulent), fluid type (viscous and non-viscous), entrance length and friction. Friction drag, as an inherent feature of any flowing fluid, has implications for a variety of engineering applications, such as long distance transport of piped oil. Researches have investigated several drag reduction methods, some of them with biomedical applications [243]. Because friction is an important flow parameter, a number of friction factor correlation equations for engineering applications at high Reynolds numbers have been developed [367]. These formulas are used to calculate the friction factor in pipe flow under laminar and turbulent flow.

The effect of curvature on flow, such as reduced flow rate and skewing of velocity profile, have been highlighted since early in the 19<sup>th</sup> century in some of the work by Dean [263]. Since then, fluid flow characteristics in curved tubes of various configurations have been extensively studied, as demonstrated in the review by Naphon and Wongwises [242]. Curved tube flow has numerous applications that take advantage of its effective mixing and mass transport characteristics. These include industrial heating and cooling [368], biochemical or biomedical microreactors and micromixers for oxygenation [369, 370]. Although the curvature increases the Reynolds number point of transition to turbulent flow, the curvature-induced pressure loss and friction can be a concern due to its effect on wall shear stress. A number of friction factor correlations have been developed for both smooth and rough tubes of specific roughness. Table 3-8 presents some of the equations that may be applicable to a curved loop model, such as the Chandler loop. Therefore, the purpose of this work was to determine the friction factor for the Chandler loop model and analyze the relevance of friction in an *in vitro* model since it is an important feature of fluid flow, especially in curved geometry.

**Table 3-8. Typical friction factor equations for laminar flow**

Tube type	Friction factor	Ref
Straight smooth	Fanning: $f_0 = \frac{16}{R_e}$  Darcy: $f_0 = \frac{64}{R_e}$	[346]
Curved smooth	$f = 0.5 \left( \frac{D_n}{16} \right)^{0.2} + 1.5$	[262]
Curved smooth non-rotating pipe	$\frac{f}{f_D} = 0.0899 D_n^{0.5} (1 + 12.4 D_n^{-0.701})$	[371]
Straight rough (helical-finned)	$f = 0.108 R_e^{-0.283} N^{0.221} \left( \frac{\varepsilon}{D} \right)^{0.785} \varphi^{0.78}$	[372]

$D_n$  is Dean number,  $\varepsilon$  is internal rib height,  $D$  is internal tube diameter,  $N$  is number of rib starts and  $\varphi$  is helix angle

#### 3.4.4.1 Loop friction factor

There is little discussion on the issue of friction in the Chandler loop model, with or without stents. It is therefore necessary to determine its significance in this model. Most applications where a friction factor is determined, the tube is filled with fluid or a sufficiently large volume is assumed. However, in some applications, such as the Chandler loop *in vitro* model, the existence of a liquid-air interface mimics open channel flow. This requires special attention since the blood cells do not experience the same magnitude of shear all the time.

The friction equation for curved smooth pipes has been previously described by Soeberg [262] and Ishigaki [371]. Comparison of these friction factors based on the parameters of the model as described in Table 3-5 shows that they provide very similar friction approximations up to low Dean numbers, Figure 3-6. However, examination of the equations reveals that the Ishigaki equation does not reduce well to a straight tube. Thus, for brevity we adopt the curved flow friction factor equation by Soeberg [262], as the friction factor for the Chandler loop model. This is expressed as,

$$f_{cs} = \frac{32}{R_e} \left[ 0.5 \left( \frac{D_n}{16} \right)^{0.6} + 1.5 \right] \quad (25)$$

where  $D_n = R_c \sqrt{R/R_0}$  is the Dean number and the subscript *cs* denotes a curved smooth tube.

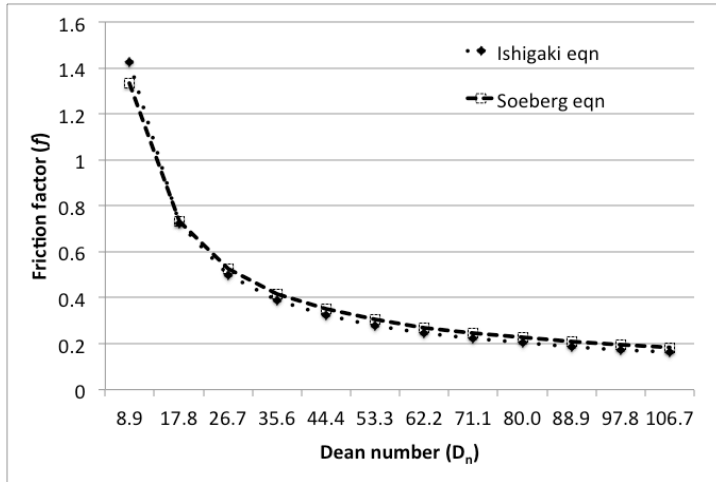


**Figure 3-6. Comparison of friction factor equations for curved smooth tubes**

### 3.4.4.2 Loop friction factor with model stent

To perform fluid dynamics analysis of the flow model in the presence of model stents, it was necessary to incorporate a stent with specific geometric and structural measurements. To this end, helical shaped model stents were designed and fabricated, as described in Chapter 4. The parameter specifications for the model stents are as presented Table 4-2.

In the presence of stents, the stent struts introduce wall roughness, which causes friction and flow disturbance. Studies have demonstrated the effect of stent strut design height and shape on hemodynamics; in straight tubes [373, 374] as well as inter-connections in curved tubes [375, 376]. The hemodynamic effect of stent design may translate to development of in-stent thrombosis. Therefore, it is necessary to develop analytical equations that describe the effect of each stent design (such as the one used in this research) on flow friction in a curved tube that mimics the curvature of the coronary arteries.

To derive a suitable friction factor equation for the Chandler loop with a helical model stent, the stent struts can be represented as fins within a tube and it is necessary to know the stent design struts dimensions and shape. For brevity, the Fanning friction factor equation for a straight helical-finned tube previously developed by Li and Webb [372], was adopted. Assuming fully developed flow, this is expressed as,

$$f_{sr} = 0.108 R_e^{-0.283} \left( \frac{\varepsilon}{D} \right)^{0.785} N^{0.221} \varphi^{0.78} \quad (26)$$

where  $\varepsilon$  is the internal rib height,  $D$  is the internal tube diameter,  $N$  is number of rib starts,  $\varphi$  is the helix angle of the ribs and the subscript  $sr$  denotes a straight rough tube. For the purpose of this research, model helical stents with parameters presented in Table 4-2 are used.

Since equation (26) is for a rough straight tube, it is necessary to introduce a correction factor in order to derive an appropriate equation suitable for the curved loop with a helical roughness. The correction factor can be expressed as [377],

$$f_r = \frac{f_{sr}}{f_{ss}} \quad (27)$$

where  $f_{ss} = 16/R_e$  is the Fanning friction factor for a smooth straight tube [378]. Hence the corrected friction factor for a rough curved tube is then expressed as,

$$f_{cr} = f_{cs} \frac{4f_{sr}}{f_0} \quad (28)$$

where  $f_0 = 64/R_e$  is the Darcy friction factor for a straight smooth pipe with laminar flow. The factor of 4 was introduced since equation (24) was based on the Fanning friction factor. Therefore, the friction factor equation for a circular curved loop model with helical roughness, is given by equation (29),

$$f_{cr} = 0.054 \left[ 0.5 \left( \frac{D_n}{16} \right)^{0.6} + 1.5 \right] R_e^{-0.283} \left( \frac{\varepsilon}{D} \right)^{0.785} N^{0.221} \varphi^{0.78} \quad (29)$$

This is the in-stent friction factor equation for the Chandler loop with a helical stent. In order to appreciate the impact of the friction factor on flow, it is necessary to relate it to wall shear stress.

#### 3.4.4.3 Loop shear stress with model stent

To relate equations (25) and (29) to shear stress, the Blasius equation correlating wall shear stress with friction factor is applied. This is expressed as [378],

$$\tau = f \rho \frac{v^2}{2} \quad (30)$$

where  $\tau$  is wall shear stress and  $v$  is average velocity. After rearranging the terms as described in Appendix B, the wall shear stress is given by equation (31),

$$\tau = f \left( \frac{R_e}{16} \right) \tau_w \quad (31)$$

where  $\tau_w$  is wall shear stress as defined by equation (19). Therefore, the wall shear stress for the smooth loop without the stent becomes,

$$\tau_s = f_{cs} \left( \frac{R_e}{16} \right) \tau_w \quad (32)$$

The wall shear stress for the loop with roughness becomes,

$$\tau_r = f_{cr} \left( \frac{R_e}{16} \right) \tau_w \quad (33)$$

In establishing the above equations for the circulation loop, an implicit assumption was that the whole lumen of the loop has helical roughness. However, in the case of the Chandler loop model, only a small portion of the lumen has roughness due to the stent; there is a defined length of roughness. In addition, the sample volume does not occupy the whole tube. Therefore, further analysis is necessary to take the stent length and sample volume into account. This would make the friction factor appropriate for the *in vitro* model used.

Due to the cyclical nature of the flow, the time period that the stent experiences shear stress in one cycle is only  $\lambda T$ , where the period  $T$  is as previously defined. If the ratio of stent length to tube length is defined as  $\alpha$ , then the periodic time fraction for the stent can be defined as  $\beta T = \alpha \lambda T$ . The period circulation of the stent in and out of the fluid sample can be represented by a square wave superimposed on Figure 3-5. The resulting pulse train wave event is depicted on Figure 3-7.

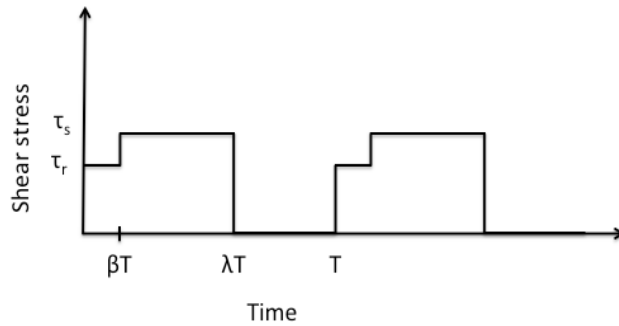


**Figure 3-7. Pulse wave representation of circulating blood sample with model stent**

Since shear stress is time-dependent, it is appropriate to introduce the concept of time-averaged wall shear stress for this model. Then using the time-averaged wall shear stress as defined by equation (19), the integral for the pulse train in Figure 3-7 becomes,

$$\tau = \frac{1}{T} \left[ \int_0^{\beta T} \tau_r dt + \int_{\beta T}^{\beta T + \lambda T} \tau_s dt \right] \quad (34)$$

Substituting equations (32) and (33), it can be shown that the loop fluid time-averaged wall shear stress for the Chandler loop model with a model stent can be expressed by equation (35).

$$\tau = \frac{\tau_w R_e}{16} [\beta f_{cr} + (\lambda - \beta) f_{cs}] \quad (35)$$

This can also be written as,

$$\tau = \frac{\tau_w R_e}{16} \lambda [\alpha f_{cr} + (1 - \alpha) f_{cs}] \quad (36)$$

In the absence of a stent, equation (36) reduces to the time-averaged wall shear stress for the Chandler loop with the friction factor term, which is,

$$\tau = \frac{\tau_w R_e}{16} f_{cs} \lambda \quad (37)$$

Equation (37) represents the time-averaged wall shear stress for a stationary point in the loop outer wall, in the place of a stent. For the fluid element, the flow is assumed relatively continuous for the reasons previously discussed. In detail, the time-averaged wall shear stress for the Chandler loop model with and without a helical stent can be expressed as equations (38) and (39), respectively.

$$\tau_{TAWSS} = \frac{\pi \omega \mu \lambda R_e}{120 \kappa} \left[ 0.5 \left( \frac{D_n}{16} \right)^{0.6} + 1.5 \right] \left[ \left( 0.00675 R_e^{0.717} \left( \frac{\varepsilon}{D} \right)^{0.875} N^{0.221} \varphi^{0.78} - 1 \right) \alpha + 1 \right] \quad (38)$$

$$\tau_{TAWSS} = \frac{\pi \omega \mu \lambda R_e}{120 \kappa} \left[ 0.5 \left( \frac{D_n}{16} \right)^{0.6} + 1.5 \right] \quad (39)$$

To predict the effect of the selected sample volume and stent lengths on time-averaged wall shear stress, the weighting factors for the stent and loop friction factor terms, equation (36), were determined based on the volume of the circulation tube (6.644 ml), Table 3-5. When the sample volume is doubled without changing the stent length, both weighting factors for the stent and loop friction factor terms ( $\alpha$  and  $1-\alpha$ , respectively) are unchanged, Table 3-9. The counter effect of the volume increase on the surface area-to-volume ratio is a decrease by a factor of two. For this case, the sample volume fraction seems to be the dominant parameter, in terms of influencing both the surface-area-to-volume ratio and the friction factor. However, when doubling the sample volume is accompanied by an increase in stent length to maintain similar surface area-to-volume ratios, the stent friction factor weighing term ( $\alpha$ ) increases 1.8-fold and the loop friction term ( $1-\alpha$ ) barely changes. In this case, the combined effect of volume and stent has a higher effect on friction factor. Similarly, if both samples have increased sample volume (4 ml) and the stent length is almost doubled, the stent friction factor increases 1.8-fold and there is almost no change with loop friction factor term. Thus, for these parameters, the combined effect of sample volume and stent length has greater influence on friction factor weighting, and hence time-averaged wall shear stress, especially at larger sample volumes.

**Table 3-9. Volume and stent ratio effect on friction factor weighting**

	2 ml + 20 mm	4 ml + 20 mm		4 ml + 35 mm		
			Fold-increase relative to 2ml+20mm		Fold-increase relative to 2ml+20mm	Fold-increase relative to 4ml+20mm
$\lambda$	0.3012	0.6024	2.00	0.6024	2.00	1.00
$\alpha$	0.0539	0.0539	1.00	0.0943	1.75	1.75
$1-\alpha$	0.9461	0.9461	1.00	0.9057	0.96	0.96

The effect of the weighting factors on shear stress are explored further by plotting equations (19), (38) and (39) in Figure 3-8. There are three interesting points to note: (i) compared to Eqn 19, wall shear stress in the Chandler loop is nonlinear and is much higher than estimated by the original equation (19), (ii) there is an interesting grouping of the data plots around 2 ml and 4 ml samples and

(iii) the time-averaged wall shear stress for samples with stents is slightly lower than for samples without stents. The data plot grouping by volume indicated the dominating effect of sample volume.

The results indicate that in the presence of a stent, time-averaged wall shear stress depends on both stent length and sample volume. Comparison of the 2 ml curve with the 4 ml curves shows that for the selected parameters, time-averaged wall shear stress is much more sensitive to sample volume than stent length, especially at higher rotational velocities. The low sensitivity of shear stress to stent length suggests that at the same angular velocity, stent surface area may play a bigger role compared to friction, for samples with the same volume but different stent lengths. On the other hand, for samples with comparable surface area-to-volume ratios, activation may be more shear-dependent, which is influenced by sample volume fraction. Taken together, these results indicate that time-averaged wall shear stress for the Chandler loop model is nonlinear and much higher than previously thought. In addition, sample volume, as well as stent length, have an effect on wall shear stress.

Typical wall shear stress/rate values for 25 RPM and 45 RPM, read from Figure 3-8 are presented on Table 3-10. As observed above, the original equation (19) did not take into account the sample volume fraction or the presence of a stent, and hence the time-averaged wall shear stress is the same as the wall shear stress magnitude for this case. On the other hand, the new time-averaged wall shear stress reflects the effect of changes in sample volume and stent length on fluid dynamics.

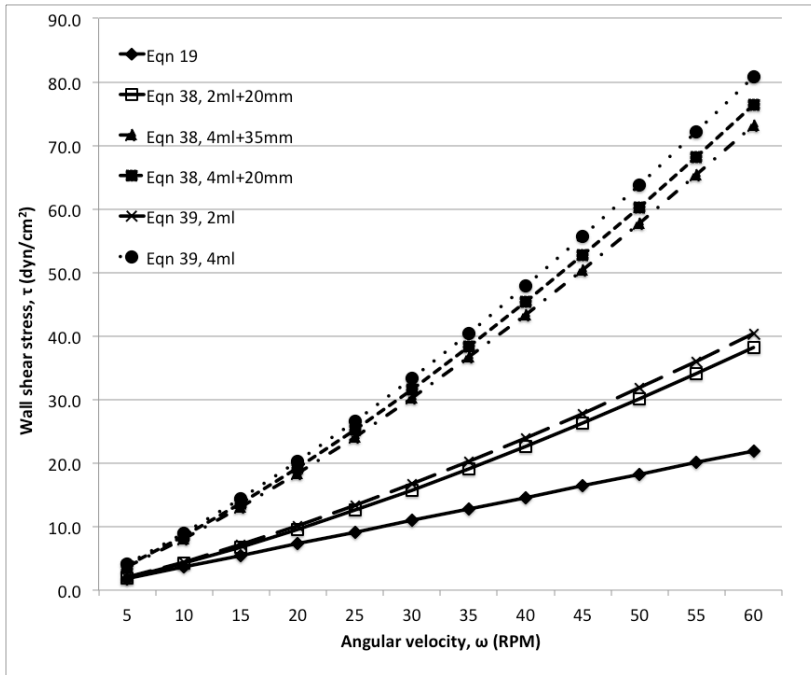


**Figure 3-8. Time-averaged wall shear stress as a function of angular velocity.** For this study,  $\lambda=0.3012$  and  $0.6024$ ,  $\alpha=0.0539$  and  $0.0943$  ( $\beta=0.0162$ ,  $0.0325$  and  $0.0568$ )

**Table 3-10. Time-averaged wall shear stress for selected sample volumes and stent samples**

Experimental groups	Wall shear stress (rate) at 24 RPM		Wall shear stress (rate) at 45 RPM	
	Eqn 19, dyn/cm <sup>2</sup> (s <sup>-1</sup> )	Eqn 36, dyn/cm <sup>2</sup> (s <sup>-1</sup> )	Eqn 19, dyn/cm <sup>2</sup> (s <sup>-1</sup> )	Eqn 36, dyn/cm <sup>2</sup> (s <sup>-1</sup> )
<b>2 ml</b>	9.1 (260.0)	13.3 (380.0)	16.4 (468.6)	27.8 (794.3)
<b>4 ml</b>	9.1 (260.0)	33.3 (951.4)	16.4 (468.6)	55.7 (1591.4)
<b>2 ml+20 mm</b>	9.1 (260.0)	12.6 (360.0)	16.4 (468.6)	26.3 (751.4)
<b>4 ml+20 mm</b>	9.1 (260.0)	25.2 (720.0)	16.4 (468.6)	52.7 (1505.7)
<b>4 ml+35 mm</b>	9.1 (260.0)	24.1 (688.6)	16.4 (468.6)	50.4 (1440.0)

NB. 2 ml + 35 mm stent samples were not used because it results in very low surface area-to-volume ratio. Eqn (36) is equivalent to equation (38).

In the above analysis of the model fluid dynamics, it was inherently assumed that the effect of air in the loop was minimal. However, the possible implications and limitations on controlling the blood-to-air ratio have been previously raised [29]. If it is now assumed that the loop is occupied by two incompressible and immiscible fluids, which remain separate during flow, then a new analysis is necessary. In this case the pulse wave representation of Figure 3-7 can be represented as Figure 3-9, where the period 0 to  $\lambda T$  is occupied by one fluid and  $\lambda T$  to  $T$  is the other fluid.

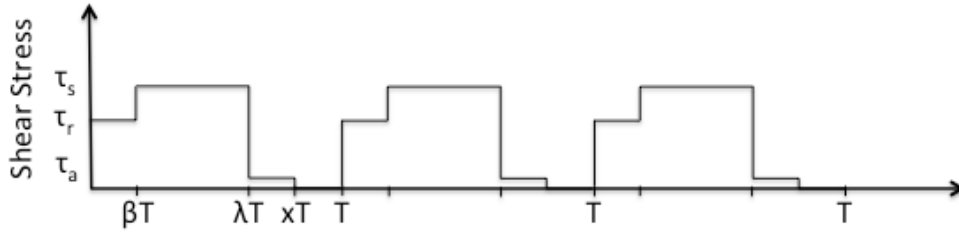


**Figure 3-9. Pulse wave representation of circulating blood sample with model stent, including effect of air.  $xT=(\lambda+\beta)T$ , which accounts for the stent sample in the air portion of the loop.**

Suppose that the two fluids are defined by characteristic parameters  $\rho_1, \mu_1, v_1$  and  $\rho_2, \mu_2, v_2$ , where  $\rho, \mu, v$  are their density, viscosity and average velocity, respectively. Then equation (34) with two fluids becomes,

$$\tau = \frac{1}{T} \left[ \int_0^{\beta T} \tau_{r1} dt + \int_{\beta T}^{\lambda T} \tau_{s1} dt + \int_{\lambda T}^{\lambda T + \beta T} \tau_{r2} dt + \int_{\lambda T + \beta T}^T \tau_{s2} dt \right] \quad (40)$$

Using Blasius correlation equation (30) to substitute for the shear stress terms, the above equation becomes,

$$\tau = \frac{\rho_1 v^2}{2} [\beta f_{cr1} + (\lambda - \beta) f_{cs1}] + \frac{\rho_2 v^2}{2} [\beta f_{cr2} + (1 - \lambda - \beta) f_{cs2}] \quad (41)$$

where the subscript on the velocity was dropped because the two fluids have the same velocity and it is assumed that the friction factors as discussed previously are applicable for both fluids. Suppose the first fluid is blood and the second fluid is air. Then it can be noted that the first fluid terms can be replaced by equation (35). However, the equation for wall shear stress as defined by Gardner [354], is not applicable for the air sample. Therefore, equation (41) becomes,

$$\tau = \frac{\tau_w R_e}{16} [\beta f_{cr} + (\lambda - \beta) f_{cs}] + \frac{\rho_a v^2}{2} [\beta f_{cra} + (1 - \lambda - \beta) f_{csa}] \quad (42)$$

In the absence of a stent, equation (42) can be expressed as,

$$\tau = \frac{\tau_w R_e}{16} \lambda f_{cs} + \frac{\rho_a v^2}{2} (1 - \lambda) f_{csa} \quad (43)$$

Since blood is composed of almost 50% water, the water vapor saturation pressure was used to calculate the density of moist air in the loop, see Appendix C for details on vapor pressure determination. From the calculation, the density of humid air in the loop at 37°C is  $\rho_a = 1.1166 \text{ kg/m}^3$  and the air viscosity  $\mu_a = 19.03 \times 10^{-6} \text{ Pa}\cdot\text{s}$ . Using these values, the second terms of equations (42) and (43), representing shear stress contribution from the air sample, are plotted in Appendix C. From the data, the highest time-averaged wall shear stress due to air is less than  $0.04 \text{ dyn/cm}^2$ . The combined effect of blood and air samples on wall shear stress, as expressed by equations (42) and (43), are plotted on Figure 3-10.

Based on comparison of Figure 3-8 and Figure 3-10, it is clear that the effect of air shear stress is minimal. Therefore, ignoring the effect in the previous analysis is acceptable. It was however, informative to perform the analysis and prove that the air effect can be ignored, which has not been done previously. Therefore, from a hemodynamic stand point, the air sample volume can be neglected and equations (38) and (39) can be used as time-averaged wall shear stress equations for the Chandler loop model with and without a helical model stent.

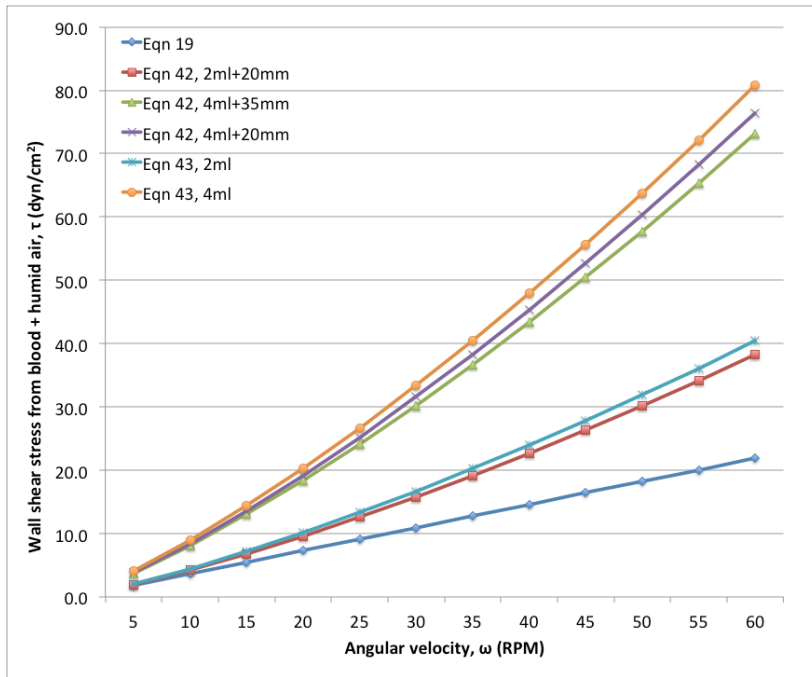


**Figure 3-10. Combined time-averaged wall shear stress due to blood and air in the loop**

### 3.4.5 Discussion

The design parameters of an *in vitro* model greatly influence its relevance and accuracy. Although previous studies have made important contributions to the understanding of the fluid dynamics of the Chandler loop model [354], the importance of sample volume in this model has not been addressed. In this section, the importance of blood sample volume in the Chandler loop model was highlighted and demonstrated through analysis and characterization of the model fluid dynamics. A method for determining the appropriate blood sample volume for the Chandler loop model was also developed through the CLSVF criterion. In addition, time-averaged wall shear stress analysis was provided.

The importance of blood sample volume in *in vitro* blood-biomaterial interaction studies has been emphasized by the development of a guidance standard, the ISO 10993 Standard, which stipulates a material surface area-to-blood volume ratio of 0.5 to 6.0 cm<sup>2</sup>/ml. This parameter (surface area-to-volume ratio) can easily be met under static conditions, but under flow conditions the selected

sample volume may violate some of the fluid dynamics assumptions. Therefore, under flow conditions, it is necessary to consider the hemodynamics of the selected sample volume since inappropriate sample volume can result in wrong assumptions and incorrect hemodynamic parameters, which has implications on interpretation of experimental results. In the Chandler loop model with a stent, the significance of blood sample volume is three-fold; (i) it affects the ISO 10993 Standard compliance, (ii) it influences the fully developed flow condition and (iii) it influences the length of time shear stress is applied to a model stent. Putting all these together, the CLSVF criterion was developed as guidance for determining the appropriate sample volume fraction and the concept of time-averaged wall shear stress was introduced as an important aspect of this model.

Another important parameter of the Chandler loop model that has not been considered is the friction factor. In coronary arteries, friction may be introduced by curvature or the presence of a stent implant. Similarly, in the circulation loop model, the curved flow and introduction of model stent introduce friction drag. In this work, flow and friction factor for the Chandler loop model were appropriately characterized, an element that had been absent in the literature. An analytical friction factor equation was derived for the Chandler loop, which can be used with any stent with a defined friction factor. For this research, the particular equation was for a helical stent model. Consequently, a time-averaged wall shear stress equation, dependent on friction, was also derived. It was demonstrated that in the presence of a model stent, wall shear stress is not only influenced by friction, but is influenced by blood sample volume and stent length.

Analysis of the wall shear stress equation plots revealed that the loop shear stress is nonlinear and much higher than the prediction from the original equation. The difference in linearity and magnitude between the original equation and the new developed equation is partly due to the fact that the new equation includes some of the important parameters in curved tube flow not included in the original equation. It was also interesting to note the grouping of the data around sample sizes, which suggests the critical role played by the sample volume in time-averaged wall shear stress, with or without stents. The effect of sample volume in this model was not previously discussed in the literature. The other interesting point is that the time-averaged wall shear stress for samples with stents is slightly lower than that for samples without stents. A decrease in the in-stent wall shear stress, dependent on stent design, has been previous shown in *in vitro* [379] and computational fluid dynamics simulations [380], which can be exacerbated by overlapping stents [380, 381]. The shear recovery at the distal end, which may be higher than inlet shear at the proximal end, is partly due to

the sudden flow disturbance vortex as the fluid enters the stent. There are also recirculation zones within the stent that would reduce the flow. In our case, the shear at specific locations within the stent cannot be determined without numerical simulation, but the overall observed results may be partly explained by what has been reported in the literature.

There was also a difference in the effect of stent length on time-averaged shear stress when samples with similar volume size but different stent lengths were compared. The longer stent shows a slightly lower time-averaged wall shear stress compared to the shorter stent samples. The difference in spatial distribution of in-stent wall shear stress between long and short stents has previously been shown in a different model; straight tube model with no volume effect [381]. The difference between the previously reported measurement results and our analytical results is that time-averaged wall shear stress is lower for the longer stent. This may be partly due to the curvature in our case versus a straight tube in their model and the sample volume-stent length interaction. The impact of a longer stent on blood activation is increased residence time from reduced shear and increased recirculation zones, which would have implications for blood activation. Indeed, longer stents have been associated with adverse clinical outcomes, more so first generation DES than second generation DES [382]. The information on the impact of stent length is important for interpreting the effect of hemodynamics on blood activation using the Chandler loop model.

Like any other model, the Chandler loop model has some limitations. These include the fact that, (i) it cannot exactly reproduce the physiological conditions, (ii) it is closed-loop and (iii) there is air in the circulation loop. The first limitation is a limitation of all *in vitro* models. The effect of this limitation has been addressed in the design and analysis of model parameters as described in the previous sections of this chapter. The second limitation is inherent due the design of the model, but limiting the experimental time can reduce its effects. The third limitation, although recognized and acknowledged in previous studies, has not been analyzed. Therefore, analysis was performed and it was demonstrated that the air-blood interface has an intermittent shear stress effect, which depends on the sample volume. However, analysis of the wall shear stress effect of the air sample demonstrated that the air sample had minimal effect on the overall wall shear stress of the model. Thus, from the analysis the air sample can be considered to have little additional hemodynamic effect. While the effect of the air sample on shear stress was analyzed, the biochemical effect, which may be caused by such factors as the difference in oxygen partial pressure between the air and the blood samples,

remains to be investigated. Nonetheless, the proposed time-averaged wall shear stress equations for the Chandler loop models can be used without loss of generality.

### 3.5 Implementing the model

The main components of the *in vitro* flow model are the rotor, the rotating disk turntable connected to the rotor by a shaft and the tubing loop for containing the blood. Therefore, to implement the model, a rotor (Roto-Torque™, model RT50, Cole-Palmer Instrument Co., IL, USA) was used to drive a single plane turntable where the sample loops were mounted, Figure 3-11. The rotor speed could vary from 0 to 60 revolutions per minute (RPM), which was calibrated with a model 461831 Digital Stroboscope Tachometer (Extech Instruments, Melrose, MA, USA). The calibration procedure is summarized in Appendix D. The turntable had brackets located at approximately 60 mm and 100 mm from its center, which were used for holding blood sample tube loops. With modification, additional loops of similar or larger radii may be mounted, if necessary. When the sample loops were mounted, the turntable was positioned in a vertical orientation. The blood sample loop tubes were non-permeable medical grade Silastic silicone tubes (VWR, PA, USA). The tubes were spliced with similar silicone tube approximately 25 mm long, 7.95 mm internal diameter and 12.70 mm external diameter, to complete the loop. The splicing piece was kept short to reduce its impact on the smoothness of the loop curvature. Incorporation of the stents also did not alter the loop geometry, i.e. did not alter both the tube diameter and the smoothness of the loop. While the silastic tubing is a biomaterial, the use of the term biomaterial in this study only refers to the materials under test (model stent), unless otherwise stated.

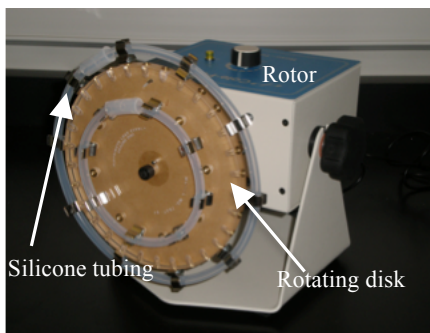


**Figure 3-11. Rotor with rotation disk and loops used as the *in vitro* flow model**

Before performing *in vitro* experiments, the model was tested to ensure that the leading edge of the blood sample would not spill over when either volume or rotational speed was increased. For this, the circulation loop was filled with either a 2 ml or 4 ml blood sample. For each blood sample volume, the loop was rotated at 24 and 45 RPM, at separate times, making a total of four experimental runs. For each experiment, it was confirmed, through visual observation of the meniscus level, that the fluid did not spill over during rotation. After 2 hours of testing, no obvious clots were observed in the tube.

### **3.6 Summary**

This work has demonstrated that although wall shear stress is an important parameter that characterizes flow both *in vivo* and *in vitro*, it does not entirely define the flow characteristics as it is only one of the many parameters that characterize flow. Some of the important flow characteristics are the geometry of the flow (e.g. tube vs plate flow or straight vs curved tube flow) and the type of flow (e.g. continuous vs pulsatile flow). Hence in the selection or design of a flow model, other parameters that characterize flow in the physiological location of interest need to be considered. This guiding principle, which was based on the systems approach framework proposed in Chapter 2, was applied in determining and designing/selecting the appropriate model for this research. Hence, the Chandler loop model was found to be a reasonably appropriate model for this research because of its geometry and flow characteristics. For this research, the model geometric parameters were based on the coronary system.

The model flow characteristics were analyzed and a time-averaged wall shear stress (TAWSS) equation was developed. Although the TAWSS equation was based on previously validated work, further numerical validation of the developed equation may be necessary. The TAWSS, which depends on blood sample volume, loop friction factor (with or without stent) and the model stent length, greatly contributes to the understanding of flow in the Chandler loop model. Appropriate flow characterization is important for understanding blood activation as well as drug delivery kinetics [383]. Since a method for determining the appropriate blood sample volume did not exist, a method was developed for the same. Overall the method and critical analysis presented in this work are significant for understanding the Chandler loop model and further investigations of its fluid dynamics.

### 3.7 Conclusion

In this chapter a systems approach was used for the design of the *in vitro* flow model and its parameters. A systems approach by its very nature ensures consideration of all the necessary factors and their linkages. Therefore, it facilitates the implementation of a comprehensive model. Hence, using a systems approach as a guiding method, this work developed a method for determining the sample volume, characterized flow and introduced the concept of time-averaged wall shear stress for the Chandler loop model. More importantly, an improved time-averaged wall shear equation for this model has been proposed. An analysis to show the hemodynamic effect of air in the loop was also presented. Further investigation into the biochemical effect is necessary. Overall the results support the hypothesis that a systems approach is better suited for designing *in vitro* flow model that mimics the physiological location of interest. In general, this work also supports the hypothesis that sample volume consideration is important in this model, especially in biomaterial studies. The improved time-averaged wall shear stress will go a long way in providing appropriate model design parameters, which will not only facilitate interpretation of *in vitro* results, but also provide a reasonable approximation of physiological parameters. The next step in this work is to characterize blood activation in the Chandler loop model in relation to the new model fluid dynamics characterization. Simulation studies would also be useful.

## Chapter 4

### Model Stent Design, Fabrication and Characterization

#### 4.1 Introduction

Coronary stents come in various strut shapes, sizes and structural design patterns, regardless of whether they are bare-metal or drug-eluting stents. The strut design [374] and pattern of connectors [376, 379] have implications on hemodynamics and subsequent in-stent thrombosis. The design of such stents requires expensive and time-consuming laser patterning. As a result, stents are too expensive to use in *in vitro* experiments unless the numbers are limited. The cost of bare metal stents varies but can be estimated in the range of \$500 to \$1000 per unit, based on a 2009 review [384]. Therefore, in order to study blood biomaterial interactions that mimic physiological conditions with an implanted stent it was necessary to design model stents for cost considerations. Furthermore, the use of in kind donation of commercial stents may also come with restrictions on publication of the data.

As discussed in Chapter 2, some of the commercially available metallic biomaterials are made from Nitinol and Ti-6Al-4V. These materials are already commonly used in a variety of applications, such as dental fixtures, orthopedic devices and coronary stents. As discussed in Chapter 2, Ti-6Al-4V has both an alpha phase, which is soft and ductile, and a beta phase, which is harder and stronger. The presence of the two phases in Ti-6Al-4V, alpha and beta, allows it to be heat treated to stabilize it at desired phase proportions [385, 386]. For example, at high temperatures, above 1010°C ( $\beta$  transus) it exists predominately in the beta phase. The rate of heating and cooling cycles determines the transformation dynamics [386]. This property is exploited in making model stents for this research. In addition, the spontaneous formation of a surface oxide layer makes these materials reasonably biocompatible. Hence, these materials were selected for use in model stents.

The role of material surface characteristics in determining interfacial phenomena, and thus blood-biomaterial interactions, was described in Chapter 2. Since material surface characteristics play an important role in influencing protein adsorption and subsequent cell activation and adhesion, there are several standards addressing material properties, such as qualitative and quantitative parameter description of surface morphology, ASTM F2791-09 standard [271]. For that reason, material surface characterization is an integral part of both *in vitro* and *in vivo* investigation of material interaction

with biological systems. Hence, there was a need to undertake surface characterization of the fabricated stents to ascertain their suitability for *in vitro* studies.

Although studies have been done with materials in different shapes and configurations, the use of a model stent in this study was considered more appropriate for stented coronary flow studies. The design of model stents with specific structural patterns provides motivation for detailed analysis of the effect of stent design on hemodynamic parameters, such as fluid friction. Thus, the purpose of this part of the thesis was to design, fabricate and characterize model stents.

## **4.2 Model stent design and fabrication**

### **4.2.1 Materials and methods**

Nitinol and Ti-6Al-4V ELI wires, specified at 0.005” (0.127 mm) diameter, were purchased from Fort Wayne Metals, Fort Wayne, USA. The surface was specified as smooth. These titanium alloys were selected for my experiments because they are both commonly used in implants. Ti-6Al-4V ELI (extra low interstitial) is a higher purity alloy with lower iron and carbon elements compared to the standard Ti-6Al-4V. Threaded A4 stainless steel rod (the metric equivalent of 316 stainless steel) and nuts were purchased from Spaenaur, Waterloo, ON, Canada.

The choice of the diameter of the threaded rod was based on the internal diameter of the selected silicone tube. The threaded rod was selected with the aid of the machinery handbook [387], to find a minor diameter that would produce the appropriate stent diameter, Table 4-1. The choice of the rod was made with allowance for sharp pitch, which means the wire leaves a gap in the groove when wound along the threads. One of the challenges encountered was the difficulty in matching the threaded rod with the tube internal diameter to a precise fit. This is because when the two are manufactured under different measurement systems, i.e. one metric and the other imperial, the conversion of one measurement unit to the other introduces errors and small differences.

**Table 4-1. Matching the tube to the rod. WD is the wire diameter, 0.005”.**

<b>Tube IDxOD inch. (mm)</b>	<b>Screw thread minor diameter = ID-2(WD) inch. (mm)</b>	<b>Closest screw type</b>	<b>Coupler IDxOD inch.</b>
0.188x0.313 (4.775x7.950)	0.178 (4.521)	(#12-28) 0.1711/0.1722	(#62999-884) 0.313x0.500

A typical cross-section of the threaded rod, with 0.005” wire, is depicted on Figure 4-1, not drawn to scale.

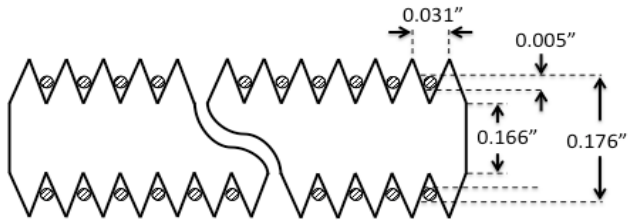


**Figure 4-1. Schematic of the longitudinal section view of the threaded rod with wire**

In addition, threaded mandrels were machined from 316 stainless steel rods in the University of Waterloo Machine Shop. These mandrels were designed to accommodate either the round wire or the flat wire strip, 0.02” width and 0.005” thickness. Since they were customized, they were designed so that stents would fit better in the tube. Figure 4-2 is a schematic cutout of the mandrel with specifications, not drawn to scale.

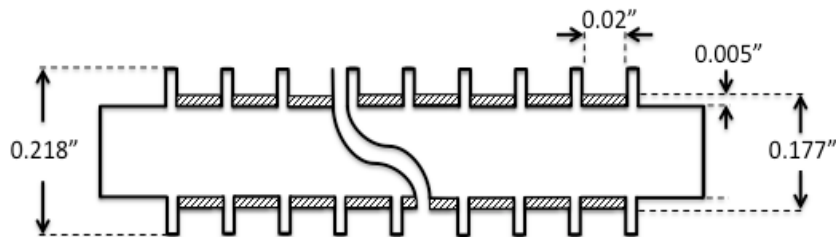


**Figure 4-2. Schematic of longitudinal section view of the mandrel with wire strip**

#### 4.2.1.1 Sample preparation

Ti-6Al-4V ELI wire was first cleaned by wiping with 70% ethanol. The threaded rod sections were cut into lengths between 40 mm and 65 mm. The mandrels were cut into lengths of about 30 mm. The threaded rod sections and mandrels and nuts were first cleaned in 30% nitric acid for 10 minutes in an ultrasonic cleaner. Wire segments were then wound around mandrels or threaded rod sections, along the threads, and held at both ends with nuts.

#### 4.2.1.2 Model stent shape setting

Four methods were used for shape setting model stents.

- (i) Furnace – In this method, the furnace was preheated to 800°C. The wire-rod/mandrel assemblies were placed on a 316 stainless steel open container and then inserted into the oven bore. The oven was closed and the assemblies were left to bake for 20 minutes at 800°C and taken out of the oven after baking. The assemblies were either air-cooled or water quenched for quick cooling.
- (ii) Furnace with argon – The wire-rod/mandrel assemblies were heated in a furnace, in 99.999% flowing argon at 2L/min. Heating rate was 25°C/min up to 500°C with a 20 minute hold at 500°C. The furnace power was then shut off to cool as fast as possible to room temperature (~60°C/min).
- (iii) Vacuum oven – This method used a large vacuum oven, model VAH 1220 HV-2 (Vac Aero International Inc., Oakville, ON, Canada). The assemblies were placed inside the oven in crucibles. The oven was held at a vacuum of -3 torr and heated at 25°C/min up to 800°C, with a 20 minute hold at 800°C. The vacuum was cooled slowly with water circulating in the oven jacket.
- (iv) Furnace (vacuum-sealed tubes) – In this method, the assemblies were vacuum-sealed at about  $1.5 \times 10^{-3}$  mbar in quartz tubes, which were then heat treated in an oven at 800°C. Figure 4-3(a) and (b) depict sealed tubes after heat treatment. The oven was held at 800°C for 20 minutes and then turned off to cool slowly. The tubes were kept sealed until it was necessary to use the model stents, at which time the stents were unwound from the threads. However, contamination from the mandrel or nuts can easily remain on the surface of the stent and the tube due to small space. This was observed with some of the samples being discolored after oven treatment, Figure 4-3(b).



**Figure 4-3. Picture of mandrels with stents sealed in a quartz tube after heat treatment. (a) Purchased mandrel and (b) Machined mandrel, showing contamination**

#### **4.2.2 Results and discussion**

Regardless of the method used, the results of shape setting 0.005" (0.127 mm) diameter Ti-6Al-4V ELI wires on mandrels produced helical shaped model stents, Figure 4-4. The 800°C heat treatment produced an  $\alpha$ - $\beta$  microstructure [386]. However, the surface texture varied considerably depending on the method. The first method produced model stents with a thick oxide layer because of heating and cooling in air. When the stents were water quenched, the oxide layer was found to be thick and flakey in some cases, Figure 4-5. Some preliminary experiments were done with stents from this treatment but because it produced an unpredictable surface oxide thickness layer, it was not pursued. The furnace with argon method generally produced model stents with a smooth surface. There were limited cases of a rough textured oxide layer. Stents from this method produced consistent results, but unfortunately the oven was removed from service.

The vacuum oven produced model stents with a very consistent surface layer. This method was desirable but expensive because of the size of the oven. Unfortunately, this oven was also taken

out of service. The sealed vacuum tube method produced good results when the seal was good. In some cases the seal may not have been complete as the stent surfaces showed a thick oxide layer. The sealed vacuum tube was the method of choice for the rest of the research.

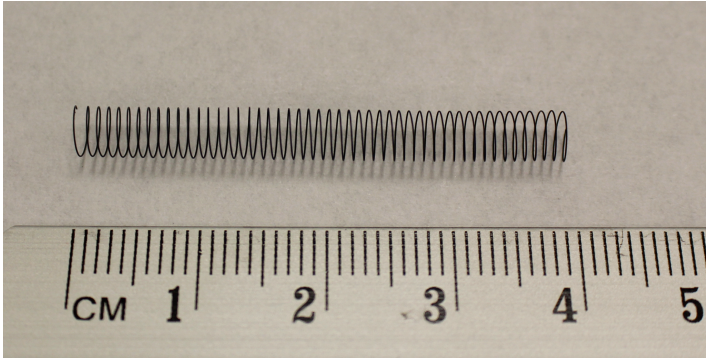


**Figure 4-4. Typical model stent**

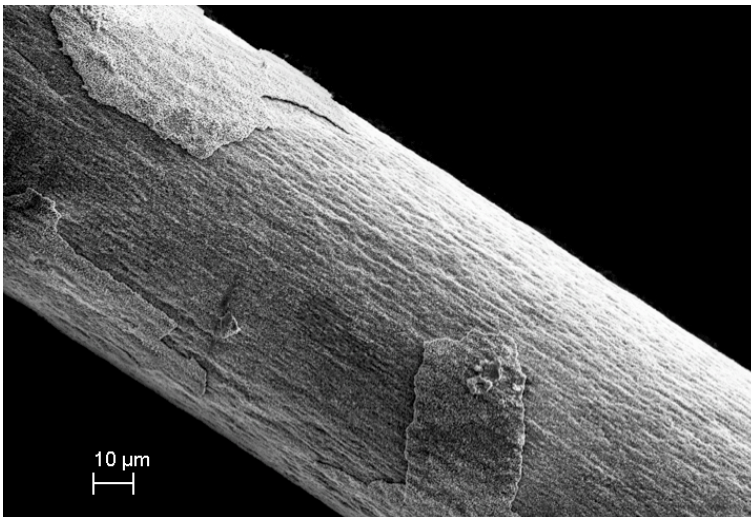


**Figure 4-5. Scanning electron micrograph of stent surface heat treated and quenched in air**

For this research, model stents were cut into two sets of lengths, 20 mm and 35 mm. Typical model stent parameters for the machined mandrel are as presented in Table 4-2. It should be noted that for some of the stents made with a mandrel as specified in Table 4-1, the diameters would be slightly different. After heat treatment, it was necessary to determine the surface characteristic of the stents before performing *in vitro* experiments.

**Table 4-2. Typical model stent parameters.** For conversion,  $3.224^\circ = 0.056$  radians.

Stent length (mm)	No. of ribs $\aleph$	Pitch $P$ (mm)	Strut diameter $\varepsilon$ (mm)	Stent diameter (mm)			Surface area $A$ (cm <sup>2</sup> )	Coil/helix angle $\varphi = \tan^{-1}\left(\frac{P}{\pi D_m}\right)$
				Outside $D_0$	Inside $D_i$ ( $D_0 - 2\varepsilon$ )	Mean $D_m = \frac{D_0 - D_i}{2}$		
20	25	0.8	0.127	4.775	4.521	4.521	1.46	$3.22^\circ$
35	44	0.8	0.127	4.775	4.521	4.521	2.47	$3.22^\circ$

### 4.3 Model stent surface characterization

#### 4.3.1 Materials and methods

In order to ensure the suitability of the designed model stents for application in *in vitro* investigations, it was necessary to carry out material surface characterization. Material surface characteristics that are of particular interest are surface topography and roughness, surface chemistry, wettability and electrochemistry.

There are several qualitative and quantitative methods available for characterization of material surface morphology, chemistry and thermodynamics [294]. The characterization methods used in this study include scanning electron microscopy (SEM), atomic force microscopy (AFM), X-ray-photoelectron spectroscopy, contact angle analysis and cyclic voltammetry. Before each characterization, Ti-6Al-4V wire samples and model stent samples were cleaned with 70% ethanol for 10 minutes in an ultrasonic cleaner and rinsed at least twice with a phosphate buffer saline (PBS) solution. Sample stents were first cleaned with 30% nitric acid before ethanol cleaning. The samples were air dried in a sterile safety cabinet for at least 20 hours.

##### 4.3.1.1 Scanning electron microscopy

Scanning electron microscopy (SEM) is used to evaluate qualitative material surface topography and roughness. In SEM, the material sample surface is scanned and bombarded with a high-energy electron beam, which causes emission of secondary electrons from the material sample [294]. Information from the secondary electrons is translated into a qualitative image of the surface

topography. Scanning electron microscopy was used to qualitatively evaluate surface topographical differences between the wires and model stents after heat treatment. Ti-6Al-4V wire and model stent samples were mounted on SEM discs with conductive tape. Surface topography and roughness characterization for both samples was performed with scanning electron microscopy LEO 1530 Gemini (Zeiss, USA) set at 10kV in secondary electron mode (SE2).

#### 4.3.1.2 Atomic force microscopy

Atomic force microscopy (AFM) is used to characterize quantitative surface roughness. In AFM, the material sample surface is scanned by the sharp tip of the cantilever-tip assembly and as the tip interacts with the sample surface, the interaction forces cause deflections, which are detected by the laser-photodiode assembly [294]. The deflections are translated into topography information, and used to construct the high-resolution 3D surface topography of the sample image. AFM also provides detailed quantitative roughness information.

Qualitative surface roughness for the Ti-6Al-4V wire and model stent samples, before and after heat treatment, were determined with the Nanoscope III atomic force microscope (Digital Instruments, Santa Barbara, CA), using Veeco software (Veeco Instruments, USA) for analysis. A scan rate of 1 Hz was used for this experiment. To reduce the error due to the wire curvature, a scan area of 10  $\mu\text{m}$  x 10  $\mu\text{m}$  was used to measure surface roughness. The maximum allowable scanning area was determined as described in Appendix E. Surface roughness was measured in terms of average roughness ( $R_a$ ) and root mean square (RMS) or  $R_q$ .  $R_a$  is the arithmetic mean, which measures the average deviation of roughness from the mean roughness profile while  $R_q$  is the quadratic mean [388].  $R_q$  is generally considered more sensitive to surface texture than  $R_a$  since surfaces with very different textures can still have similar  $R_a$  [271]. Both parameters are commonly used to describe surface texture, but there are other additional parameters that can be included to provide a much more complete information about the surface morphology [270, 388]. Hence, surface area (SA) and surface area difference ( $S_d$ ) parameters were also measured.  $S_d$ , which is a measure of surface area enlargement, is determined from the topographic area with respect to the projected or scanned area [270]. For the purpose of this research, these general surface characterization parameters were considered adequate and hence characterization was not performed to the level of detail referred to above.

#### 4.3.1.3 Contact angle analysis

Contact angle measurements characterize surface wettability, which indicates material hydrophobicity/hydrophilicity, commonly performed by either the sessile drop and the Wilhelmy method [294]. The method of choice may depend on the size and shape of the sample. For small wires or strips, the most suitable method is the dynamic contact angle analysis (DCA) using Wilhelmy method because of its operation principle [389]. Hence, this was the method of choice for this study. Details of the dynamic contact angle analysis method are described in Appendix F. The instrument used was the tensiometer Sigma 700 (KSV Instruments, Helsinki, Finland) with Milli-Q™ water. The analysis was performed with the following settings; immersion and emersion speed: 10 mm/min, start depth: 10mm, immersion depth: 20 mm and the first 2 mm were ignored.

#### 4.3.1.4 X-ray-photoelectron spectroscopy

X-ray-photoelectron spectroscopy (XPS) is one of the methods that are used to characterize material surface chemistry. The others include secondary ion mass spectrometry-time of flight (SIMS-TOF) and Fourier transform infrared spectroscopy (FTIR) [390]. These have advantages and disadvantages in accuracy and specificity, which may depend on the material surface composition. In this research, material surface chemistry was determined with XPS because it is available and is easy to interpret. XPS was performed at 15 kV, 150W. TiO<sub>2</sub> powder was used as reference standard. The reference standard was 99.9% metal basis titanium (IV) oxide powder with density of 3.9-4.23g/cm<sup>3</sup> at 20°C (Alfa Aesar, Ward Hill, MA, USA). Identification and quantification of surface element concentrations were performed with CasaXPS (Casa Software Ltd., Cheshire, UK).

#### 4.3.1.5 Cyclic voltammetry

To characterize material surface film stability and corrosion resistance, potentiodynamics polarization measurements were performed using cyclic voltammetry. Test methods for cyclic potentiodynamics polarization measurements are described in ASTM F2129-08 standard [391]. In cyclic voltammetry (CV), the potential is cycled in both the positive and negative direction (anodic and cathodic polarization), within predetermined limits. The current is monitored as a function of time or potential. The current versus potential curve provides information on the susceptibility of the material for corrosion in a given solution. The point at which the current suddenly drops at a given potential is an indicator of the surface breakdown. The higher the potential at which the current drops, the higher the corrosion resistance or surface stability.

Cyclic voltammetry method was used to check the stability of the material surface and ensure that it is the same as commercially available material. Model stent samples, 20 mm long, were used for CV electrochemical tests with Ag/AgCl and platinum as reference and center electrodes, respectively. A simulated body fluid, sometime referred to as physiological solution, with ionic concentrations similar to blood plasma and pH 7.4 was used for electrochemical tests. The simulated body fluid was prepared from analytical chemistry as per procedure previously described by Oyane [392], summarized in Appendix G. The measurements were performed with the solution kept at 37°C. Cyclic voltammetry, with current cycled between -500mV and +1500 mV and scan rate of 1 mV/s, was used for the polarization test. During the test, nitrogen was bubbled through the physiological solution to reduce oxidation of the sample surface.

### 4.3.2 Results

#### 4.3.2.1 Surface topography and roughness

Scanning electron microscopy was used to qualitatively evaluate surface roughness and topographical differences between the wires and model stents after heat treatment. The SEM surface topography micrographs for the Ti-6Al-4V wire and the model stent are depicted on Figure 4-6. Comparison of the two surfaces does not show obvious differences in surface topography and roughness.

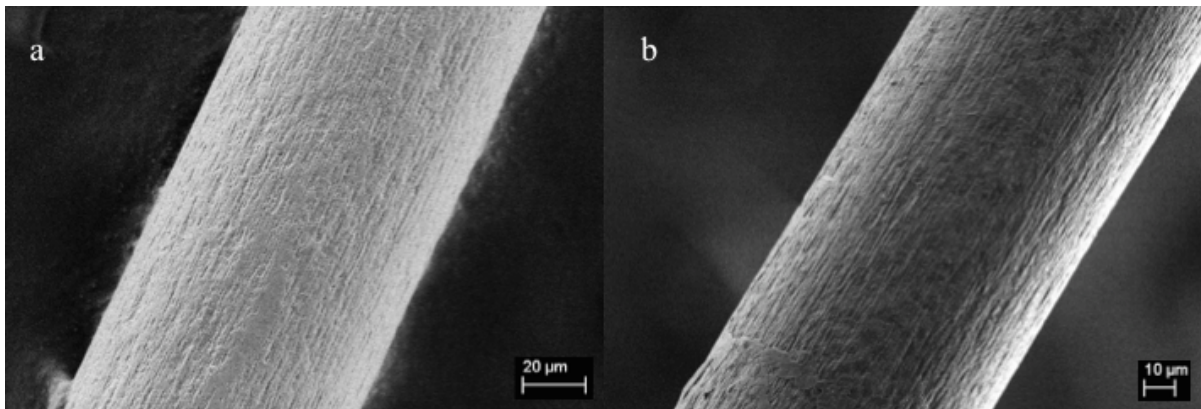


**Figure 4-6. Ti-6Al-4V SEM surface topography and roughness.** (a) The wire surface before heat treatment shows patterned ridges or grooves, oriented along the length of the wire. (b) The model stent surface shows that the pattern is retained after heat treatment. Magnification for both micrographs at 1KX.

Surface topography and roughness were also evaluated by atomic force microscopy. Randomly selected areas were examined with AFM. Figure 4-7 depicts surface topography images of randomly selected typical samples. Three randomly selected areas on the untreated wire (control) were scanned with AFM and roughness values were averaged. Two randomly selected heat-treated stents, not from the same vacuum-sealed tube, were also examined with AFM. Two examination areas were scanned on each sample and the roughness values were averaged.

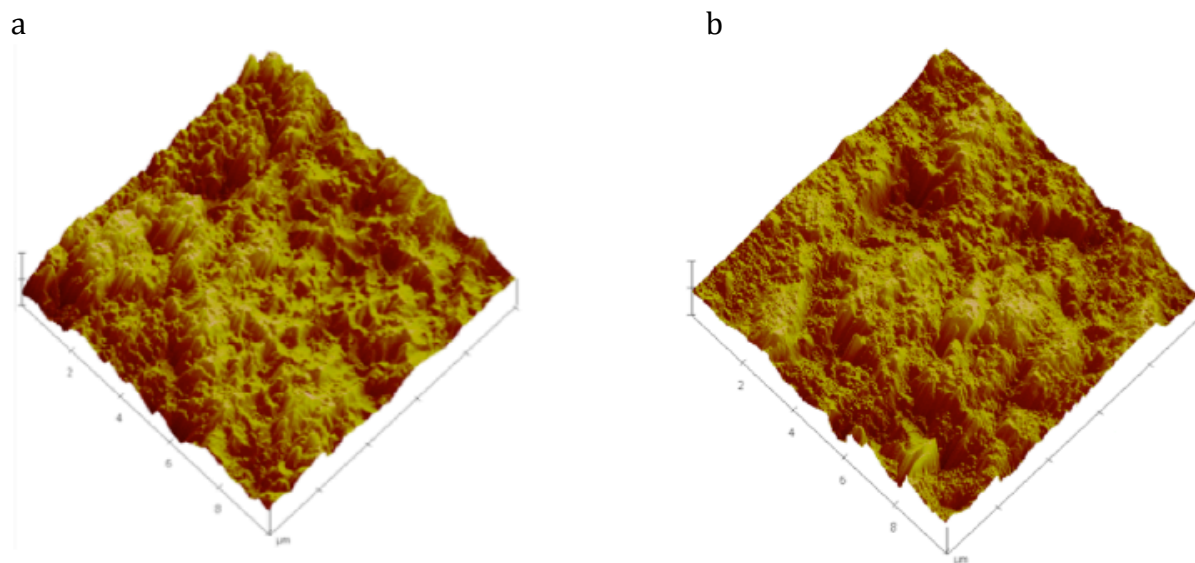


**Figure 4-7. Ti-6Al-4V AFM surface topography and roughness.** (a) Wire before heat treatment. Horizontal axis at 2  $\mu\text{m}/\text{div}$  and vertical axis at 550 nm/div. (b) Model stent after heat treatment. Horizontal axis at 2  $\mu\text{m}/\text{div}$  and vertical axis at 500 nm/div.

A summary data of the roughness values is presented on Table 4-3. The results show a slight increase in Ti-6Al-4V roughness after heat treatment. However, there was no difference in surface areas (SA) or surface area enlargement ( $S_d$ ) between treated and untreated samples. A statistical 2-tailed *t*-test comparison of the means between unheated and heat-treated samples showed that the increase in all roughness values on Table 4-3 was non-significant ( $p>0.6$ ). The level of increase or decrease in roughness after heat treatment is very dependent on the treatment environment. An increase in roughness was previously observed after treatment in air [267]. It should be noted that, as highlighted by other investigators [393], these roughness parameters, though generally used, do not

adequately describe the geometric surface characteristics. Therefore, ideally a detailed 3D characterization would be necessary to adequately characterize the surface texture.

**Table 4-3. Ti-6Al-4V surface characteristics from AFM. Results are mean  $\pm$  SD. n=3.**

	Z range (nm)	Ra (nm)	Rq (nm)	SA ( $\mu\text{m}^2$ )	S <sub>d</sub> (%)
<b>Before heat treatment</b>	996.1 $\pm$ 275.0	113.0 $\pm$ 21.4	148.0 $\pm$ 33.9	114.0 $\pm$ 2.7	14.0 $\pm$ 0.03
<b>After heat treatment</b>	1065.4 $\pm$ 190.5	122.5 $\pm$ 31.5	155.0 $\pm$ 38.0	114.1 $\pm$ 2.2	14.1 $\pm$ 0.03

#### 4.3.2.2 Wettability

Surface wettability was determined with the dynamic contact angle analysis method. The results of measurements for 6 cycle loops are presented on Table 4-4. A substantial difference between the advancing and receding contact angles was observed for the stent wires. Thermodynamic hysteresis has been associated with surface roughness and irregularities [389]. As observed from the roughness and topography characterization in the previous section, the experimental samples were not smooth, which may influence the wettability results. When hysteresis kinetics occurs, the advancing angle is used as the representative contact angle [393]. Therefore, the average contact angle for the wire sample is  $65.39^\circ \pm 1.54^\circ$  and the surface tension is  $21.46 \pm 1.28$  mN/m. It has previously been suggested that the approximate cutoff for hydrophobicity/hydrophilicity is at  $65^\circ$ , i.e. hydrophobic surfaces have contact angle  $\theta > 65^\circ$  (water adhesion tension  $< 30$  mN/m) and hydrophilic surfaces have contact angle  $\theta < 65^\circ$  (water adhesion tension  $> 30$  mN/m) [394]. Based on this cutoff and using the adhesion tension map [394], the Ti-6Al-4V samples can be characterized as weakly hydrophobic with water adhesion tension of approximately 21.5 mN/m ( $\theta \approx 65.4^\circ$ ).

**Table 4-4. Contact angle measurements**

Sample	Cycle	Advancing (degrees)			Receding (degrees)		
		Surface tension, F/L (mN/m)	Cos $\theta$	$\theta$ ( $^{\circ}$ )	Surface tension, F/L (mN/m)	Cos $\theta$	$\theta$ ( $^{\circ}$ )
Wire	1	18.861	0.366	68.54	62.076	1.204	0.00
	2	21.956	0.426	64.80	61.479	1.192	0.00
	3	22.044	0.428	64.69	60.813	1.179	0.00
	4	22.140	0.429	64.57	60.729	1.178	0.00
	5	21.794	0.423	65.00	60.373	1.171	0.00
	6	21.966	0.427	64.75	60.823	1.180	0.00

#### 4.3.2.3 Surface composition

Surface composition of the reference TiO<sub>2</sub> powder and two stent samples (unetched and acid-etched) was performed with X-ray photoelectron spectroscopy (XPS). The survey spectra of the reference sample and the stent samples are shown on Figure 4-8. The titanium (Ti) and oxygen (O) spectral signals on the stent samples were similar to the reference sample, indicating that the stent sample surface was composed of titanium oxide (TiO<sub>2</sub>). However, the carbon (C) signal was very high on the stent surfaces. The presence of C on the stent samples, normally in the form of hydrocarbons, may be due to the atmospheric contamination, which is difficult to avoid [395], although it can be reduced through appropriate sample preparation and handling. Other contaminating elements such as nitrogen can be extracted from the spectra, but they were much lower than carbon and therefore were not included for simplicity.

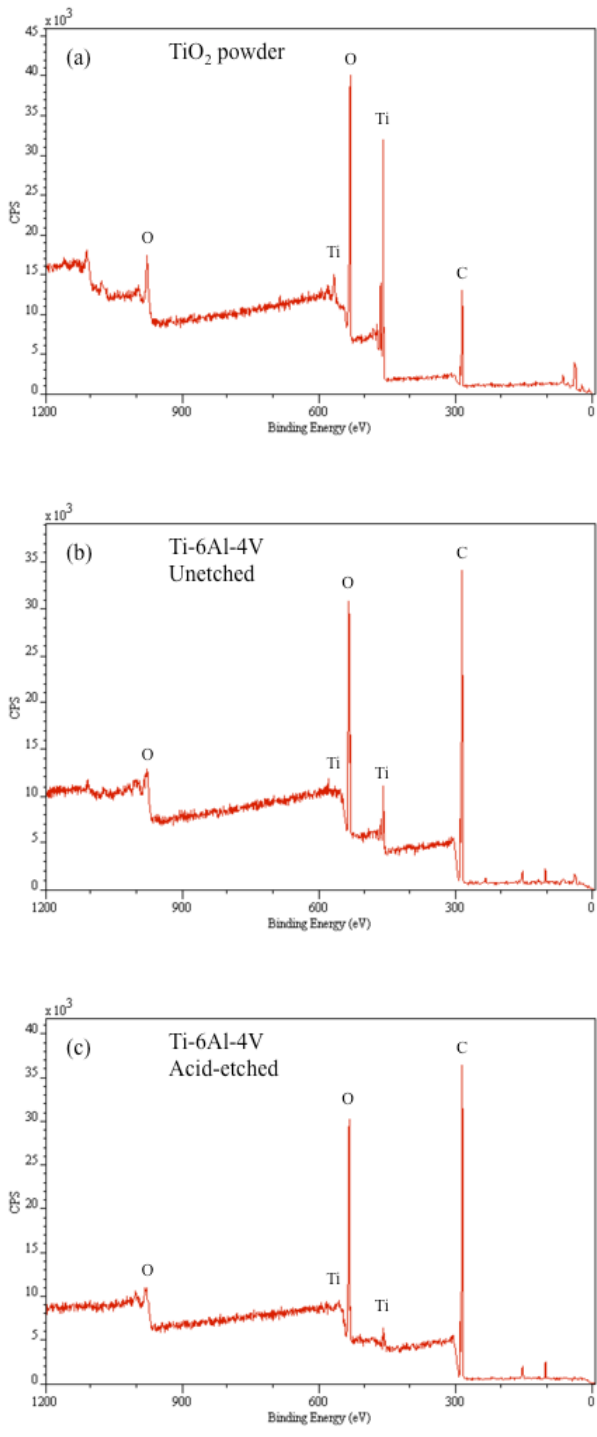


**Figure 4-8.** XPS survey spectra from (a)  $\text{TiO}_2$  powder, (b) unetched stent sample and (c) acid-etched stent sample. CPS: count per second (arbitrary units)

The concentrations of surface elements, in terms of atomic percentages, are listed on Table 4-5. The carbon levels were relatively high for all the samples, but the lowest was observed on the reference sample, at 47%. Carbon levels for the unetched and acid-etched stent samples were approximately 75% and 80%, respectively. The fact that even the reference sample had a high level of carbon suggests all the samples may have been exposed to the atmosphere for an extended period of time. The samples were processed by a third party and therefore there was little control on the handling process. Overall the analysis demonstrated that the samples had a TiO<sub>2</sub> layer.

**Table 4-5. Relative concentration (atomic %) of surface elements**

Sample	C 1s	O 1s	Al 2p	Ti 2p	V 2p
TiO <sub>2</sub> powder	47.11	39.13	0	13.76	0
Ti-6Al-4V (unetched)	74.75	22.83	0	2.42	0
Ti-6Al-4V (acid-etched)	78.57	20.53	0	0.90	0

#### 4.3.2.4 Electrochemistry

Figure 4-9 depicts the cyclic voltammetry curve for a Ti-6Al-4V model stent. The loop on the graph is produced by the reversal in the applied potential. The results show surface breakdown potential at about 1.2V, which is comparable to previously reported value for commercial Ti-6Al-4V for clinical use [282]. The small loop suggests that the surface is repassivated when the potential is reversed, after breakdown. While this test is mostly used as an indicator of corrosion resistance, here it is used to show that the material does not have any defect and is similar to commercially used material and that the titanium oxide layer formed after material treatment is stable. Thus, the results suggest that model stents have the characteristics of a stable passivation surface.

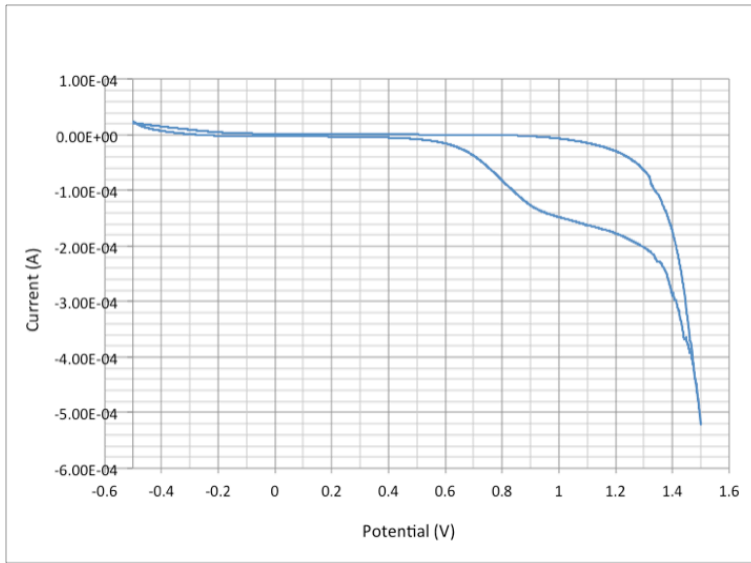


**Figure 4-9. Cyclic voltammety curve for Ti-6Al-4V model stent. The small loop suggests surface repassivation when the potential is cycled.**

#### 4.4 Summary and conclusion

In this part of the thesis, an inexpensive method was used to design and fabricate stents from Ti-6Al-4V ELI wires. In order to ensure that the surface titanium oxide layer was rutile type, model stents were shape-set in the oven at 800°C. Although other heat treatment methods can be used, it was found that the sealed vacuum treatment methods had the advantage of not requiring a special oven for heat treatment. The sealing also ensures consistency in surface oxide layer thickness since the stents can remain sealed until they need to be used. For simplicity, the design of model stents was based on a helical spring form. This facilitates analysis of the stent strut effect on flow, such as friction. Besides model stent geometry, surface characteristics are equally important. The investigation of surface characteristics of the fabricated model stents revealed that the prepared model stents had topography and roughness characteristics that were not significantly altered by heat treatment. In addition, the surface exhibited a stable titanium oxide passivation layer.

This work has demonstrated an inexpensive method for fabricating model stents for *in vitro* studies. The work also highlights some of the advantages and disadvantages of different stent preparation and oven treatment methods. This would be beneficial to other investigators so that they do not have to reinvent the wheel.

## Chapter 5

# Effect of Sample Volume on *In Vitro* Evaluation of Material-Induced Thrombogenicity

### 5.1 Introduction

In device-tissue investigations, a number of investigation methods can be used, both *in vitro* and *in vivo*. In all the methods, one of the common requirements is the standardization of processes to ensure comparability of experimental results. To that end, a number of standardization bodies, such as the International Organization for Standardization (ISO) and the American Standards for Testing and Measurement (ASTM) and AAMI/ANSI, have developed various equivalent guidance standards dealing with requirements for processing or testing of medical devices. The standards dealing with methods for testing for host response include ISO 10993-4:2002 Biological evaluation of medical devices – part 4: selection of tests for interactions with blood. *In vivo* investigations strictly adhere to these guidance standards. *In vitro* blood-biomaterial interaction studies, on the other hand, may or may not follow all or some of the guidance standards. This is despite the fact that *in vitro* studies are precursors for *in vivo* investigations. They play an important role in the initial investigation of complex biological systems and interpretation of their results serves as a guide on any decisions taken regarding further investigations or translation to the *in vivo* situation. It is therefore, important that attempts are made to follow guidance standards as well as standardize model parameters in order to improve the relevance of experimental results and facilitate comparison.

One of the important requirements in *in vitro* blood-biomaterial interaction studies is the relationship between the biomaterial sample size and the amount of blood sample, which is expressed using surface area-to-volume ratio. The significance of blood sample volume with regards to this parameter under flow conditions has been addressed in Chapter 3. While the ISO 10993 Standard compliance is important for maintaining a standard surface area-to-volume ratio, the length of time shear is applied to a stent has direct impact on time-averaged wall shear stress, one of the important physiological parameters. The other important factor is that sample volume affects the assumption of fully developed flow. For colloidal fluids like blood, whether the flow is fully developed or not is important because it influences particle-wall interaction, such as platelet dispersion [149], which affects the biochemical processes at the wall. Therefore, in using the Chandler loop model, it is necessary to ensure that all three conditions are met. Taking all these factors into consideration, the

CLSVF criterion was introduced in Chapter 3 to provide guidance on the selection of appropriate sample volume when the Chandler loop model is used with a model stent.

In addition to developing the CLSVF criterion, flow in the model was characterized. Appropriate characterization of flow is important because it has been shown that the flow type influences a number of phenomena, such as particle dispersion [56, 57, 149, 339], platelet aggregation [204] and adhesion [396] and tissue factor expression [129, 397]. As a result of flow characterization, the effect of sample volume on hemodynamics was analytically described, with and without model stents. It was demonstrated that sample volume did not have a significant effect on shear stress in the absence of model stents, except for an immobilized particle. In addition, a time-averaged wall shear stress equation was developed, taking into account the blood sample volume and stent parameters, equation (38) in Chapter 3. This equation provides an improved estimate for wall shear stress in the Chandler loop model since it incorporates some of the important curved tube flow parameters. However, it is not sufficient to characterize hemodynamics without characterizing biological implications. Hence, the next step was to experimentally validate the theoretical analysis and the new equations.

Since the time-averaged wall shear stress was shown to be dependent on blood sample volume, it was hypothesized that sample volume in the Chandler loop model influenced flow dynamics and consequently blood cell (platelets and leukocytes) activation. Therefore, the sensitivity of platelet and leukocyte activation and aggregation to sample volume, in the absence and presence of model stents, was investigated. Platelets are a key component of the hemostatic system but play diverse roles in inflammatory response and thrombosis [398]. Extracellular phospholipids exposed after activation act as binding surfaces for proteins of both the contact and coagulation systems. In addition, activated platelets produce pro/anti-inflammatory agents, form microparticles and express a variety of surface receptors [189]. Microparticles, which are cell fragments or microvesicles of 100-1000 nm size [399], are a common feature of activated platelets and other cells, both *in vitro* and *in vivo* [209, 210, 400-403]. They are estimated to account for 25% of activated platelet activity [404]. The key receptor, which has fibrinogen as its ligand, is the glycoprotein receptor GPIIb/IIIa (integrin  $\alpha_{IIb}\beta_3$ ). Platelets are activated by a variety of biological agonists as well as shear stress [202-204] and biomaterials, through adsorbed fibrinogen [155, 160]. Although platelets have been extensively studied because of their relative importance, their activation and aggregation is dependent on the characteristics of the model. Hence, it was important to include them in this study in order to understand the effect of these particular model characteristics on platelet activation. Platelet activation

was mainly characterized by platelet microparticle formation, a common feature in cardiovascular diseases [209] as well as *in vitro* and expression of the glycoprotein receptor GPIIb/IIIa (integrin  $\alpha_{IIb}\beta_3$ ). These are, at the minimum, key indicators of platelet activation.

Leukocytes are a key component of the innate immune response and therefore play an important role in biological response to implants [182]. Hence, blood-biomaterial studies would not be complete without leukocytes. In this research, leukocyte activation was investigated by expression of several surface receptors; Mac-1 (CD11b/CD18), tissue factor (TF, CD142), complement C3a receptor (C3aR) and toll-like receptor-4 (TLR-4). Mac-1 is one of the leukocyte integrin family of receptors that play important roles in health and disease [101]. Mac-1 is generally stored in the intracellular vesicles in quiescent leukocytes and expressed on the surface after activation by a variety of agonists [124]. It is a multifunctional leukocyte activation indicator and an important receptor in thrombosis because of its affinity to a variety of ligands, such as fibrinogen, soluble CD40 ligand (sCD40L), iC3b, and factor X (FX). In particular, Mac-1 has highest affinity for fibrinogen and FX zymogen, with dissociation constant  $K_d=2.2 \mu\text{M}$  and 20 nM, respectively [194]. Both of these proteins participate in the coagulation cascade. Although Mac-1 is usually upregulated by shear stress, there is evidence that there is a point at which it is down-regulated by high shear [168]. Therefore, Mac-1 response under the shear stress conditions predicted by Figure 3-8 (Chapter 3) is of particular interest in this study.

Tissue factor is regarded as a key protein in the initiation of blood coagulation. It is a transmembrane receptor not constitutively expressed on leukocytes but expressed on the surface through transcription and translation upon activation [135]. Monocytes are the main leukocyte source of TF, which is also expressed on their microparticles. TF can be initiated by a vast number of stimulants under both *in vitro* and *in vivo* conditions [127]. TF, together with activated platelets, are key risk factors for acute in-stent thrombosis [405]. TF is also induced by biomaterial surface characteristics [170]. It has been correlated with TLR4 on monocytes [406]. It has also been implicated in a number of pathological conditions. Therefore, it is an important protein in material induced thrombosis. It is however, not an enzyme and its activity in coagulation is limited to complexing with FVIIa, which is the active component. Hence, it is investigated in this research on the understanding that it provides an indirect indication of the activity of the enzyme complex.

As discussed in Chapter 2, complement protein C3 plays a key role in the complement cascade because it is a vital component of both the C3 and C5 convertases. The activation anaphylatoxin fragments C3a and C5a, and the opsonin iC3b play an important role in facilitating

inflammation and phagocytosis, respectively. To facilitate leukocytes activation and recruitment, leukocytes constitutively express complement fragment receptors, such as C3a receptor (C3aR) [69, 107]. Previous studies have suggested that the presence of C3a, which is produced from complement amplification, causes internalization of its receptor, C3aR [407]. Since C3aR is an important receptor in inflammation, it is one of the receptors that play a role in complement-mediated thrombogenicity. The ligand-receptor specificity of C3a-C3aR also makes it an interesting receptor for possible diagnosis or intervention methods. Therefore, its regulation under different experimental conditions is of particular interest in this research.

TLR4 as previously described in Chapter 2, is one of the ten human toll-like receptor family, which are the main pattern recognition receptors in innate immunity [67]. In an inflammatory response, it is engaged in leukocyte activation [66] and chemotaxis [92]. TLR4 is a receptor for LPS, which seems to have affinity to titanium surfaces [104, 105]. In addition, TLR4 was previously shown to be down-regulated by titanium particles in a murine monocyte/macrophage cell line [408]. More importantly, its stimulation on blood from normal subjects has been shown to correlate with TF [406] and modulate CD11b expression on blood of coronary artery disease patients [409]. Therefore, TLR4 is an important parameter in blood-biomaterial investigations. Although it has been studied before, it has not been characterized under the flow conditions described in this model. Hence, the need to investigate its expression in this research.

In addition to investigating platelet and leukocyte activation in the fluid phase, cell adhesion on model stent surfaces was investigated in this chapter. Surface adhesion is important when investigating material thrombogenicity. Leukocyte adhesion has been shown to be both material and shear-dependent [19, 26, 27]. The negative correlation between shear and leukocyte adhesion has also been shown in a stenotic model [332]. On polymeric materials, adherent leukocyte sensitivity to shear stress was reduced above  $7 \text{ dyn/cm}^2$  and in general leukocyte adhesion seems to be highest in the  $1\text{-}4 \text{ dyn/cm}^2$  shear stress range [332]. Interestingly, at high shear stress when shear sensitivity is lost, material-dependent adhesion may also be lost [19], although this might depend on other model parameters as a stent material effect was still observed after 2 hours in a loop model [26]. It is also interesting that inflammatory mediators such as PAF and fMLP can suppress leukocyte shear sensitivity in a dose dependent manner [410]. Thus, there are possible diverse leukocyte responses that depend on a variety of factors. The purpose of this part of the study was to investigate cell adhesion sensitivity to volume, in light of the new flow characterization, under different experimental conditions.

Therefore, the purpose of this study was to test the analytical predictions and the developed equations from Chapter 3 using numerical simulation and *in vitro* experimental investigations. While numerical investigation was only used to test the sample volume effect without model stents, *in vitro* experimental investigations were performed with and without model stents. Numerical simulation results have been previously published [411]. *In vitro* experiments were performed with the Chandler loop model parameters designed to closely mimic coronary arterial geometry and hemodynamics as depicted on Table 3-5. It was hypothesized that under shear and stent conditions, blood sample volume has an effect on blood cell activation and surface adhesion. To test this hypothesis in line with a systems approach, whole blood samples were used to investigate platelet and leukocyte activation and platelet-leukocyte aggregation. Although whole blood experiments are much more complex to interpret because isolating cause-effect is not straight forward, it provides a more appropriate biochemical environment [178] compared to isolated blood components.

## **5.2 Materials and methods**

### **5.2.1 Flow model**

The flow model was made from a rotor and turntable as previously described in Chapter 3. The turntable for mounting blood sample tube loops was fixed in a vertical position. The sample tube loops were medical grade Silastic tubes (VWR, PA, USA) with 4.78 mm internal diameter. The tubes were cut into 371 mm long sections and spliced into loops with internal loop radius of about 59 mm. The loop volume was 6.64 ml. The wall shear stress for this model is as described by equation (19), and the improved time-averaged wall shear stress is equation (39), Chapter 3.

### **5.2.2 Model stent design**

Model stents were made from Ti-6Al-4V 0.005” diameter wire (Fort Wayne Metals, Fort Wayne, IN, USA) as described in Chapter 4. Detailed specifications for the model stents are as described in Table 4-2. The stents were cut into sections of 20 mm and 35 mm lengths, giving surface area of 1.46 cm<sup>2</sup> and 2.47 cm<sup>2</sup>, respectively. The stents were first ultrasonically cleaned in 30% nitric acid to reduce the endotoxin (LPS) contamination since LPS has been shown to have high affinity for titanium surfaces [105]. After rinsing with distilled water, the stents were ultrasonically cleaned in 70% alcohol solution for about 10 minutes, and then rinsed at least twice in PBS (50 mM sodium phosphate plus 100 mM sodium chloride, pH 7.4). The prepared stents were stored in PBS at 4°C and used within 4 hours.

### **5.2.3 Antibodies and reagents**

Fluorescein isothiocyanate conjugated mouse monoclonal antibody against human glycoprotein GPIIb/IIIa (CD61-FITC), R-phycoerythrin monoclonal antibody against P-selectin (CD62-PE), Fluorescein isothiocyanate conjugated mouse monoclonal antibody against Mac-1 (CD11b-FITC), R-phycoerythrin monoclonal antibody against tissue factor (CD142-PE), anti-C3a receptor (PE hC3aRZ8) and R-phycoerythrin-cytochrome 5 conjugated monoclonal antibody against PAN leukocytes (CD45-PE-Cy5) were purchased from BD Biosciences (San Diego, CA, USA). Anti-human Toll-Like receptor 4 (CD284-PE) was purchased from eBioscience (San Diego, CA, USA). FACS lysing solution was purchased from BD Biosciences (San Diego, CA, USA). Phosphate-buffered saline (PBS) was purchased from Fisher Scientific Inc (Ottawa, ON, Canada). Lipopolysaccharide (Escherichia coli serotype 0111:B4) (LPS), 50% glutaraldehyde solution, and paraformaldehyde were purchased from Sigma-Aldrich Co (Oakville, ON, Canada). HEPES Tyrode Buffer (HTB) solution pH 7.4 was made in the laboratory with a final concentration of 137mM NaCl, 2.7mM KCl, 5mM MgCl<sub>2</sub>, 3.5mM HEPES, 1g/L Glucose, and 2g/L BSA (bovine serum albumin).

### **5.2.4 Blood sample collection**

This study received ethics clearance from the University of Waterloo Research Ethics Office. Peripheral venous blood samples were drawn with formal consent from healthy volunteers, of age range 20 to 50 years, who indicated that they had not taken any medication in the last 72 hours. There was no restriction placed on the participants' physical activity, the type of diet and eating time. Participants were however advised to drink lots of water ahead of the blood draw. Samples were drawn with a 21 Gauge Vacutainer needle and syringe (BD Biosciences, San Diego, CA, USA) by a qualified phlebotomist. Blood was immediately transferred into 10 ml conical tubes containing heparin (5U heparin/ml). Heparin was the anticoagulant of choice because it has previously been shown to cause less inhibition of platelet-monocyte aggregation, compared to other anticoagulants [412] and has also been found suitable for whole blood experiments [317]. Blood samples were kept in an insulated container and used in the blood activation experiments within 30 minutes of collection.

### **5.2.5 Platelet and leukocyte activation and platelet-leukocyte aggregation**

To assess the volume effect, either 2 ml or 4 ml blood samples were transferred into silicone tube loops, which had been prepared by rinsing with PBS, less than 30 minutes before use. To assess

the sample volume effect in the presence of biomaterial, either 20 mm or 35 mm model stents were included with the 2 ml and 4 ml blood samples, respectively. Additionally, 20 mm model stents were included with 4 ml samples to assess the effect of surface area-to-volume ratio. These gave surface area-to-volume ratios of 0.71 cm<sup>2</sup>/ml for 2 ml + 20 mm stents, 0.62 cm<sup>2</sup>/ml for 4 ml + 35 mm stents and 0.35 cm<sup>2</sup>/ml for 4 ml + 20 mm stents. Therefore, the experiments were carried out in three groups, Table 5-1. Experimental group one was composed of 2 ml blood samples with and without 20 mm stents, group two was 4 ml samples with and without 35 mm stents and group three was 4 ml samples with and without 20 mm stents. To assess shear effect, each experimental group was exposed to the two experimental conditions; each composed of two setups. Experimental condition one setups were gentle agitation on a mini-shaker (VWR, PA, USA) and rotation at 24 RPM. Experimental condition two setups were gentle agitation on a mini-shaker and rotation at 45 RPM. For all the experiments, control samples were static and included blood alone (negative control/resting sample) and blood with lipopolysaccharide (LPS) (1 µg/mL) as a positive control. All samples were incubated at 37°C for 2 hours. The 2 hour experimental time was selected because it has been reported as the typical time required for steady state protein surface adsorption [174] and steady state leukocyte receptor expression [178].

**Table 5-1. Experimental conditions**

		Experimental condition 1		Experimental condition 2	
Experimental groups		Agitate	Rotate 24 RPM	Agitate	Rotate 45 RPM
<b>I</b>	<b>2 ml</b>	x	x	x	x
	<b>2 ml + 20 mm</b>	x	x	x	x
<b>II</b>	<b>4 ml</b>	x	x	x	x
	<b>4 ml + 35 mm</b>	x	x	x	x
<b>III</b>	<b>4 ml</b>	x	x	x	x
	<b>4 ml + 20 mm</b>	x	x	x	x

### 5.2.6 Immunolabelling and flow cytometry analysis

At the end of the 2-hour incubation, small blood samples were diluted in test tubes and incubated with respective antibodies for 30 minutes for receptor-antibody binding. To assess platelet

activation and platelet microparticle (PMPs) formation, 5  $\mu\text{L}$  blood samples (about  $1.25\text{-}2\times 10^6$  platelets/sample) were diluted with 50  $\mu\text{L}$  HTB in test tubes and incubated for 30 minutes at  $4^\circ\text{C}$  with fluorescently-labeled antibodies against GPIIb/IIIa (CD61-FITC) and P-selectin (CD62PE). Following incubation, samples were further diluted with 200  $\mu\text{L}$  HTB, fixed with 200  $\mu\text{L}$  2% paraformaldehyde and stored at  $4^\circ\text{C}$  before flow cytometry analysis.

To assess leukocyte activation and platelet-leukocyte aggregation, 30 $\mu\text{L}$  of blood samples (about  $150\text{-}300\times 10^3$  leukocytes/sample) were diluted with 50  $\mu\text{L}$  HTB in test tubes and incubated for 30 minutes at  $4^\circ\text{C}$  with appropriate antibodies. Leukocytes were identified by PAN leukocyte marker (CD45 PE-Cy5.5). Leukocyte activation was identified by antibodies against Mac-1 (CD11b-FITC) and tissue factor (CD142-PE) on leukocytes. Leukocyte activation was additionally identified with antibodies against C3a receptor (anti-C3aR) and TLR4 (CD284-PE). Platelet-leukocyte aggregation was identified by antibodies against GPIIb/IIIa (CD61-FITC) on leukocytes. Following 30 minutes incubation, 700  $\mu\text{L}$  of FACS Lyse solution was added to lyse red blood cells. Aliquots were concentrated by centrifuging at 1200g for 6 minutes and discarding supernatant. Resuspended pellets were washed and then diluted with 150  $\mu\text{L}$  HTB and fixed with 150  $\mu\text{L}$  2% paraformaldehyde. All samples were stored at  $4^\circ\text{C}$  and analyzed on a BD FACS Calibur flow cytometer with CellQuest Pro software (BD Diagnostics, San Diego, CA, USA), within 5 days.

In flow cytometry, cells can be isolated on the basis of size, granularity and antibody fluorescence colors and intensity. Cell size is indicated by forward scatter laser channel (FSC-H) signal, granularity is indicated by side scatter laser channel (SSC-H) signal and fluorescence levels are determined by the specific filter, labeled FL-1 (green), FL-2 (yellow) and FL-3 (red). Flow cytometry provides both qualitative and quantitative data. There are publications on the fundamentals of flow cytometry [413] and methods to reduce background fluorescence signal noise [414]. Fluorescence intensities are reported as median intensities by normalizing the geometric mean with the geometric mean of the respective positive control. This method is commonly used because it is independent of the shape of the histogram.

### **5.2.7 Scanning electron microscopy**

After the experiment, stent samples were prepared for protein and cell surface adhesion analysis with a scanning electron microscope on a later date. Samples were first rinsed with 0.2M sodium phosphate buffer, pH 7.2 followed by fixing in 2.5% glutaraldehyde and storage at  $4^\circ\text{C}$ . Fixed

samples were then prepared for SEM analysis. Briefly, stent samples were first immersed and washed in 0.2M sodium phosphate buffer, pH 7.2. This was followed by dehydration through a series of steps in 10%, 25%, 50%, 70%, 90% and 100% ethanol. Samples were dried overnight and then coated with a thin layer of gold (8-10nm) in a vacuum chamber (Denton Vacuum, Desk II, USA) for 120sec, set at 50millitorr and 15 mA. Analysis was done with LEO 1530 Gemini (Zeiss, USA) set at 10kV in secondary electron mode (SE2). No specific marking was used to distinguish between the inner and outer stent wall, as it relates to the loop curvature.

### **5.2.8 Statistical analysis**

Statistical analysis was done with the IBM SPSS Statistics version 20. Data were analyzed using analysis of variance (2-way ANOVA). For post-hoc analysis, Least Significant Difference (LSD) method was used to determine significant difference between groups. No specific analysis was performed to account for donor variability. Overall effects are not reported due to the complexity of the data; in some cases there are fewer than three groups, e.g. volume and stent samples. All data are presented as mean±standard deviation of a minimum of 3 separate experiments from different donors. For all analysis,  $p < 0.05$  was used to indicate significant difference.

## **5.3 Results**

### **5.3.1 Effect of experimental groups and conditions on shear stress/rate**

Data from Table 3-9 and equations (38) and (39) can be used to calculate the shear stress and shear rate values, Table 5-2. These values correspond to values read directly from Figure 3-8, Chapter 3. As previously observed, the new time-averaged wall shear stress reflects the effect of changes in sample volume and stent length on fluid dynamics. Hence, for the same angular velocity, the wall shear stress is different, depending on the sample volume and model stent length.

**Table 5-2. Time-averaged wall shear stress/rate for the experimental groups and conditions**

Experimental groups	Time-averaged wall shear stress/rate at 24 RPM		Time-averaged wall shear stress/rate at 45 RPM	
	$\tau$ (dyn/cm <sup>2</sup> )	$\gamma$ (s <sup>-1</sup> )	$\tau$ (dyn/cm <sup>2</sup> )	$\gamma$ (s <sup>-1</sup> )
2 ml	13.3	380.0	27.8	794.3
4 ml	33.3	951.4	55.7	1591.4
2 ml+20 mm	12.6	360.0	26.3	751.4
4 ml+20 mm	25.2	720.0	52.7	1505.7
4 ml+35 mm	24.1	688.6	50.4	1440.0

### **5.3.2 Effect of sample volume, shear stress and stent on platelet activation**

The effect of volume on platelet activation was investigated under three conditions; without model stents, with model stents at similar surface area-to-volume ratio and at different surface area-to-volume ratios.

#### **5.3.2.1 Effect of volume and shear on platelet activation – without stents**

After a 2-hour incubation, activated platelets were characterized by formation of platelet microparticles (PMPs), expression of receptor GPIIb/IIIa (CD61) on platelets and PMPs, and P-selectin expression on platelets. Since both activated platelets and PMPs express CD61, circulating PMPs were distinguished from platelets and platelet aggregates based on size (flow cytometry forward light scatter). P-selectin expression was determined based on fluorescence levels. Figure 5-1 depicts typical flow cytometry data analysis plots for circulating PMPs, activated platelets, excluding platelet aggregates with other platelets, leukocytes and RBC (region R3). PMPs are expressed as percentage of total events (platelets + PMPs) or number of particles per 100 platelets and microparticles.

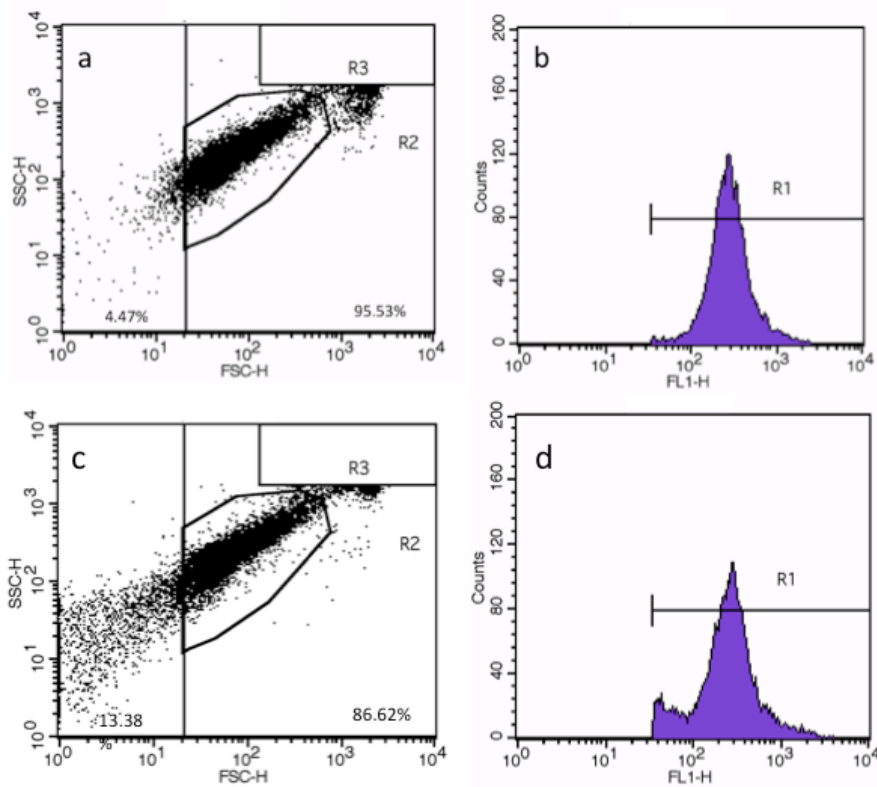


**Figure 5-1. Characteristic flow cytometry analysis plots of platelet activation in whole blood.** Negative control (rest) sample: (a) light scatter dot plot showing PMPs (4.47%) distinguished by the forward light scatter signal and (b) histogram of events (platelets and PMPs) positive for CD61. Platelet activation after model stent contact under shear ( $360 \text{ s}^{-1}$ ) for 2 ml + 20 mm stent: (c) light scatter dot plot showing PMPs (13.38%) and (d) histogram of events (platelets and PMPs) positive for CD61. FL1-H = CD61.

As shown on Table 5-3, sample volume did not have any significant effect on platelet activation, as indicated by PMP formation and CD61 under all experimental conditions. However, there was a significant difference in P-selectin expression when sample volumes were compared at 45 RPM ( $p < 0.05$ ). Shear stress did not have any significant effect on platelet activation for rotational speeds up to 45 RPM. The observed decrease in CD61 expression and P-sel increase at 45 RPM are consistent with platelet degranulation upon PMP formation.

**Table 5-3. Effect of sample volume and shear rate on platelet activation**

		Activation marker (Negative control)		
		% Platelet microparticle formation (5±1%)	CD61+ Platelets and PMPs (235±38)	P-sel Platelets (21±7)
<b>2 ml sample</b>	<b>Agitate</b>	5±1	241±42	18±4
	<b>24 RPM (380 s<sup>-1</sup>)</b>	7±1	260±10	17±6
	<b>45 RPM (790 s<sup>-1</sup>)</b>	7±2	217±24	21±2
<b>4 ml sample</b>	<b>Agitate</b>	5±2	228±36	24±8
	<b>24 RPM (950 s<sup>-1</sup>)</b>	5±1	231±30	24±3
	<b>45 RPM (1590 s<sup>-1</sup>)</b>	7±3	214±47	31±16 *

Percentages for PMPs are based on size (forward scatter signal). CD61 and P-sel expressions are reported as arbitrary fluorescent units. Bold indicates significant difference. \*significantly different from 2 ml sample at 45 RPM ( $p<0.05$ ). Results are mean ± SD,  $n=3-6$ .

### 5.3.2.2 Effect of volume and shear on platelet activation – with stents

To investigate the effect of volume on platelet activation in the presence of model stents, experiments were carried out with 2 ml + 20 mm and 4 ml + 35 mm stent samples, giving relatively similar surface area-to-volume ratios of 0.71 cm<sup>2</sup>/ml and 0.62 cm<sup>2</sup>/ml, respectively. Figure 5-2 depicts the results of PMP formation in the presence of model stents. Although shear stress alone did not have a significance effect on PMP formation, in the presence of model stents, a significant shear effect was observed for the 4 ml samples ( $p<0.01$ ). When 2 ml + 20 mm and 4 ml + 35 mm samples were compared under rotational conditions, 1.5 and 2.0-fold increase in PMP formation was observed at 24 and 45 RPM, respectively; this was a significant volume effect ( $p<0.02$ ). In addition, within the same volume sample and under identical rotational conditions, the presence of a stent resulted in a significant increase in PMP formation when compared with corresponding no-stent samples ( $p<0.02$ ). Furthermore, the combined effect of shear stress and material produced significant effect when stent samples under shear were compared with agitated samples ( $p<0.03$ ).

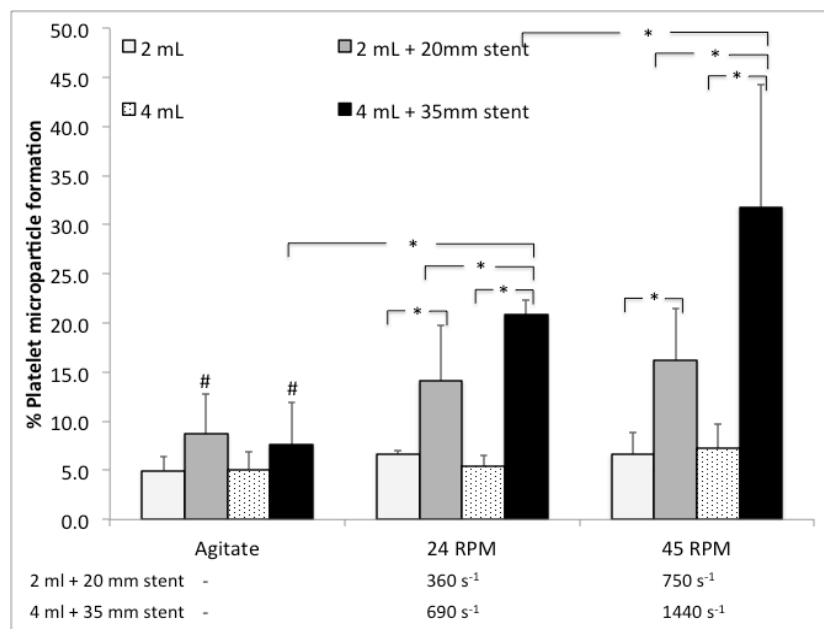


**Figure 5-2. Effect of volume, shear and stent on platelet microparticle formation.** Percentages for PMPs are based on size (forward scatter signal). \*:  $p < 0.02$ . #significantly different from corresponding stent samples under shear ( $p < 0.03$ ). Results are mean  $\pm$  SD,  $n = 3$  to 6.

Further confirmation of platelet activation was investigated by CD61 and P-selectin expression on platelets, Table 5-4. Similar to PMP formation, a significant material effect on CD61 expression on platelets and PMPs was observed under rotational conditions ( $p < 0.05$ ). When stent samples were compared with no-stent samples under rotational conditions, material effect was only significant for the 4 ml samples ( $p < 0.01$ ). However, the combined effect of shear stress and material, when compared with agitated stent samples, was significant for both 2 and 4 ml samples at 45 RPM ( $p < 0.04$ ). P-selectin on the other hand did not show significant sensitivity to shear and/or biomaterial. In general, the results suggest that for wall shear stress up to  $56 \text{ dyn/cm}^2$ , shear alone did not have a significant effect on platelet activation. On the other hand, shear in the presence of model stents resulted in significant platelet activation for the 4 ml samples. Similarly, there was a significant material effect under shear stress. Overall, the combined effect of sample volume, stent material and shear stress caused significant platelet activation.

**Table 5-4. Effect of volume, shear and stent on CD61 and P-selectin expression**

Experimental conditions		Activation marker (Negative control)	
		CD61 <sup>+</sup> Platelets and PMPs (235±38)	P-sel Platelets (21±7)
2 ml sample	Agitate	241±42	18±4
	24 RPM (380 s <sup>-1</sup> )	260±10	17±6
	45 RPM (790 s <sup>-1</sup> )	217±24	21±2
4 ml sample	Agitate	228±36	24±8
	24 RPM (950 s <sup>-1</sup> )	231±30	24±3
	45 RPM (1590 s <sup>-1</sup> )	214±47	31±16**
2ml+20mm sample	Agitate	225±40	17±5
	24 RPM (360 s <sup>-1</sup> )	222±37	17±7
	45 RPM (750 s <sup>-1</sup> )	184±25 <sup>@</sup>	22±4
4ml+35mm sample	Agitate	216±30	22±3
	24 RPM (690 s <sup>-1</sup> )	166±13 * # <sup>@</sup>	22±2
	45 RPM (1440 s <sup>-1</sup> )	143±39 * # <sup>@</sup>	24±2

CD61 and P-sel expression are reported as arbitrary fluorescent units. \*Significantly different from corresponding 2 ml + 20 mm stent sample (p<0.05), # significantly different from corresponding no-stent sample (p<0.01), @significantly different from corresponding agitated stent sample (p<0.04). \*\*significantly different from 2 ml sample at 45 RPM (p<0.05). Results are mean ± SD, n=3 to 6.

### 5.3.2.3 Effect of material surface area-to-volume ratio on platelet activation

To investigate the effect of material surface area-to-volume ratio on platelet activation, experiments were performed with 4 ml + 20 mm and 4 ml + 35 mm stent samples, giving surface area-to-volume ratios of 0.35 cm<sup>2</sup>/ml and 0.62 cm<sup>2</sup>/ml, respectively. While the surface area-to-volume ratio of 0.35 cm<sup>2</sup>/ml (20 mm stent) caused a non-significant increase in PMP formation, the surface area-to-volume ratio of 0.62 cm<sup>2</sup>/ml (35 mm stent) resulted in a significant increase in platelet activation under shear conditions (p<0.01), Figure 5-3. Comparison of PMP formation at the two

surface area-to-volume ratios revealed that a 1.8-fold increase in surface area-to-volume ratio resulted in a significant ( $p<0.01$ ) 2.6 and 3.7-fold increase in PMP formation at 24 and 45 RPM, respectively.

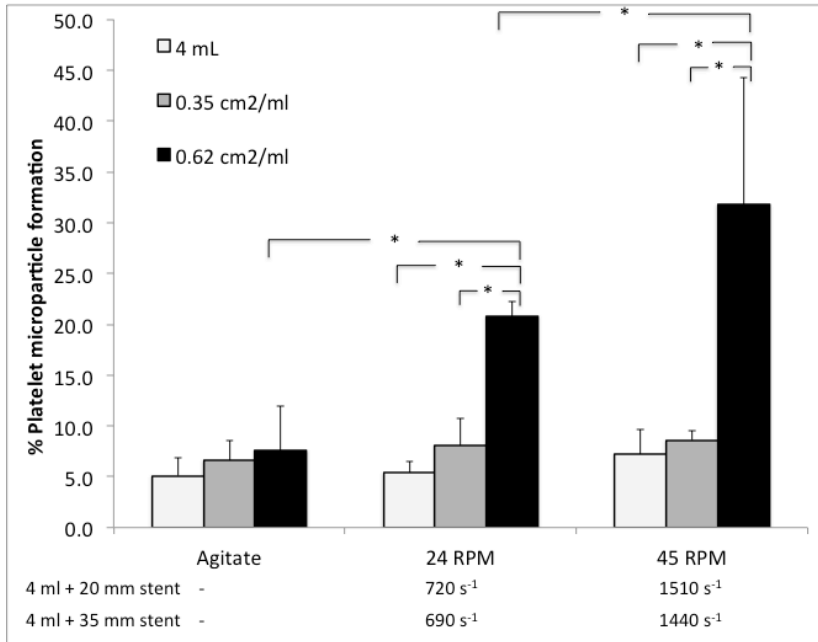


**Figure 5-3. Effect of surface area-to-volume ratio on platelet microparticle formation.** PMP percentages are based on size (forward scatter signal). \*:  $p<0.02$ . Results are mean  $\pm$  SD,  $n=3$  to 5.

Platelet activation at  $0.35 \text{ cm}^2/\text{ml}$  versus  $0.62 \text{ cm}^2/\text{ml}$  was also reflected in CD61 expression. The presence of 35 mm stents ( $0.62 \text{ cm}^2/\text{ml}$ ) caused a significant CD61 decrease on platelets and PMPs ( $p<0.01$ ), while 20 mm stents ( $0.35 \text{ cm}^2/\text{ml}$ ) caused a non-significant decrease, Table 5-5. When CD61 expression was compared between the two surface area-to-volume ratios, a significant difference was observed at 24 RPM ( $p<0.02$ ). As in previous experiments, no changes were observed in P-sel expression. The results show that at low surface area-to-volume ratio (below  $0.5 \text{ cm}^2/\text{ml}$ ), the combined effect of shear and biomaterial was not sufficient to cause a significant platelet activation under experimental conditions for this study. However, when the surface area-to-volume ratio was increased above  $0.5 \text{ cm}^2/\text{ml}$ , the lower limit of the recommended range, a significant increase in PMP formation was observed under both shear conditions. This suggests that shear significantly augments material-induced PMP formation only when there is sufficient surface-area-to volume ratio. Thus, our results suggest that PMP formation is surface area dependent.

**Table 5-5. Effect of surface area-to-volume ratio on CD61 and P-sel expression**

Experimental conditions		Activation marker	
		(Negative control)	
		CD61 <sup>+</sup> Platelets and PMPs (235±38)	P-sel Platelets (21±7)
4 ml sample	24 RPM (950 s <sup>-1</sup> )	231±30	24±3
	45 RPM (1590 s <sup>-1</sup> )	214±47	31±16
0.35 cm <sup>2</sup> /ml sample	24 RPM (720 s <sup>-1</sup> )	220±17	24±5
	45 RPM (1510 s <sup>-1</sup> )	180±40	33±17
0.62 cm <sup>2</sup> /ml sample	24 RPM (690 s <sup>-1</sup> )	166±13 * #	22±2
	45 RPM (1440 s <sup>-1</sup> )	143±39 #	24±2

CD61 and P-sel expression are reported as arbitrary fluorescent units. \*Significantly different from corresponding 0.35 cm<sup>2</sup>/ml sample (p<0.02), #significantly different from corresponding no-stent sample (p<0.01). Results are mean ± SD, n=3 to 5.

### 5.3.3 Effect of sample volume, shear stress and stent on leukocyte activation

Similar to platelet activation, the effect of volume on leukocyte activation was investigated under three conditions; without model stents, with model stents at similar surface area-to-volume ratio and at different surface area-to-volume ratios.

#### 5.3.3.1 Effect of sample volume and shear on leukocyte activation – without stents

Leukocytes were determined by expression of CD45 and leukocyte sub-populations (monocytes, PMNs and lymphocytes) were distinguished by side and forward light scatter signals, i.e. cell granularity and size, respectively. Activated leukocytes were characterized by surface expression of CD11b (Mac-1) and TF (CD142) and complement C3a receptor (C3aR). Preliminary investigation of toll-like receptor 4 (TLR-4) expression on leukocytes was also performed.

The effect of sample volume on leukocyte activation, as indicated by the percentage of monocytes expressing TF, and Mac-1 and C3aR expression on leukocytes, are presented in Table 5-6. Changing blood sample volume in the absence of model stents did not result in any changes in the

percentage of monocytes expressing TF. While volume changes did not affect TF expression on monocytes, a decrease in Mac-1 expression on monocytes was observed when sample volume was changed from 2 to 4 ml, which was significant at 24 RPM ( $p=0.05$ ). The increase in volume also had a slight down-regulation effect on Mac-1 expression on PMNs. On the other hand, volume change did not have a significant effect on C3aR expression on both monocytes and PMNs.

Unlike change in volume, increase in shear rate ( $380\text{ s}^{-1}$  to  $790\text{ s}^{-1}$  for 2 ml and  $950\text{ s}^{-1}$  to  $1590\text{ s}^{-1}$  for 4 ml sample) had a down-regulation effect on percentage of monocytes expressing TF, Table 5-6. Increasing shear also had a down-regulation effect on Mac-1 expression on leukocytes. Similar to TF and Mac-1, C3aR expression was down-regulated when shear was increased. C3aR expression was significantly down-regulated compared to agitated samples on both monocytes and PMNs,  $p<0.01$  and  $p<0.03$ , respectively. In general, increasing volume in the absence of stents had an insignificant effect on TF and C3aR expression, but had a down-regulation effect on Mac-1 expression on leukocytes. Shear stress had a down-regulation effect on all the leukocyte activation markers.

Preliminary investigations on the effect of volume and shear on TLR-4 expression on leukocytes were also performed and the results are presented in Table 5-7. Although there was a significant volume effect on some samples, conclusions on TLR-4 expression cannot be drawn from the preliminary data due to the small number of samples ( $n=2$ ).

**Table 5-6. Effect of volume and shear on leukocyte activation**

Marker (Negative control)	Experimental condition			<i>p</i> -value				
	$\omega$ , RPM	2 ml sample	4 ml sample	2ml vs 4ml	Agitate vs 2ml	Agitate vs 4ml	24 vs 45 RPM (2ml)	24 vs 45 RPM (4ml)
% Monocytes expressing TF (9±2)	Agitate	18±6	17±4	0.81				
	24 RPM	20±6	20±9	0.92	0.81	0.49		
	45 RPM	16±4	15±7	0.90	0.70	0.74	0.55	0.33
Mac-1 expression on monocytes (%) (29±12)	Agitate	34±5	35±10	0.87				
	24 RPM	55±4	39±16	<b>0.05</b>	<b>0.01</b>	0.43		
	45 RPM	45±7	33±8	0.09	0.10	0.78	0.25	0.33
Mac-1 expression on PMNs (%) (23±6)	Agitate	18±6	26±7	0.11				
	24 RPM	26±4	20±9	0.43	0.26	0.26		
	45 RPM	24±14	18±5	0.30	0.31	0.11	0.85	0.66
C3aR expression on monocytes (%) (115±18)	Agitate	123±18	128±22	0.69				
	24 RPM	111±6	118±16	0.68	0.44	0.39		
	45 RPM	99±20	96±26	0.87	0.10	<b>0.01</b>	0.52	0.12
C3aR expression on PMNs (%) (144±29)	Agitate	150±17	137±32	0.36				
	24 RPM	131±17	126±16	0.84	0.34	0.47		
	45 RPM	110±29	123±40	0.49	<b>0.03</b>	0.36	0.36	0.86

Bold indicates significant difference. Shear rate: 2 ml at 24 and 45 RPM is equivalent to 380 s<sup>-1</sup> and 790 s<sup>-1</sup>, 4 ml at 24 and 45 RPM is equivalent to 950 s<sup>-1</sup> and 1590 s<sup>-1</sup>. Results are mean ± SD, n=3 to 5.

**Table 5-7. Effect of volume and shear on TLR-4 expression on leukocytes**

Marker (Negative control)	Experimental conditions			<i>p</i> -value		
		2 ml	4 ml	2 ml vs 4 ml	24 vs 45 RPM (2ml)	24 vs 45 RPM (4ml)
<b>TLR4 expression on monocytes (%)</b> (88±16)	<b>Agitate</b>	87±32	101±19	0.22		
	<b>24 RPM</b>	85±11	105±22	0.21		
	<b>45 RPM</b>	87±30	85±13	ND	ND	0.33
<b>TLR4 expression on PMNs (%)</b> (92±21)	<b>Agitate</b>	67±16	97±14	<b>0.003</b>		
	<b>24 RPM</b>	69±11	94±11	<b>0.05</b>		
	<b>45 RPM</b>	70±2	97±14	ND	ND	0.79

Bold indicates significant difference. Shear rate: 2 ml at 24 and 45 RPM is equivalent to 380 s<sup>-1</sup> and 790 s<sup>-1</sup>, 4 ml at 24 and 45 RPM is equivalent to 950 s<sup>-1</sup> and 1590 s<sup>-1</sup>. 2 ml samples: n=5 except for samples at 45 RPM (n=2); 4 ml samples: n=3 to 5. ND: not determined due to small sample size. Results are mean ± SD.

### 5.3.3.2 Effect of sample volume and shear on leukocyte activation – with model stents

The effect of sample volume on leukocyte activation was also investigated in the presence of model stents. To perform this investigation, experiments were carried out with 2 ml + 20 mm stents and 4 ml + 35 mm stents sample, giving relatively similar surface area-to-volume ratios of 0.71 cm<sup>2</sup>/ml and 0.62 cm<sup>2</sup>/ml, respectively and thus allowing us to assess the potential effect of sample volume on activation.

The effect of volume on percentage of monocytes expressing TF is depicted on Figure 5-4. Changing blood sample volume in the presence of model stents did not result in any changes in the percentage of monocytes expressing TF. When stent samples were compared with no-stent samples, the presence of stents did not result in significant changes in TF expression under agitation while a significant increase in the percentage of monocytes expressing TF (*p*<0.01) was observed at both 24 RPM and 45 RPM regardless of volume. Thus, the combined shear-stent interaction had a significant effect on TF expression.

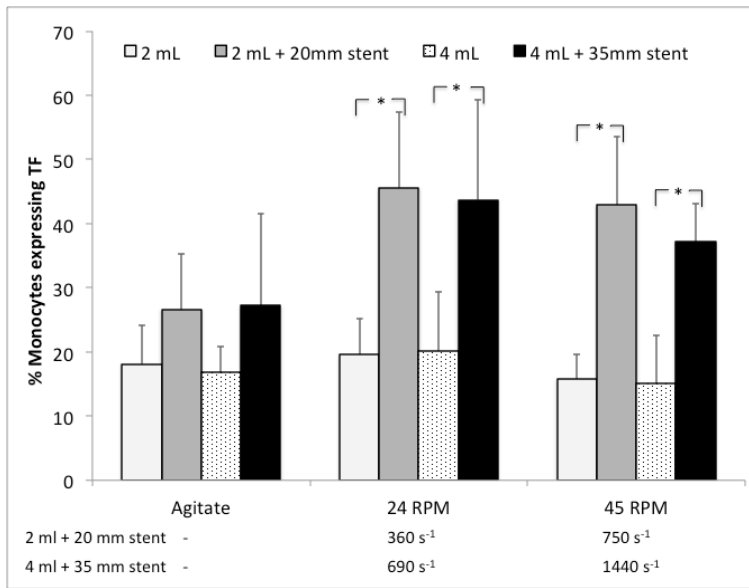


**Figure 5-4. Effect of volume, shear and stent on percentage of monocytes expressing TF.** \*:  $p < 0.05$ . Results are mean  $\pm$  SD,  $n = 3$  to  $5$ .

Table 5-8 depicts the results of the effect of sample volume on Mac-1 and C3aR receptor expression on leukocytes in the presence of model stents, for similar surface area-to-volume ratios. The presence of a stent led to an increase in Mac-1 expression on monocytes and PMNs. The increase in Mac-1 expression on monocytes was significant ( $p < 0.02$ ) for all 4 ml samples under all experimental conditions. Mac-1 expression on PMNs was significant ( $p < 0.02$ ) for all samples under agitate and 24 RPM. At 45 RPM, Mac-1 expression in both stent and non-stent samples was down regulated to the range of control values, and hence the difference between the samples was not significant.

For C3aR expression on leukocytes, unlike TF and Mac-1 expression, the presence of stents did not result in any significant difference under all experimental conditions. In general, volume did not have a significant effect on Mac-1 and C3aR expression on leukocytes for samples with similar surface area-to-volume ratio. However, the results generally show a significant material effect on Mac-1 and TF expression and limited effect on C3aR expression.

TLR-4 expression was also investigated and preliminary results are presented in Figure 5-5. Based on the 4 ml samples, the presence of stents under shear caused a significant upregulation in TLR-4 expression ( $p < 0.02$  for monocytes and  $p < 0.04$  for PMNs). In addition, the results suggest that

shear stress had a down regulation effect on TLR-4 expression on leukocytes. However, conclusions cannot be drawn due to the limited number of samples.

**Table 5-8. Effect of volume in the presence of model stent on Mac-1 and C3aR expression on leukocytes**

Marker (Negative control)	Experimental condition					p-value		
	$\omega$ , RPM	2ml	2ml + 20mm	4ml	4ml + 35mm	2ml vs 2ml+20mm	4ml vs 4ml+35mm	2ml+20mm vs 4ml+35mm
% Mac-1 expression on monocytes (29±12)	Agitate	34±5	49±10	35±10	55±19	<b>0.01</b>	<b>0.001</b>	0.33
	24 RPM	55±4	63±2	39±16	61±3	0.36	<b>0.01</b>	0.81
	45 RPM	45±7	58±12	33±8	70±13	0.11	<b>&lt;0.001</b>	0.14
% Mac-1 expression on PMNs (23±6)	Agitate	18±6	33±8	26±7	44±14	<b>0.01</b>	<b>0.001</b>	<b>0.03</b>
	24 RPM	26±4	44±5	20±9	43±8	<b>0.02</b>	<b>0.002</b>	0.84
	45 RPM	24±14	27±18	18±5	26±13	0.64	0.21	0.88
% C3aR expression on monocytes (115±18)	Agitate	123±18	140±21	128±22	143±40	0.21	0.22	0.80
	24 RPM	111±6	125±16	118±16	144±27	0.46	0.12	0.33
	45 RPM	99±20	114±42	96±26	104±42	0.37	0.64	0.59
% C3aR expression on PMNs (144±29)	Agitate	150±17	143±16	137±32	124±45	0.64	0.40	0.26
	24 RPM	131±17	125±19	126±16	138±33	0.80	0.58	0.59
	45 RPM	110±29	112±41	123±40	111±62	0.91	0.57	0.97

Bold indicates significant difference. Shear rates: 24 RPM with 2 ml and 4 ml = 380 s<sup>-1</sup> and 950 s<sup>-1</sup>; 45 RPM with 2 ml and 4 ml = 790 s<sup>-1</sup> and 1590 s<sup>-1</sup>; 24 RPM with 2 ml + 20 mm and 4 ml + 35 mm stent = 360 s<sup>-1</sup> and 690 s<sup>-1</sup>; 45 RPM with 2 ml + 20 mm and 4 ml + 35 mm = 750 s<sup>-1</sup> and 1440 s<sup>-1</sup>. Results are mean ± SD, n=3 to 5.

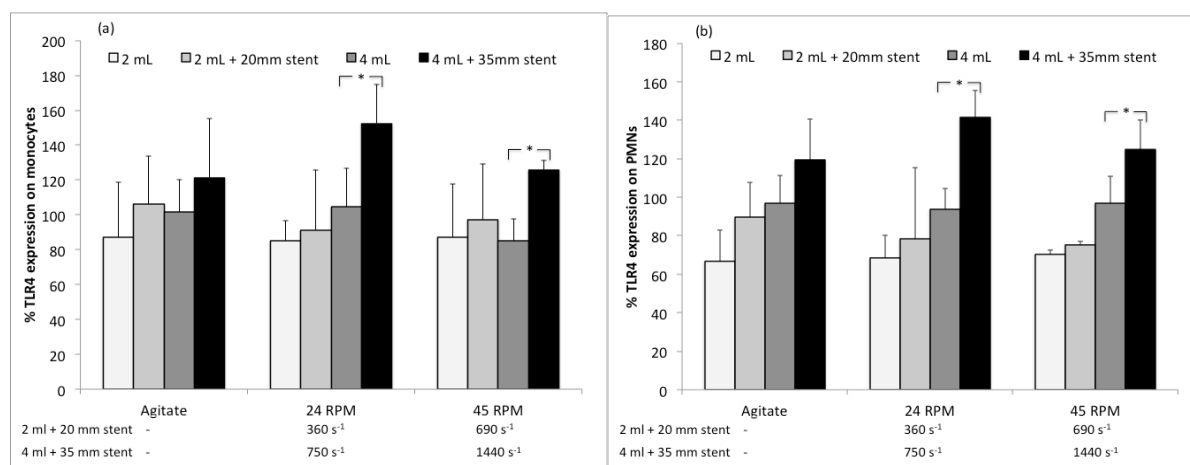


**Figure 5-5. Effect of volume, shear and stent on TLR-4 expression.** \*:  $p < 0.04$ . Results are mean  $\pm$  SD. 2 ml samples:  $n=5$  except for samples at 45 RPM ( $n=2$ ); 4 ml samples:  $n=3$  to 5.

The effect of sample volume on Mac-1 and C3aR receptor expression on leukocytes in the presence of model stents, for similar surface area-to-volume ratios, were further investigated in Table 5-9. Mac-1 expression on monocytes was not significantly changed by changing blood sample volume while keeping the surface area-to-volume ratio constant, for agitated and rotational samples. Increasing shear rate (by increasing rotational speed from 24 RPM to 45 RPM) in the presence of stents down-regulated Mac-1 expression on monocytes for the 2 ml + 20 mm stent but was upregulated for the 4 ml + 35 mm samples. Similar to Mac-1 expression on monocytes, changing the sample volume while keeping the surface area-to-volume ratio constant did not result in significant changes in Mac-1 expression on PMNs. However, unlike Mac-1 expression on monocytes, increasing shear rate in the presence of stents resulted in a significant down-regulation in Mac-1 expression on PMNs for both samples ( $p < 0.05$ ).

There was also no observed significant difference in C3aR expression on leukocytes between samples with similar surface area-to-volume ratio when sample volume was changed, Table 5-9. However, similar to TF and Mac-1 expression, increasing shear stress in the presence of stents down-regulated C3aR expression on leukocytes, which was significant ( $p=0.04$ ) on monocytes for 4 ml + 35 mm samples. It is interesting to note that the samples showing significant decrease in C3aR expression correspond to the samples with increased Mac-1 expression, which was contrary to other samples.

Although volume did not generally have a significant effect on Mac-1 expression on leukocytes for samples with similar surface area-to-volume ratio, the results suggest some differences under shear. Increasing shear rate generally down regulated Mac-1 expression, except for Mac-1 expression on monocytes for the 4 ml with 35 mm stent samples.

**Table 5-9. Effect of volume, shear and stent on Mac-1 and C3aR expression on leukocytes**

Marker (Negative control)	Experimental condition			p-value			
	$\omega$ , RPM	2ml + 20mm sample	4ml + 35mm sample	Agitate vs 2ml+20mm	Agitate vs 4ml+35mm	24 vs 45 RPM (2ml+20mm)	24 vs 45 RPM (4ml+35mm)
% Mac-1 expression on monocytes (29±12)	Agitate	49±10	55±19				
	24 RPM	63±2	61±3	0.06	0.43		
	45 RPM	58±12	70±13	0.19	<b>0.05</b>	0.53	0.30
% Mac-1 expression on PMNs (23±6)	Agitate	33±8	44±14				
	24 RPM	44±5	42±8	0.10	0.79		
	45 RPM	27±18	26±13	0.32	<b>0.01</b>	<b>0.02</b>	<b>0.04</b>
% C3aR expression on monocytes (115±18)	Agitate	140±21	143±40				
	24 RPM	125±16	144±27	0.39	0.94		
	45 RPM	114±42	104±42	0.09	<b>0.02</b>	0.54	<b>0.04</b>
% C3aR expression on PMNs (144±29)	Agitate	143±16	124±45				
	24 RPM	125±19	138±33	0.38	0.52		
	45 RPM	112±41	111±62	0.10	0.54	0.59	0.27

Bold indicates significant difference. Shear rates: 24 RPM with 2 ml + 20 mm and 4 ml + 35 mm stent =  $360 \text{ s}^{-1}$  and  $690 \text{ s}^{-1}$ ; 45 RPM with 2 ml + 20 mm and 4 ml + 35 mm =  $750 \text{ s}^{-1}$  and  $1440 \text{ s}^{-1}$ . Results are mean  $\pm$  SD, n=3 to 5.

### 5.3.3.3 Effect of surface area-to-volume ratio on leukocyte activation

Since material surface area-to-volume ratio is an important factor, as previously discussed, its effect on leukocyte activation was investigated further. To investigate the effect of material surface area-to-volume ratio, experiments were performed with 4 ml + 20 mm and 4 ml + 35 mm stent samples, giving surface area-to-volume ratios of 0.35 cm<sup>2</sup>/ml and 0.62 cm<sup>2</sup>/ml, respectively. While the presence of a 20 mm stent did not cause a significant increase in Mac-1 expression on monocytes (Figure 5-6(a)), the presence of 35 mm stent resulted in a significant increase in Mac-1 expression under all experimental conditions (p<0.01). When the samples with stents were compared, higher Mac-1 expression was observed on the samples with higher surface area-to-volume ratio, which was significant at 45 RPM (p<0.01). Increasing shear rate resulted in Mac-1 down-regulation for the 20 mm stent samples and upregulation for the 35 mm samples. The upregulation was significant when compared with agitated samples (p<0.05).

Unlike Mac-1 expression on monocytes, there was a significant difference in Mac-1 expression on PMNs (p<0.05) between 0.35 cm<sup>2</sup>/ml and 0.62 cm<sup>2</sup>/ml samples, for agitated and 24 RPM conditions, Figure 5-6(b). Comparison of stent samples shows higher Mac-1 expression on samples with higher surface area-to-volume ratio, similar to expression on monocytes. Increasing shear significantly down regulated Mac-1 expression on PMNs (p<0.04), for both stent samples. The down-regulation was also significant when compared with the agitated samples (p<0.02).

Overall, Mac-1 expression on leukocytes was upregulated with surface area-to-volume ratio. Shear rate had an upregulation effect on Mac-1 expression on monocytes for the 0.62 cm<sup>2</sup>/ml sample, but generally had a significant down-regulation effect on PMNs.

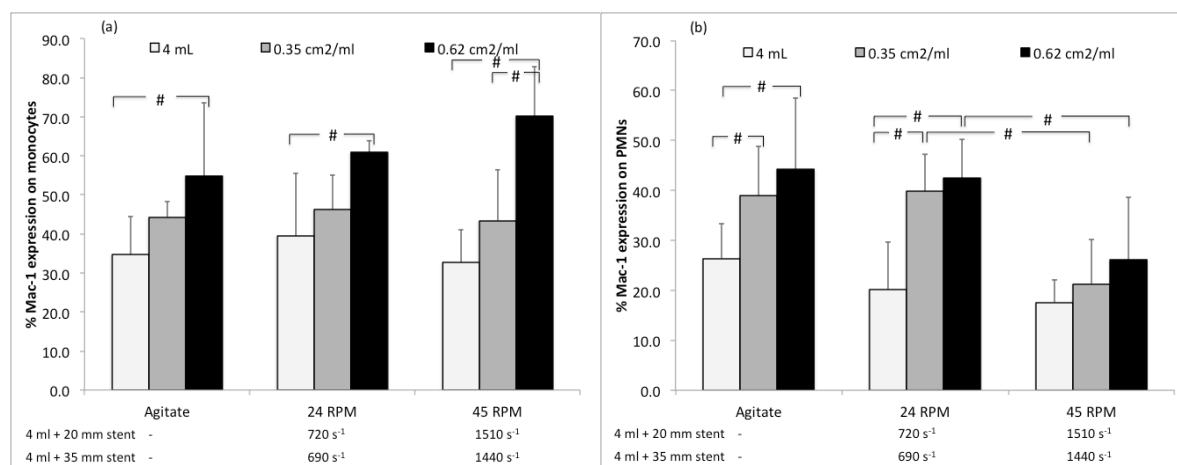


**Figure 5-6. Effect of surface area-to-volume ratio on Mac-1 expression on (a) monocytes, (b) PMNs. #:  $p < 0.05$ . Results are mean  $\pm$  SD,  $n = 3$  to 5.**

For C3aR expression on both monocytes and PMNs, neither the presence of model stents nor the difference in surface area-to-volume ratio had any significant effect, Table 5-10. Comparison of stent samples shows a slight upregulation in C3aR expression on both monocytes and PMNs with increased surface area-to-volume ratio at 24 RPM for the 0.62 cm<sup>2</sup>/ml sample (690 s<sup>-1</sup>) compared with the 0.35 cm<sup>2</sup>/ml sample (720 s<sup>-1</sup>). However, at 45 RPM the results are opposite; expression on the 0.62 cm<sup>2</sup>/ml (1440 s<sup>-1</sup>) is lower compared to the 0.35 cm<sup>2</sup>/ml (1510 s<sup>-1</sup>). When shear rate was increased (24 RPM to 45 RPM), a down-regulation in C3aR expression on monocytes was observed on both stent samples, which was significant for the 0.62 cm<sup>2</sup>/ml sample ( $p < 0.05$ ). Similarly, increase in shear rate down-regulated C3aR expression on PMNs for the high surface area-to-volume ratio samples, albeit non-significant, but slightly upregulated C3aR expression for the low surface area-to-volume ratio. Therefore, C3aR sensitivity to surface area was not significant but there was significant shear sensitivity on monocytes.

TLR-4 expression on the other hand showed sensitivity to material surface area-to-volume ratio, Table 5-10. TLR-4 expression on leukocytes was upregulated in the presence of model stents, when compared with non-stent samples, which was significant for the higher surface area-to-volume ratio under all shear conditions ( $p < 0.05$ ). When stent samples were compared, higher TLR-4 expression was observed on samples with high surface area-to-volume ratio compared with low surface area-to-volume samples. The difference was significant for PMN at 24 RPM. Although increasing shear rate (24 RPM to 45 RPM), resulted in the down-regulation of TLR-4 on all stent

samples, no definitive conclusion can be drawn from this observation due to the small number of samples at 45 RPM. In general, leukocytes showed sensitivity to material surface area-to-volume ratio.

**Table 5-10. Effect of surface area-to-volume ratio on C3aR and TLR-4 expression on leukocytes**

Marker (Negative control)	Experimental condition				p-value				
	$\omega$ , RPM	4ml sample	0.35 cm <sup>2</sup> /ml sample	0.62 cm <sup>2</sup> /ml sample	4ml vs 0.35 cm <sup>2</sup> /ml	4ml vs 0.62 cm <sup>2</sup> /ml	0.35 cm <sup>2</sup> /ml vs 0.62 cm <sup>2</sup> /ml	24 vs 45 RPM (0.35 cm <sup>2</sup> /ml)	24 vs 45 RPM (0.62 cm <sup>2</sup> /ml)
% C3aR expression on monocytes (115±18)	Agitate	128±22	143±23	143±40	0.26	0.22	0.99		
	24 RPM	118±16	127±8	144±27	0.60	0.12	0.37		
	45 RPM	96±26	119±15	104±42	0.19	0.64	0.45	0.69	<b>0.04</b>
% C3aR expression on PMNs (144±29)	Agitate	137±32	145±19	124±45	0.62	0.40	0.25		
	24 RPM	126±16	111±7	138±33	0.48	0.58	0.28		
	45 RPM	123±40	132±10	111±62	0.68	0.57	0.40	0.41	0.27
% TLR-4 expression on monocytes (88±17)	Agitate	101±19	110±6	121±34	0.41	<b>0.05</b>	0.36		
	24 RPM	105±22	127±19	153±22	0.12	<b>0.001</b>	0.11		
	45 RPM	85±13	101±12	126±6	0.35	<b>0.01</b>	0.17	0.15	0.10
% TLR-4 expression on PMNs (94±21)	Agitate	97±14	107±12	119±21	0.25	<b>0.01</b>	0.20		
	24 RPM	94±11	116±16	142±14	0.06	<b>&lt;0.001</b>	<b>0.05</b>		
	45 RPM	97±14	100±22	125±15	0.83	<b>0.02</b>	0.09	0.28	0.20

Bold indicates significant difference. Results are mean ± SD, n = 2 to 5 (n=2 for TLR4-4 0.35 cm<sup>2</sup>/ml, 45 RPM).

### **5.3.4 Effect of sample volume, shear and stent on platelet-leukocyte aggregation**

To understand and relate the effect of platelet and leukocyte activation on platelet-leukocyte aggregation, the effect of blood sample volume on fluid phase platelet-leukocyte aggregation was also investigated under three similar conditions as above. Platelet-leukocyte aggregates were characterized by GPIIb/IIIa expression on CD45 expressing leukocytes. Orthogonal light scatter, as previously described, was used to distinguish leukocyte sub-population aggregates.

#### **5.3.4.1 Effect of volume and shear on platelet-leukocyte aggregation – without stents**

The results of sample volume effect on platelet-leukocyte aggregation, in the absence of model stents, are depicted on Table 5-11. When 2 ml and 4 ml samples were compared under the same experimental conditions, lower platelet-leukocyte aggregation was observed for the 4 ml samples, although non-significant. Increasing shear rate by increasing angular velocity (24 to 45 RPM) resulted in a decrease in platelet-leukocyte aggregation in both 2 ml and 4 ml samples. The platelet-monocyte aggregation decrease was significant in the 4 ml sample at 45 RPM ( $1590 \text{ s}^{-1}$ ) compared with the agitated sample ( $p < 0.01$ ).

In general, higher platelet-monocyte aggregation was observed compared with platelet-PMN aggregation under all experimental conditions. A noticeable but non-significant difference in platelet-leukocyte aggregation was observed between the volume samples under shear. Generally, shear rate had a reducing effect on platelet-leukocyte aggregation.

**Table 5-11. Effect of volume and shear on platelet-leukocyte aggregation**

Marker (Negative control)	Experimental condition			<i>p</i> -value				
	$\omega$ (shear rate)	2 ml sample	4 ml sample	2 ml vs 4ml	Agitate vs 2ml	Agitate vs 4ml	24 vs 45 RPM (2ml)	24 vs 45 RPM (4ml)
<b>Platelet-monocyte aggregates</b> (180.8±109.9)	<b>Agitate</b>	381±132	287±105	0.17				
	<b>24 RPM (380 s<sup>-1</sup>)</b>	379±147	189±63	0.06	0.98	0.17		
	<b>45 RPM (790 s<sup>-1</sup>)</b>	247±164	72±28	0.06	0.13	<b>0.003</b>	0.22	0.15
<b>Platelet-PMN aggregates</b> (33.3±15.7)	<b>Agitate</b>	67±39	51±24	0.66				
	<b>24 RPM (950 s<sup>-1</sup>)</b>	112±53	58±24	0.30	0.33	0.88		
	<b>45 RPM (1590 s<sup>-1</sup>)</b>	17±2	16±3	0.97	0.23	0.32	0.07	0.34

Platelet-monocyte/PMN aggregates are reported as arbitrary fluorescent units. Results are mean ± SD, n=3 to 5.

#### 5.3.4.2 Effect of volume and shear on platelet-leukocyte aggregation – with stents

To investigate the effect of volume on leukocyte activation in the presence of model stents, experiments were carried out with different sample volumes but relatively similar surface area-to-volume ratio; 2 ml + 20 mm stents ( $0.71 \text{ cm}^2/\text{ml}$ ) and 4 ml + 35 mm stents sample ( $0.62 \text{ cm}^2/\text{ml}$ ). The presence of model stents produced a significant increase ( $p < 0.01$ ) in platelet-monocyte aggregation under all experimental conditions, Figure 5-7(a). Comparison of stent samples under the same experimental conditions showed that there was no sample volume effect on platelet-monocyte aggregation for agitated and 24 RPM conditions. However, a significant volume effect was observed at 45 RPM ( $p < 0.03$ ). When shear was increased, a decrease in platelet-monocyte aggregation was observed for the 2 ml + 20 mm stent sample while an increase was observed for the 4 ml + 35 mm stent sample, which was significant when compared with the agitated sample ( $p < 0.01$ ). In fact, both 4 ml + 35 mm stent samples under shear were significantly higher than the agitated sample ( $p < 0.01$ ).

For platelet-PMN aggregation, the presence of model stents resulted in a significant increase in platelet-PMN aggregation ( $p < 0.02$ ), except for the 2 ml + 20 mm samples at 45 RPM ( $p = 0.64$ ), Figure 5-7(b). Similar to platelet-monocyte aggregation, there was no significant volume effect observed either when the stent samples were compared under the same conditions. When shear was increased, there was a significant decrease in platelet-PMN aggregation for both stent samples ( $p < 0.05$ ).

In general sample volume did not have a significant effect on platelet-leukocyte aggregation for similar surface area-to-volume ratio samples, except at high shear. The presence of model stents produced significant aggregation, which was diminished at high shear due to the significant shear-dependent decrease in platelet-leukocyte aggregation. The exception was platelet-monocyte aggregation, which was increased at high shear.

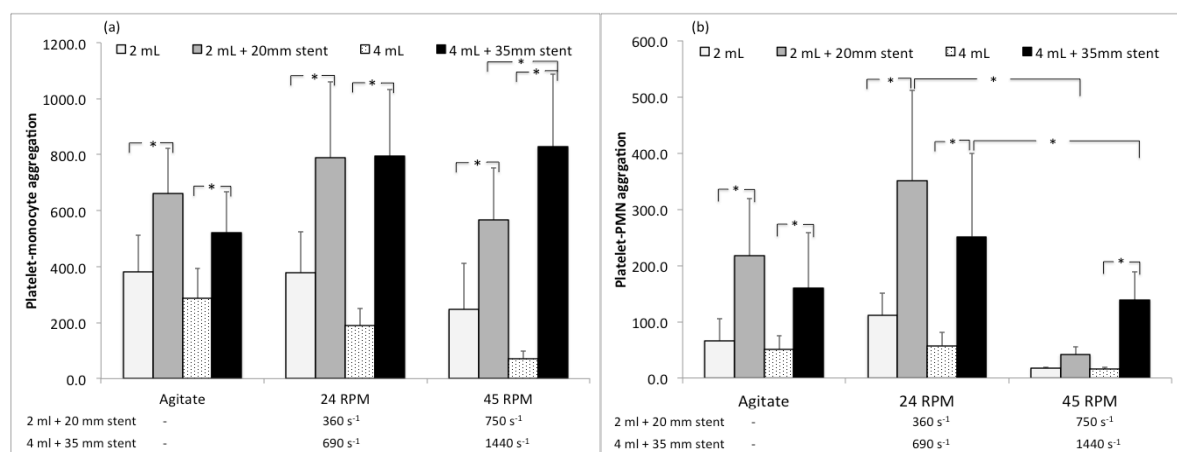


**Figure 5-7. Effect of volume, shear and stent on platelet-leukocyte aggregation: (a) platelet-monocyte and (b) platelet-PMN aggregation. \*** : $p < 0.05$ . Results are mean  $\pm$  SD,  $n=3$  to 5.

#### 5.3.4.3 Effect of material surface area-to-volume ratio on platelet-leukocyte aggregation

To investigate the effect of material surface area-to-volume ratio on platelet-leukocyte aggregation, experiments were performed with 4 ml + 20 mm ( $0.35 \text{ cm}^2/\text{ml}$ ) and 4 ml + 35 mm ( $0.62 \text{ cm}^2/\text{ml}$ ) stent samples. The presence of model stents had a significant effect on platelet-monocyte aggregation under all conditions ( $p < 0.04$  for  $0.35 \text{ cm}^2/\text{ml}$  and  $p < 0.01$  for  $0.62 \text{ cm}^2/\text{ml}$  samples), Figure 5-8(a). When stent samples were compared at the same experimental conditions, a significant surface area-to-volume ratio dependent difference in platelet-monocyte aggregation was observed under shear conditions ( $p < 0.01$ ). The introduction of shear (agitate to 24 RPM) resulted in a significant increase ( $p < 0.01$ ) in platelet monocyte-aggregation for the  $0.62 \text{ cm}^2/\text{ml}$  sample. On the other hand, the increase in shear (24 RPM to 45 RPM) significantly decreased platelet-monocyte aggregation ( $p < 0.04$ ) for the  $0.35 \text{ cm}^2/\text{ml}$  sample but increased aggregation for the  $0.62 \text{ cm}^2/\text{ml}$  sample, which was significantly higher compared with the agitated sample ( $p < 0.01$ ).

For the platelet-PMN aggregation, the presence of stents had a significant effect under agitation and 24 RPM for both surface area-to-volume ratios ( $p \leq 0.05$ ), Figure 5-8(b). At 45 RPM, a significant effect of the presence of a stent was observed for the 35 mm samples ( $p < 0.02$ ). The difference in surface area-to-volume ratio had a significant effect on platelet-PMN aggregation at high shear rate ( $p < 0.04$ ). When shear was introduced, an increase in aggregation was observed for the

high surface area-to-volume ratio and when shear was increased, there was a significant decrease in aggregation ( $p < 0.02$  for the  $0.35 \text{ cm}^2/\text{ml}$  samples and  $p < 0.05$  for the  $0.62 \text{ cm}^2/\text{ml}$  samples).

In general the higher surface area-to-volume ratio samples had significantly higher platelet-leukocyte aggregation under shear. Increasing shear generally had decreasing effect on platelet-leukocyte aggregation for most samples, with the exception of monocytes for the high surface area-to-volume samples.

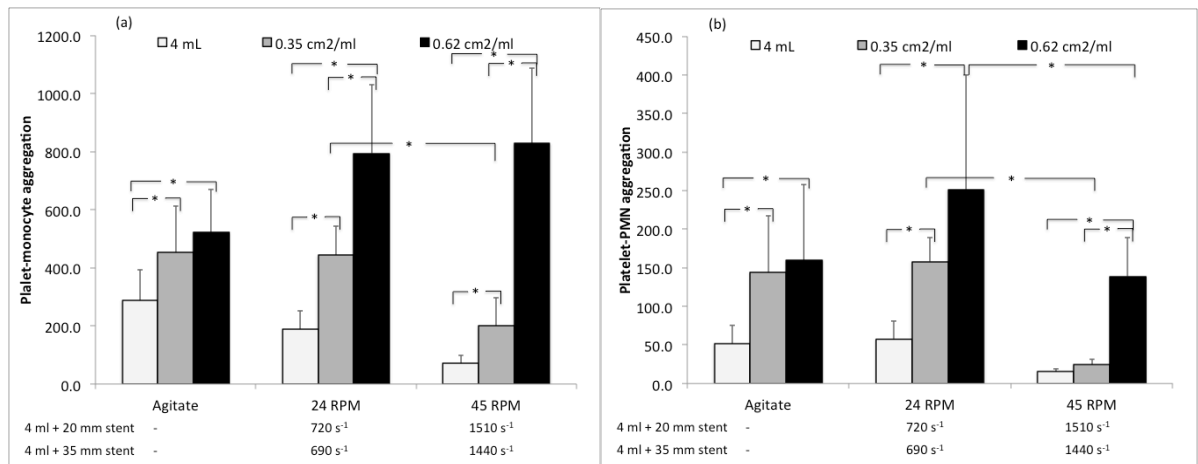


**Figure 5-8. Effect of surface area-to-volume ratio on platelet-leukocyte aggregation. \***  $p \leq 0.05$ . Results are mean  $\pm$  SD,  $n=3$  to 5.

### 5.3.5 Effect of sample volume and shear on surface adhesion

To investigate the effect of sample volume and shear stress on protein adsorption and cell adhesion after a 2-hour incubation, model stent samples were fixed in 2.5% glutaraldehyde and subsequently prepared for examination with a scanning electron microscope (SEM), as described under Materials and methods. Figure 5-9 to Figure 5-11 depict typical SEM results for some of the experimental conditions for 2 ml + 20 mm, 4 ml + 20 mm and 4 ml + 35 mm stent samples, respectively.

There was visible variation in the morphology of surface adherent leukocytes. While some samples show rugged morphology, even membrane blebbing (Figure 5-9), some show pancake morphology (Figure 5-10). However, these variations could not be associated with either specific material/experimental conditions or individual variability. In general, the pattern of cell adhesion

showed a shear-dependent reduction in adherent leukocytes when shear samples were compared with agitated samples.

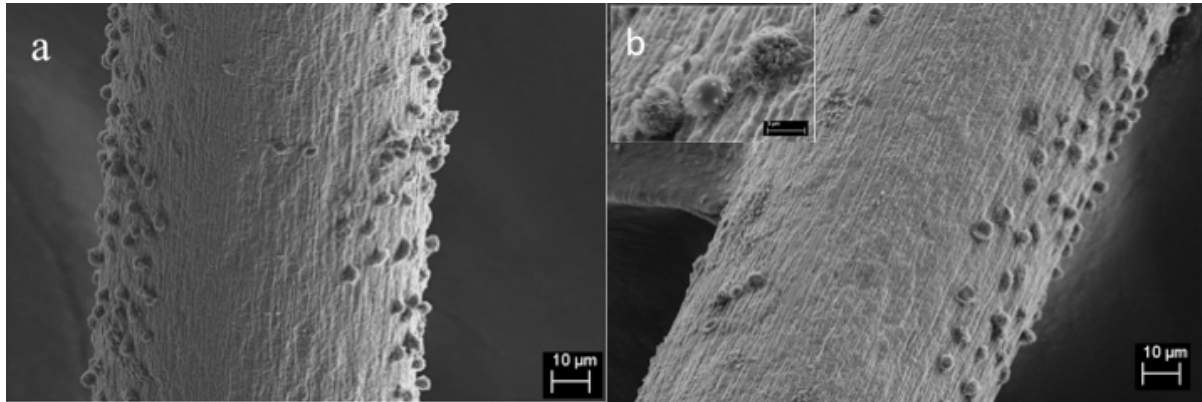


**Figure 5-9. Scanning electron micrograph of cell adhesion pattern for 2 ml + 20 mm stent samples. (a) Agitated sample at 500X and (b) 24 RPM (13 dyn/cm<sup>2</sup>) sample at 500X (insert at 5kX).**

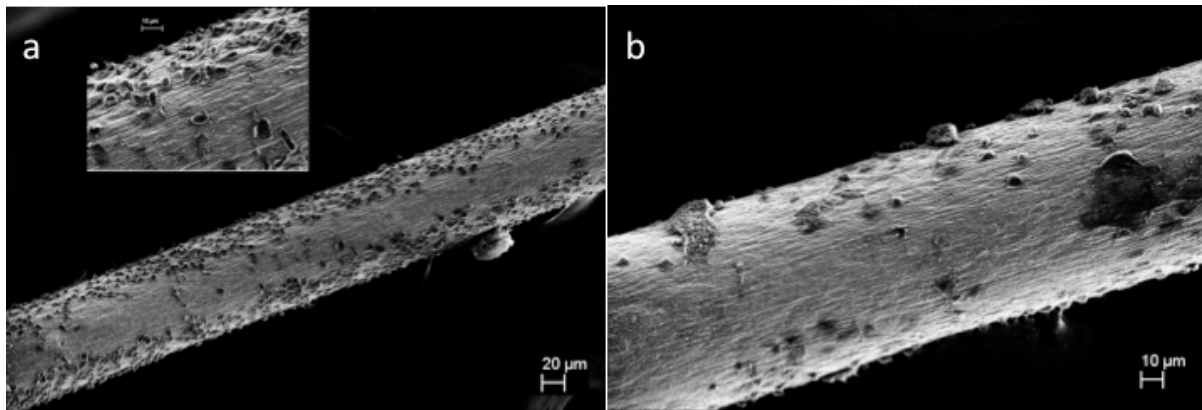


**Figure 5-10. Scanning electron micrograph of cell adhesion pattern for 4 ml + 20 mm stent samples. (a) Agitated sample at 500X (2.52kX insert) and (b) 45 RPM (53 dyn/cm<sup>2</sup>) sample at 1.01kX**

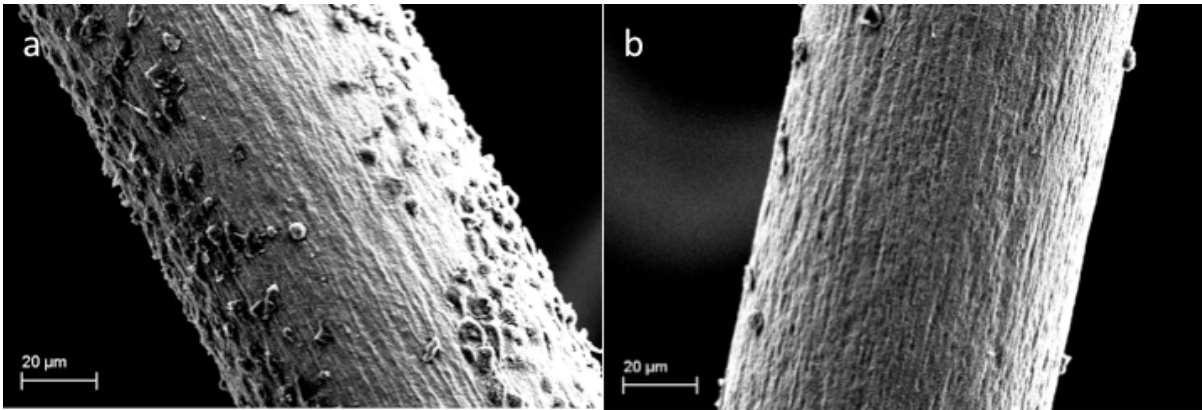


**Figure 5-11. Scanning electron micrograph of cell adhesion pattern for 4 ml + 35 mm stent samples.** (a) Agitated sample at 500X and (b) 24 RPM (24 dyn/cm<sup>2</sup>) sample at 500X.

## 5.4 Discussion

The purpose of this work was to investigate the effect of blood sample volume, in the presence of shear stress and/or material, on blood activation, using the Chandler loop as described in Chapter 3. Since the model time-averaged wall shear stress equation proposed in Chapter 3 is a function of sample volume fraction and model stent parameters, the combined effect of volume-shear-material interaction was of particular interest. Hence, investigations on the effect of sample volume and shear stress were performed with and without model stents.

In this investigation, whole blood was used and a variety of cell activation parameters were investigated. This is in line with the need to provide a parameter profile in a systems approach to experimental investigations. Although the listed parameters are far from providing the profile necessary to characterize transient interactions, they are meant to demonstrate the need to take into account the various factors in the investigations.

### 5.4.1 Effect of experimental groups and conditions on shear stress/rate

Comparison of wall shear stress developed in the loop as predicted by the original Gardner equation [354] and the proposed time-averaged wall shear stress [29] suggest that the shear stress in the loop is much higher than originally thought. The effect of sample volume is particularly observable. This was also obvious in Chapter 3 (Figure 3-8), where the plot lines were clustered by sample volume. Although the time-averaged wall shear rate at the highest angular velocity for this

study, 45 RPM, is much higher compared with the unmodified equation, it is still within the low range of what is considered pathologically high shear stress, since physiological shear rate range is 100-1000  $s^{-1}$  [52] or even up to 1200  $s^{-1}$  [229].

#### 5.4.2 Platelet activation

This study has demonstrated that, in the absence of model stents, blood sample volume did not have a significant effect on platelet activation for the rotational speeds used in this study, i.e. up to the highest time-averaged wall shear stress/rate without stents of 56  $\text{dyn/cm}^2$  (1590  $s^{-1}$ ). This is consistent with the theoretical prediction as discussed in Chapter 3. It is also in agreement with the results of numerical simulation [411] and a previously published study [29]. Minimal shear-dependent platelet activation has also been reported in previously published studies with whole blood but different *in vitro* models [168, 415]. A microfluidic model with porcine blood also did not show any platelet aggregation at shear rates below 1500  $s^{-1}$  [416]. These results suggest that under a physiological shear range, shear alone may not significantly activate platelets in whole blood. It should be noted that the results of platelet activation within physiological shear in whole blood experiments, as observed in this and previous studies [168, 415], are contrary to results from platelet rich plasma (PRP) experiments [204]. This implies that the use of whole blood is important as also demonstrated by the difference in material-dependent thrombin-antithrombin complex generation and platelet activation in a different model [417]. Since isolated platelets are very sensitive to shear stress compared to platelets in whole blood, and there is a difference in material response, it is important to take into consideration the platelet environment when interpreting and comparing results of the effect of shear stress on platelets.

Although low shear stress did not significantly affect platelet activation, pathologically high shear stress has been shown to activate platelets in whole blood [415, 418]. The physiological relevance of the results of the current study is consistent with previous findings that, except in the reactive lumen, leukocytes play a bigger role in thrombosis at low shear rates while platelets play a key role at higher shear rates, since they have developed the mechanism to adhere even at high shear rates [419]. At high wall shear rates, above 1000  $s^{-1}$ , the platelets receptor complex GPIb-IX-V is able to bind to the vWF factor [420, 421]. *In vivo*, the importance of vWF at arterial shear has been demonstrated by correlation of vWF deficiency with reduced prevalence of arterial thrombosis [422]. This work has emphasized the importance of using whole blood versus blood components because it may affect interpretation and translation of results.

The presence of a stent resulted in platelet activation, which was significant under shear conditions. Numerous studies have demonstrated material-induced platelet activation under static [317] and flow conditions [27, 349]. The observed difference in platelet activation in the presence of model stents, for samples with similar surface area-to-volume ratio, even at the same rotational speed can be attributed to the effect of volume and stent on shear rate. It was previously hypothesized in Chapter 3 that the combined effect of volume and stent, for the same surface area-to-volume ratio is high shear stress, dominated by a volume effect. This is non-linear and increases rapidly with rotational speed and the Dean number as depicted on Figure 3-8, Chapter 3. Thus, the difference in time-averaged wall shear stress ( $\approx 63\%$ ), at the same rotational speed, partly explains the observed difference in platelet activation.

Another variable that is important to consider in the volume-stent interaction is the shear exposure time to the stent, which is related to the periodic circulation of the sample volume in the loop. The fractional period of circulation for the sample volume can be expressed as  $T_c = 30\lambda/\pi\omega$ , where  $\lambda$  is the dimensionless volume fraction as previously defined and  $T_c$  is in seconds. When the volume fraction is doubled, the exposure period is also doubled. Since platelet activation is sensitive to shear exposure time [204, 415], although to a less extent compared to shear level [204], the fractional difference in volume, and hence exposure time, may contribute to the difference in platelet activation observed at the same rotational speed. That means, in reality the effective interaction is volume-stent-time-frequency. Hence the material effect in semi-static conditions (where material effect is only in terms of surface area) is not significant but becomes significant under shear (surface area + friction). In line with these explanations, was the observed significant platelet activation, for the 4 ml + 35 mm stent samples, when rotational speed was increased from 24 to 45 RPM, which increases the shear rate and the volumetric flow rate. This suggests that it is the combined shear-volume-stent-time-frequency interaction that is responsible for the observed results.

One of the consequences of shear-volume-stent-time interactions was observed when the surface area-to-volume ratio was decreased below the ISO Standard. No significant increase in platelet activation was observed under all experimental conditions (Figure 5-3). This suggests that if the surface area-to-volume ratio is low, below the ISO range, then the threshold for platelet activation is high, since high shear rate of  $1510 \text{ s}^{-1}$  did not produce significant activation. However, for sufficient surface area-to-volume ratio, the threshold for platelet activation is low. Therefore, when a material is included *in vitro* studies, it is important to maintain an appropriate surface area-to-volume ratio in order to ensure that results are not misinterpreted. For that reason, sample volume, as it relates

to surface area-to-volume ratio, is an important parameter in this model. Thus, this study has demonstrated the importance of sample volume in platelet activation, in the presence of a model stents, not only for hemodynamic conditions but, for sufficient surface area-to-volume ratio as per the ISO 10993 Standard. This effect could not be predicted using the existing shear rate equation developed by Gardner [354]. It is worth noting that under all experimental conditions, there was no condition that had any significant effect on P-selectin expression. This seems to agree with previous suggestions that P-selectin is more time-dependent than shear dependent [423]. *In vivo* P-selectin tracking in baboons showed a half-life of 5 minutes and remained relatively unchanged beyond 20 minutes [424]. In general, the results suggest that sample volume has an effect in the Chandler loop model and are in agreement with the theoretical predictions.

### **5.4.3 Leukocyte activation**

Leukocyte activation was also investigated in this study. The tissue factor results showed great variability, which is a recognized phenomenon [137, 406, 425]. Generally the monocyte subpopulation expressing TF decreased at high shear rate, for both samples with and without stents. The presence of model stents significantly increased the monocyte subpopulation expressing TF under shear conditions. Material-dependent TF expression has previously been shown [170]. The observed decrease in monocytes expressing TF with increasing shear seems to agree with previous studies in whole blood [418] as well as endothelial cell type [426]. Interestingly, studies on endothelial cell type have shown TF expression at about  $400\text{s}^{-1}$  peaked at 2hrs, followed by a decrease [427]. Although this was a different cell type, it suggests that TF peak for our experiment at high shear could have occurred before the 2hr end point, resulting in observed down-regulation.

The mechanism of TF down-regulation is not clear at this point but there has been evidence of time-dependent TF internalization on fibroblasts in the presence of FVIIa, peaking at 60 minutes [138]. If monocytes follow the same mechanism, this suggests mechanical stimulus may directly or indirectly mediate other mechanisms that induced TF down-regulation. This may include shear-dependent leukocyte reduced sensitivity to shear through internalization of formyl peptide receptor (FPR) and retraction of pseudopods [94, 166]. More so, TF has been shown to be upregulated by FPR ligand, formyl-methionyl-leucyl-phenylalanine (fMLP) [140]. In addition, monocytes form microparticles upon stimulation, which express TF. Although leukocyte microparticles were not characterized in this study, it is possible that the release of TF bearing microparticles may also provide partial explanation for TF down-regulation on leukocytes under shear. Since TF expression

and activity are sensitive to the type [129] and level [249] of flow shear, further studies would be necessary to elucidate the interaction of shear, volume and material influence on TF expression.

Similar to TF expression, Mac-1 expression on monocytes and PMNs showed shear-dependent down-regulation in the absence of stents. However, in the presence of stents, Mac-1 on monocytes showed upregulation, which seemed to correspond with PMP formation, while PMNs showed down-regulation. This was also reflected on the difference in surface-area-to-volume ratios. The results suggest that in stent-shear interactions, Mac-1 expression on monocytes was sensitive to the level of platelet activation while PMNs were sensitive to shear. This agrees with previous studies, although using a different model and biomaterial, that suggested that platelet activation in the bulk did not necessarily translate into leukocyte activation [178]. The down-regulation in leukocyte Mac-1 expression at higher shear rates has been observed previously in different *in vitro* models [166, 168, 428]. This may be partly due to the shear-induced proteolytic cleavage of the  $\beta_2$  integrin, CD18 [429] or inactivation of  $\alpha_M\beta_2$  [166], resulting in internalization of formyl peptide receptor and retraction of pseudopods [94, 166] and reduced leukocyte sensitivity to shear stress. However, further studies are necessary to quantify the trigger point for Mac-1 down-regulation in our whole blood model. The results of isolated neutrophils in Hank's buffered salt solution in the cone and plate model suggested the trigger point at about  $0.75 \text{ dyn/cm}^2$  [166]. In general, volume did not appear to have a significant effect on Mac-1 expression except in terms of surface area-to-volume ration under high shear.

An important aspect of Mac-1 expression is the relationship to function under different conditions. Although Mac-1 expression is an important leukocyte activation marker, there is evidence that receptor affinity may be more important than density [430]. There is also evidence that Mac-1 affinity to its ligands can be increased by extracellular adenosine 5'-diphosphate (ADP), which increases affinity to fibrinogen and FX through up-regulation of cytosolic  $\text{Ca}^{2+}$  concentration without increasing Mac-1 expression [194]. Since activated platelets produce ADP, it follows that leukocyte adhesion will be increased in the presence of platelets. This supports the previously reported findings that leukocyte adhesion seems to depend on the presence of platelets [178]. Much of the research has examined material-induced Mac-1 expression but not affinity. Therefore, in addition to the effect of specific biomaterial characteristics on Mac-1 expression, the question of whether there is material-mediated affinity under specific flow conditions is a valid question that needs further investigation.

The result of leukocyte constitutively expressed receptor, C3aR, did not show any significant sensitivity to sample volume in the absence of model stents. In the presence of model stents, C3aR expression was slightly upregulated mostly on monocytes. The results of the effect of surface area-to-

volume ratio seemed to suggest a complex shear-dependent interaction. Shear had a down regulating effect on C3aR expression on leukocytes, which was significant for the 4 ml sample corresponding to significant Mac-1 upregulation. Since complement activation was expected to produce C3a in these experiments, the results seem to agree with previous findings that the presence of C3a causes C3aR internalization [407]. It is interesting to note that although previously studies have shown that monocytes and PMNs express fewer C3aR than C5aR and monocytes express 2-fold more C3aR than PMNs [108], this difference is not manifested in the above results. This may be explained by the fact that monocyte response to C3a has been found to be quite diverse, suggesting a subpopulation not responding to C3a [107]. In this study, this was also observed. Since these receptors seem to have distinct roles in other conditions [431], their roles reach further than merely recruitment and activation. There is need to investigate their signaling role simultaneously in blood-biomaterial studies. Further investigations are necessary to elucidate relative expression of C3aR to C5aR under different conditions.

TLR-4 expression on leukocytes seemed to be influenced by sample volume. Shear increase seemed to down-regulate TLR-4 expression. The presence of stents resulted in increased TLR-4 expression, as did the high surface area-to-volume ratio. On the contrary, titanium particles in mice have been found to down regulate TLR-4 expression [408]. The regulation of TLR-4 under the current experimental condition is not clear. As previously discussed, conclusions cannot be drawn on TLR-4 expression from this study. However, since TLR-4 may play an important role in material recognition [432], further studies are necessary to elucidate its regulation mechanism in the presence of biomaterials.

#### **5.4.4 Platelet-leukocyte aggregation**

Platelet-leukocyte aggregation results showed preferential aggregation of platelets with monocytes compared with PMNs (minimum 3-fold) under all experimental conditions, which has been previously observed [178, 424]. A general material and shear-dependent platelet-leukocyte aggregation was also observed. Samples with higher surface area-to-volume ratio, which seemed to correspond with PMP formation, CD11b and TLR4 expression. While platelet-leukocyte aggregation generally exhibited shear-dependent decrease, platelet-monocyte aggregation was increased for samples corresponding to Mac-1 upregulation and increased PMP formation at high shear. The preferential platelet aggregation with monocytes, which has been observed *in vivo* [424], may partly explain the observed low sensitivity of platelet-monocyte aggregation to shear. Extracellular ADP

from activated platelets may contribute to this shear-resistant aggregation since ADP induces integrin  $\alpha_{IIb}\beta_3$  (GPIIb/IIIa) expression as well increases Mac-1 affinity to fibrinogen without increasing Mac-1 expression [194]. Moreover, there is evidence that receptor affinity may be more important than density [430]. Yet another contributing factor to the stability of the platelet-monocyte aggregate may be the role played by FXIIa, which can directly interact with activated platelets and fibrin(ogen) to stabilize the network [184]. Hence, factors emanating from increased platelet activation may result in increased platelet-monocyte aggregation.

On the other hand, the general decrease in platelet-leukocyte aggregation could be due to shear inactivation of Mac-1. The decrease could also be due to the previously reported shear-induced increase in coagulation time; partly linked to change in kinetics at higher shear rate [354] or the dissociation of the platelet P-selectin and leukocyte PSGL-1 bond, which is an important platelet-leukocyte bond under flow [97, 99]. Moreover, P-selectin did not show significant increase in the experiments. However, there is also the possibility of the *in vitro* model “closed-loop effect”. The in-circuit leukocytes activation in cardiopulmonary bypass is a known phenomenon [433], which may lead to leukocyte exhaustion leading to subsequent clearance by phagocytosis. Indeed, a noticeable C5b-9 increase was previously observed after 1 hour in a loop model at a shear rate of  $530\text{ s}^{-1}$  [349]. The question of whether the dose and time-dependent increase in C5b-9 on platelets [434] does not come into effect at the higher shear rate for the length of time in our experiments also arises. An interesting twist to the presence of C5b-9 on platelets is that it has been shown to cause formation of microparticles, which contain the complement C5b-9 pores [78, 79]. More interestingly, complement C5b-9-induced increase in PMP formation is accompanied by increased expression of GPIIb/IIIa, which is incompetent in binding fibrinogen [435]. This would suggest the possibility of observing increased PMP and GPIIb/IIIa but without necessarily a corresponding increase in platelet-leukocyte aggregation. While this phenomenon was not investigated in this study, it is possible that it may partly explain the observed low platelet-leukocyte aggregation even though PMP formation was high, especially for 4 ml + 35 mm samples at 45 RPM ( $1440\text{ s}^{-1}$ ). Therefore, the disaggregation from shear may not be the only explanation for the observed results. Further studies are necessary to elucidate the dominant mechanism and the critical influencing factors.

Another interesting question that arises from the results of complement-induced PMP formation is whether PMP formation is only for hemostatic and pro/anti-inflammatory response as generally thought. The fact that C5b-9 is carried on the microparticles raises the curious question of platelet survival. The issue of cell survival has been discussed [403], but PMP formation as a form of

platelet survival is not usually discussed. This may be a subject that warrants further investigation as it may influence their function. Combining the two observations, it is possible that platelets PMP formation takes two paths – inflammatory path, which has competent GPIIb/IIIa and the survival path, which has incompetent GPIIb/IIIa. It makes sense that the survival path may not bind fibrinogen because by so doing it will defeat the purpose as it will result in amplified platelet degranulation. If that is the case then the use of PMP formation as a biomarker [436] without accompanying information on functional capacity, may in some case be only accurate for platelet activation, but not for prediction of thrombogenicity. This is particularly important because 80% of circulating PMPs have been shown to lack procoagulant activity as assessed by annexin V binding [437]. Moreover procoagulant activity is dependent on the agonist [437] and PMP formation seems to be dependent on the type of platelet subsets [438]. It remains unclear whether there is any difference in phosphatidylserine expression, i.e. functional/procoagulant capacity, between suggested inflammatory path activated degranulation (IPAD) and survival path activated degranulation (SPAD) PMPs. Because PMPs are responsible for a variety of functions, including contact system-dependent coagulation [162], it would be informative to establish this fact with different biomaterials.

Therefore, several mechanisms may be responsible for the observed shear and material-dependent platelet-leukocyte aggregation. In general there was no volume effect except at high shear, which may be partly due to the complex stent-shear interactions. This suggests a complex cell activation and aggregation function, which may be generally expressed as,  $C_a = f(\tau, \sigma, \xi, t)$ , where  $\tau$  is wall shear stress,  $\sigma$  is surface area-to-volume ratio,  $\xi$  is collision efficiency/frequency and  $t$  is exposure time. This proposed function is an expansion of the generally accepted platelet activation function, which is shear and time-dependent. Based on experimental results in this study and previous studies, the effect of shear stress on platelet and leukocyte activation and aggregation can be illustrated by the schematic in Figure 5-12. The general broad implication of the schematic is that shear-induced TF-dependent thrombogenicity occurs at low shear while PMP-dependent thrombogenicity occurs at high shear as previously described. Furthermore, from a systems approach point of view, the results illustrate the importance of a holistic approach to blood-biomaterial interaction studies as it assists in understanding the effects of a stimulus on different activation pathways, and hence provide better guidance for appropriate intervention methods. Hence, from an intervention perspective, the result suggest that while a balanced approach is always necessary, at low shear, emphasis may be better placed in reducing leukocyte activation, which could partly be

achieved through complement inhibition. Further investigation into the effect of complement inhibition on cell activation at nominal shear is necessary.

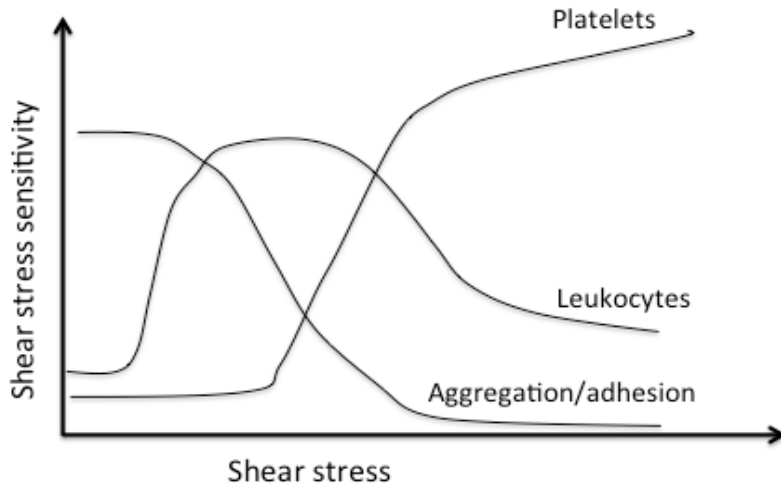


**Figure 5-12. Schematic of shear stress sensitivity of platelet and leukocyte activation and platelet-leukocyte aggregation**

#### **5.4.5 Surface adhesion**

Cell surface adhesion was reduced in shear samples compared to agitated samples, which is in agreement with previous findings of shear-dependent leukocyte adhesion on different surfaces [19, 332, 334]. The threshold for isolated adherent leukocyte diminished sensitivity to shear has previously been shown to be above 7 dyn/cm<sup>2</sup> in a rotating disc model [19] and flow chamber [419]. The threshold of leukocyte sensitivity to shear stress was not investigated in this study. However, examination of the data suggests that it may be above time-averaged wall shear stress of 13 dyn/cm<sup>2</sup> (360 s<sup>-1</sup>), but depends on the experimental conditions. The level of shear stress and type (intermittent vs continuous) and the exposure time will affect the threshold of shear sensitivity. Shear-dependent adhesion has been linked to integrin molecules,  $\alpha_M\beta_2$  [166] and  $\alpha_4\beta_1$  [439]. Thus, the observed reduction in leukocyte adhesion at higher shear may be due to the cleavage/inactivation of the Mac-1 integrin receptors, as discussed previously, since they also act as surface adhesion molecules. However, shear stress does not affect cell adhesion only through its influence on cell receptors. It also affects protein adsorption [440, 441], which subsequently would affect cell adhesion. Of particular

interest to this study is the previously reported loss of fibrinogen which was observed in a curved tube model due to secondary flow effects [441]. Although the loss of proteins was not specifically investigated in this study, it may also play a role. In general, the combined effect of shear on protein adsorption and cell cytoskeleton and subsequent receptor expression could partly explain previous observations that when leukocyte shear sensitivity is lost at high shear stress, material-dependent adhesion may also be lost [19].

The shapes of adherent leukocytes showed some variations. These differences could not be linked to specific parameters in this study. It was also not possible to quantify adhesion in this study but in general the observed cell adhesion is consistent with other previous studies. A detailed characterization of surface adhesion is necessary in order to elucidate the effect of volume-stent-shear on cell adhesion.

A summary of overall observations on the effect of experimental conditions on platelet and leukocyte activation and aggregation is presented on Table 5-12. The summarized observations are for the maximum observed effect, except where it was necessary to specify the sample volume. The summary is for samples with similar surface area-to-volume ratio only. The general observation was that all the three variables, shear stress, sample volume and model stent had varying effects on platelet and leukocyte activation and aggregation. Sample volume, which is of particular interest in this study, had direct effects as well as indirect effects upon interaction with the other variables. It is important to note that the lack of significant difference in some of the parameters in no way diminishes the importance of the results. The fact that sample volume without stent did not show significant effect is important because it suggests that in the absence of stents, it may not be necessary to use large volumes of blood.

**Table 5-12. Summary of the effects of experimental conditions on platelets and leukocytes**

	No stent		Similar surface area-to-volume ratio			
	Volume	Shear	Volume (low shear)	Volume (high shear)	Stent (low shear)	Shear
<b>PMP formation (%)</b>	—	—	↑	↑	↑	↑
<b>Monocytes expressing TF (%)</b>	—	↓	—	—	↑	↓
<b>Mac-1 expression on monocytes (%)</b>	↓	↓	—	↑	↑	↓↑
<b>Mac-1 expression on PMNs (%)</b>	↓	↓	—	—	↑	↓
<b>Platelet-monocyte aggregates</b>	↓	↓	—	↑	↑	↓
<b>Platelet-PMN aggregates</b>	↓	↓	—	↑	↑	↓
<b>C3aR expression on monocytes (%)</b>	—	↓	↑	↓	↑	↓
<b>C3aR expression on PMN (%)</b>	—	↓	↑	—	↓↑	↓

— No effect or barely discernible effect

↓, ↑ Non-significant decrease or increase, respectively

↓, ↑ Significant decrease or increase, respectively

↓↑ 2 ml decrease and 4 ml increase

NB. The effect of the presence of stent is depicted only when the shear effect is minimum (low shear). At high shear, the combined effect is included under volume (high shear).

## 5.5 Conclusions

In this chapter, the effect of blood sample volume under shear, with and without model stents, was investigated. The results are interpreted using an improved time-averaged wall shear stress for

the Chandler loop model. While the effect of sample volume without stents was minimum as analytically predicted in Chapter 3, there was a volume effect in the presence of model stents. The fact that data interpretation may vary depending on the blood sample volume, even with similar surface area-to-volume ratio has significant implications when screening materials for blood compatibility. Therefore, the results confirm the importance of selecting appropriate model parameters to reflect a reasonable simulation of *in vivo* parameters to reduce misinterpretation of *in vitro* results due to experimental parameters.

The effect of sample volume in the presence of model stents is reflected in surface-area-to-volume ratio, in shear rate and in differences in the fraction time of exposure per cycle. Analysis suggests that the interaction of all the variables in this model is much more complex than previously thought. The combined volume-stent-time-shear-frequency interactions, as a result of changes in volume, can have a significant effect on *in vitro* model results. Hence, the results of this chapter overall support the hypothesis that sample volume plays an important role in influencing the results of this *in vitro* model. This in turn would have implications for the investigation of biomaterials and comparison of results. Therefore, sample volume selection for this model needs to be considered carefully.

Besides highlighting the complex interactions, this work raises a number of pertinent questions with regards to cell activation and aggregation mechanisms. The importance of Mac-1 affinity vs expression level, the trigger level for Mac-1 and TF cleavage/internalization, the issue of platelet survival path under high shear stress ( $>50 \text{ dyn/cm}^2$ ), the effect of material on constitutively expressed receptors in thrombosis and the possibility of reducing leukocyte activation through complement inhibition. Further experimental studies and simulation would be necessary to elucidate the mechanism of shear-volume-stent-time interaction effect on flow characteristics and blood activation, at different experimental conditions and for a wider range of physiological and pathologic shear stress.

## Chapter 6

# Effect of Complement Inhibition on Platelet and Leukocyte Response to Shear and Biomaterials

### 6.1 Introduction

In Chapter 2, the important role that complement proteins play in health as well as in a variety of disease conditions was described. More importantly, the central role that complement plays through its elaborate intrinsic pathways and the cross-talk interactions with extrinsic pathways from platelets and the coagulation system was highlighted. These interactions present additional challenges for blood-biomaterial interaction investigators because, besides pathologic conditions, complement also plays an important role in blood-biomaterial interactions [7, 22, 82, 182]. Complement role in this regard has been demonstrated both *in vitro* [85, 442] as well as *in vivo* in medical devices such as hemodialysis [443], extracorporeal circuits [442] and coronary stents [88]. These findings place complement at the center of blood-biomaterial interaction investigations.

*In vivo*, complement anaphylatoxins C5a and C3a have common as well as distinct physiological and inflammatory effects. Their inflammatory effect on leukocytes can be detrimental as activated leukocytes, particularly PMNs, generate reactive oxygen species (ROS), which can cause tissue damaging oxidative stress. Complement fragment C5a, the most potent in foreign body response, has been correlated with implantation of drug-eluting stents, while C3a has correlated with development of in-stent thrombosis [88]. However, both have been correlated with late lumen loss in drug-eluting stents [88], which incidentally delays reendothelialization [43, 444] and can leave stent struts uncovered for up to 2 years [444]. The exposed struts result in chronic inflammation, which consequently causes late in-stent thrombosis and adverse patient outcomes, raising questions about their cost-effectiveness [445] and long-term patient outcome [446]. These developments, which are evidently linked to complement activation, show the central role that complement plays in influencing inflammatory response and thrombosis under a variety of conditions. For that reason, complement has lately been a subject of intense investigations with the aim of developing therapeutic interventions.

We previously showed indirectly, through investigation of material-dependent complement C3aR expression, that complement was activated in our *in vitro* model [447]. This was also shown in Chapter 5. Furthermore, in Chapter 5, the effect of shear and the presence of model stents on platelet

and leukocyte activation and surface adhesion were demonstrated. Activated platelets express P-selectin, which binds C3b of the alternative pathway [448], as well as the global C1q receptor (gC1qR), which binds C1q of the classical pathway to activate platelets and/or complement [449]. Consequently, platelet activation has been associated with increased complement C3a and C5a fragments [74]. The capacity of platelets to activate either the classical or alternative pathway depends on the stimulant, with shear preferentially activating the classical pathway [74]. Regarding leukocytes, they constitutively express complement receptors C3aR and C5aR [108]. Therefore, any initial complement activation produces anaphylatoxins that induce expression of CD11b and TF in leukocytes [141]. TF expression initiates the TF-dependent coagulation cascade, which produces thrombin. Thrombin, which has a variety of physiological functions, in turn activates complement [450] and platelets, thus creating feedback loops. Certainly, blood activation involves complex cross-talk and co-stimulation between the various systems, with platelet, complement and leukocytes playing an important role in material-induced thrombogenicity [317]. Since complement plays such an important part in the initiating and amplification of the inflammatory response, it would be informative to understand the level of its contribution under specific experimental conditions. We hypothesized that complement inhibition should significantly reduce platelet and leukocyte activation under simulated physiological conditions.

The divergent roles that the complement system plays in disease conditions as well as material-induced thrombogenicity, has made complement proteins and receptors targets for possible therapeutic interventions. A number of inhibitors and blockers have been investigated experimentally and clinically [70, 451]. The number of proteins involved in complement activation and regulation pathways means that there are enumerable points at which complement inhibition or modulation can be achieved [451]. Hence, efforts have been placed on specific as well as broad spectrum inhibitors. Some of the specific targets include the C5aR-C5a complex [452]. Inhibition of specific complement pathways (classical and alternative) has also been targeted with the soluble complement receptor 1 (sCR1) inhibitor, which has been shown to reduce leukocyte activation and adhesion in a cardiopulmonary circuit model [453]. Inhibitors have also targeted the central protein C3 from cleavage, which has seen the development of inhibitors such as compstatin [454]. Compstatin has been shown to inhibit complement activation and cell surface adhesion in an extracorporeal model [455] and has been advocated for hemodialysis because of its broad implications on complement activation [456]. Another inhibitor with broad anti-inflammatory effects that has been used in dialysis is nafamostat mesilate (FUT-175) [457], which has found use in other clinical conditions. Although

some of the therapeutic intervention methods have been proven to function *in vivo*, there is still no consensus on one method of inhibition, especially in blood-biomaterial interactions.

Nafamostat mesilate (FUT-175) or futhan is of particular interest in blood-biomaterial interactions because it is a general serine protease inhibitor and an inhibitor of the complement classical and alternative pathways [458]. Since FUT-175 has broad specificity, it has been used in other clinical conditions, such as an anticoagulant option in cardiopulmonary bypass surgery [459]. Serine proteases make one third of known proteases and they form an intricate activation and inhibition network between the cascade systems [460]. Hence, their inhibition can have great effect on coagulation and thrombosis. FUT-175 is appropriate for complement inhibition since many of the complement activation interactions are the result of serine protease activity. Its specific inhibition effects on C3a, C4a and C5a, which are all mediators of inflammation, have been previously demonstrated [458]. While futhan has a broad spectrum inhibition effect on complement and coagulation systems, both *in vitro* and *in vivo*, to our knowledge there is generally limited investigations on its effect in whole blood in the presence of biomaterials using the Chandler loop circulation model with metallic stents, especially with the new fluid dynamics characterization. Therefore, the purpose of this research was to investigate the effect of complement inhibition by FUT-175 on platelet and leukocyte activation and aggregation in the presence of model stents, under flow simulating nominal physiological shear conditions. It was hypothesized that under flow and stent conditions, complement inhibition reduces leukocyte and platelet activation and surface adhesion. The overall objective was to understand its relevance for application in material-induced thrombogenicity, with broad applications for stent implantation.

## **6.2 Materials and methods**

### **6.2.1 Flow model**

The flow model was made from a rotor and turntable as previously described in Chapter 3. The turntable for mounting blood sample tube loops was fixed in a vertical position. The sample tube loops were medical grade Silastic tubes (VWR, PA, USA) with 4.78 mm internal diameter. The tubes were cut into 371 mm long sections and spliced into loops with internal loop radius of about 59 mm. The wall shear stress for this model is as previously described with the improved time-averaged wall shear stress [29].

### 6.2.2 Model stents

Model stents were made from Ti-6Al-4V 0.005" diameter wire (Fort Wayne Metals, Fort Wayne, IN, USA) as described in Chapter 4. Detailed specifications for the model stents are as described in Table 4-2. The stents were cut into sections of 20 mm lengths, giving surface area of 1.46 cm<sup>2</sup>. The stents were first ultrasonically cleaned in 30% nitric acid to reduce the endotoxin (LPS) contamination, followed by rinsing with distilled water. The stents were then ultrasonically cleaned in 70% alcohol solution for about 10 minutes, and then rinsed at least twice in (PBS; 50 mM sodium phosphate plus 100 mM sodium chloride, pH 7.4). The prepared stents were stored in PBS at 4°C and used within 4 hours.

### 6.2.3 Antibodies and reagents

Fluorescein isothiocyanate conjugated mouse monoclonal antibody against human glycoprotein GPIIb/IIIa (CD61-FITC), R-phycoerythrin monoclonal antibody against P-selectin (CD62-PE), Fluorescein isothiocyanate conjugated mouse monoclonal antibody against Mac-1 (CD11b-FITC), R-phycoerythrin monoclonal antibody against tissue factor (CD142-PE), anti-C3a receptor (PE hC3aRZ8), R-phycoerythrin-cytochrome 5 conjugated monoclonal antibody against PAN leukocytes (CD45-PE-Cy5) and FUT-175 (Futhan, chemical name: 6-amidino-2-naphthyl *p*-guanidinobenzoate dimethanesulfonate) were purchased from BD Biosciences (San Diego, CA, USA). Anti-human Toll-Like receptor 4 (CD284-PE) was purchased from eBioscience (San Diego, CA, USA). FACS lysing solution was purchased from BD Biosciences (San Diego, CA, USA). Phosphate-buffered saline (PBS) was purchased from Fisher Scientific Inc (Ottawa, ON, Canada). Lipopolysaccharide (*Escherichia coli* serotype 0111:B4) (LPS), 50% glutaraldehyde solution, and paraformaldehyde were purchased from Sigma-Aldrich Co (Oakville, ON, Canada). Hepes Tyrode Buffer (HTB) solution PH 7.4 was made in the laboratory with a final concentration of 137mM NaCl, 2.7mM KCl, 5mM MgCl<sub>2</sub>, 3.5mM HEPES, 1g/L Glucose, and 2g/L BSA.

### 6.2.4 Blood sample collection

This study received ethics clearance from the University of Waterloo Research Ethics Office. Peripheral venous blood samples were drawn with formal consent from healthy volunteers, of age range 20 to 50 years, who indicated that they had not taken any medication in the last 72 hours. There was no restriction placed on the participants' physical activity, the type of diet and eating time. Participants were however advised to drink lots of water ahead of the blood draw. Samples were

drawn with a 21 Gauge Vacutainer safety-lok blood collection set and syringe (BD Biosciences, San Diego, CA, USA) by a qualified phlebotomist. Blood was immediately transferred into 10 ml conical tubes containing heparin (5U heparin/ml). Blood samples were kept in an insulated container and used in the blood activation experiments within 30 minutes of collection.

### **6.2.5 Platelet and leukocyte activation and platelet-leukocyte aggregation**

To assess complement inhibition effects, collected blood samples were first mixed with FUT-175 (Futhan) at 10  $\mu\text{l/ml}$ . Futhan is a synthetic serine protease inhibitor with a half-life of approximately 8 minutes [458]. 2 ml blood samples were then transferred into silicone tube loops, which had been prepared by rinsing with PBS, as illustrated on Figure 6-1. To assess the effects of complement inhibition in the presence of biomaterials, 20 mm model stents were included with the blood samples. For this study, only setups composed of 2 ml blood samples with and without 20 mm stents were used, which gave surface area-to-volume ratios of 0.71  $\text{cm}^2/\text{ml}$ . To assess activation effects under shear, half of the experimental sample loops were mounted on the flow model turntable set to rotate at either 24 RPM and the other half were placed on a mini-shaker (VWR, PA, USA) set at 200 RPM for the semi-static condition. The equivalent wall shear stresses for the 24 RPM rotation is 13  $\text{dyn/cm}^2$ , which changes very little in the presence of a stent, as was shown in Chapter 5, Table 5-2. This shear stress was chosen to simulate nominal physiological shear stress, which is approximately 15  $\text{dyn/cm}^2$  [250]. For all the experiments, control samples were static and included only blood (negative control/resting sample) and blood with lipopolysaccharide (LPS) (1  $\mu\text{g/mL}$ ) as a positive control. All samples were incubated at 37°C for 2 hours.

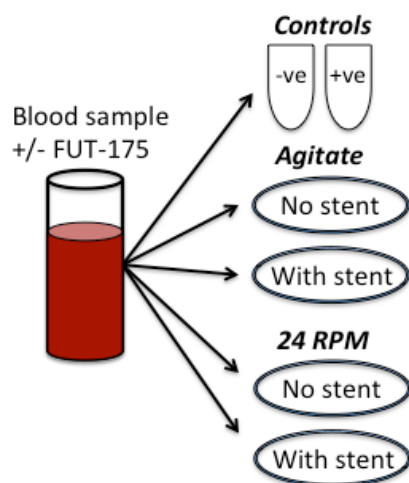


**Figure 6-1. Schematic of experimental conditions**

### **6.2.6 Immunolabelling and flow cytometry analysis**

At the end of the 2-hour incubation, small blood samples were diluted in test tubes and incubated with respective antibodies for 30 minutes for receptor-antibody binding. To assess platelet activation and platelet microparticle (PMPs) formation, 5  $\mu\text{L}$  blood samples (about  $1.25\text{-}2 \times 10^6$  platelets/sample) were diluted with 50  $\mu\text{L}$  HTB in test tubes and incubated for 30 minutes at  $4^\circ\text{C}$  with fluorescently-labeled antibodies against GPIIb/IIIa (CD61-FITC) and P-selectin (CD62PE). Following incubation, samples were further diluted with 200  $\mu\text{L}$  HTB, fixed with 200  $\mu\text{L}$  paraformaldehyde (1% final concentration) and stored at  $4^\circ\text{C}$  before flow cytometry analysis.

To assess leukocyte activation and platelet-leukocyte aggregation, 30  $\mu\text{L}$  of blood samples (about  $150\text{-}300 \times 10^3$  leukocytes/sample) were diluted with 50  $\mu\text{L}$  HTB in test tubes and incubated for 30 minutes at  $4^\circ\text{C}$  with appropriate antibodies. Leukocytes were identified by PAN leukocyte marker (CD45 PE-Cy5.5). Leukocyte activation was identified by antibodies against Mac-1 (CD11b-FITC) and tissue factor (CD142-PE) on leukocytes. Leukocyte activation was additionally identified with antibodies against C3a receptor (anti-C3aR) and TLR4 (CD284-PE). Platelet-leukocyte aggregation was identified by antibodies against GPIIb/IIIa (CD61-FITC) on leukocytes. Following 30 minutes incubation, 700  $\mu\text{L}$  of FACS Lyse solution was added to lyse red blood cells. Aliquots were concentrated by centrifuging at 1200g for 6 minutes and discarding supernatant. Resuspended pellets were washed and then diluted with 150  $\mu\text{L}$  HTB and fixed with 150  $\mu\text{L}$  2% paraformaldehyde. All

samples were stored at 4°C and analyzed on a BD FACS Calibur flow cytometer with CellQuest Pro software (BD Diagnostics, San Diego, CA, USA), within 5 days.

### **6.2.7 Scanning electron microscopy**

After the experiments, stent samples were prepared for protein and cell surface adhesion analysis with a scanning electron microscope on a later date. Samples were first rinsed with 0.2M sodium phosphate buffer, pH 7.2 followed by fixing in 2.5% glutaraldehyde and storage at 4°C. Fixed samples were then prepared for SEM analysis. Briefly, stent samples were first immersed and washed in 0.2M sodium phosphate buffer, pH 7.2. This was followed by dehydration through a series of steps in 10%, 25%, 50%, 70%, 90% and 100% ethanol. Samples were dried overnight and then coated with a thin layer of gold (8-10nm) in a vacuum chamber (Denton Vacuum, Desk II, USA) for 120sec, set at 50millitorr and 15 mA. Analysis was done with LEO 1530 Gemini (Zeiss, USA) set at 10kV in secondary electron mode (SE2). No specific marking was used to distinguish between the inner and outer stent wall, as it relates to the loop curvature.

### **6.2.8 Statistical analysis**

Statistical analysis was done with the IBM SPSS Statistics version 20. Data were analyzed using analysis of variance (2-way ANOVA). For post-hoc analysis, Least Significant Difference (LSD) method was used to determine significant difference between groups. No specific analysis was performed to account for donor variability. Overall effects are not reported due to the complexity of the data; in some cases there are fewer than three groups, e.g. volume and stent samples. All data are presented as mean  $\pm$  standard deviation of a minimum of 3 separate experiments. For all analysis,  $p < 0.05$  was used to indicate significant difference.

## **6.3 Results**

### **6.3.1 Effect of complement inhibition on platelet response to shear and model stents**

After a 2-hour incubation, activated platelets were characterized by formation of platelet microparticles (PMPs), expression of receptor GPIIb/IIIa (CD61) on platelets and PMPs, and P-selectin (CD62) expression on platelets. Since both activated platelets and PMPs express CD61, circulating PMPs were distinguished from platelets and platelet aggregates based on size (flow cytometry forward light scatter). P-selectin expression was determined based on fluorescence levels. Figure 6-2 depicts typical flow cytometry data analysis dot plots for platelet activation, as

characterized by circulating PMPs, with and without complement inhibition. PMPs are expressed as a percentage of total events (platelets + PMPs) or number of particles per 100 platelets and microparticles. As can be observed, PMP formation is reduced in the negative control/resting sample in the presence of complement inhibitor.

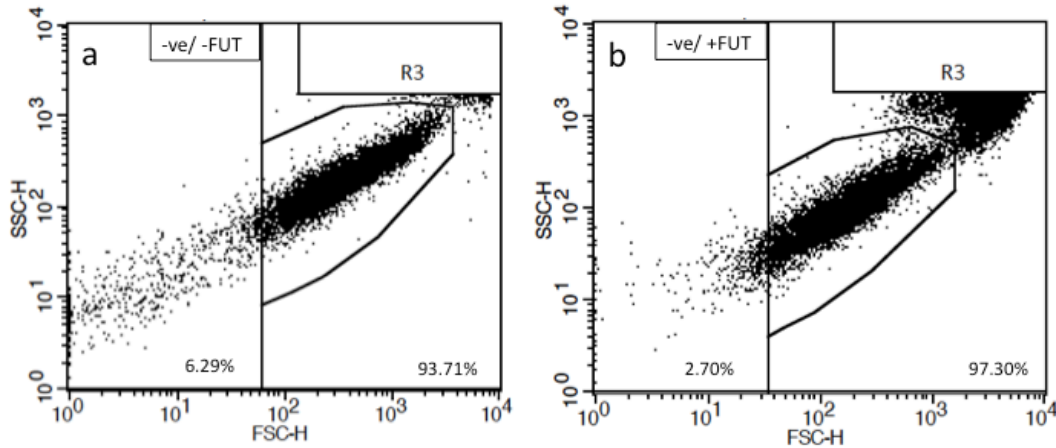


**Figure 6-2. Characteristic flow cytometry analysis dot plots for platelets forward (FSC-H) versus side (SSC-H) light scatter events.** Negative control (rest): (a) without FUT-175, (b) with FUT-175. All events are positive for CD61, hence platelet microparticles are distinguished based on size (forward light scatter). Events in region R3 represent aggregates and are not included in PMP percentage determination.

The results of platelet activation as illustrated by PMP formation are presented on Figure 6-3. The presence of stent under shear had a significant effect ( $p < 0.001$ ) on PMP formation when compared to shear alone. In general, complement inhibition reduced PMP formation under all experimental conditions. However, complement inhibition had a higher effect in reducing PMP formation on samples with stents compared to non-stent samples. The inhibition effect was significant in stent samples under shear ( $p < 0.001$ ).

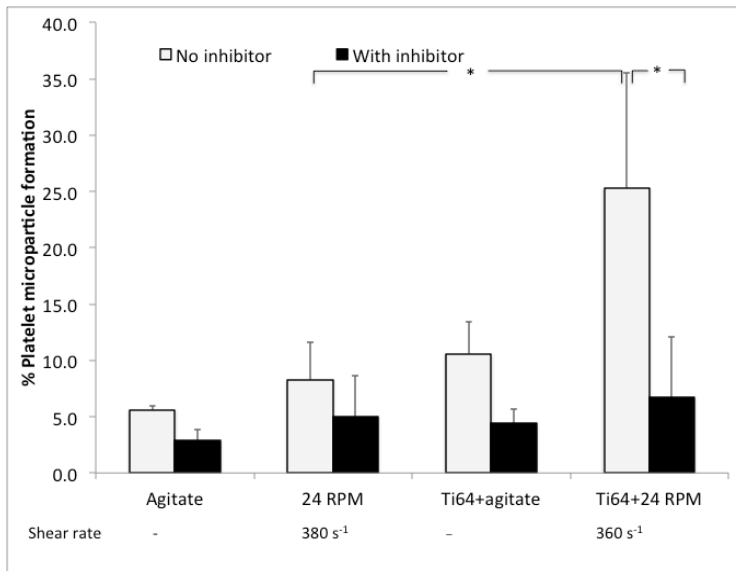


**Figure 6-3. Effect of complement inhibition on platelet microparticle formation.** Percentage microparticles are based on size (forward scatter signal) and expressed relative to total events (platelet + microparticles). Negative control:  $6\pm 1\%$  and  $4\pm 1\%$  (inhibitor). \*:  $p < 0.001$ . Comparison of agitated stent samples gives  $p = 0.07$ . Results are mean  $\pm$  SD,  $n = 3$  to 4. Ti64: Ti-6Al-4V stent.

The effect of complement inhibition on platelet activation was also investigated by CD61 and P-selectin expression on platelets. In the absence of the inhibitor, the presence of a stent under shear had a significant effect on platelet consumption ( $p = 0.05$ ), Table 6-1. Consistent with PMP formation, the results of CD61 expression suggest complement inhibitor induced less platelet consumption compared to samples with no inhibitor. P-selectin on the other hand did not show sensitivity to complement inhibition. In general the results suggest that complement inhibition influenced CD61 expression, but did not show any effect on one of the recognized platelet activation markers, P-selectin.

**Table 6-1. Effect of complement inhibition on CD61 and P-sel expression on platelets**

		CD61 <sup>+</sup> Platelets and PMPs		P-sel platelets	
Experimental conditions		Without FUT-175 (259±67)	With FUT-175 (205±74)	Without FUT-175 (18±4)	With FUT-175 (12±5)
<b>2 ml</b>	<b>Agitate</b>	249±54	214±51	19±4	15±4
	<b>24 RPM (380 s<sup>-1</sup>)</b>	240±61	207±29	20±3	16±2
<b>Ti64</b>	<b>Agitate</b>	222±46	210±48	19±3	17±5
	<b>24 RPM (360 s<sup>-1</sup>)</b>	163±56* <sup>#</sup>	194±22	19±4	17±1

Negative control: CD61 and P-sel expressions are reported as arbitrary fluorescent units.

\*significantly different from corresponding shear without stent (p=0.05), <sup>#</sup>significantly different from corresponding control (p<0.001). Results are mean ± SD, n=3 to 4. n=2 for P-sel with inhibitor.

### **6.3.2 Effect of complement inhibition on leukocyte response to shear and model stents**

To investigate the effect of complement inhibition on leukocytes, experiments were carried out with and without inhibitor, under semi-static and shear conditions. In addition to shear, activation was induced by the presence of model stents in some of the samples. Activated leukocytes were characterized by expression of CD11b (Mac-1) and TF. Constitutively expressed receptors, C3aR and TLR4, were also investigated. Typical flow cytometry data analysis plots for negative and positive controls, for CD11b expression on monocytes and PMNs, are depicted on Figure 6-4 and Figure 6-5, respectively. Only CD11b is presented to illustrate the difference with and without FUT-175. As illustrated, the geometric means for the samples with the inhibitor FUT-175 are lower than for samples without the inhibitor.

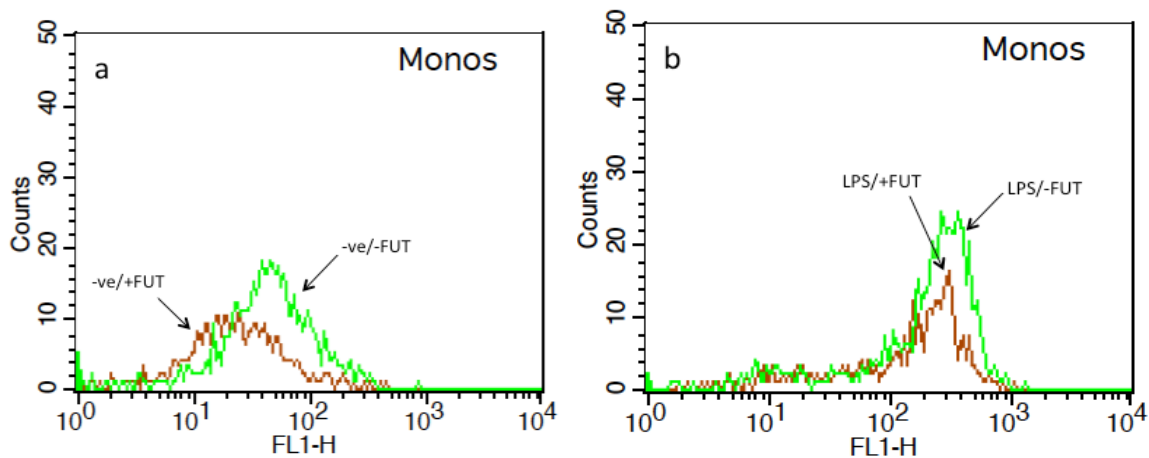


**Figure 6-4. Characteristic flow cytometry events histogram plots for CD11b on monocytes.** (a) Negative control (rest) samples and (b) positive control (LPS) samples. Histograms are in arbitrary fluorescent intensity units. A higher relative decrease in fluorescent intensity is observed in negative control samples compared with positive control, in the presence of FUT-175. FL1-H = CD11b.

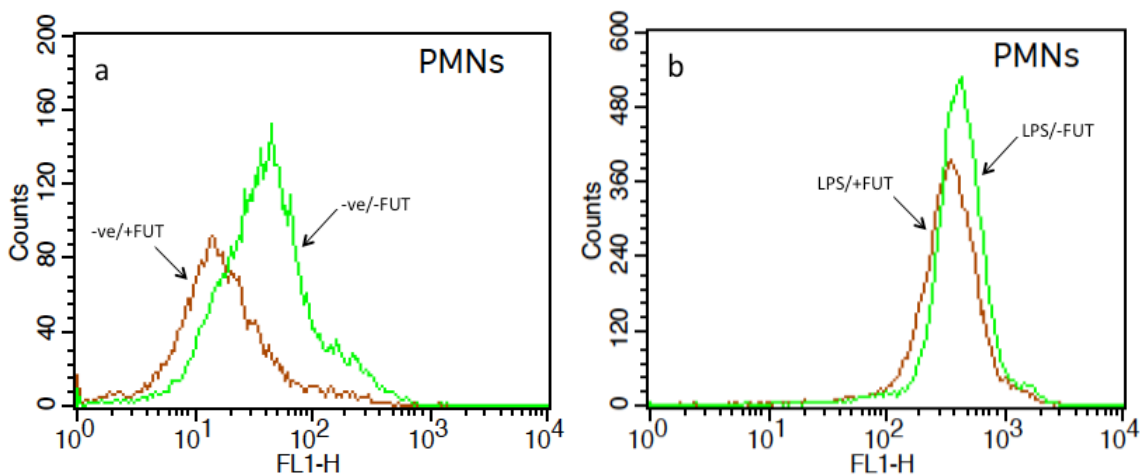


**Figure 6-5. Characteristic flow cytometry events histogram plots for CD11b on PMNs.** (a) Negative control (rest) samples and (b) positive control (LPS) samples. Histograms are in arbitrary fluorescent intensity units. A decrease in the fluorescent intensity is observed in the presence of FUT-175. FL1-H = CD11b. FL1-H = CD11b.

As shown on Figure 6-6, the percentage of monocytes expressing TF, which corresponds to TF expression on monocytes, was dependent on shear and the presence of a stent in the absence of FUT-175. Although in the presence of FUT-175 the results seem to show inhibition of TF expression, conclusions cannot be drawn because of the limited number of samples.

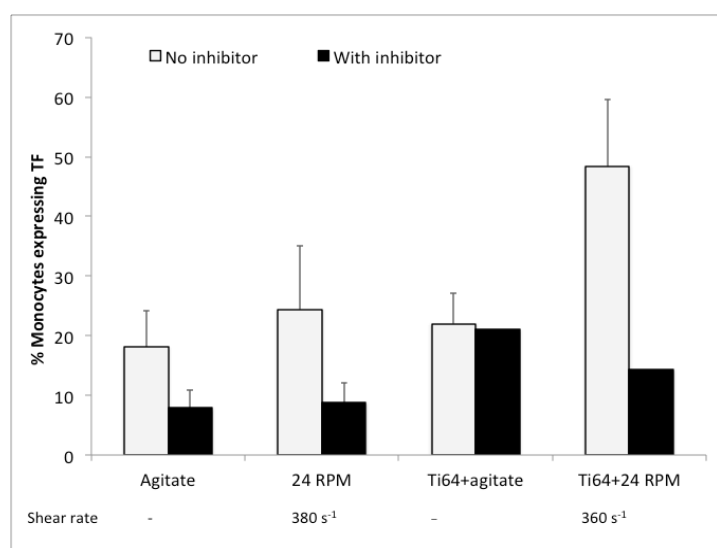


**Figure 6-6. Effect of complement inhibition on percentage of monocytes expressing TF.** Negative control: 10±3 and 8±5 (inhibitor). Results are mean ± SD, n=4 except for samples with inhibitor (n=1 to 2).

The effect of FUT-175 on Mac-1 expression on leukocytes in the presence of a model stent is depicted in a typical flow cytometry data analysis plot, Figure 6-7. The reduction in fluorescent intensity or geometric mean in samples with futhan illustrates the effect of complement inhibition on Mac-1 expression. The average results of Mac-1 expression on monocytes and PMNs are as depicted on Figure 6-8 and Figure 6-9, respectively. In the absence of model stents, FUT-175 down-regulated Mac-1 expression on monocytes, which, while non-significant on agitated samples ( $p=0.06$ ), was significant for samples at shear rate of 380 s<sup>-1</sup> ( $p<0.001$ ). Parallel to this observation, in the presence of model stents, FUT-175 did not induce a significant down regulation of Mac-1 on agitated stent samples but induced a significant down regulation ( $p<0.001$ ) in stent samples under shear (360 s<sup>-1</sup>). Since FUT-175 did not significantly reduce Mac-1 expression in agitated stent samples, consequently,

a significant ( $p < 0.01$ ) Mac-1 upregulation on monocytes was still observed under inhibition; when agitated stent samples with the inhibitor were compared to agitated samples without inhibitor.

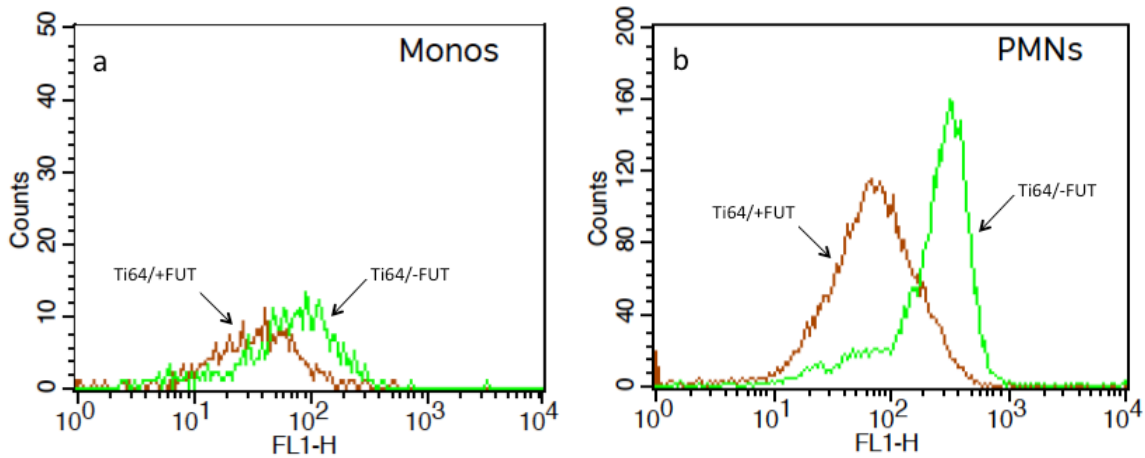


**Figure 6-7. Representative flow cytometry histogram plots showing FUT-175 effect on Mac-1 expression in stent samples at  $360 \text{ s}^{-1}$ .** Histograms are in arbitrary fluorescent intensity units. A decrease in the fluorescent intensity is observed in the presence of FUT-175. FL1-H = CD11b.

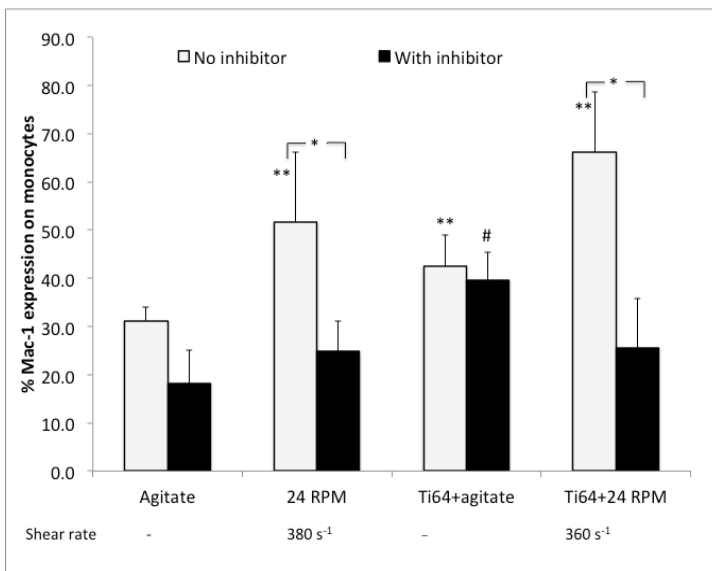


**Figure 6-8. Effect of complement inhibition on Mac-1 expression on monocytes.** Percentages are expressed relative to positive control (LPS). Negative control:  $20 \pm 1\%$  and  $16 \pm 10\%$  (inhibitor). \*:  $p < 0.001$ . \*\*Significantly different from negative control with no inhibitor ( $p < 0.01$ ), #significantly

different from corresponding agitated sample with inhibitor ( $p < 0.01$ ). Results are mean  $\pm$  SD,  $n = 3$  to 4.

Similar to what was observed with monocyte samples, FUT-175 did not induce a significant Mac-1 down regulation on agitated PMN samples ( $p = 0.09$ ) while it induced a significant ( $p < 0.01$ ) down regulation on samples at  $380 \text{ s}^{-1}$ , Figure 6-9. Likewise, in the presence of model stents, FUT-175 did not induce significant Mac-1 down regulation on agitated samples while a significant ( $p < 0.001$ ) Mac-1 down regulation was observed on stent sample at shear rate  $360 \text{ s}^{-1}$ . Mac-1 expression was significantly ( $p < 0.02$ ) upregulated when agitated stent samples with inhibitor were compared with corresponding agitated samples. On the whole, FUT-175 down regulated Mac-1 expression on leukocytes under all experimental conditions, although not always at a level that reached statistical significance of 0.05. The inhibition effect was not significant for samples with stents only but was significant for all shear samples, with or without model stents.

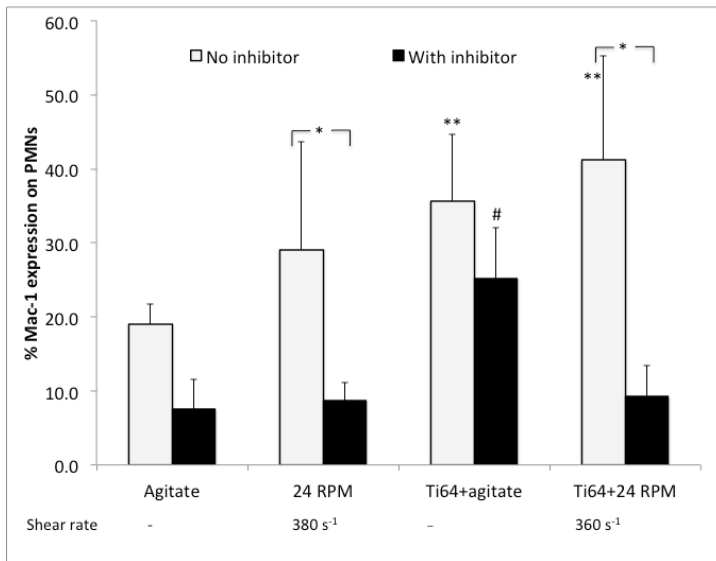


**Figure 6-9. Effect of complement inhibition on Mac-1 expression on PMNs.** Percentages are expressed relative to positive control (LPS). Negative control:  $17 \pm 4\%$  and  $9 \pm 8\%$  (inhibitor). \*:  $p < 0.01$ . \*\*Significantly different from negative control with no inhibitor ( $p < 0.01$ ), #significantly different from corresponding agitated sample with inhibitor ( $p < 0.02$ ). Results are mean  $\pm$  SD,  $n = 3$  to 4.

Regarding C3aR expression, complement inhibition did not show any significant effect on both monocytes and PMNs, Table 6-2. FUT-175 caused a slight C3aR upregulation on non-stent shear samples on monocytes but had little effect for PMNs. On the other hand, for shear samples with stents, FUT-175 showed little effect on monocytes but induced slight C3aR upregulation on PMNs. Shear induced general C3aR down regulation, with some exceptions. In the case of TLR-4 receptor, complement inhibition resulted in consistent upregulation of TLR-4 expression under all conditions, for both monocytes and PMNs. However, definitive conclusions are not possible due to the limited number of samples.

**Table 6-2. Effect of complement inhibition on C3aR and TLR4 expression**

<b>Marker</b> (Control: without, with FUT-175) (%)	<b>Experimental condition</b>	<b>Without FUT-175 (%)</b>	<b>With FUT-175 (%)</b>	<b>p-value FUT-175 Vs No FUT-175</b>
<b>C3aR expression on monocytes (%)</b> (-FUT: 115±12, +FUT: 132±34)	<b>Agitate</b>	135±16	130±29	0.77
	<b>24 RPM (380 s<sup>-1</sup>)</b>	112±5	124±19	0.52
	<b>Ti64+Agitate</b>	149±27	132±30	0.34
	<b>Ti64+24 RPM (360 s<sup>-1</sup>)</b>	124±17	125±16	0.99
<b>C3aR expression on PMNs (%)</b> (-FUT: 164±15, +FUT: 180±70)	<b>Agitate</b>	164±15	174±80	0.81
	<b>24 RPM (380 s<sup>-1</sup>)</b>	129±21	129±21	0.42
	<b>Ti64+Agitate</b>	154±15	151±52	0.94
	<b>Ti64+24 RPM (360 s<sup>-1</sup>)</b>	128±15	163±70	0.40
<b>TLR4 expression on monocytes (%)</b> (93±11, 94±25)	<b>Agitate</b>	71±30	112±17	ND
	<b>24 RPM (380 s<sup>-1</sup>)</b>	81±12	116±7	ND
	<b>Ti64+Agitate</b>	90±6	128±22	ND
	<b>Ti64+24 RPM (360 s<sup>-1</sup>)</b>	85±24	114±41	ND
<b>TLR4 expression on PMNs (%)</b> (80±6, 88±18)	<b>Agitate</b>	57±16	89±7	ND
	<b>24 RPM (380 s<sup>-1</sup>)</b>	66±8	93±14	ND
	<b>Ti64+Agitate</b>	79±14	105±17	ND
	<b>Ti64+24 RPM (360 s<sup>-1</sup>)</b>	75±32	90±22	ND

Percentages for C3aR and TLR4 are expressed relative to positive control (LPS). n=3 except for TLR-4 samples with inhibitor (n=2). ND: not determined due to small sample size. Results are mean  $\pm$  SD.

To further examine the difference in the leukocyte expression of Mac-1, C3aR and TLR-4 receptors, the results of the controls were compared, Table 6-3. For each control, when samples with and without inhibitor were compared, the presence of the complement inhibitor did not result in any significant difference in Mac-1 expression on leukocytes. Mac-1 expression was generally lower on samples with inhibitor. However, significant Mac-1 down-regulation was observed in samples with inhibitor when compared to samples without inhibitor, under shear conditions (Figure 6-8 and Figure 6-9). Therefore, the fact that the inhibitor did not induce significant differences in Mac-1 expression under control conditions, and Mac-1 expression was lower in inhibitor samples, suggests that the differences observed in the experimental results were related to the experimental conditions and not due to the control samples. It is interesting to note that the difference in Mac-1 expression between the negative control and the corresponding positive control, with and without inhibitor, are both significant.

Similar to Mac-1 expression, the presence of the FUT-175 did not result in a significant difference in C3aR expression in the control samples. C3aR expression also seemed to be lower for samples with inhibitor. Since the low C3aR expression in LPS control samples with FUT-175 did not correspondingly produce high C3aR expression in all experimental results with FUT-175 (Table 6-2), this suggests that the observed experimental results may not have been influenced by the control samples.

For TLR-4, the presence of complement inhibitor in either control sample did not result in a significant difference in TLR-4 expression on leukocytes. Complement inhibition had minimal effect on monocytes but slightly discernible effect on PMNs. In the absence of inhibitor, the results also showed slight increase in TLR-4 expression on leukocytes. Since TLR-4 expression seemed to show an increase in the presence of FUT-175, under all experimental conditions (Table 6-2), this suggests that the differences observed in the experimental results were not due to the control samples. Thus, the results of Mac-1, C3aR and TLR-4 expression can generally be attributed to experimental conditions.

**Table 6-3. Comparison of inhibitor effects on controls for Mac-1, C3aR and TLR-4. All markers are reported as arbitrary fluorescent units.**

Marker expression		Negative control		Positive control		p-value	
						Negative	Positive
		- FUT	+ FUT	- FUT	+ FUT	-FUT vs +FUT	-FUT vs +FUT
<b>Mac-1</b>	<b>Monocytes</b>	21±3	18±8	106±12 <sup>#</sup>	126±34 <sup>*</sup>	0.83	0.17
	<b>PMNs</b>	63±30	35±37	353±95 <sup>#</sup>	318±105 <sup>*</sup>	0.62	0.55
<b>C3aR</b>	<b>Monocytes</b>	135±24	92±60	119±31	70±44	0.25	0.19
	<b>PMNs</b>	162±23	128±71	100±19	79±43	0.37	0.58
<b>TLR-4</b>	<b>Monocytes</b>	246±5	251±55	268±36	269±14	ND	ND
	<b>PMNs</b>	212±13	250±79	270±14	282±31	ND	ND

Results are mean ± SD. n=3-4 except TLR-4 samples with inhibitor (n=2). <sup>#</sup>Significantly different from corresponding negative control without inhibitor (p<0.001), <sup>\*</sup>significantly different from corresponding negative control with inhibitor (p<0.002)

### **6.3.3 Effect of complement inhibition on platelet-leukocyte aggregation response to shear and model stents**

In addition to leukocyte activation, platelet-leukocyte aggregation was investigated with and without complement inhibitor. In the absence of model stents, complement inhibition did not have a significant effect on platelet-monocyte aggregations, Figure 6-10. It was observed that the presence of model stents in the absence of the inhibitor caused significant platelet-monocyte aggregation when compared with corresponding non-stent agitate (p<0.02) and shear (p<0.001) samples. The presence of complement inhibitor significantly (p<0.001) reduced platelet-monocyte aggregation at shear rate 360 s<sup>-1</sup>. Generally, complement inhibition reduced platelet-monocyte aggregation.

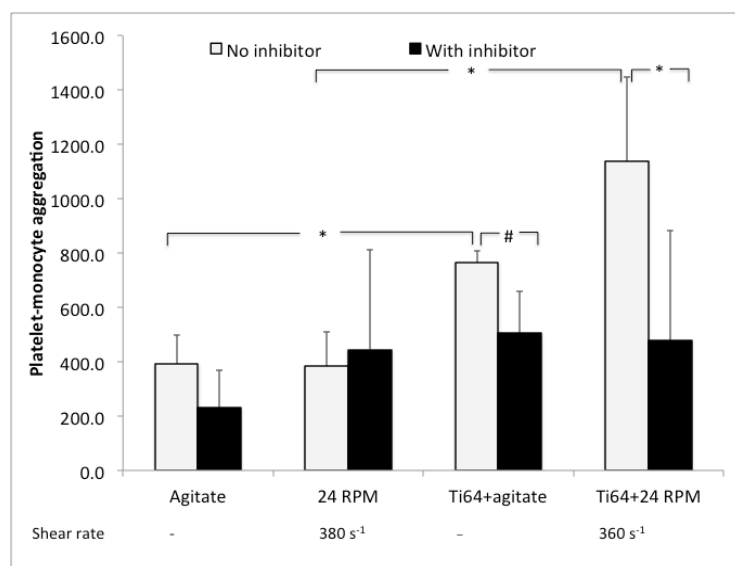


**Figure 6-10. Effect of complement inhibition on platelet-monocyte aggregation.** Aggregation values are reported as arbitrary fluorescent units. Negative control: 166±77 and 119±106 (inhibitor). \*: p<0.02, #: p=0.12. Results are mean ± SD, n=3 to 4.

Similar to platelet-monocyte aggregation, in the absence of a stent, platelet-PMN aggregation was not significantly affected by complement inhibition, Figure 6-11. The presence of a stent in the absence of the inhibitor caused significant platelet-PMN aggregation when compared to corresponding non-stent agitate (p<0.001) and shear (p<0.001) samples. In the presence of model stents, complement inhibition significantly (p<0.001) reduced platelet-PMN aggregation under both agitation and shear conditions. In general, complement inhibition reduced platelet-leukocyte aggregation, which seems to be more effective on platelet-PMN aggregation. Overall the effect of complement inhibition on platelet-leukocyte aggregation was greater for stent samples and was significant under shear.

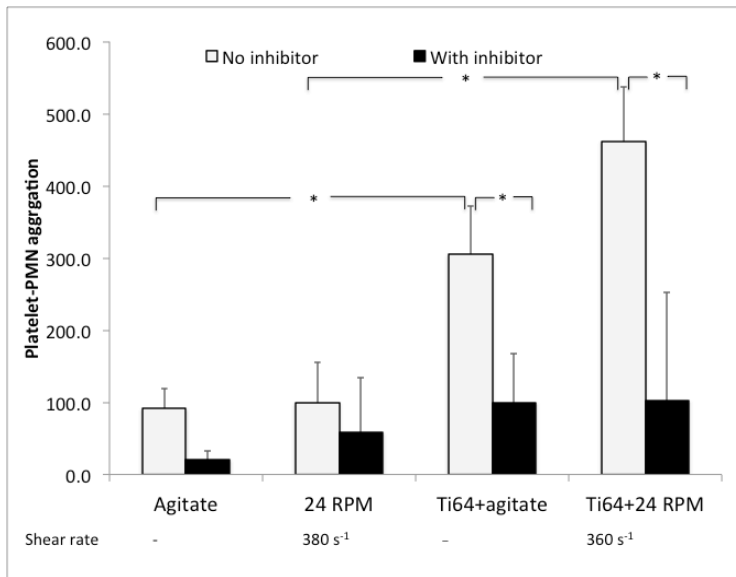


**Figure 6-11. Effect of complement inhibition on platelet-PMN aggregation.** Aggregation values are reported as arbitrary fluorescent units. Negative control: 41±16 and 31±34 (inhibitor). \*: p<0.001. Results are mean ± SD, n=3 to 4.

### 6.3.4 Effect of complement inhibition on surface adhesion

Figure 6-12 depicts typical scanning electron microscopy images of protein deposition and cell adhesion on model stent samples with and without complement inhibitor. Adherent leukocytes can be observed on both samples without inhibitor, Figure 6-12(a) and (b), although the morphologies are different. Agitated sample shows pancake morphology while shear sample shows rugged surface morphology. It should be noted that some of the cells may be RBCs. Agitated sample with inhibitor, Figure 6-12(c), shows predominantly adherent platelets, although there are some leukocytes. What appear like floating cells are actually cells that have fallen onto the adhesion tape. For shear sample, Figure 6-12(d), platelets can still be observed with even fewer leukocytes. There also seems to be a layer of protein deposition as shown by the insert in (d), which is presented in a magnified view in Figure 6-13.

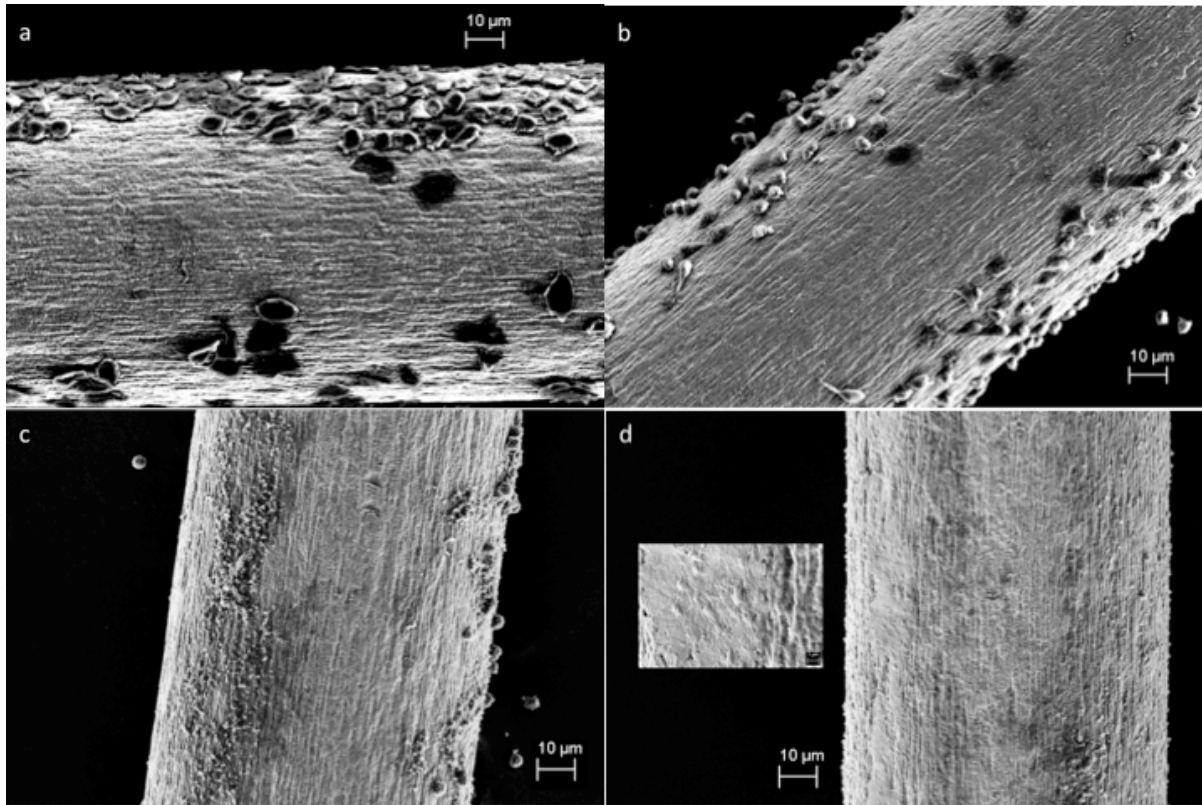


**Figure 6-12. SEM cell adhesion pattern for sample with and without inhibitor.** Samples without inhibitor: (a) agitated sample and (b) 24 RPM ( $360 \text{ s}^{-1}$ ) sample; samples with inhibitor: (c) agitated and (d) 24 RPM sample. SEM magnification for all samples at 500X (insert at 5kX).

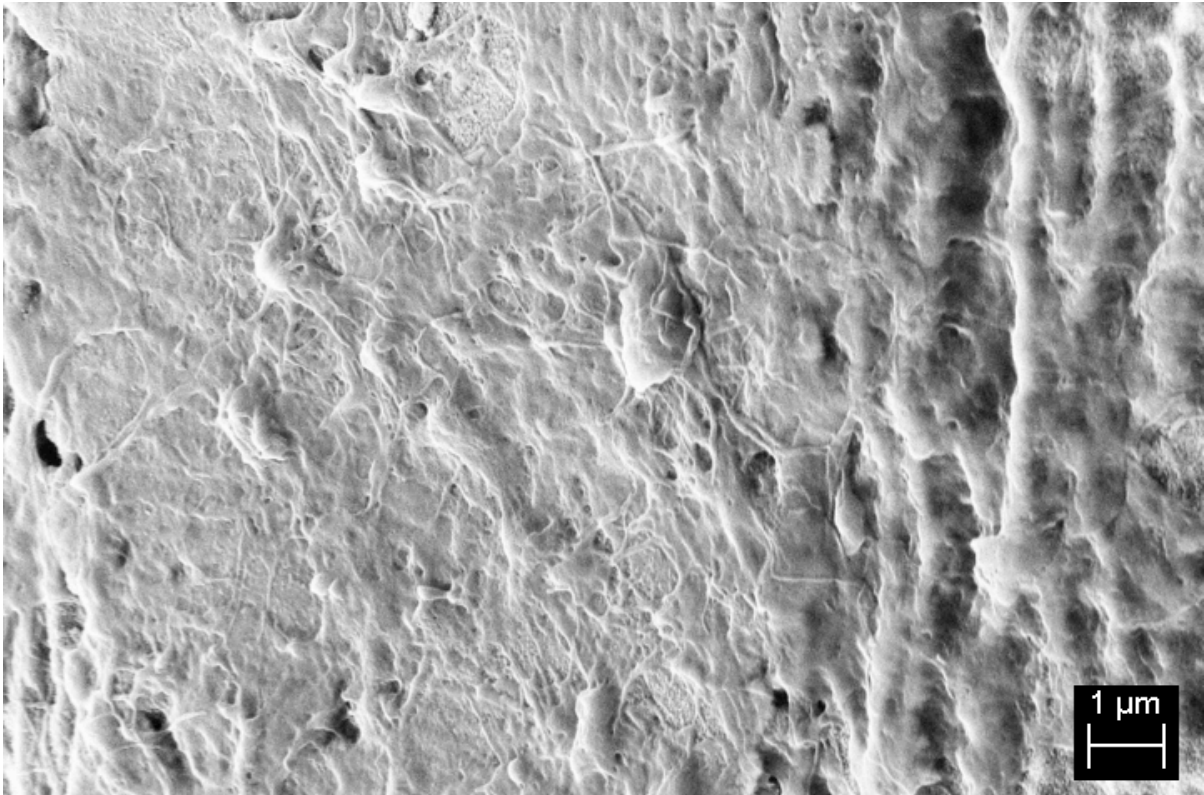


**Figure 6-13. Magnified SEM cell adhesion pattern for sample with inhibitor.** 24 RPM sample, magnification at 5kX.

## **6.4 Discussion**

Blood-biomaterial interaction involves a lot of cross-talk and co-stimulation of blood cells from the various systems. In this study, the effect of broad spectrum complement inhibition, which eliminated some of the co-stimulators, was investigated with the complement inhibitor FUT-175. FUT-175 was introduced at 10 $\mu$ l/ml into the blood samples at the beginning of the experiments. Following 2-hour whole blood incubation under mild agitation and shear, with and without model stents, platelet and leukocyte activation and aggregation were characterized to determine the effect of complement inhibition.

### **6.4.1 Platelet activation**

The level of shear in this study did not significantly increase platelet activation in the absence of model stents; it was below the threshold of platelet activation in whole blood. Hence, complement

inhibition did not significantly reduce platelet activation, as characterized by PMP formation. This seems to be consistent with previous findings that the ability of platelets to activate complement is time and shear dependent [434]. While some of our values appear to be different from values reported in Chapter 5, this is due to the fact that the donor samples in these experiments were not necessarily the same as donors compared to the initial experiments in Chapter 5 where low platelet response donors were present.

However, in the presence of model stents, FUT-175 significantly inhibited material-induced PMP formation. Platelet activation in the presence of a biomaterial can be induced through a number of mechanisms, which include complement activation fragments such as C5b-9 [78], thrombin from the coagulation system,  $\text{Ca}^{2+}$  bound to the negatively charged  $\text{TiO}_2$  [461] and binding of platelet integrin receptor GPIIb/IIIa to fibrinogen [219], which also binds metallic biomaterials [220]. In order to significantly reduce platelet activation, as characterized by PMP formation, FUT-175 would have to inhibit complement activation as well as the other mechanisms that contribute to platelet activation. Since FUT-175 inhibits complement activation [458], it blocks the formation of C5b-9 and therefore, the reduction in PMP formation in the presence of FUT-175 is understandable. Regarding calcium, futhan can inhibit intracellular platelet calcium mobilization in a dose-dependent manner, with or without extracellular calcium [462]. In addition, it is possible that FUT-175 interacts with the platelet calcium channels as another mechanism of regulating PMP formation. Indeed, there has been evidence of futhan blocking acid-sensing ion channels [463] and in another model, futhan was shown to preferentially target ion channels; abolishing calcium influx [464]. Hence, it is plausible that a similar inhibition mechanism could occur with platelets and thus, partly explain the reduction in PMP formation in the presence of futhan. Concerning platelet activation from the binding of integrin receptor GPIIb/IIIa to material-bound fibrinogen, FUT-175 may also be interfering with the platelet receptor GPIIb/IIIa. Futhan can certainly antagonize the GPIIb/IIIa receptor since it has been shown to inhibit platelet aggregation from a variety of agonists, such as ADP [462, 465]. This is further supported by the reported disaggregation of platelets after ADP stimulation in the presence of futhan [465]. Thus, the interaction of futhan with GPIIb/IIIa, which would interfere with the outside-in signaling effects, such as mobilization of intracellular calcium, may also provide an explanation for reduced platelet activation.

The reported double role of futhan, reduced PMP formation and aggregation, has significance for thrombosis reduction. The reduction in PMP formation by complement inhibition has some clinical relevance since PMPs, and other cell microparticles, are associated with a variety of clinical

conditions, including arterial thrombosis. While the results have promising applications, there is a need to further elucidate the mechanism of inhibition.

The results of platelet consumption as characterized by GPIIb/IIIa expression suggest that futhan reduced platelet consumption. This is interesting because under physiological conditions it means activation is controlled, as demonstrated by suppression of PMP formation, and the preservation of platelets. The reduction in platelet consumption seems to agree with the results of an extracorporeal model using futhan, which showed that platelet count was preserved after 2 hours of circulation [466]. Thus, futhan could reduce platelet participation in material-induced thrombosis.

#### **6.4.2 Leukocyte activation**

Complement inhibition down regulated Mac-1 expression on leukocytes under all conditions. However, the down regulation of Mac-1 on both monocytes and PMNs was only significant in samples under shear, with and without a model stent. Interestingly, both samples (shear alone and shear with model stents) were reduced to similar levels. Shear is known to activate leukocytes and induce CD11b upregulation or down-regulation as shown in Chapter 5 and other studies [168, 428]. In the presence of model stents under mild agitation, complement inhibition caused minimal reduction in CD11b expression. Taken together, these results suggest shear-dependent inhibition of Mac-1 expression. The question that arises is whether shear sensitizes leukocytes to futhan inhibition, regardless of material presence. Mac-1 down regulation has also been observed in other *in vitro* and *in vivo* models using compstatin [443, 467]. However, in a 2-hour extracorporeal circulation model, no effect was observed on CD11b expression [466]. The interesting aspect of the extracorporeal model results was that they showed reduction in PMN F-actin. This did not only suggest preserved PMN deformability under flow but also suggested that futhan may interact with leukocyte mechanosensing receptors that control the intracellular calcium-dependent cytoskeleton filaments. If that is the case, then this may partly explain our observed shear-dependent Mac-1 inhibition.

Furthermore, platelets under shear have been reported to preferentially activate the classical pathway [74], which could be through C1q of the classical pathway either binding to the global C1q receptor (gC1qR) on activate platelets [449] or to chondroitin sulfate A released from  $\alpha$ -granules of activated platelets [468, 469]. Since this pathway will add to leukocyte activation, it may be a major contributing pathway to leukocyte activation under nominal physiological shear through amplification. If so, that would also be a factor in explaining the observed shear-dependent leukocyte CD11b down regulation.

Futhan had limited effect on Mac-1 expression in the presence of model stents under mild agitation. In fact, CD11b expression was significantly higher than the corresponding agitated samples without stents. In a polymeric bead model using sCR1, CD11b expression was previously found to be material dependent [317]. This then raises the question of whether in the absence of shear, futhan inhibition is material dependent. However, since futhan is reported to have a short half-life of approximately 8 minutes, the question is whether the CD11b expression is time and material-dependent. Indeed blood activation is known to be time and material dependent. More importantly it has previously been shown that CD11b expression rate on titanium surfaces was dependent on surface characteristics. CD11b expression was found to increase slowly on hydrophobic surfaces [293]. Interestingly, in Chapter 4, the characterization of the stent wire revealed a weakly hydrophobic contact angle of  $65.4^\circ$  (water adhesion tension approximately  $21.5 \text{ dyn/cm}^2$ ). If the increase in CD11b expression was indeed slow due to the surface wettability, then in a semi-static condition with other agonists inhibited, it may be even slower. Thus, as futhan effects diminished, CD11b expression increased. Therefore, this may provide another explanation for the observed increase in CD11b expression even with futhan inhibition. Yet, another factor could be related to the previously alluded binding of calcium to titanium oxide [461]. If it indeed plays a role in platelet activation, this would support the observed platelet inhibition in agitated stent samples and no inhibition on leukocytes for the corresponding samples.

Tissue factor expression, which is also anaphylatoxin induced [141], was down regulated by futhan in a similar manner as Mac-1. Complement inhibitor mediated TF down regulation has also been reported in a hemodialysis model using another broad effect inhibitor, compstatin, [443]. Although the TF samples were limited, the results suggest shear-dependent down regulation and limited effect in the presence of model stents under agitation, similar to Mac-1 expression. It is plausible that the mechanism responsible for Mac-1 pattern of regulation may be similar as they both can be induced by complement. It should be noted however that the implications of TF upregulation or down regulation for material-induced thrombogenicity in the presence of futhan would have been limited anyway due to the fact that the activity of the TF/FVIIa would be reduced by futhan inhibition [470].

The effect of complement inhibition on C3aR expression on leukocytes was minimal. It has previously been shown that complement activation and the presence of C3a fragment causes internalization of C3aR [407]. Therefore, when complement activation is inhibited, the lack of C3a from either the classical or alternative pathway would keep the C3aR expression at the basal level.

Since FUT-175 also blocks serine protease thrombin, which is another pathway for generating C3a, there are limited pathways for contributing C3a. This is not surprising that no significant change was observed in C3aR expression.

The initial results for TLR-4 expression suggest that it was upregulated in the presence of complement inhibitor. Since LPS, without inhibitor, can increase TLR-4 mRNA [406], the question of possible influence from the positive control was raised. However, our LPS investigation revealed no influence from positive control, especially on monocytes, which predominantly express the LPS receptor (CD14) compared with PMNs [125]. This seems to agree with the results of a rabbit model in which futhan did not have any effect on endotoxin-induced inflammation [458]. Therefore, the observed increase in TLR-4 expression was not due to futhan effect on LPS. It is possible that in the absence of other co-stimulators as a result of complement inhibition, activation of compensatory mechanisms, could occur since there is cross-talk between complement and TLR-4 mediated pathways. Additional studies are necessary to elucidate the mechanisms at play.

#### **6.4.3 Platelet-leukocyte aggregation**

The presence of model stents under all experimental conditions resulted in a significant increase in fluid phase platelet-leukocyte aggregation, without an inhibitor. The presence of FUT-175 in samples with stents substantially reduced platelet-leukocyte aggregation; platelet-monocyte, up to 2-fold, and platelet-PMN aggregation up to 5-fold. Platelet-leukocyte aggregation is facilitated by platelet P-selectin and leukocyte PSGL-1 interaction as well as fibrinogen bridging between platelet GPIIb/IIIa and leukocyte Mac-1; the latter interaction proving to be the most stable binding. In the platelet and leukocyte investigations, it was shown that complement inhibition significantly reduced both platelet and leukocyte activation under shear conditions, in the presence of model stents. Hence aggregation receptors were reduced for both platelets and leukocytes, resulting in reduced platelet-monocyte and platelet-PMN aggregation, 2.4-fold and 4.5-fold, respectively.

For agitated stent samples, platelet PMP activation was still substantially reduced. Mac-1 expression was also down regulated, albeit not significantly. The combined effect was reduced platelet-leukocyte aggregation. It is interesting to note that consistent with previously observed preferential platelet aggregation with monocytes compared to PMNs [29, 178, 424], the reduction in platelet-monocyte aggregation (1.5-fold) was not significant while it was significant for platelet-PMN aggregation (3-fold). The reduction in platelet-leukocyte aggregation is desirable since these

aggregates have the potential to adhere to the stent surface and therefore contribute to material-induced thrombosis.

#### **6.4.4 Surface adhesion**

In the absence of complement inhibitor, qualitative evaluation showed that there was visible shear-dependent leukocyte adhesion to the model stents. While there was still shear-dependent adhesion in the presence of FUT-175, complement inhibition substantially reduced cell adhesion under both conditions. For samples under shear, leukocyte adhesion was almost abolished while there was still limited platelet adhesion and visible protein adsorption. Complement inhibition would generally result in reduced availability of anaphylatoxins and the iC3b fragment, which is a Mac-1 ligand for leukocyte surface adhesion. In addition, complement inhibition reduced Mac-1 expression, especially under shear, hence the observed reduction in leukocyte adhesion. The decrease in leukocyte adhesion has significance for material-induced thrombosis since adherent leukocytes, especially monocytes because of their persistence in foreign body response, express TF and C3aR, which play a role in thrombosis. Tissue factor [405] as well as the C3aR ligand, C3a [88], have been associated with development of in-stent thrombosis. In addition, inhibition of leukocyte adhesion has significance for reducing possible leukocyte oxidative stress at the surface, which has beneficial effect *in vivo*. This suggests that complement may be one of the main driving forces behind leukocyte mediated foreign body response. Hence, control of complement activation could be one of the possible mechanisms to regulate material-induced thrombosis.

Platelets, on the other hand, even not activated can still bind surface adsorbed fibrinogen through GPIIb/IIIa and be activated, since fibrinogen is not directly affected by complement inhibition. As a result, platelet adhesion was not completely abolished. Since proteins generally unfold and expose binding epitopes upon contact and adsorption to biomaterial surfaces, targeting proteins such as inhibiting complement or blocking conformational change may be one of the better ways to reduce the effect of material-induced thrombogenicity. It is interesting to note that similar results were observed in a different model using complement inhibitor compstatin, where leukocyte adhesion was reduced but platelet adhesion was not affected [455]. However, the rate of platelet activation is limited partly because feedback loops for some of the agonists, such as thrombin, are reduced by futhan inhibition. In general the results suggest that futhan may have the potential to reduce material-induced thrombosis.

The effects of complement inhibition on platelet and leukocyte activation and aggregation are summarized on Table 6-4. An interesting aspect of this inhibition is that even though FUT-175 has a short half-life and its effects are reversible, the inhibition effects were still significant after 2-hour incubation. Thus, the mode of interaction in an *in vitro* model is unclear. The results of this study raise important questions about the mechanisms of inhibition of shear and material-induced complement activation with futhan. Further investigations are necessary to elucidate these mechanisms.

**Table 6-4. Summary of inhibition effect. Arrows show comparison of samples with and without FUT-175 at each experimental condition. Ti64: Ti-6Al-4V stent sample.**

		<b>Agitate</b>	<b>Shear</b>	<b>Ti64+agitate</b>	<b>Ti64+shear</b>
<b>Platelets</b>	<b>PMP formation (%)</b>	↓	↓	↓	↓
	<b>CD61</b>	↓	↓	↓	↑
	<b>P-seletin</b>	—	—	—	—
<b>Monocytes (% expression)</b>	<b>% expressing TF</b>	↓	↓	↓	↓
	<b>Mac-1</b>	↓	↓	↓	↓
	<b>C3aR</b>	↓	↑	↓	—
	<b>TLR-4</b>	↑	↑	↑	↑
<b>PMNs (% expression)</b>	<b>Mac-1</b>	↓	↓	↓	↓
	<b>C3aR</b>	↑	—	↓	↑
	<b>TLR-4</b>	↑	↑	↑	↑
<b>Platelet-monocyte aggregates</b>		↓	—	↓	↓
<b>Platelet-PMN aggregates</b>		↓	↓	↓	↓

— No effect or barely discernible effect

↓, ↑ Non-significant decrease or increase, respectively

↓ Significant decrease

## 6.5 Conclusion

This study has demonstrated that complement inhibition with futhan provides an effective method to reduce platelet and leukocyte activation and adhesion to a Ti-6Al-4V surface. This in turn

may reduce the local production of superoxides from leukocytes, which can have detrimental effects *in vivo*, such as lumen loss. The interesting aspect of this compound is that from this and other studies, it did not completely impair platelet function. This would be important *in vivo* for active hemostasis with reduced coagulation effects. The importance of this finding is that while under normal circumstances platelet adhesion correlates with leukocyte adhesion, when complement is inhibited, the correlation does not seem to exist or is substantially reduced. Which means platelet adhesion can occur with limited influence on leukocyte adhesion, thus reducing the effect of the coagulation cascade and subsequent thrombosis.

This study has also raised important questions regarding the mode of interaction and the effect of inhibiting material-induced complement activation. Further investigations are necessary to elucidate the specific extent and time course of activation of each complement pathway in material-induced thrombogenicity. Such information is crucial for *in vivo* applications in developing drug strategies throughout the healing process after stent implantation. The interaction of futhan with cell receptors also needs further examination. Detailed studies are necessary to elucidate the futhan effect on platelet receptors such as P-selectin and other receptors that play a role in the regulation of PMP formation. Studies are also necessary to elucidate the possible interaction of futhan with constitutively expressed leukocyte receptors, such as C3aR, as well as activation receptors, such as Mac-1. These investigations would go a long way in understanding the effect of futhan on platelet and leukocyte functions. Furthermore, there is an important issue of cell adaptation in the absence of co-stimulators, which remains unclear. This can possibly occur if there is stimulus imbalance in an environment where cross-talk and co-stimulation play an essential role.

Material-dependence was also raised in this study. Whether futhan interacts with the metallic implant is not clear. The effect of material chemistry, in this case titanium oxide, in blood activation and subsequently determining the effect of futhan is an important factor that needs to be investigated. These studies were performed under nominal shear conditions. The effect of experimental conditions on the threshold of inhibition remains undetermined. Therefore, further studies are necessary to elucidate the effect of inhibition under high physiologic and pathologic shear conditions. Overall the study supports the hypothesis that complement inhibition could reduce material-induced thrombogenicity. The results have significance in further investigation of the use of futhan in reducing material-induced thrombosis.

## **Chapter 7**

# **Effect of Surface Roughness on Blood Activation and Complement Inhibition**

### **7.1 Introduction**

Biomaterial surface characteristics, such as surface chemistry, morphology (roughness and topography), wettability, energy, and their effects on blood-biomaterial interaction were described briefly in Chapter 2. All the surface characteristics are equally important in blood-biomaterial interaction because any material surface can be uniquely described by a specific combination of parameters pertaining to these characteristics. Hence, the specific combination of surface characteristics influences the sequence of events at the blood-biomaterial interface, such as protein conformational change and subsequent adsorption and cell adhesion; a sequence which ultimately is associated with the level of material thrombogenicity. Thus, considering all other factors equal (such as individual immune response and hemodynamics [471]), material thrombogenicity is uniquely determined by its surface characteristics. Although the question of the relationship between the different material characteristics and biological system response has long been asked [472], and despite years of research in blood-biomaterial interactions, “the fundamental principles of the causation of specific cellular responses as a result of the influence of materials are still not well known” [50]. Therefore, there is need for continued investigation of the relationship between material surface properties and protein and cell behavior.

One material surface characteristic that is of particular interest is surface morphology, which is often described in terms of roughness and topography. As previously described in Chapter 2, roughness and topography are often used interchangeably since they both describe surface texture. However, surface roughness is usually quantitative, in terms of either an average or root-mean-square value but topography is often qualitative, e.g. surface waviness, although it can also be specified quantitatively if the topography is defined. Hence, topography can be used as a distinguishing qualitative description for surfaces with diverse geometries but similar average or root-mean-square roughness values. For that reason, at the minimum, the description of surface morphology requires the inclusion of both the topographic and the quantitative description of roughness. Both parameters are equally important in blood/cell-biomaterial studies. In this study, both roughness and topography are used but the use of roughness alone will be understood to include topography.

Surface roughness, with or without defined topography, is one of the significant biomaterial properties that can easily be modified during or after manufacturing to influence both specific and non specific surface binding, for a variety of applications, which include cardiovascular stents [473, 474]. Surface roughness and topography define both the physical and thermodynamic characteristics of the material. They influence biological response through three main mechanisms; (i) physical increase in surface area, (ii) physical patterned guidance of cell response and (iii) the thermodynamics of wettability and the related surface energy. The physical increase in surface area, as well as the level and structure/topography of roughness have been shown to influence cell adhesion and proliferation [272-274, 475]. These physical properties also have implications for the contact system and recognition molecules, such as complement, and regulation of cell responses. The level and structure of roughness have certainly been found to be important factors in influencing material roughness-induced complement activation and adhesion [25, 85] and endothelialization [476-478]. The activation of complement, which results in the formation of anaphylatoxins C3a and C5a, whose main function is activation and recruitment of leukocytes through their respective receptors C3aR and C5aR. These receptors are constitutively expressed by leukocytes [69, 107] and their regulation by agonists/antagonists has pharmacological relevance. Their ligand specificity, particularly C3aR, whose ligand has been used as an indicator of complement activation [85], suggests the possibility of its use for leukocyte activation studies. Indeed, C3aR can be regulated by a variety of agonists and antagonists [479]. However, there is limited understanding on how it is regulated in the presence of a biomaterial with specific physical characteristics such as roughness. The receptor regulation by biomaterial characteristics such as roughness is of particular interest as it may have implications for leukocyte recruitment and material-induced thrombogenicity.

Furthermore, surface patterning of vascular implants has enhanced endothelialization [476-478], suggesting possible use of stent surface roughness to reduce thrombogenicity. While stent endothelialization is desirable *in vivo*, it occurs in a longer time scale than an acute inflammatory response or blood activation, which occurs in a matter of seconds for platelets (10 seconds) and minutes for PMNs (10 minutes) [171, 480]. Surface roughness has indeed been shown to influence blood cell activation and adhesion. It also influences platelet activation and adhesion [480-483] and tissue factor expression [170], which are key risk factors for acute in-stent thrombosis [405]. Therefore, any continued surface exposure of either bare-metal stents or drug-eluting stents, raises concern for a roughness-induced inflammatory response. Incidentally, drug-eluting stents have been shown to leave stent struts uncovered for up to 2 years in 20% of the patients [444], and the late

lumen loss has been correlated with complement anaphylatoxins C3a and C5a [88]. Furthermore, drug-eluting stents have been associated with late in-stent thrombosis [484, 485]. Although recent studies suggest comparable performance between metallic and polymer coated drug-eluting stents [486, 487], without the use of anticoagulant/antiplatelet therapies there is still increased likelihood of material-induced thrombosis once the drug release is complete. So, while surface roughness has some applications in drug delivery to promote endothelialization, it also raises concerns for triggering some of the immune response systems and possible material-induced thrombosis.

Besides, the physical effects, the level of roughness influences the thermodynamics of surface wettability [50, 304], which is also related to surface energy. Surface thermodynamics specifically influences water structure at material surface [59], which in turn influences protein adsorption and conformational change, e.g. activation of the complement [85] and contact system [488], and subsequent cell adhesion. Thus, surface roughness and topography induce a variety of effects on blood activation, from the initial water and protein interaction to cell activation and the development of thrombosis. Since complement plays an important role in material-induced inflammation, complement inhibition was previously investigated in Chapter 6. However, the effect of material surface properties on the effectiveness of complement inhibition with FUT-175 remains unclear.

Therefore, the purpose of this chapter was two-fold; (i) to investigate the effect of multiscale roughness on blood activation using helical model stents as previously described and (ii) to investigate the effect of roughness on the effectiveness of complement inhibition. We hypothesized that, under flow conditions, multiscale roughness with relatively heterogeneous topography has an effect on blood activation as well as complement inhibition. Interaction between surface roughness and biological systems has implications for material-induced thrombogenicity since roughness influences activation of the various biological systems (complement, contact, coagulation and hemostatic systems). For that reason, the effect of roughness on complement inhibition is also investigated. Investigating the mechanism of roughness effect on platelet and leukocyte activation and adhesion is of particular interest as they play a key role in coagulation and thrombosis.

## **7.2 Materials and methods**

### **7.2.1 Flow model**

The Chandler loop model, with a silastic tube of 4.78 mm internal diameter and 59 mm loop diameter, as previously described in Chapter 3, was used for this experiment.

### **7.2.2 Model stents surface treatment**

Model stents were made as described in Chapter 4. Before forming stents, one set of stent wires was acid-etched to create surface roughness and the other set was used as obtained from the manufacturer. Acid etching was done by immersing the wires in a mixture of 15% hydrofluoric acid, 40% nitric acid and 45% distilled water at room temperature for 10 seconds. This acid mixture has previously been used by other investigators, sometimes with different concentrations [306]. Model stents were ultrasonically cleaned in 30% nitric acid for 20 minutes, followed by rinsing in distilled water and ultrasonic cleaning in 70% ethanol for 10 minutes. Stents were then rinsed at least twice in phosphate buffer saline (PBS) and stored at 4°C, for use within 4 hours.

### **7.2.3 Model stent surface characterization**

Surface characterizations, using a scanning electron microscope, atomic force microscopy and contact angle measurements were conducted as described in Chapter 4.

### **7.2.4 Antibodies and reagents**

Fluorescein isothiocyanate conjugated mouse monoclonal antibody against human glycoprotein GPIIb/IIIa (CD61-FITC), R-phycoerythrin monoclonal antibody against P-selectin (CD62-PE), Fluorescein isothiocyanate conjugated mouse monoclonal antibody against Mac-1 (CD11b-FITC), R-phycoerythrin monoclonal antibody against tissue factor (CD142-PE), anti-C3aR PE hC3aRZ8 and R-phycoerythrin-cytochrome 5 conjugated monoclonal antibody against PAN leukocytes (CD45-PerCP-Cy5.5) were purchased from BD Biosciences (San Diego, CA, USA). FACS lysing solution was purchased from BD Biosciences (San Diego, CA, USA). Phosphate-buffered saline (PBS) was purchased from Fisher Scientific Inc (Ottawa, ON, Canada). Lipopolysaccharide (Escherichia coli serotype 0111:B4) (LPS), 50% glutaraldehyde solution, and paraformaldehyde were purchased from Sigma-Aldrich Co (Oakville, ON, Canada). Hepes Tyrode Buffer (HTB) solution PH 7.4 was prepared in the laboratory with a final concentration of 137mM NaCl, 2.7mM KCl, 5mM MgCl<sub>2</sub>, 3.5mM HEPES, 1g/L Glucose, and 2g/L BSA.

### **7.2.5 Blood sample collection**

This study received ethics clearance from the University of Waterloo Research Ethics Office. Peripheral venous blood samples were drawn with formal consent from healthy volunteers, of age range 20 to 50 years, who indicated that they had not taken any medication in the last 72 hours. There

was no restriction placed on the participants' physical activity, the type of diet and eating time. Participants were however advised to drink lots of water ahead of the blood draw. Briefly, blood samples were drawn with a 21G Vacutainer safety-lok blood collection set and syringe (BD Biosciences, San Diego, CA, USA) by a qualified phlebotomist. Blood was immediately transferred into 10 ml conical tubes containing heparin (5U heparin/ml). Blood samples were kept in an insulated container and used in the blood activation experiments within 30 minutes of collection.

### 7.2.6 Platelet, complement and leukocyte activation and aggregation

To assess material effect on blood activation, 2 ml blood samples were transferred into silicone tube loops, with or without appropriate 20 mm model stents. Therefore, the experiments were carried out in two groups. Group one was composed of 2 ml blood samples with 20 mm un-etched stents and group two was 2 ml samples with 20 mm acid-etched stents. To assess activation effects under shear, experiments were performed under two conditions, Figure 7-1. Experimental condition one was composed of gentle agitation and rotation at 24 RPM on a mini-shaker (VWR, PA, USA) and experimental condition two was composed of gentle agitation and rotation at 45 RPM. For all the experiments, control samples were static and included only blood (negative control/resting sample) and blood with lipopolysaccharide (LPS) (1  $\mu\text{g}/\text{mL}$ ) as a positive control. All samples were incubated at 37°C for 2 hours.

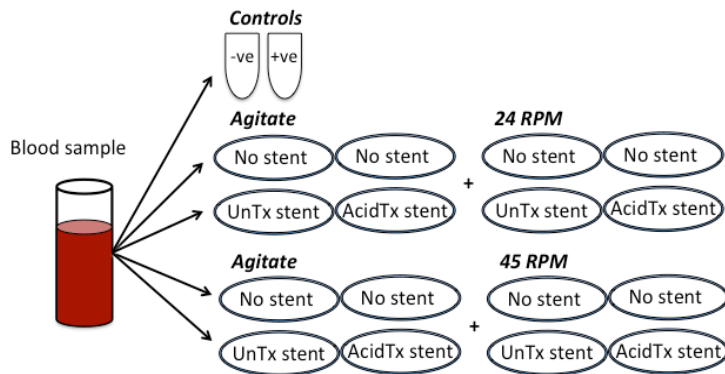


**Figure 7-1. Schematic of experimental conditions.** UnTx: un-etched, AcidTx: acid-etched.

### **7.2.7 Immunolabelling and flow cytometry analysis**

At the end of the 2-hour incubation, aliquots of blood samples were incubated in tubes containing fluorescently-labeled antibodies for flow cytometry. To assess platelet activation and platelet microparticle (PMPs) formation, 5  $\mu$ L blood samples were diluted with 50  $\mu$ L HTB in test tubes and incubated for 30 minutes at 4°C with fluorescently-labeled antibodies against GPIIb/IIIa (CD61-FITC). Following incubation, samples were further diluted with 200  $\mu$ L HTB, fixed with 200  $\mu$ L 2% paraformaldehyde and stored at 4°C before flow cytometry analysis. In flow cytometry analysis, platelets and PMPs are distinguished on the basis of size. First, events are acquired based on anti-CD61 expression. Light scatter analysis on granularity and size then distinguishes the events related to PMP, platelet and platelet aggregates. Based mostly on size, PMPs, which are smaller than platelet, are then reported as percentage of the total events (PMP + platelets).

To assess complement and leukocyte activation and platelet-leukocyte aggregation, 30 $\mu$ L of blood samples were diluted with 50  $\mu$ L HTB in test tubes and incubated for 30 minutes at 4°C with appropriate antibodies. Leukocytes were identified by PAN leukocyte marker (CD45 PE-Cy5). The effect of complement activation was assessed with anti-C3aR PE hC3aRZ8. Leukocyte activation was identified by antibodies against Mac-1 (CD11b-FITC) and tissue factor (CD142-PE) on leukocytes. Platelet-leukocyte aggregation was characterized with antibodies against GPIIb/IIIa (CD61-FITC) on leukocytes. Following 30 minutes incubation, 700  $\mu$ L of FACS Lyse solution was added to lyse red blood cells. Aliquots were concentrated by centrifuging at 1200g for 6 minutes and discarding supernatant. Resuspended pellets were washed and then diluted with 200  $\mu$ L HTB and fixed with 200  $\mu$ L paraformaldehyde (1% final concentration). All samples were stored at 4°C and analyzed on a BD FACS Calibur flow cytometer with CellQuest Pro software (BD Diagnostics, San Diego, CA, USA), within 5 days.

### **7.2.8 Surface adhesion characterization**

After the experiment, stent samples were first rinsed with 0.2M sodium phosphate buffer, pH 7.2. Adherent proteins and cells were then fixed in 2.5% glutaraldehyde and stored at 4°C until analyzed. To prepare fixed samples for SEM analysis, samples were first immersed and washed in 0.2M sodium phosphate buffer, pH 7.2. This was followed by dehydration through a series of steps in 10%, 25%, 50%, 70%, 90% and 100% ethanol. Samples were dried overnight and then coated with a thin layer of gold (8-10nm) in a vacuum chamber (Denton Vacuum, Desk II, USA) for 120sec, set at

50 millitorr and 15 mA. Analysis was done with a LEO 1530 Gemini (Zeiss, USA) set at 10kV in secondary electron mode (SE2). No specific marking was used to distinguish between the inner and outer stent wall, as it relates to the loop curvature.

### 7.2.9 Statistical analysis

Statistical analysis was done with the IBM SPSS Statistics version 20. Data were analyzed using analysis of variance (2-way ANOVA). For post-hoc analysis, Least Significant Difference method was used to determine significant difference between groups. No specific analysis was performed to account for donor variability. Overall effects are not reported due to the complexity of the data; in some cases there are fewer than three groups, e.g. volume and stent samples. All data are presented as mean  $\pm$  standard deviation of a minimum of 3 separate experiments. For all analysis,  $p < 0.05$  was used to indicate significant difference.

## 7.3 Results

### 7.3.1 Lumen characterization

Model stent struts introduce roughness inside the tube lumen as previously described by the friction factor in Chapter 2. As a result, there were two levels of roughness – the macro level roughness due to the stent struts and the stent surface nano/micro level roughness. Hence, part of the lumen is characterized by a roughness with a length scale of  $127 \mu\text{m}$ , which is the thickness of the stent strut. An illustration of the lumen roughness is depicted on Figure 7-2. The effective strut size to lumen diameter is  $\epsilon/D = 2.7\%$ . The length scale of stent surface roughness ( $\epsilon'$ ) is characterized in section 7.3.2.

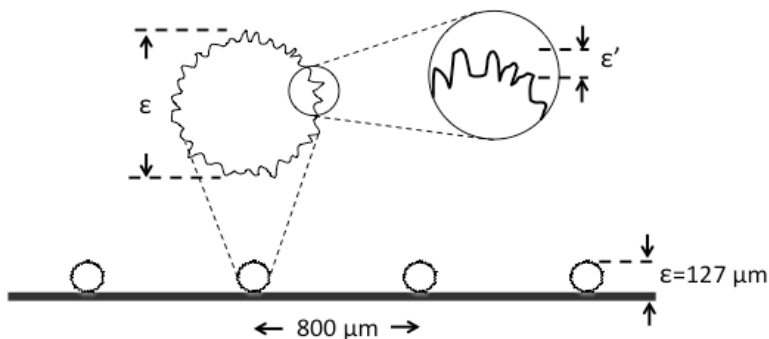
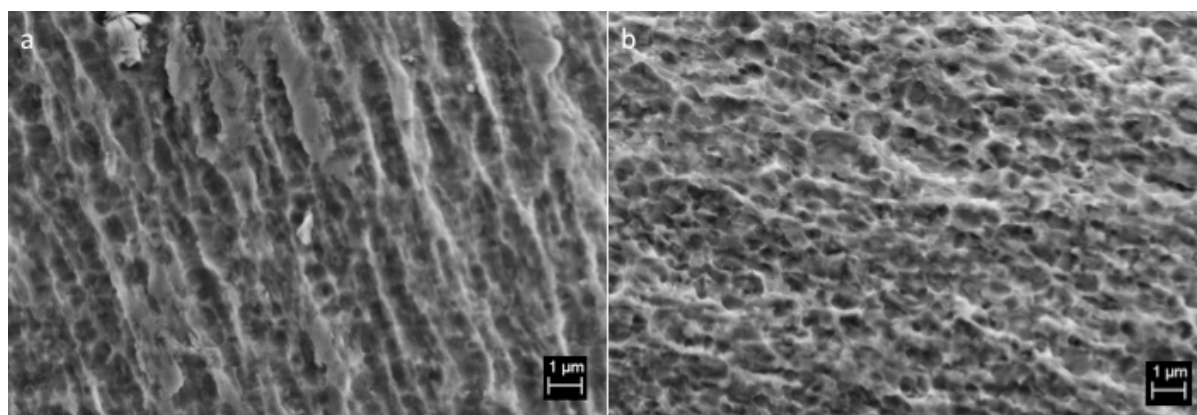


Figure 7-2. Schematic illustration of lumen and stent surface roughness (not drawn to scale)

### 7.3.2 Model stent characterization

Model stent surface characterization by scanning electron microscopy (SEM) is depicted in Figure 7-3. The unetched surface (Figure 7-3(a)) had somewhat heterogeneous multi-scale roughness with a general pattern of rugged grooves with sharp cliffs, predominately aligned along the length of the wire. The grooves varied in length, depth and width (average approximately 1  $\mu\text{m}$  wide). In addition, the spacing between the grooves was found to be random; from approximately 0.1  $\mu\text{m}$  to 2  $\mu\text{m}$ . There were also some round grooves or pits. While the acid-etched surface (Figure 7-3(b)) also showed multi-scale roughness, it had a different morphology from the unetched surface. The acid-etched surface had a high degree of sharp-edged and irregular cavities or pits, which varied in size from sub-micron to 1  $\mu\text{m}$ . The average diameter of the deep pits was approximately 0.5  $\mu\text{m}$ . Although the acid-etched surface was relatively rugged, it was generally uniform compared to the unetched surface. Visual observation of both surfaces suggests that the maximum depth of roughness grooves occurred on unetched stent, Figure 7-3(a). Since both the unetched and acid-etched stents were heat treated under the same oven conditions, it can be safely assumed that the titanium oxide layers would be similar in chemistry; in particular the rutile  $\text{TiO}_2$ . Hence, surface roughness and the related surface energy would be the key differentiating factor between the two types of stent surfaces. In addition, visual inspection suggests that the number of valleys or pits is higher on the acid-etched surfaces compared to the unetched surface.



**Figure 7-3. SEM micrograph comparison of unetched and acid-etched stent surfaces.** (a) Unetched surface, shows random rugged grooves along wire length, mag 15KX and (b) 10 sec acid-

etched wire surface, shows more uniform random pattern roughness varying up to 1  $\mu\text{m}$  wide, mag 15KX.

Model stents were also characterized by atomic force microscopy to determine surface profile and quantitative roughness values under dry conditions, Figure 7-4. The scan area was  $10 \times 10 \mu\text{m}^2$  at a scan rate of 1 Hz, in tapping mode. The difference in AFM surface profile between unetched surface (Figure 7-4(a)) and acid-etched surface (Figure 7-4(b)) was observed to be similar to topographic difference observed with SEM, Figure 7-3. As observed in SEM topography analysis, the unetched surface (Figure 7-4(a)) showed a higher peak to valley depth than the acid-etched surface, (Figure 7-4(b)).

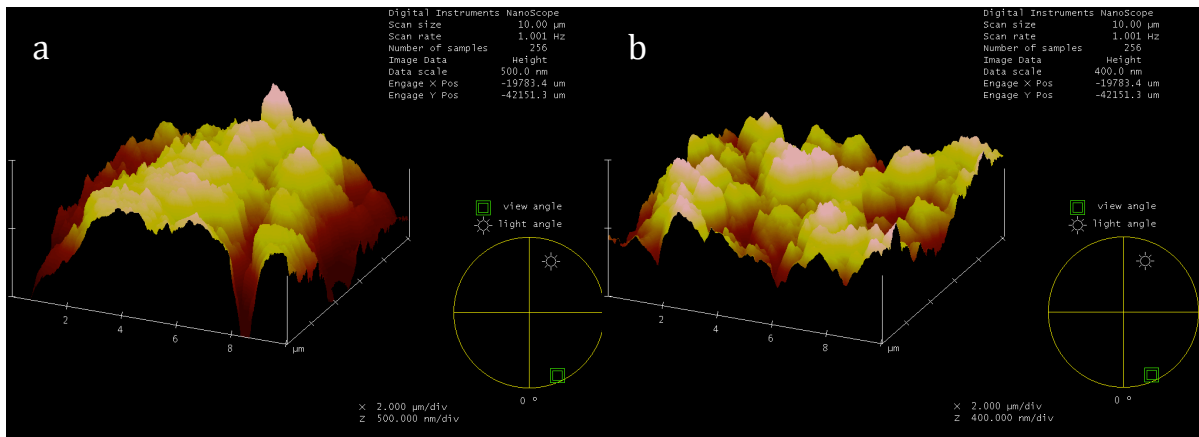


**Figure 7-4. Atomic force micrograph of model stent surface topography and roughness. (a) Unetched surface. Horizontal axis at 2  $\mu\text{m}/\text{div}$  and vertical axis at 500 nm/div. (b) Acid-etched surface. Horizontal axis at 2  $\mu\text{m}/\text{div}$  and vertical axis at 400 nm/div.**

Quantitative surface roughness measurement values were obtained from AFM, Table 7-1. There was a non-significant increase ( $p=0.2$ ) in average roughness of the acid-etched surface compared to the unetched surface. This is partly because the unetched stent was not really smooth. In some cases, acid-etching may also reduce the surface roughness, depending on the initial processing of the material [489]. The roughness length scales of both samples can be considered to be in the upper range of the nanoscopic length scale range (1-100 nm) or at the lower range of what is sometimes referred to as the subcellular length scale ( $<10 \mu\text{m}$ ) [490]. Comparison of the surface areas

also suggests that the surface areas were similar. Thus, the main difference seems to be the surface topography, which would influence contact angle and surface energy.

Similar to what was observed with SEM, for the same AFM scan area, the number of surface peaks and valleys is higher on acid-etched stents, which may have implications in blood activation. In addition, there were deeper valleys in the unetched surface and hence a wider z-range, Table 7-2. Table 7-2 also includes a new defined ratio parameter, which may be important under flow conditions. The new parameter  $\varepsilon'/\varepsilon$  has a wider range, 0.4% to 1% ( $4.4 \times 10^{-3}$  to  $10.2 \times 10^{-3}$ ), for the unetched surface and a narrow range, 0.7% to 0.9% ( $7.3 \times 10^{-3}$  to  $9.0 \times 10^{-3}$ ), for the acid-etched surface.

**Table 7-1. Surface roughness measurements**

Surface	Parameter	Sample			Average $\pm$ SD
		1	2	3	
Unetched	Ra (nm)	137.6	103.1	98.4	113.0 $\pm$ 21.4
	RMS (nm)	187.1	128.6	128.32	148.0 $\pm$ 33.9
	Surface area (nm <sup>2</sup> )	115.0	116.1	111.0	114.0 $\pm$ 2.7
	Projected surface area	100.0	100.0	100.0	100
	Surface area difference (%)	15.0	16.1	11.0	14.0 $\pm$ 2.7
Acid-etched	Ra (nm)	144.8	121.1	204.1	156.7 $\pm$ 42.7
	RMS (nm)	178.6	149.9	251.0	193.2 $\pm$ 52.1
	Surface area (nm <sup>2</sup> )	115.1	113.4	123.4	117.3 $\pm$ 5.4
	Projected surface area	100.0	100.0	100.0	100
	Surface area difference (%)	15.1	13.4	23.4	17.3 $\pm$ 5.4

**Table 7-2. The Z range and roughness ratio**

	Z range (nm)	$\varepsilon/D$ %	$\varepsilon'/\varepsilon$ (range) %
Unetched	927 $\pm$ 368	2.7	0.7 (0.4-1.0)%
Acid-etched	896 $\pm$ 90	2.5	0.8 (0.7-0.9)%

$\varepsilon=127 \mu\text{m}$  (unetched),  $\varepsilon \approx 120 \mu\text{m}$  (acid-etched)

Contact angle analysis was conducted on both samples using the dynamic contact angle analyzer as previously described. Six immersion and emersion cycles were carried out continuously at a velocity of 10 mm/min, giving six successive time-dependent hysteresis loops. Therefore, Six advancing and receding contact angle measurements were determined from each loop and the averages were calculated, Table 7-3. The acid-etched surface had slightly higher variation than the unetched surface. Based on statistical 2-tailed *t*-test comparison of the means between unetched and acid-etched sample readings, both the surface tension and contact angle measures were significantly different ( $p < 0.03$ ).

**Table 7-3. Contact angle measurements for unetched and acid-etched samples**

	<b>Surface tension (mN/m)</b>	<b>Contact angle <math>\theta</math> (°)</b>
<b>Unetched wire</b>	21.5±1.3	65.4±1.5
<b>Acid-etched wire</b>	13.5±6.1 *	74.7±7.1 *

\*Significantly different from unetched surface ( $p < 0.03$ ). Results are mean ± SD, n=6.

### **7.3.3 Effect of surface roughness on platelet activation**

The effect of surface roughness on platelet activation as characterized by formation of platelet microparticles (PMPs) are depicted on Figure 7-5. As previously observed, shear did not have a significant effect on PMP formation in the absence of model stents. In the presence of model stents, there was a shear-dependent increase in PMP formation. Under shear conditions, both stent samples produced significant PMP formation when compared to non-stent samples. At higher shear rate, the samples with acid-etched stents produced significantly higher PMP formation compared to samples with unetched stents. In general, samples with acid-etched stents had higher PMP formation compared to samples with unetched samples.

Platelet activation was also confirmed with the expression of the integrin glycoprotein receptor GPIIb/IIIa, Table 7-4. Stent samples under shear showed a reduction in CD61 expression, which corresponded to the increase in PMP formation observed above. Increase in shear (by

increasing angular velocity from 24 to 45 RPM) also reduced CD61 expression. Acid-etched stents caused higher platelet activation compared to unetched stents.

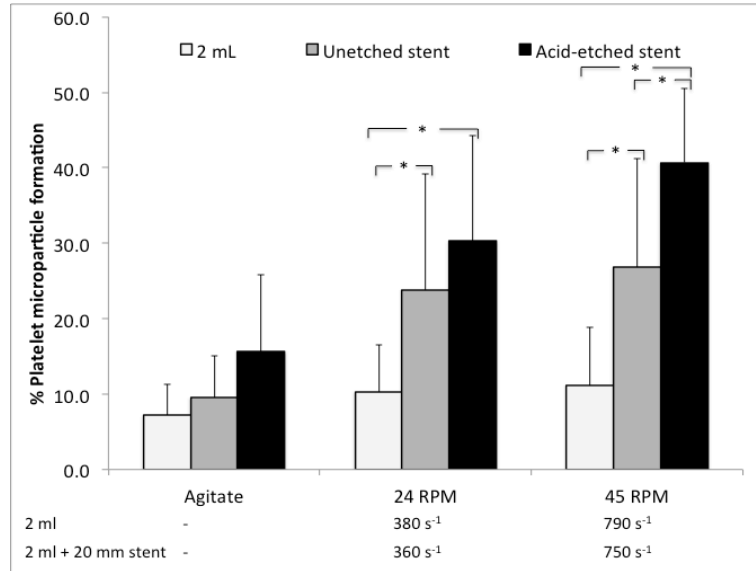


**Figure 7-5. Effect of surface roughness on PMP formation.** Percentage microparticles are based on size (forward scatter signal) and expressed relative to total events (platelet + microparticles). Negative control:  $5 \pm 2\%$ . \*:  $p < 0.01$ . Results are mean  $\pm$  SD,  $n=4$  to 6.

**Table 7-4. Effect of surface roughness on CD61 expression on platelets and PMPs**

Experimental conditions	CD61 <sup>+</sup> Platelets and PMPs			<i>p</i> -value		
	No stent sample	Unetched stent sample	Acid-etched stent sample	Unetched Vs No stent	Acid-etched Vs No stent	Unetched Vs Acid-etched
<b>Agitate</b>	214 $\pm$ 64	188 $\pm$ 75 *	195 $\pm$ 51	0.36	0.52	0.84
<b>24 RPM</b>	212 $\pm$ 58	172 $\pm$ 81 *	137 $\pm$ 60 *	0.32	0.06	0.45
<b>45 RPM</b>	179 $\pm$ 69 *	129 $\pm$ 52 *	117 $\pm$ 59 *	0.15	0.12	0.78

Negative control:  $245 \pm 67$ . CD61 expression is reported as arbitrary fluorescent units. Shear rate: 2 ml at 24 and 45 RPM is  $380 \text{ s}^{-1}$  and  $790 \text{ s}^{-1}$ , respectively; 2 ml + 20 mm stent at 24 and 45 RPM is  $360 \text{ s}^{-1}$  and  $750 \text{ s}^{-1}$ , respectively. \*Significantly different from negative control ( $p < 0.05$ ). Results are mean  $\pm$  SD,  $n=4$  to 6.

#### **7.3.4 Effect of surface roughness on leukocyte activation**

The effect of surface roughness on leukocyte activation, as characterized by TF, Mac-1 and C3aR express, was also investigated, Table 7-5. The presence of both unetched and acid-etched stents increased percentage of monocytes expressing TF, which was significant at 45 RPM ( $p < 0.03$ ). Although no significant difference in TF expression between samples with unetched and acid-etched stents was observed, no conclusions can be drawn because  $n=2$  for the acid-etched samples at 24 RPM. For Mac-1 expression, samples with acid-etched stents had slightly higher Mac-1 expression on monocytes compared to samples with unetched stents. The effect of roughness on PMNs was less discernible for samples under shear. A slight shear-dependent down-regulation of Mac-1 expression on leukocytes was observed for both stent samples. With regards to C3aR expression, similar to TF expression, no conclusions can be drawn on the effect of surface roughness because  $n=2$  for the acid-etched samples at 24 RPM. However, the effect of shear-dependent down-regulation of C3aR expression was observed for unetched stents. In general, the results suggest slightly higher leukocyte activation on samples with acid-etched stents.

**Table 7-5. Effect of surface roughness on leukocyte activation**

<b>Marker</b> (Negative control)	$\omega$	<b>No stent sample</b>	<b>Unetched stent sample</b>	<b>Acid-etched stent sample</b>
<b>% Monocytes expressing TF</b> (9±3)	<b>Agitate</b>	15±8	18±10	19±16
	<b>24 RPM</b>	26±13	46±12 *	36±18
	<b>45 RPM</b>	20±10	37±21 #	43±11 #
<b>Mac-1 expression on monocytes (%)</b> (29±14)	<b>Agitate</b>	37±12	48±10	55±15
	<b>24 RPM</b>	54±11	61±6	64±14
	<b>45 RPM</b>	42±16	55±13	61±16
<b>Mac-1 expression on PMNs (%)</b> (21±10)	<b>Agitate</b>	21±10	33±8	40±17
	<b>24 RPM</b>	24±8	38±13	38±15
	<b>45 RPM</b>	27±17	35±22	32±20
<b>C3aR expression on monocytes (%)</b> (108±15)	<b>Agitate</b>	116±21	139±22	112±20
	<b>24 RPM</b>	106±9	125±16	99±2
	<b>45 RPM</b>	95±18	106±30	115±31
<b>C3aR expression on PMNs (%)</b> (132±28)	<b>Agitate</b>	131±26	143±16	108±19
	<b>24 RPM</b>	113±27	125±19	78±15
	<b>45 RPM</b>	103±20	100±22	104±10

Shear rate: 2 ml at 24 and 45 RPM is  $380 \text{ s}^{-1}$  and  $790 \text{ s}^{-1}$ , respectively; 2 ml + 20 mm stent at 24 and 45 RPM is  $360 \text{ s}^{-1}$  and  $750 \text{ s}^{-1}$ , respectively. \*Significantly different from same shear non-stent sample ( $p < 0.05$ ), #Significantly different from same shear non-stent sample ( $p < 0.03$ ). Results are mean ± SD, n=4 to 6 (Mac-1), n=2 to 4 (TF), n=2 to 5 (C3aR), n=2 for acid-etched at 24 RPM.

### **7.3.5 Effect of surface roughness on platelet-leukocyte aggregation**

The presence of both acid-etched and unetched stent samples caused a significant increase in fluid phase platelet-monocyte aggregation ( $p < 0.001$ ), Figure 7-6. When samples with acid-etched stents were compared to samples with unetched stents, an increase in platelet-monocyte aggregation was observed, which was significant at a shear rate of  $750 \text{ s}^{-1}$  ( $p < 0.001$ ). When shear was increased, there was a significant reduction ( $p = 0.03$ ) in platelet-monocyte aggregation for non-stent and

unetched stent samples. On the other hand, the samples with acid-etched stents had an opposite effect; a slight increase in platelet-monocyte aggregation.

Similar to platelet-monocyte aggregation, the presence of both types of model stents resulted in a significant increase in platelet-PMN aggregation under shear ( $p < 0.001$ ), Figure 7-7. The presence acid-etched stents caused higher platelet-PMN aggregation compared to unetched stents, which was significant at higher shear rate ( $p < 0.001$ ). Increasing shear resulted in reduced platelet-PMN aggregation, which was significant for non-stent and unetched stent samples ( $p < 0.05$ ). In general, acid-etched stents caused higher platelet-leukocyte aggregation compared to unetched stents.

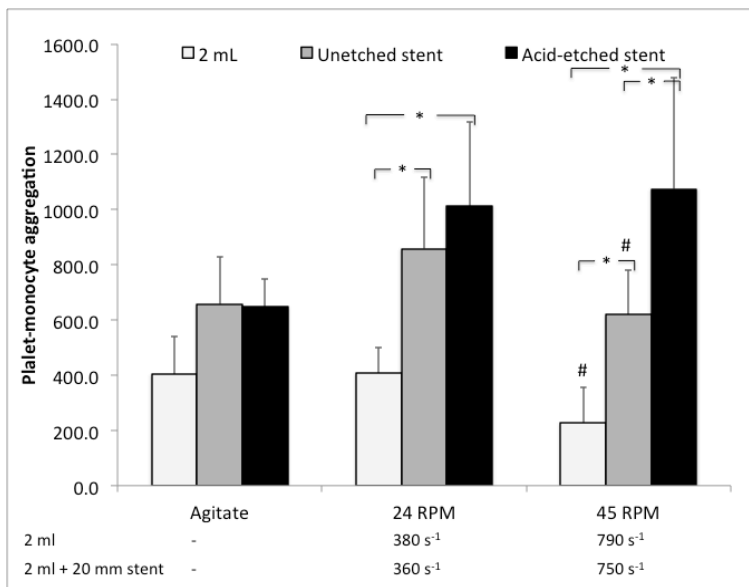


**Figure 7-6. Effect of surface roughness on platelet-monocyte aggregation.** Platelet-monocyte aggregation is reported as arbitrary fluorescent units. Negative control:  $185 \pm 99$ . \*:  $p < 0.001$ , #significantly different from corresponding sample at 24 RPM ( $p = 0.03$ ). Results are mean  $\pm$  SD,  $n = 4$  to 6.

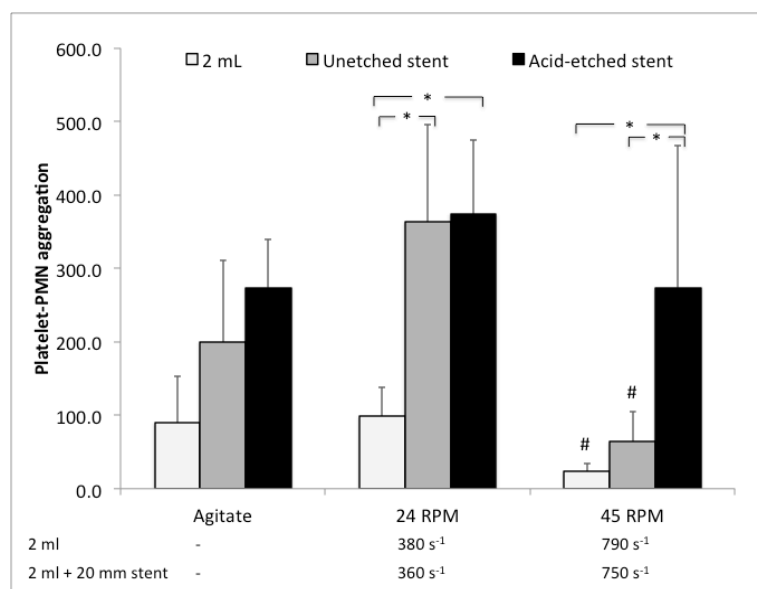


**Figure 7-7. Effect of surface roughness on platelet-PMN aggregation.** Platelet-PMN aggregation is reported as arbitrary fluorescent units. Negative control:  $45 \pm 32$ . \*:  $p < 0.001$ , # significantly different from corresponding sample at 24 RPM ( $p < 0.05$ ). Results are mean  $\pm$  SD,  $n = 4$  to 6.

### 7.3.6 Effect of surface roughness on FUT-175 efficacy

To investigate the effect of model stent roughness on the efficacy of FUT-175, experiments were carried out with 2 ml + 20 mm stent sample at an angular velocity of 24 RPM, representing a nominal time-averaged wall shear rate of  $360 \text{ s}^{-1}$ .

The results of the impact of surface roughness on the effectiveness of FUT-175 to inhibit platelet activation are presented in Table 7-6. Comparison of PMP formation results between unetched and acid-etched stent samples did not show any significant difference, suggesting minimal influence from surface roughness. Similarly, CD61 and P-selectin expression did not show any significant difference when results from unetched stent samples were compared to acid-etched stent samples. Thus, the results suggest that for the conditions of this study, surface roughness did not influence the efficacy of the complement inhibitor to reduce platelet activation.

**Table 7-6. Effect of surface roughness on FUT-175 efficacy to reduce platelet activation**

<b>Marker</b> (Negative control)	<b><math>\omega</math></b>	<b>FUT-175</b> <b>+</b> <b>Non-stent</b> <b>sample</b>	<b>FUT-175</b> <b>+</b> <b>Unetched</b> <b>stent sample</b>	<b>FUT-175</b> <b>+</b> <b>Acid-etched</b> <b>stent sample</b>
<b>% PMP formation</b> (5±1)	<b>Agitate</b>	4±1	5±1	5±2
	<b>24 RPM</b>	6±3	7±5	7±3
<b>CD61<sup>+</sup> expression on platelets +</b> <b>PMPs (233±68)</b>	<b>Agitate</b>	227±47	210±48	225±51
	<b>24 RPM</b>	218±49	194±22	215±60
<b>P-sel expression</b> (14±3)	<b>Agitate</b>	16±3	17±5	18±1
	<b>24 RPM</b>	17±2	17±1	18±1

CD61 and P-sel expressions are reported as arbitrary fluorescent units. Shear rate: 2 ml at 24 RPM is 380 s<sup>-1</sup>; 2 ml + 20 mm stent at 24 RPM is 360 s<sup>-1</sup>. Results are mean ± SD, n=2-3, n=2 for P-sel.

The influence of roughness on the efficacy complement inhibition was also investigated on leukocytes. No conclusions could be drawn from TF expression due to the limited number of samples. For Mac-1, under mild agitation, the presence of both stent samples resulted in a significant increase (p<0.02) in Mac-1 expression on leukocytes, when compared to non-stent samples, Table 7-7. This suggests that, in the presence of model stents, complement inhibition was not effective in reducing Mac-1 expression on leukocytes under agitation. However, there was no significant difference in Mac-1 expression between unetched and acid-etched stent samples under all experimental conditions, suggesting minimal impact of roughness on the effectiveness of FUT-175. Similar to Mac-1 expression, no significant difference in C3aR and TLR-4 expression on leukocytes was observed when unetched stent samples were compared to acid-etched stent samples. No significant difference was observed on platelet-leukocyte aggregation either when stent samples were compared. The results suggest that for the conditions in this study, surface roughness did not significantly influence the efficacy of complement inhibitor FUT-175.

**Table 7-7. Effect of surface roughness on FUT-175 efficacy to reduce leukocyte activation**

<b>Marker</b> (Negative control)	<b>ω</b>	<b>FUT-175</b> <b>+</b> <b>Non-stent</b> <b>sample</b>	<b>FUT-175</b> <b>+</b> <b>Unetched</b> <b>stent sample</b>	<b>FUT-175</b> <b>+</b> <b>Acid-etched</b> <b>stent sample</b>
% Monocytes expressing TF (8±5)	<b>Agitate</b>	8±3	21	7
	<b>24 RPM</b>	9±3	14	13
% Mac-1 expression on monocytes (12±8)	<b>Agitate</b>	18±6	40±6 *	32±13 *
	<b>24 RPM</b>	24±6	25±10	23±8
% Mac-1 expression on PMNs (8±6)	<b>Agitate</b>	9±4	25±7 #	26±4 #
	<b>24 RPM</b>	11±5	9±4	14±6
% C3aR expression on monocytes (114±29)	<b>Agitate</b>	135±16	132±30	114±10
	<b>24 RPM</b>	121±22	125±16	108±10
% C3aR expression on PMNs (153±54)	<b>Agitate</b>	151±57	151±52	122±12
	<b>24 RPM</b>	146±51	163±70	130±20
% TLR-4 expression on monocytes (93±20)	<b>Agitate</b>	112±22	128±22	112±28
	<b>24 RPM</b>	116±17	114±41	115±23
% TLR-4 expression on PMNs (82±12)	<b>Agitate</b>	89±9	105±17	89±12
	<b>24 RPM</b>	92±11	90±22	90±11
<b>Platelet-monocyte aggregation</b> (109±76)	<b>Agitate</b>	277±104	505±153	391±78
	<b>24 RPM</b>	520±265	479±405	618±460
<b>Platelet-PMN aggregation</b> (27±24)	<b>Agitate</b>	23±10	100±69	53±11
	<b>24 RPM</b>	65±56	102±149	123±101

Platelet-leukocyte aggregation is reported as arbitrary fluorescent units. Shear rate: 2 ml at 24 RPM is  $380 \text{ s}^{-1}$ ; 2 ml + 20 mm stent at 24 RPM is  $360 \text{ s}^{-1}$ . \*Significantly different from corresponding non-stent sample ( $p < 0.02$ ), #Significantly different from corresponding non-stent sample ( $p < 0.001$ ). Results are mean ± SD, n=2-3, n=2 for TLR-4 acid-etched samples and n=1-2 (TF).

### 7.3.7 Surface adhesion

The effect of roughness on cell adhesion was observed on acid-etched stents, Figure 7-8. A thick mesh covering the whole stent was observed on the agitated acid-etched stent sample, Figure 7-8(a). The acid-etched stent sample under shear showed reduced surface adhesion, but the fiber mesh seemed dense and adherent platelets were visible, Figure 7-8(b). Adherent leukocytes were not visible. There was increased adhesion compared to adhesion on unetched stent samples as previously presented on Chapter 5.

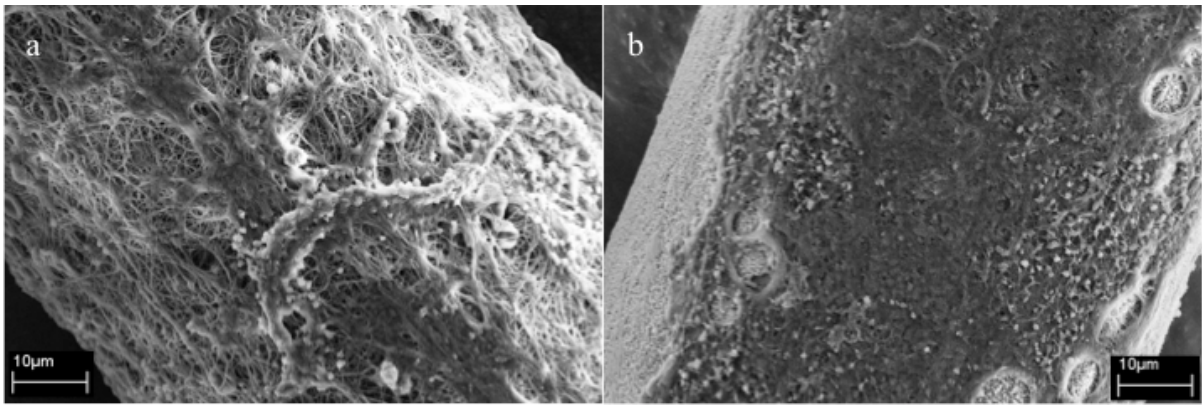


**Figure 7-8. SEM of cell adhesion pattern on acid-etched samples.** (a) Agitated sample at 1.0 KX and (b) 45 RPM ( $750 \text{ s}^{-1}$ ) sample at 1.0 KX. Acid-etching increased surface adhesion

Figure 7-9 depicts typical scanning electron microscopy images of cell adhesion on acid-etched stent samples with complement inhibitor, FUT-175. While adherent leukocytes can be observed on the agitated sample (Figure 7-9(a)), there are no visible leukocytes on samples at shear rate of  $360 \text{ s}^{-1}$  (Figure 7-9(b)). However, adherent platelets can be observed on the sample at shear, as indicated by the magnified SEM, Figure 7-9(c). Thus, leukocyte adhesion is abolished but some platelet adhesion is retained.

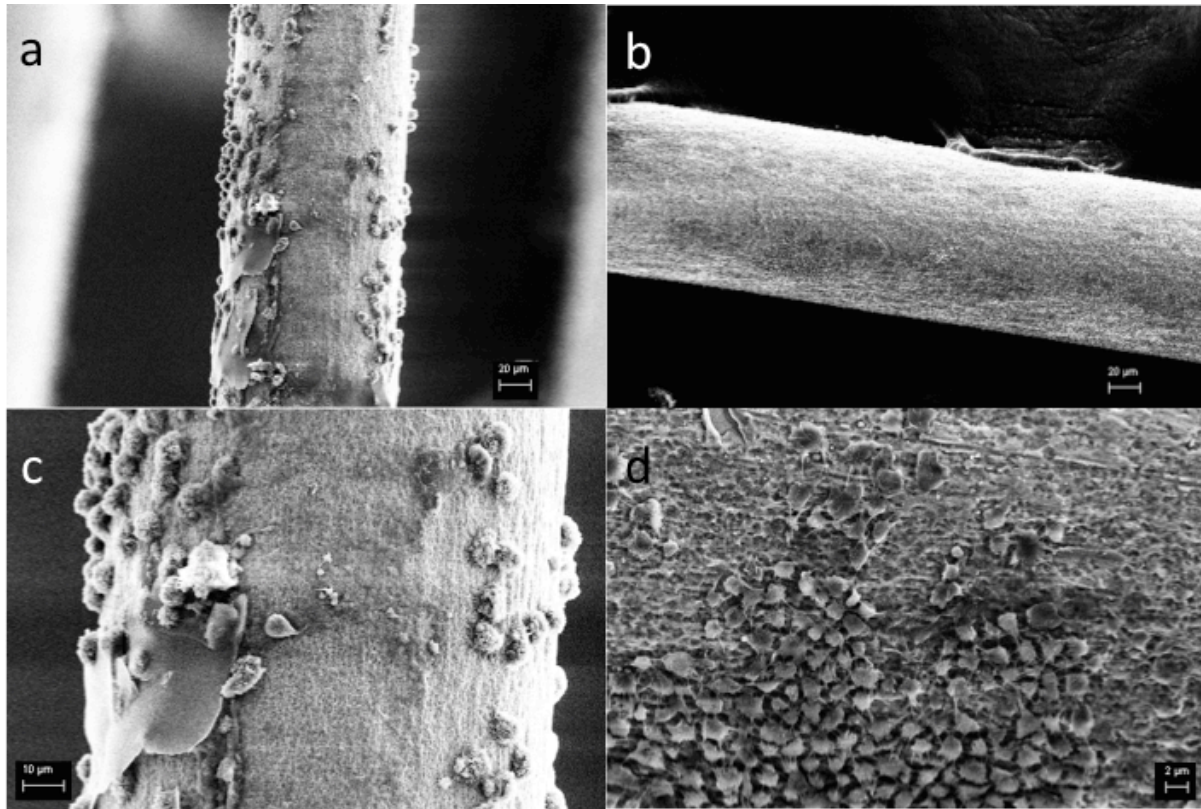


**Figure 7-9. SEM of cell adhesion pattern on acid-etched sample, with inhibitor.** (a) Agitated sample at 1.0 KX, (b) 24 RPM ( $360 \text{ s}^{-1}$ ) sample at 1.0 KX, (c) agitated sample (same as (a)) at 2.58 KX, (d) 24 RPM sample (same as (b)) at 6.96 KX. FUT-175 abolished leukocyte adhesion.

## 7.4 Discussion

Biomaterial surface roughness is known to induce a variety of cell responses [491] and hence can be exploited for bone integration and anchoring [492]. In stent technology, surface patterning can be used for drug delivery on polymer covered or metallic stents [493]. However, once the drug is exhausted, the bare metal surface may still cause roughness-induced thrombosis because evidence suggests surface roughness enhances blood activation and cell adhesion [483, 494]. While this is known, there is still no defined roughness for specific blood-biomaterial applications. Furthermore, it is not clear if material surface topography has an effect on the efficacy of one of the complement inhibitors, FUT-175.

In this chapter, the effect of material surface (model stent) roughness was investigated to elucidate some of the important factors to consider under flow conditions. For this study, two levels of roughness were considered – the macro-level introduced by the stent struts and the micro-level introduced by acid etching of the stent struts. The macro-level lumen roughness has been shown to influence time-averaged wall shear stress [29], [495] as well as platelet deposition [496], and hence activation. For this investigation, the macro-level roughness was held constant while the micro-level, model stent surface roughness, was changed. Acid etching was considered appropriate due to the multiscale nature of the roughness, which is suitable since biomolecules come in different sizes and shapes.

#### **7.4.1 Surface roughness**

The surface morphology of the acid-etched model stent was generally multiscale roughness with sharp-edged pits, which was comparable to other acid-etched titanium surfaces [393, 497]. The averaged roughness was found to be similar to the unetched stent although the morphology was different. These differences were only qualitatively observed from SEM and AFM micrographs. Due to time constraints, no quantitative 3D analysis was performed. It is important to note that the difference in morphology would also be reflected in the surface energy and contact angle, which is further confirmed by some of the differences observed in our surface energy and contact angle results. It has been previously shown that in some cases, acid-etching may also reduce the surface roughness, depending on the initial processing of the material [489]. The roughness length scale for both samples was in the nanoscopic (1-100 nm) to the subcellular (<10  $\mu\text{m}$ ) length scale, which falls in the range of cell receptors and other proteins [490]. One parameter that was defined in this investigation was the ratio of the surface stent strut roughness to the macroscopic roughness. There is no benchmark for this ratio that was found but it is possible that this may impact the thickness of the wetting film during the circulation gas phase. This emanates from the fact that the circulation loop is partly filled with blood, and hence there is a liquid and a gas phase in the loop. This parameter may introduce the boundary layer problem, which is not discussed in this thesis. However, this parameter may need to be incorporated into the broad activation and aggregation function discussed in Chapter 5. Further studies are necessary to elucidate the implications of the strut surface roughness on the surface flow dynamics.

Contact angle measurements for both unetched and acid-etched wires could be characterized as hydrophobic based on the previously suggested approximate cutoff for hydrophobicity/

hydrophilicity of  $65^\circ$  [394]. Also based on the adhesion tension map [394], it is noted that both samples fall in the region where both dispersive and polar components of the surface energy play an important role, which has implications for blood activation. It has previously been shown that titanium oxide wettability is greatly influenced by treatment and storage conditions [305, 497]. The reduction of expected metallic hydrophilicity is not only due to the formation of the  $\text{TiO}_2$  but also the atmospheric hydrocarbons [395, 497]. As a result the contact angle on a titanium surface increases when stored in air [497]. This effect could partly explain the observed hydrophobic tendency of the samples used in this study.

#### **7.4.2 Platelet activation**

Acid-etched stents used in this study caused an increase in platelet activation when compared to unetched stents, which was significant at high shear rate. Material-induced platelet activation is mediated by a number of material-dependent mechanisms, which include the density of surface bound fibrinogen [498], complement activation fragment C5b-9 [417],  $\text{Ca}^{2+}$  bound to the negatively charged  $\text{TiO}_2$  [461] and thrombin from the coagulation system [417]. Fibrinogen, which can adsorb on a variety of metallic surfaces [220, 499, 500], activates platelets by binding to the integrin glycoprotein receptor GPIIb/IIIa. Fibrinogen surface adsorption is influenced by surface chemistry [501] as well as surface energy and roughness [499, 502]. Although fibrinogen adsorption was not investigated in this study, some surface adsorption would be expected on weakly hydrophobic surfaces, like the ones used in this study. It is a key protein in platelet activation and adhesion and hence any roughness-mediated surface adsorption that may occur, as in the above quoted studies, would partly explain the observed increase in platelet activation in this study. Characterization of fibrinogen adsorption would be necessary to elucidate the relationship with platelet activation and adhesion.

Protein interaction with material surfaces is also influenced by electrolytes [503]. The influence of electrolytes on protein-material interaction is an important phenomena because blood contains electrolytes, which would not only interact with the material surface, but would also influence cell activation and function, such as  $\text{Ca}^{2+}$ -dependent platelet activation in the presence of biomaterials [217] and phospholipid expression on platelets [504]. The impact of material-mediated electrolyte platelet activation has also been previously demonstrated by the activation of platelet from  $\text{Ca}^{2+}$  bound to  $\text{TiO}_2$  surface [461]. The implications of the acid-etched surface on the presence of hydrated cations, which influences the material surface charge and subsequently fibrinogen adsorption, is not clear. Although this was not investigated in this study, it may contribute to the

observed platelet activation. Therefore, further studies are necessary to elucidate the effect of roughness on electrolyte surface retention and subsequent influence on fibrinogen adsorption and its implications for roughness-induced thrombogenicity.

Material-induced complement fragments also activate platelets [82]. The classical pathway complement C1q, which binds to material adsorbed immunoglobulins like IgG [25, 85], enhances platelet activation by binding to the global C1q receptor (gC1qR) on activated platelets [449] or through binding to chondroitin sulfate A secreted from activated platelet  $\alpha$ -granules [469]. Complement C5b-9, which is also dependent on surface characteristics [349, 417, 494, 505], induces platelet  $\alpha$ -granule secretions and PMP formation [196]. Besides complement, another mechanism that may contribute to platelet activation is the roughness-induced contact system activation [417, 494]. Contact system activation would induce thrombin formation and subsequent platelet activation. Thus, a variety of roughness-mediated mechanisms may contribute to the increased platelet activation as observed in this study. Under shear, which has been shown to activate platelets in the presence of model stents (Chapters 5 and 6), the effect of these mechanisms may be amplified through feedback, resulting in significant platelet activation as observed at high shear.

In addition to surface adsorbed protein-mediated platelet activation, isolated platelet adhesion and activation in direct contact with material have been shown to be dependent on the type as well as the pattern of TiO<sub>2</sub> topography [506]. Thus, the results of isolated platelets and whole blood flow models [27, 494] generally agree with our findings that acid-etched roughness, directly and indirectly, increased platelet activation. However, in whole blood and under flow conditions, the stimulus and response are much more complex as discussed above and hence, the cause and effect cannot be easily deduced. Therefore, further studies, which incorporate the issues raised above, such as fibrinogen adsorption, electrolyte surface retention, complement and contact system activation, are necessary to elucidate the impact of patterned surfaces on platelet activation. In particular, it is necessary to elucidate the conditions that may emphasize one system or synergistically amplify all systems.

### **7.4.3 Leukocyte activation**

Unetched and acid-etched stents samples caused similar leukocyte activation, although Mac-1 expression on monocytes seemed to be slightly higher in samples with acid-etched stents. Some of the material-dependent mechanisms that mediate leukocyte activation are linked to platelet activation [182]. These include surface bound fibrinogen [507] and complement activation [22]. Nanoparticle size and roughness-dependent fibrinogen conformational change exposes the C-terminus of the  $\gamma$ -

chain, which binds and activates leukocyte integrin receptor Mac-1 [507]. It is interesting to note that similar to fibrinogen density-dependent platelet activation [498], leukocyte Mac-1 binding to fibrinogen on nanoparticles was also found to be size and density-dependent – increasing with decreasing fibrinogen density [507]. Fibrinogen binding to Mac-1 activates the nuclear factor-kappa B (NF- $\kappa$ B) transcription factor pathway [507, 508], and thus induces inflammatory mediators [507]. Since the NF- $\kappa$ B is also one of the pathways for TF expression, this may partly explain the observed material-dependent TF expression. However, the roughness effect on TF expression was not observed.

Leukocyte activation could also occur as a result of material-induced complement activation and formation of anaphylatoxins [25, 85, 417, 494], since complement plays an important role in immune response to biomaterials [7, 22, 82, 182]. Moreover, C3 fragments can even adsorb on other plasma proteins [83]. Complement activation anaphylatoxins induce Mac-1 and TF expression on leukocytes [141, 443] and anaphylatoxin C3a has also been shown to induce internalization of C3a receptor (C3aR) on leukocytes [407]. Therefore, the observed material-induced leukocyte activation for both unetched and acid-etched stent samples may partly be mediated by complement activation. However, the effect of roughness on leukocyte activation was not obvious.

Although the results of this study generally suggest increased blood activation with roughness as found by others [27], other results have suggested the contrary [509]. Several factors may account for the seemingly contradictory results. One main factor, as already alluded to in this discussion, is the fact that roughness alone cannot be used to explain the blood activation. The slight differences in surface thermodynamics, electrostatics and chemistry play an important role. Hence, further studies with profiled surface characteristics are necessary to elucidate material surface effect on all the factors that mediate blood activation.

#### **7.4.4 Platelet-leukocyte aggregation**

Platelet-leukocyte activation was higher in samples with acid-etched stents compared to samples with unetched stents, which seemed to correspond with increased platelet and leukocyte activation. Platelet-leukocyte aggregation is facilitated by fibrinogen as it can bind with both platelet and leukocyte integrin receptors GPIIb/IIIa and Mac-1, respectively. Under shear, the platelet P-selectin and leukocyte PSGL-1 receptor interactions facilitate platelet-leukocyte aggregation. Thus, increased activation from acid-etched stents would result in increased platelet-leukocyte aggregation as observed in this study.

However, as discussed in previous sections, other biochemical entities, such as thrombin and calcium play an important role in platelet activation. More importantly thrombin and calcium have been shown to mediate platelet aggregation independent of fibrinogen and von Willebrand factor [510]. Thus, a variety of mechanisms may contribute to the observed increase in platelet-leukocyte aggregation.

#### **7.4.5 Surface adhesion**

Acid-etched stents had greater surface adhesion than unetched stents, which was previously observed [511]. The fact that the acid-etched surface was slightly more hydrophobic suggests the possibility of increased protein adsorption, such as fibrinogen and complement fragment iC3b. Fibrinogen is a ligand for both platelet and leukocyte integrin receptors GPIIb/IIIa and Mac-1, respectively. Complement iC3b is a ligand for Mac-1 receptor. Hence, adsorption of both fibrinogen and iC3b facilitates cell adhesion. Moreover, both platelets and leukocytes were activated in acid-etched stents. Under flow conditions, platelet and leukocyte aggregation and adhesion is also facilitated by interaction of platelet P-selectin with leukocyte PSGL-1 receptors. Thus, these conditions increased the likelihood of surface adhesion.

Furthermore, the results seem to agree with another whole blood loop model study comparing electropolished and unpolished stents [27]. This is supported by the finding that increased roughness resulted in increased cell resistance to shear detachment in microsphere roughness [512] and nanopores roughness [513]. This may partly explain the observed adhesion on acid-etched stents because of increased surface peaks and valleys than the unetched stents, in spite of similar average roughness values.

#### **7.4.6 Complement inhibition effect**

Since material properties influence the distribution of electrolytes at the surface, there is a possibility that some of the drugs, such as the complement inhibitor FUT-175, could interact with the surface. We are not aware of investigations into the effect of patterned titanium oxide on the efficacy of FUT-175. Hence, the effect of model stent roughness on complement inhibitor, FUT-175, was investigated in this study.

Complement inhibition in the presence of model stents reduced the level of platelet and leukocyte activation to similar values. The possible mechanisms through which FUT-175 can reduce platelet and leukocyte activation and aggregation were discussed in Chapter 6. The fact that FUT-175

reduced platelet and leukocyte activation to similar levels suggests that surface roughness did not have an effect on the efficacy of the complement inhibitor, FUT-175. Thus, the results imply that FUT-175 could have the potential to be used with nano/micro-structured surfaces, without affecting its efficacy. These results have relevance for drug eluting stents since they have patterned surfaces. More detailed studies are necessary to elucidate inhibition under different surface structures.

The presence of FUT-175 abolished leukocyte adhesion to acid-etched surfaces. This is important because leukocytes play an important role in material-induced thrombosis. However, some platelets were still adherent, although the whole surface was not covered. The results are similar to what was observed in Chapter 6. This may be possibly due to the fact that unactivated platelets can still adhere to surface adsorbed fibrinogen. The results suggest that FUT-175 has the potential to reduce material-induced thrombosis on rough surface material.

Overall, the issues raised in this study, taken together with other studies that have demonstrated the various parameters that influence the interactions at the biomaterial surface, suggest that the material-protein interaction is really material-electrolyte-water-protein-cell interactions [175], and therefore needs to be modeled appropriately. Hence, efforts made to investigate and/or control material-protein interactions need to take all the system factors into account. While efforts are made to control the specific interactions at the biomaterial surface, it is not clear if there are surface modifications that may inadvertently promote non-specific binding. Regardless of the binding mechanism, it is necessary to characterize and investigate further the key contributing factors to material-induced blood activation.

Furthermore, the limitations in the use of 2D roughness parameters should be noted. Materials with the same average roughness values and different topographies can produce very different responses [272], and therefore 2D roughness parameters, although commonly used, are not sufficient to completely characterize surface roughness [388]. They are sufficient as a proof of concept, as done in this study, but for detailed surface interaction studies, it would be necessary to perform 3D characterization.

## **7.5 Conclusion**

In this chapter, the effect of acid-etched surface roughness on platelet activation and platelet-leukocyte activation was demonstrated. For the roughness surface used in this study, leukocyte activation markers were relatively similar between the different surfaces. It is not clear if there are some parameters that are more sensitive to material surface area and roughness and some that are

more sensitive to other factors, such as surface water, electrolytes and plasma proteins, which may be influenced by subtle differences between surfaces that have similar average roughness values. Thus, although the effect of roughness was demonstrated, the precise details of how the specific surface characteristics influence the synergistic contribution of each biological system are not clear. Further studies are necessary to investigate the contributory role of the various factors.

The possible role of the parameter relating the stent strut surface nano/micro scale roughness and the macro scale lumen roughness in surface flow dynamics was also raised in this chapter. Although no defined relationship was established, this parameter may have implications for fluid-solid interface and subsequent platelet and leukocyte activation and aggregation. Detailed investigations are necessary to establish the relationship and possible role of this parameter in blood activation. There is also need for surface profiling in order to elucidate the contributions of surface thermodynamics, electrostatics and chemistry.

The results of the investigation into the impact of surface roughness on the effectiveness of FUT-175 suggest that there was little or no impact. Thus, these results disprove the hypothesis that roughness has an effect on complement inhibition. The lack of a roughness effect on complement inhibition has possible significance for micro-structured devices such as drug eluting stents as this suggests the possibility of using FUT-175 to reduce complement activation without loss of efficacy. Further investigations are however necessary, with different surface structures, such as pores versus surface roughness and at different shear rates.

## Chapter 8

### Summary of Contributions and Future Work

#### 8.1 Summary and perspectives

The approach taken in this thesis was to link fundamentals with system interactions and the broader picture and in so doing highlight the significance of a systems approach in blood-biomaterial interaction studies.

##### 8.1.1 Significance of a systems approach

In this thesis, the significance of a systems approach has been highlighted and demonstrated. More importantly, the case for a systems approach in blood-biomaterial studies has been presented, together with examples that demonstrate the importance of this approach in analyzing complex systems such as the blood-biomaterial interaction system. In addition, a framework for a systems approach was developed. This provides the basis for further development and refinement of this concept. The significance of a systems approach was demonstrated by the analysis and design of the *in vitro* flow model used in the experiments. Furthermore, by using a systems approach and examining system components, it allowed for the examination of the main functions such as activation and regulation of the inhibition control mechanism. Thus, making it possible to identify some of the missing links regarding activation control by inhibition, such as factors that influence platelet and leukocyte inhibition under different flow and material surface conditions, and other mechanisms. A lot of work has been done. It is time to put the pieces of the big puzzle together. Somewhere in the vast number of combinations lies the solution for the key to the holy grail of biocompatibility.

##### 8.1.2 A systems approach to *in vitro* model design

The systems approach proposed in this thesis was used to design the *in vitro* model parameters. From all the physiological parameters, a systematic method was followed to rationalize the selection of parameters to ensure appropriate mimicking of the physiological location of interest by the *in vitro* model. Therefore, the contribution of this work was in demonstrating the usefulness of a systems approach in model design for blood-biomaterial interaction studies.

### **8.1.3 Model stent design, fabrication and characterization**

Model stents were designed, fabricated and characterized. In designing the model stents, strut and stent geometry were considered as well as strut surface characteristics. Although basic surface characterization parameters were determined, it was noted that there is a need to consider detailed surface characterization as other surface parameters besides roughness may be equally important. There are other pertinent parameters that may be relevant. These include the stent surface area to its volume or to its surface structure/morphology. Thus, the contribution of this work is in demonstrating model stent fabrication and raising pertinent material parameters that may need closer attention.

### **8.1.4 A method for determining appropriate blood sample volume**

Although the Chandler loop model has been used by a number of investigators, there has been little discussion on the appropriateness of the sample volume, the sample volume selection method and its implications on fluid dynamics. Thus, there has been no guidance on the method for determining the appropriate sample volume for the Chandler loop model. For that reason, this study developed a method for determining the blood sample volume that takes into account the hemodynamic and biochemical requirements for the Chandler loop model. The proposed criterion is named the Chandler loop sample volume fraction (CLSVF) equation. The significance of the criterion is that it is general and therefore can be used with any defined range of the surface area-to-volume ratio.

This study has demonstrated that the sample volume influences the fluid mechanics of the Chandler loop model. This is important because fluid mechanics greatly influence thrombus formation. Hence, appropriate fluid mechanics characterization is very beneficial in investigating the effect of shear on material-induced molecular/cellular activity in initiating, dissolving or enhancing thrombus formation. Therefore, the contributions of this work are in developing a tool for determining sample volume (the CLSVF criterion) and demonstrating the effect of sample volume on the loop fluid mechanics.

### **8.1.5 Fluid mechanics of the Chandler loop model**

Although the fluid mechanics of the Chandler loop model was previously developed, the wall shear stress equation approximation did not incorporate some of the key parameters that characterize curved tube flow. In this study, fluid flow was appropriately characterized and a new time-averaged wall shear stress equation was developed. Appropriate flow characterization is important because

blood activation is influenced by the level as well as the type of flow. The significance of the developed equation is that it can be used for any stent with defined friction factor. The equation can also be used in the absence of a stent to evaluate the effect of shear on blood activation or to evaluate protein adsorption on new tube material under appropriately characterized flow conditions. Thus, the major contributions of this work are appropriate flow characterization and the development of a better approximation of the time-averaged wall shear stress equation for the Chandler loop model.

#### **8.1.6 Effect of sample volume on platelet and leukocyte activation**

The contribution of the experimental investigation was in validating the effect of blood sample volume on platelet and leukocyte activation. This fact was demonstrated by the experimental results, especially in the presence of model stents.

#### **8.1.7 Effect of complement inhibition on platelet and leukocyte activation**

The effect of futhan on blood activation was demonstrated under different experimental conditions. The contribution of this work was in demonstrating the potential for futhan to be used to reduce material-induced thrombogenicity under flow and possibly retaining the platelet hemostatic functions.

#### **8.1.8 Effect of surface roughness**

The effect of surface roughness on blood activation was demonstrated in this research. It was also demonstrated that roughness did not reduce the effectiveness of complement inhibition. The contribution of this work was in demonstrating the possible use of futhan to reduce material-induced thrombosis on devices with patterned surfaces, such as drug-eluting stents.

#### **8.1.9 Perspectives on receptor expression and function**

The importance of leukocytes in material-induced thrombosis has previously been highlighted. Platelets also seem to regard leukocytes as key partners in aggregation – they express receptors/ligands to bind leukocytes and then they enhance the Mac-1 binding affinity through ADP without increasing expression. Mac-1 expression and affinity are interesting because there has also been evidence that fMLP increases Mac-1 expression without increasing affinity – quite the opposite of ADP. To some extent, one may see the logic behind the fMLP effect, as it is a chemoattractant. The interesting thing is that this expression without function is also observed with platelet microparticle formation. The curious question that arises then is whether most agonists fall into these

two categories of either inducing expression or affinity. If that is the case then it may be time to consider classifying agonists as activators (the ones that activate function/affinity) and stimulators (stimulate expression). This is particularly important because targeting, in this case a stimulator, for therapeutic intervention may not be as effective as targeting an activator. Further studies are necessary to elucidate the validity of this classification. Even if the classification is not generalized, it is still necessary to understand if material characteristics, all or some, induce either or both expression and function. An additional point is to consider a standard to investigate both expression and function such as the SAXSA sequence.

## **8.2 Major contributions**

- (a) Proposed a pyramid and cube representation for blood-biomaterial interaction
- (b) Proposed the SAXSA sequence to understand and visualize mode of interaction
- (c) Proposed a systems approach framework for blood-biomaterial interaction studies
- (d) Developed a method to determine the appropriate blood sample volume and demonstrated the importance of selecting appropriate sample volume
- (e) Characterized fluid mechanics and developed improved time-average wall shear stress equation for the Chandler loop model
- (f) Experimentally demonstrated the effect of blood sample volume in blood-biomaterial investigations with model stents
- (g) Proposed an improved cell activation and aggregation model function that incorporates surface area-to-volume ratio as well as roughness
- (h) Demonstrated the possible use of complement inhibitor, futhan, as an effective intervention to control coagulation and material-induced thrombosis
- (i) Demonstrated that although roughness affects cell activation, it did not have an effect on futhan, which has possible applications for reducing material-induced thrombosis from patterned surfaces such as on drug-eluting stents.

## **8.3 Future work**

In this section, a brief discussion of possible future work is presented to build on this thesis, taking into consideration information from other studies.

### *A systems approach*

The development of the framework for systems design is only the beginning. There is need to build on this work and develop a framework with established parameters that can be accepted by consensus and will guide future research in blood-biomaterial interaction studies. The weighting factors for the relative importance of various physiological parameters for databases with some of the important parameters, such as the surface concentrations of ions or molecules on specific surfaces, under specific conditions, e.g.  $\text{OH}^-$ ,  $\text{Ca}^{2+}$ , fibrinogen, etc., are necessary. Some of these data may already exist but may need to be compiled.

In order to elucidate the cause and effect relationship between material surface characteristics and blood cell activation, it is necessary to clearly identify and characterize all the entities involved at the blood-biomaterial interface, as previously discussed in chapter 2. A schematic of the system interactions at the surface is provided to highlight the key players that should be investigated simultaneously, Figure 8-1.

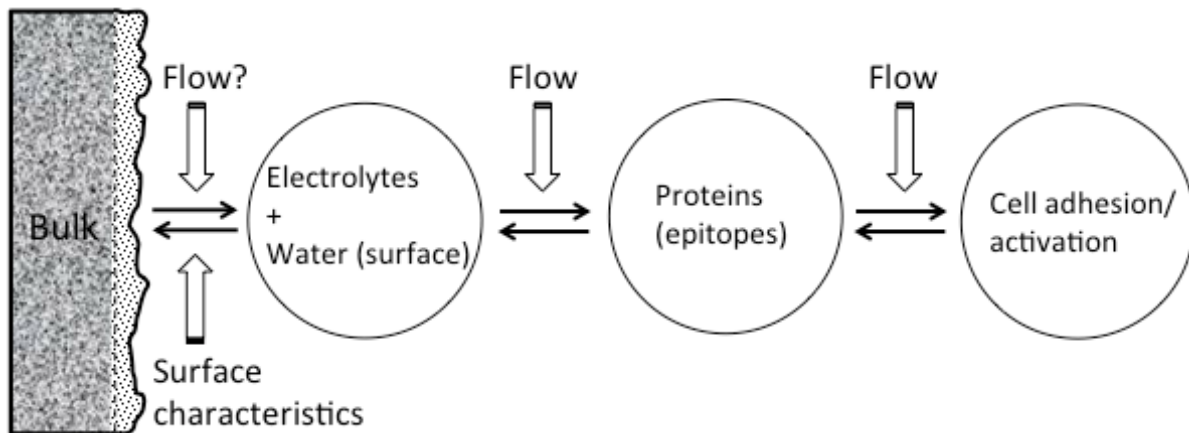


**Figure 8-1. Schematics of events at a material surface and mediating factors.** Closed arrows represent interactions and open arrows represent mediating factors. Question mark means, depending on the level of roughness, surface flow may mediate some the interactions.

### *The butterfly effect*

The idea that butterfly wings can cause a hurricane is well known in physics. This understanding is founded on chaos theory, which states that small perturbations can result in very large and divergent effects or system responses over time. With the complexity of the biological system, it is entirely possible that while we often look for statistically significant changes, some of the changes that are not significant may have subsequent large effects. It is possible that in some cases the significant differences may indicate terminal change and the seemingly insignificant changes may be hiding the true effects that cause final undesirable consequences. This idea needs to be explored in blood-biomaterial interaction studies because it has not been disproved that it is not applicable. With current computing simulation power, this needs closer attention in models that have been refined through appropriate and valid assumptions. Hence, chaos theory may hold the key to some of the unanswered questions.

#### ***In vitro model parameters***

While there will continue to be innovation and inventions in the development of new *in vitro* models, it is important to ‘standardized’ or determine the minimum design parameters necessary for models used for investigating blood-biomaterial interaction studies related to specific physiological locations of interest. Here the use of a systems approach and engineering design methods would be invaluable. If there is to be progress in standardization, it is in the interest of the biomaterials community to take the development of such guidelines as a priority. This will greatly facilitate comparison of experimental results.

#### ***In vitro model air-to-blood sample ratio***

It was shown in this thesis that there is little hemodynamic (shear) effect from the air sample in the loop. However, from a biochemical point of view, there are other factors such as the difference in oxygen partial pressure between the air and blood sample that need to be considered. The effect of this difference is not clear and therefore further investigation is warranted.

#### ***Time-averaged wall shear stress (TAWSS)***

This work has introduced the concept of time-averaged wall shear stress for the circulating loop model. While this concept is also applied *in vivo*, the time-averaged oscillatory shear index is deemed to be a better indicator for the shear effect. The question then is whether for *in vitro* models the time-averaged wall shear stress is the ultimate indicator of the shear effect or if it has some

limitations. This is because different combinations of the circulation period and shear magnitude for the same experimental model may theoretically produce similar time-averaged wall shear stress but different activation results. Therefore, there is a need to explore whether there is a better indicator based on TAWSS for *in vitro* studies using the Chandler loop model.

There is also a need to develop a platelet activation model, which incorporates surface-area-to-volume ratio. The current shear and time depend model is not sufficient to explain activation in the presence of biomaterials.

### ***Computational fluid dynamics***

It is necessary to further explore the fluid dynamics of the Chandler loop model with numerical methods, especially in the presence of stents. This will assist with investigating shear sensitivity to various model parameters.

### ***Leukocyte activation and adhesion kinetics***

The dynamics adsorption and desorption of proteins, especially complement fragments, plays a key role in building surface bound convertases and subsequent leukocyte activation and adhesion. Real-time monitoring of the different hydroxyl and amino bonds and the related complement fragments would be informative in elucidating the point at which the combinations may tip the scale to thrombus growth.

It is known that ADP from platelets enhances the affinity of Mac-1 to its ligands, e.g. FX and fibrinogen, but the kinetics of the ADP and other agents and how they relate to fibrinolytic agents in an *in vitro* model is not well understood. It is not clear if any of the agents are depleted in an *in vitro* model and at what time-point. This information would be useful in understanding and explaining observations at both short and long experimental end points.

The effect of intermittent flow on cell adhesion was not studied in detail in this research. Since there is a possibility that intermittent flow, as in this model, may increase cell adhesion due to the possibility of adhesion stabilizing during the reduced shear part of the cycle, it can be hypothesized that intermittent flow could increase cell adhesion. Therefore, it would be informative to further examine the effect of frequency in this model.

TF-FVIIa complex and FXa play much more diverse roles through PAR signaling. It is therefore important that in investigating coagulation, the effects of these proteins are not confined to extracellular roles only as the signaling effects occur concurrently with coagulation. These

investigations would be useful in understanding some of the observations, such as down-regulation of TF at high shear rates. This is in line with the idea of profiling receptors that are not normally included in coagulation investigations and yet play an important role.

The issue of material-induced Mac-1 affinity has not been addressed. There has been evidence that while receptor density is important, affinity may be a much more deciding factor. This makes sense because expression is not equivalent to activity. Expressed receptors may be incompetent in activity and may depend on the sub-population. Therefore, further work is necessary to elucidate the issue of affinity.

The effect of biomaterial on TF expression is known but the exact mechanism is not well understood. Hence, it is not possible to predict the outcome based on a set of material input parameters/characteristics. This is due to a lack of quantitative parameters that characterize the network as well as the kinetics of the multiple contributing factors. An argument for a systems approach has been presented. That will ensure that both experimental and computational simulations are carried out hand in hand to understand the mechanism of activation and signal propagation and control.

Some of the constitutively expressed receptors were investigated in this research. However, further investigations are necessary to elucidate their regulation in the presence of biomaterials.

### ***Contact system in thrombosis***

There is evidence that the contact system may be playing a bigger role in the structure, and thus the stability, of thrombi. Since biomaterial implants, depending on their surface characteristics, could bind FXII as well as fibrinogen and fibrin, it is possible that this combination could contribute to propagation of material-induced thrombosis. Therefore, further investigations are necessary to elucidate the role of the contact system in material-induced thrombosis, in light of the new information.

### ***Role of inhibitory pathways in blood-biomaterial interactions***

While it is known that inhibitory pathways work in tandem with activation pathways, a lot of effort is placed on elucidating the cell activation mechanism and not enough is done to examine the effect of materials on the various inhibitory mechanisms. It will be difficult to understand the cause and effect without accounting for the equally important regulatory mechanisms. Therefore, regulatory mechanisms need to be investigated and profiled in the presence of biomaterials.

For those measurements that are not sensitive to the current measurement methods, it is necessary to either amplify their signal to noise ratio since they may be designed to work under small concentrations but may still have information that is buried in the noise.

## Chapter 9

### Summary of Conclusions

#### **The use of a systems approach in blood-biomaterial studies is invaluable in the analysis of the response of complex biological networks to biomaterial stimulus**

Numerous blood-biomaterial interaction studies, both *in vitro* and *in vivo*, have produced enormous amounts of information and data. These complex interactions cannot be understood without the use of a complex systems methods. The case for a systems approach in blood-biomaterial interaction studies has been presented and a framework was proposed as a starting point to develop methods in this area.

#### **Geometric and hemodynamics parameters of *in vitro* models are important to mimic physiological location of interest**

The design of appropriate model parameters to mimic the physiological location of interest cannot be over emphasized. In this study, geometric parameters were selected based on the physiological location of interest. For hemodynamic parameters, flow was appropriately characterized and an improved time-averaged wall shear stress equation was proposed. This equation is considered more accurate than the original equation as it takes into account some of the curved tube flow parameters not included in the Gardener equation.

Furthermore, the results suggest that data interpretation may vary depending on whether one is looking at the results from exposing stents to 2 ml or 4 ml of blood, even with similar surface area-to-volume ratio. Therefore, the results confirm the importance of selecting appropriate model parameters to reflect a reasonable simulation of *in vivo* parameters as *in vitro* results may be misinterpreted due to experimental parameters. Simulation and further experimental studies would be necessary to elucidate the mechanism of a shear-volume-stent interaction effect on flow characteristics and blood activation, over a wider range of physiological and pathologic shear stress.

#### **Blood sample volume has multifactorial effects on *in vitro* flow model experimental results**

In blood-biomaterial interaction studies, blood sample volume is an important parameter because of its implications on hemodynamics and biochemical processes. Under flow conditions, it is necessary to have sufficient sample volume that exceeds entrance length to ensure the assumption of

fully developed flow conditions. In the presence of a biomaterial, an additional consideration is surface area-to-volume ratio, as stipulated by the ISO standard. Furthermore, sample volume determines shear exposure time. For these reasons, sample volume is a critical parameter in the shear-volume-stent-time interaction effect on blood activation. In this study, the effect of sample volume on platelet and leukocyte activation was demonstrated. The possibility of misinterpretation of results due to differences in volume, even at the same surface area-to-volume ratio, has significant implications when screening materials for blood compatibility. Overall this study supports the hypothesis that sample volume consideration is important in this model, especially in biomaterial studies.

#### **Complement inhibition could reduce leukocyte activation and adhesion.**

We have demonstrated that leukocyte adhesion on Ti-6Al-4V can be reduced without reducing platelet adhesion. The formation of an adsorbed protein layer was also not affected. The importance of these results, if extrapolated to possible *in vivo* implications, is that complement inhibition could be one mechanism to reduce leukocyte adhesion and possible localized effects of superoxide production on vascular walls.

Furthermore, it was also demonstrated that surface patterning did not reduce the effectiveness of complement inhibition with futhan. This suggests possible application with drug-eluting stents to reduce material-induced thrombosis. Further investigations are necessary to elucidate the implications of these findings.

## References

1. Black, J., *Biological performance of materials: fundamentals of biocompatibility*. 4th ed. 2006, Boca Raton: CRC Taylor & Francis. 497 p.
2. Murphy, K., Travers, P. and Walport, M., *Janeway's Immunobiology*. 7th ed. 2008, New York: Garland Science, Taylor & Francis Group.
3. Athey, T.H., *Systematic Systems Approach: An integrated method for solving systems problems*. 1982, New Jersey: Prentice-Hall, Inc. 366.
4. Ratner, B.D., Horbett, T. A., *Evaluation of blood-materials interactions*, in *Biomaterials Science: An Introduction to Materials in Medicine*, 3rd Edition, B.D. Ratner, Hoffman, A. S., Schoen, F. J., Lemons, J. E., Editor. 2013, Elsevier Inc: London. p. 617-634.
5. Gorbet, M.B., Sefton, M.V., *Biomaterial-associated thrombosis*, in *Hemostasis and Thrombosis: Basic principles and clinical practice*, R.W. Colman, Marder, V.J., Clowes, A.W., George, J.N., Goldhaber, S.Z., Editor. 2006, Lippincott Williams & Wilkins: NY.
6. Lévesque, J., Dubé, D., Fiset, M., Mantovani, D., *Materials and properties of coronary stents*. *Advanced Materials and Processes*, 2004. **162**(9): p. 45-48.
7. Gorbet, M.B., Sefton, M. V., *Biomaterial-associated thrombosis: roles of coagulation factors, complement, platelets and leukocytes*. *Biomaterials*, 2004. **25**(26): p. 5681-703.
8. Ratner, B.D., *The catastrophe revisited: blood compatibility in the 21st Century*. *Biomaterials*, 2007. **28**(34): p. 5144-7.
9. Anderson, J.M., A. Rodriguez, and D.T. Chang, *Foreign body reaction to biomaterials*. *Semin Immunol*, 2008. **20**(2): p. 86-100.
10. Gorbet, M.B., *The importance of platelets and complement in material-induced leukocyte activation in vitro*. 2001, PhD Thesis, University of Toronto. p. 239.
11. Vienken, J., *The need for a systems approach in biomaterials testing*. *Med Device Technol*, 2007. **18**(5): p. 12-4, 16-7.
12. Chatterjee, M.S., et al., *Systems biology of coagulation initiation: kinetics of thrombin generation in resting and activated human blood*. *PLoS Comput Biol*, 2010. **6**(9).
13. Panteleev, M.A., et al., *Task-oriented modular decomposition of biological networks: trigger mechanism in blood coagulation*. *Biophys J*, 2010. **98**(9): p. 1751-61.
14. Ratner, B.D., *The blood compatibility catastrophe*. *J Biomed Mater Res*, 1993. **27**(3): p. 283-7.
15. Chandler, A.B., *In vitro thrombotic coagulation of the blood; a method for producing a thrombus*. *Lab Invest*, 1958. **7**(2): p. 110-4.
16. Sakariassen, K.S., et al., *A perfusion chamber developed to investigate platelet interaction in flowing blood with human vessel wall cells, their extracellular matrix, and purified components*. *J Lab Clin Med*, 1983. **102**(4): p. 522-35.
17. Hong, J., et al., *A new in vitro model to study interaction between whole blood and biomaterials. Studies of platelet and coagulation activation and the effect of aspirin*. *Biomaterials*, 1999. **20**(7): p. 603-11.
18. Turitto, V.T. and C.L. Hall, *Mechanical factors affecting hemostasis and thrombosis*. *Thromb Res*, 1998. **92**(6 Suppl 2): p. S25-31.
19. Patel, J.D., et al., *Phospholipid polymer surfaces reduce bacteria and leukocyte adhesion under dynamic flow conditions*. *J Biomed Mater Res A*, 2005. **73**(3): p. 359-66.
20. Niinomi, M., *Metals for biomedical devices*. 2010, Oxford: Woodhead Publishing Ltd. xvii, 420 p.

21. Pandit, A., Planell, J., Navarro, M., *Titanium and Nitinol (NiTi)*, in *Biomaterials Science: An Introduction to Materials in Medicine*, 3rd Edition, B.D. Ratner, Hoffman, A. S., Schoen, F. J., Lemons, J. E., Editor. 2013, Elsevier Inc.: London. p. 120-124.
22. Ekdahl, K.N., et al., *Innate immunity activation on biomaterial surfaces: a mechanistic model and coping strategies*. *Adv Drug Deliv Rev*, 2011. **63**(12): p. 1042-50.
23. Mitchell, R.N., *Innate and adaptive immunity: the immune response to foreign materials*, in *Biomaterials Science: An Introduction to Materials in Medicine*, 3rd Edition, B.D. Ratner, Hoffman, A. S., Schoen, F. J., Lemons, J. E., Editor. 2013, Elsevier Inc: London. p. 512-533.
24. Breitenstein, A., G.G. Camici, and F.C. Tanner, *Tissue factor: beyond coagulation in the cardiovascular system*. *Clin Sci (Lond)*, 2010. **118**(3): p. 159-72.
25. Moghimi, S.M., et al., *Material properties in complement activation*. *Adv Drug Deliv Rev*, 2011. **63**(12): p. 1000-7.
26. Sinn, S., et al., *A novel in vitro model for preclinical testing of the hemocompatibility of intravascular stents according to ISO 10993-4*. *J Mater Sci Mater Med*, 2011. **22**(6): p. 1521-8.
27. Tepe, G., et al., *Thrombogenicity of various endovascular stent types: an in vitro evaluation*. *J Vasc Interv Radiol*, 2002. **13**(10): p. 1029-35.
28. Celi, A., et al., *P-selectin induces the expression of tissue factor on monocytes*. *Proc Natl Acad Sci U S A*, 1994. **91**(19): p. 8767-71.
29. Gaamangwe, T., Peterson, S. D., Gorbet, M. B., *Investigating the effect of blood sample volume in the Chandler loop model: Theoretical and experimental analysis*. *Cardiovascular Engineering and Technology*, 2014. **5**(2): p. 133-144.
30. Mendis, S., Puska, P., Norrving, B., *Global Atlas on Cardiovascular Disease Prevention and Control*. 2011, World Health Organization: Geneva. p. 164.
31. WHO. *Cardiovascular Diseases (CVDs)*. March 2013 [cited 2013 December 19]; Fact sheet No. 317]. Available from: <http://www.who.int/mediacentre/factsheets/fs317/en/index.html>.
32. Go, A.S., et al., *Heart Disease and Stroke Statistics--2014 Update: A Report From the American Heart Association*. *Circulation*, 2013.
33. Canada, P.H.A.o., *Tracking heart disease and stroke in Canada*, P.H.A.o. Canada, Editor. 2009.
34. Dibra, A., et al., *Effectiveness of drug-eluting stents in patients with bare-metal in-stent restenosis: meta-analysis of randomized trials*. *J Am Coll Cardiol*, 2007. **49**(5): p. 616-23.
35. Kastrati, A., et al., *Meta-analysis of randomized trials on drug-eluting stents vs. bare-metal stents in patients with acute myocardial infarction*. *Eur Heart J*, 2007. **28**(22): p. 2706-13.
36. Spaulding, C., et al., *Sirolimus-eluting versus uncoated stents in acute myocardial infarction*. *N Engl J Med*, 2006. **355**(11): p. 1093-104.
37. Steffel, J., et al., *Drug-eluting stents - what should be improved?* *Ann Med*, 2008. **40**(4): p. 242-52.
38. Dixon, S.R., C.L. Grines, and W.W. O'Neill, *The year in interventional cardiology*. *J Am Coll Cardiol*, 2009. **53**(22): p. 2080-97.
39. Capodanno, D., et al., *Meta-analysis of everolimus-eluting stents versus first-generation drug-eluting stents in patients with left main coronary artery undergoing percutaneous coronary intervention*. *Int J Cardiol*, 2013. **168**(2): p. 1718-9.
40. Dores, H., et al., *Stent thrombosis with second- versus first-generation drug-eluting stents in real-world percutaneous coronary intervention: analysis of 3806 consecutive procedures from a large-volume single-center prospective registry*. *J Invasive Cardiol*, 2013. **25**(7): p. 330-6.

41. Palmerini, T., et al., *Stent thrombosis with drug-eluting and bare-metal stents: evidence from a comprehensive network meta-analysis*. Lancet, 2012. **379**(9824): p. 1393-402.
42. Luscher, T.F., et al., *Drug-eluting stent and coronary thrombosis: biological mechanisms and clinical implications*. Circulation, 2007. **115**(8): p. 1051-8.
43. Joner, M., et al., *Pathology of drug-eluting stents in humans: delayed healing and late thrombotic risk*. J Am Coll Cardiol, 2006. **48**(1): p. 193-202.
44. Otsuka, F., et al., *Pathology of second-generation everolimus-eluting stents versus first-generation sirolimus- and Paclitaxel-eluting stents in humans*. Circulation, 2014. **129**(2): p. 211-23.
45. Moser, M., C.B. Olivier, and C. Bode, *Triple antithrombotic therapy in cardiac patients: more questions than answers*. Eur Heart J, 2014. **35**(4): p. 216-23.
46. Park, S.J., et al., *Duration of dual antiplatelet therapy after implantation of drug-eluting stents*. N Engl J Med, 2010. **362**(15): p. 1374-82.
47. Helmus, M.N., D.F. Gibbons, and D. Cebon, *Biocompatibility: meeting a key functional requirement of next-generation medical devices*. Toxicol Pathol, 2008. **36**(1): p. 70-80.
48. O'Brien, B. and W. Carroll, *The evolution of cardiovascular stent materials and surfaces in response to clinical drivers: a review*. Acta Biomater, 2009. **5**(4): p. 945-58.
49. Li, S. and J.J. Henry, *Nonthrombogenic approaches to cardiovascular bioengineering*. Annu Rev Biomed Eng, 2011. **13**: p. 451-75.
50. Matschegewski, C., et al., *Cell architecture-cell function dependencies on titanium arrays with regular geometry*. Biomaterials, 2010. **31**(22): p. 5729-40.
51. Herman, I.P., *Physics of the human body*. Biological and medical physics, biomedical engineering,. 2007, Berlin ; New York: Springer. xix, 857 p.
52. Katriasis, D., et al., *Wall shear stress: theoretical considerations and methods of measurement*. Prog Cardiovasc Dis, 2007. **49**(5): p. 307-29.
53. Thibodeau, G.A. and K.T. Patton, *Structure & function of the body*. 12th ed. 2004, St. Louis, Mo.: Mosby. 1 v. (various pagings).
54. Hall, J.E. and A.C. Guyton, *Guyton and Hall textbook of medical physiology*. 12th ed. 2011, Philadelphia, PA: Saunders/Elsevier. xix, 1,091 p.
55. Baskurt, O.K. and H.J. Meiselman, *Blood rheology and hemodynamics*. Semin Thromb Hemost, 2003. **29**(5): p. 435-50.
56. Patel, I.C. and J.A. Sirs, *Dispersion of solutes during blood flow through curved tubes*. Med Biol Eng Comput, 1983. **21**(2): p. 113-8.
57. Alonso, C., et al., *Transient rheological behavior of blood in low-shear tube flow: velocity profiles and effective viscosity*. Am J Physiol, 1995. **268**(1 Pt 2): p. H25-32.
58. Slack, S.M., *Properties of biological fluids*, in *Biomaterials Science: An Introduction to Materials in Medicine*, 3rd Edition, B.D. Ratner, Hoffman, A. S., Schoen, F. J., Lemons, J. E., Editor. 2013, Elsevier Inc.: London. p. 1479-1482.
59. Jena, K.C. and D.K. Hore, *Water structure at solid surfaces and its implications for biomolecule adsorption*. Phys Chem Chem Phys, 2010. **12**(43): p. 14383-404.
60. Ku, D.N., *Blood flow in arteries*. Ann Rev Fluid Mech, 1997. **29**: p. 399-434.
61. Glagov, S., et al., *Hemodynamics and atherosclerosis. Insights and perspectives gained from studies of human arteries*. Arch Pathol Lab Med, 1988. **112**(10): p. 1018-31.
62. Schettler, G., *Fluid dynamics as a localizing factor for atherosclerosis : the proceedings of a symposium held at Heidelberg, FRG, June 18-20, 1982*. 1983, Berlin ; New York: Springer-Verlag. x, 230 p.
63. Turvey, S.E. and D.H. Broide, *Innate immunity*. J Allergy Clin Immunol, 2010. **125**(2 Suppl 2): p. S24-32.

64. Parkin, J. and B. Cohen, *An overview of the immune system*. Lancet, 2001. **357**(9270): p. 1777-89.
65. Akira, S., S. Uematsu, and O. Takeuchi, *Pathogen recognition and innate immunity*. Cell, 2006. **124**(4): p. 783-801.
66. Iwasaki, A. and R. Medzhitov, *Toll-like receptor control of the adaptive immune responses*. Nat Immunol, 2004. **5**(10): p. 987-95.
67. Dale, D.C., L. Boxer, and W.C. Liles, *The phagocytes: neutrophils and monocytes*. Blood, 2008. **112**(4): p. 935-45.
68. Iwasaki, A. and R. Medzhitov, *Regulation of adaptive immunity by the innate immune system*. Science, 2010. **327**(5963): p. 291-5.
69. Ricklin, D., et al., *Complement: a key system for immune surveillance and homeostasis*. Nat Immunol, 2010. **11**(9): p. 785-97.
70. Ehrnthaller, C., et al., *New insights of an old defense system: structure, function, and clinical relevance of the complement system*. Mol Med, 2011. **17**(3-4): p. 317-29.
71. Sahu, A. and J.D. Lambris, *Structure and biology of complement protein C3, a connecting link between innate and acquired immunity*. Immunol Rev, 2001. **180**: p. 35-48.
72. Janssen, B.J., et al., *Structures of complement component C3 provide insights into the function and evolution of immunity*. Nature, 2005. **437**(7058): p. 505-11.
73. Sim, R.B., et al., *The covalent-binding reaction of complement component C3*. Biochem J, 1981. **193**(1): p. 115-27.
74. Peerschke, E.I., W. Yin, and B. Ghebrehwet, *Complement activation on platelets: implications for vascular inflammation and thrombosis*. Mol Immunol, 2010. **47**(13): p. 2170-5.
75. Oikonomopoulou, K., et al., *Interactions between coagulation and complement--their role in inflammation*. Semin Immunopathol, 2012. **34**(1): p. 151-65.
76. Oikonomopoulou, K., et al., *Induction of complement C3a receptor responses by kallikrein-related peptidase 14*. J Immunol, 2013. **191**(7): p. 3858-66.
77. Hattori, R., et al., *Complement proteins C5b-9 induce secretion of high molecular weight multimers of endothelial von Willebrand factor and translocation of granule membrane protein GMP-140 to the cell surface*. J Biol Chem, 1989. **264**(15): p. 9053-60.
78. Sims, P.J., et al., *Complement proteins C5b-9 cause release of membrane vesicles from the platelet surface that are enriched in the membrane receptor for coagulation factor Va and express prothrombinase activity*. J Biol Chem, 1988. **263**(34): p. 18205-12.
79. Sims, P.J. and T. Wiedmer, *Repolarization of the membrane potential of blood platelets after complement damage: evidence for a Ca<sup>++</sup>-dependent exocytotic elimination of C5b-9 pores*. Blood, 1986. **68**(2): p. 556-61.
80. Andrade, J.D. and V. Hlady, *Plasma protein adsorption: the big twelve*. Ann N Y Acad Sci, 1987. **516**: p. 158-72.
81. Morra, M., *Water in biomaterials surface science*. 2001, Chichester ; New York: Wiley. xiii, 393 p.
82. Nilsson, B., et al., *The role of complement in biomaterial-induced inflammation*. Mol Immunol, 2007. **44**(1-3): p. 82-94.
83. Andersson, J., et al., *Binding of C3 fragments on top of adsorbed plasma proteins during complement activation on a model biomaterial surface*. Biomaterials, 2005. **26**(13): p. 1477-85.
84. Andersson, J., et al., *C3 adsorbed to a polymer surface can form an initiating alternative pathway convertase*. J Immunol, 2002. **168**(11): p. 5786-91.

85. Ferraz, N., et al., *Nanoporesize affects complement activation*. J Biomed Mater Res A, 2008. **87**(3): p. 575-81.
86. Hallstrom, T., et al., *Nontypeable Haemophilus influenzae protein E binds vitronectin and is important for serum resistance*. J Immunol, 2009. **183**(4): p. 2593-601.
87. Klos, A., et al., *The role of the anaphylatoxins in health and disease*. Mol Immunol, 2009. **46**(14): p. 2753-66.
88. Speidl, W.S., et al., *Coronary late lumen loss of drug eluting stents is associated with increased serum levels of the complement components C3a and C5a*. Atherosclerosis, 2010. **208**(1): p. 285-9.
89. Chien, S., Schmid-Schonbein, G. W., Sung, K. -L. P., Schmalzer, E. A., *Viscoelastic Properties of Leukocytes*, in *White Cell Mechanics: Basic Science and Clinical Aspects*, H.J. Meiselman, Lichtman, M. A., LaCelle, P. L., Editor. 1995, Alan R. Liss Inc.: Ney York. p. 19-51.
90. Dancey, J.T., et al., *Neutrophil kinetics in man*. J Clin Invest, 1976. **58**(3): p. 705-15.
91. Semerad, C.L., et al., *G-CSF is an essential regulator of neutrophil trafficking from the bone marrow to the blood*. Immunity, 2002. **17**(4): p. 413-23.
92. Sabroe, I., S.K. Dower, and M.K. Whyte, *The role of Toll-like receptors in the regulation of neutrophil migration, activation, and apoptosis*. Clin Infect Dis, 2005. **41 Suppl 7**: p. S421-6.
93. Schmid-Schonbein, G.W., *Rheology of Leukocytes*, in *Handbook of Bioengineering*, R. Skalak, Chien, S., Editor. 1987, McGraw-Hill, Inc.: New York. p. 13.1-13.25.
94. Su, S.S. and G.W. Schmid-Schonbein, *Internalization of Formyl Peptide Receptor in Leukocytes Subject to Fluid Stresses*. Cell Mol Bioeng, 2010. **3**(1): p. 20-29.
95. McEver, R.P. and R.D. Cummings, *Perspectives series: cell adhesion in vascular biology. Role of PSGL-1 binding to selectins in leukocyte recruitment*. J Clin Invest, 1997. **100**(3): p. 485-91.
96. Page, C. and S. Pitchford, *Neutrophil and platelet complexes and their relevance to neutrophil recruitment and activation*. Int Immunopharmacol, 2013. **17**(4): p. 1176-84.
97. Ley, K., *Endothelial cell-blood cell interactions*, in *Hemostasis and Thrombosis: Basic Principles and Clinical Practice*, V.J. Marder, Aird, W. C., Bennet, J. S., Schulman, S., White, G. C. II., Editor. 2013, Lippincott Williams & Wilkins: New York. p. 598-613.
98. Sundd, P., M.K. Pospieszalska, and K. Ley, *Neutrophil rolling at high shear: flattening, catch bond behavior, tethers and slings*. Mol Immunol, 2013. **55**(1): p. 59-69.
99. Schmidtke, D.W. and S.L. Diamond, *Direct observation of membrane tethers formed during neutrophil attachment to platelets or P-selectin under physiological flow*. J Cell Biol, 2000. **149**(3): p. 719-30.
100. Paschall, C.D. and M.B. Lawrence, *L-selectin shear thresholding modulates leukocyte secondary capture*. Ann Biomed Eng, 2008. **36**(4): p. 622-31.
101. Hyun, Y.M., C.T. Lefort, and M. Kim, *Leukocyte integrins and their ligand interactions*. Immunol Res, 2009. **45**(2-3): p. 195-208.
102. Arnaout, M.A., et al., *Deficiency of a leukocyte surface glycoprotein (LFA-1) in two patients with Mo1 deficiency. Effects of cell activation on Mo1/LFA-1 surface expression in normal and deficient leukocytes*. J Clin Invest, 1984. **74**(4): p. 1291-300.
103. Gorbet, M.B., Sefton, M. V., *Endotoxin: the uninvited guest*. Biomaterials, 2005. **26**(34): p. 6811-7.
104. Harder, S., et al., *Surface contamination of dental implants assessed by gene expression analysis in a whole-blood in vitro assay: a preliminary study*. J Clin Periodontol, 2012. **39**(10): p. 987-94.

105. Nelson, S.K., et al., *Lipopolysaccharide affinity for titanium implant biomaterials*. J Prosthet Dent, 1997. **77**(1): p. 76-82.
106. Li, Y.D., et al., *NF-kappaB transcription factor p50 critically regulates tissue factor in deep vein thrombosis*. J Biol Chem, 2009. **284**(7): p. 4473-83.
107. Martin, U., et al., *The human C3a receptor is expressed on neutrophils and monocytes, but not on B or T lymphocytes*. J Exp Med, 1997. **186**(2): p. 199-207.
108. Zwirner, J., et al., *Evaluation of C3a receptor expression on human leucocytes by the use of novel monoclonal antibodies*. Immunology, 1999. **97**(1): p. 166-72.
109. Sheterline, P., J. Clayton, and J. Sparrow, *Actin*. Protein Profile, 1995. **2**(1): p. 1-103.
110. Pollard, T.D., W.C. Earnshaw, and J. Lippincott-Schwartz, *Cell biology*. 2nd ed. 2008, Philadelphia: Saunders/Elsevier. xix, 905 p.
111. Lichtman, M.A., Santillo, P.A., Kearney, E.A., Roberts, G.W., Weed, R.I., *The shape and surface morphology of human leukocytes in vitro: effect of temperature, metabolic inhibitors and agents that influence membrane structure*. Blood Cells, 1976. **2**: p. 507-531.
112. Ruf, W. and Z.M. Ruggeri, *Neutrophils release brakes of coagulation*. Nat Med, 2010. **16**(8): p. 851-2.
113. Kambas, K., I. Mitroulis, and K. Ritis, *The emerging role of neutrophils in thrombosis-the journey of TF through NETs*. Front Immunol, 2012. **3**: p. 385.
114. Hirsch, J.G., *Cinemicphotographic observations on granule lysis in polymorphonuclear leukocytes during phagocytosis*. J Exp Med, 1962. **116**: p. 827-34.
115. Stossel, T.P., *On the crawling of animal cells*. Science, 1993. **260**(5111): p. 1086-94.
116. Gronert, K., *Resolution, the grail for healthy ocular inflammation*. Exp Eye Res, 2010. **91**(4): p. 478-85.
117. Marchi, L.F., et al., *In vitro activation of mouse neutrophils by recombinant human interferon-gamma: Increased phagocytosis and release of reactive oxygen species and pro-inflammatory cytokines*. Int Immunopharmacol, 2014. **18**(2): p. 228-35.
118. Almyroudis, N.G., et al., *NETosis and NADPH oxidase: at the intersection of host defense, inflammation, and injury*. Front Immunol, 2013. **4**: p. 45.
119. Bordon, Y., *Innate Immunity an Unexpected Guest at the Regulatory Table*. Nature Reviews Immunology, 2010. **10**(1): p. 9-9.
120. Zhang, X., et al., *Coactivation of Syk Kinase and MyD88 Adaptor Protein Pathways by Bacteria Promotes Regulatory Properties of Neutrophils*. Immunity, 2009. **31**(5): p. 761-771.
121. Stampfuss, J.J., et al., *Membrane environment rather than tissue factor expression determines thrombin formation triggered by monocytic cells undergoing apoptosis*. J Leukoc Biol, 2008. **83**(6): p. 1379-81.
122. Kominsky, D.J., E.L. Campbell, and S.P. Colgan, *Metabolic shifts in immunity and inflammation*. J Immunol, 2010. **184**(8): p. 4062-8.
123. van Raam, B.J., A.J. Verhoeven, and T.W. Kuijpers, *Mitochondria in neutrophil apoptosis*. Int J Hematol, 2006. **84**(3): p. 199-204.
124. Miller, L.J., et al., *Stimulated mobilization of monocyte Mac-1 and p150,95 adhesion proteins from an intracellular vesicular compartment to the cell surface*. J Clin Invest, 1987. **80**(2): p. 535-44.
125. Sabroe, I., et al., *Toll-like receptor (TLR)2 and TLR4 in human peripheral blood granulocytes: a critical role for monocytes in leukocyte lipopolysaccharide responses*. J Immunol, 2002. **168**(9): p. 4701-10.
126. Massberg, S., et al., *Reciprocal coupling of coagulation and innate immunity via neutrophil serine proteases*. Nat Med, 2010. **16**(8): p. 887-96.

127. Shantsila, E. and G.Y. Lip, *The role of monocytes in thrombotic disorders. Insights from tissue factor, monocyte-platelet aggregates and novel mechanisms*. *Thromb Haemost*, 2009. **102**(5): p. 916-24.
128. Leatham, E.W., et al., *Increased monocyte tissue factor expression in coronary disease*. *Br Heart J*, 1995. **73**(1): p. 10-3.
129. Abe, R., et al., *Pulsatile to-fro flow induces greater and sustained expression of tissue factor RNA in HUVEC than unidirectional laminar flow*. *Am J Physiol Heart Circ Physiol*, 2011. **300**(4): p. H1345-51.
130. Kopp, C.W., et al., *Platelet-monocyte cross talk and tissue factor expression in stable angina vs. unstable angina/non ST-elevation myocardial infarction*. *Platelets*, 2011. **22**(7): p. 530-6.
131. Macey, M.G., et al., *Expression of blood coagulation factors on monocytes after exposure to TNF-treated endothelium in a novel whole blood model of arterial flow*. *J Immunol Methods*, 2009. **350**(1-2): p. 133-41.
132. Moosbauer, C., et al., *Eosinophils are a major intravascular location for tissue factor storage and exposure*. *Blood*, 2007. **109**(3): p. 995-1002.
133. Natorska, J., et al., *Evidence for tissue factor expression in aortic valves in patients with aortic stenosis*. *Pol Arch Med Wewn*, 2009. **119**(10): p. 636-43.
134. Ye, R., et al., *Circulating tissue factor positive microparticles in patients with acute recurrent deep venous thrombosis*. *Thromb Res*, 2012. **130**(2): p. 253-8.
135. Brand, K., et al., *Tissue factor mRNA in THP-1 monocytic cells is regulated at both transcriptional and posttranscriptional levels in response to lipopolysaccharide*. *Mol Cell Biol*, 1991. **11**(9): p. 4732-8.
136. Guha, M. and N. Mackman, *The phosphatidylinositol 3-kinase-Akt pathway limits lipopolysaccharide activation of signaling pathways and expression of inflammatory mediators in human monocytic cells*. *J Biol Chem*, 2002. **277**(35): p. 32124-32.
137. Egorina, E.M., et al., *Intracellular and surface distribution of monocyte tissue factor: application to intersubject variability*. *Arterioscler Thromb Vasc Biol*, 2005. **25**(7): p. 1493-8.
138. Mandal, S.K., U.R. Pendurthi, and L.V. Rao, *Cellular localization and trafficking of tissue factor*. *Blood*, 2006. **107**(12): p. 4746-53.
139. Schwertz, H., et al., *Signal-dependent splicing of tissue factor pre-mRNA modulates the thrombogenicity of human platelets*. *J Exp Med*, 2006. **203**(11): p. 2433-40.
140. Maugeri, N., et al., *Human polymorphonuclear leukocytes produce and express functional tissue factor upon stimulation*. *J Thromb Haemost*, 2006. **4**(6): p. 1323-30.
141. Ritis, K., et al., *A novel C5a receptor-tissue factor cross-talk in neutrophils links innate immunity to coagulation pathways*. *J Immunol*, 2006. **177**(7): p. 4794-802.
142. Bogdanov, V.Y., et al., *Alternatively spliced human tissue factor: a circulating, soluble, thrombogenic protein*. *Nat Med*, 2003. **9**(4): p. 458-62.
143. Mackman, N. and T. Luther, *Platelet tissue factor: to be or not to be*. *Thromb Res*, 2013. **132**(1): p. 3-5.
144. Osterud, B., *Tissue factor/TFPI and blood cells*. *Thromb Res*, 2012. **129**(3): p. 274-8.
145. Halkier, T. and P. Woolley, *Mechanisms in blood coagulation, fibrinolysis and the complement system*. 1991, Cambridge: Cambridge University Press. xvi, 467 p.
146. Bom, V.J. and R.M. Bertina, *The contributions of Ca<sup>2+</sup>, phospholipids and tissue-factor apoprotein to the activation of human blood-coagulation factor X by activated factor VII*. *Biochem J*, 1990. **265**(2): p. 327-36.
147. Zogg, T. and H. Brandstetter, *Activation mechanisms of coagulation factor IX*. *Biol Chem*, 2009. **390**(5-6): p. 391-400.

148. Krishnaswamy, S., *Coagulation Enzymology*, in *Hemostasis and Thrombosis: Basic Principles and Clinical Practice*, V.J. Marder, Aird, W. C., Bennet, J. S., Schulman, S., White, G. C. II., Editor. 2013, Lippincott Williams & Wilkins: New York. p. 41-51.
149. Hathcock, J.J., *Flow effects on coagulation and thrombosis*. *Arterioscler Thromb Vasc Biol*, 2006. **26**(8): p. 1729-37.
150. Waters, E.K. and J.H. Morrissey, *Restoring full biological activity to the isolated ectodomain of an integral membrane protein*. *Biochemistry*, 2006. **45**(11): p. 3769-74.
151. Seligsohn, U., et al., *Evidence for the participation of both activated factor XII and activated factor IX in cold-promoted activation of factor VII*. *Thromb Res*, 1978. **13**(6): p. 1049-56.
152. Persson, E., *Macromolecular substrate affinity for free factor VIIa is independent of a buried protease domain N-terminus*. *Biochem Biophys Res Commun*, 2006. **341**(1): p. 28-32.
153. Magwenzi, S.G., et al., *Factor XIII supports platelet activation and enhances thrombus formation by matrix proteins under flow conditions*. *J Thromb Haemost*, 2011. **9**(4): p. 820-33.
154. Berglin, M., et al., *Fibrinogen adsorption and conformational change on model polymers: novel aspects of mutual molecular rearrangement*. *Langmuir*, 2009. **25**(10): p. 5602-8.
155. Shiba, E., et al., *Antibody-detectable changes in fibrinogen adsorption affecting platelet activation on polymer surfaces*. *Am J Physiol*, 1991. **260**(5 Pt 1): p. C965-74.
156. Tunc, S., et al., *In situ conformational analysis of fibrinogen adsorbed on Si surfaces*. *Colloids Surf B Biointerfaces*, 2005. **42**(3-4): p. 219-25.
157. Yermolenko, I.S., et al., *The assembly of nonadhesive fibrinogen matrices depends on the alphaC regions of the fibrinogen molecule*. *J Biol Chem*, 2012. **287**(50): p. 41979-90.
158. Yongli, C., et al., *Conformational Changes of Fibrinogen Adsorption onto Hydroxyapatite and Titanium Oxide Nanoparticles*. *J Colloid Interface Sci*, 1999. **214**(1): p. 38-45.
159. Lishko, V.K., et al., *Regulated unmasking of the cryptic binding site for integrin alpha M beta 2 in the gamma C-domain of fibrinogen*. *Biochemistry*, 2002. **41**(43): p. 12942-51.
160. Hu, W.J., et al., *Molecular basis of biomaterial-mediated foreign body reactions*. *Blood*, 2001. **98**(4): p. 1231-8.
161. Kirchhofer, D., M.A. Riederer, and H.R. Baumgartner, *Specific accumulation of circulating monocytes and polymorphonuclear leukocytes on platelet thrombi in a vascular injury model*. *Blood*, 1997. **89**(4): p. 1270-8.
162. van der Meijden, P.E.J., van Schilfgaarde, M., van Oerle, R., Renne', T., ten Cate, H., Spronk, H. M. H., *Platelet- and erythrocyte-derived microparticles trigger thrombin generation via factor XIIa*. *J Thromb Haemost*, 2012. **10**: p. 1355-1362.
163. Chu, A.J., *Role of tissue factor in thrombosis. Coagulation-inflammation-thrombosis circuit*. *Front Biosci*, 2006. **11**: p. 256-71.
164. Monroe, D.M. and N.S. Key, *The tissue factor-factor VIIa complex: procoagulant activity, regulation, and multitasking*. *J Thromb Haemost*, 2007. **5**(6): p. 1097-105.
165. Ruf, W., *Coagulation-Independent Signaling of the Extrinsic Coagulation Pathway*, in *Hemostasis and Thrombosis: Basic Principles and Clinical Practice*, V.J. Marder, Aird, W. C., Bennet, J. S., Schulman, S., White, G. C. II., Editor. 2013, Lippincott Williams & Wilkins: New York. p. 579-584.
166. Mitchell, M., King, MR., *Shear-Induced Resistance to Neutrophil Activation via the Formyl Peptide Receptor*. *Biophysical Journal*, 2012. **102**: p. 1804-1814.
167. Moazzam, F., et al., *The leukocyte response to fluid stress*. *Proc Natl Acad Sci U S A*, 1997. **94**(10): p. 5338-43.
168. Chang, X. and M. Gorbet, *The effect of shear on in vitro platelet and leukocyte material-induced activation*. *J Biomater Appl*, 2013. **28**(3): p. 407-15.

169. Gorbet, M.B., Sefton, M. V., *Pathogenesis and treatment of biomaterial-associated thrombosis*, in *Hemostasis and Thrombosis: Basic Principles and Clinical Practice*, V.J. Marder, Aird, W. C., Bennet, J. S., Schulman, S., White, G. C. II., Editor. 2013, Lippincott Williams & Wilkins: New York. p. 1165-1171.
170. Fischer, M., et al., *The ability of surface characteristics of materials to trigger leukocyte tissue factor expression*. *Biomaterials*, 2010. **31**(9): p. 2498-507.
171. Eriksson, C. and H. Nygren, *Adhesion receptors of polymorphonuclear granulocytes on titanium in contact with whole blood*. *J Lab Clin Med*, 2001. **137**(1): p. 56-63.
172. Schuler, P., et al., *Adhesion of monocytes to medical steel as used for vascular stents is mediated by the integrin receptor Mac-1 (CD11b/CD18; alphaM beta2) and can be inhibited by semiconductor coating*. *Cell Commun Adhes*, 2003. **10**(1): p. 17-26.
173. Breitenstein, A., F.C. Tanner, and T.F. Luscher, *Tissue factor and cardiovascular disease*. *Circ J*, 2010. **74**(1): p. 3-12.
174. Horbett, T.A., *Principles underlying the role of adsorbed plasma proteins in blood interactions with foreign surfaces*. *Cardiovascular Pathology*, 1993. **2**(3 (Suppl.)).
175. Norde, W. and J. Lyklema, *Why proteins prefer interfaces*. *J Biomater Sci Polym Ed*, 1991. **2**(3): p. 183-202.
176. Sperling, C., et al., *Blood coagulation on biomaterials requires the combination of distinct activation processes*. *Biomaterials*, 2009. **30**(27): p. 4447-56.
177. Rapoza, R.J. and T.A. Horbett, *Postadsorptive transitions in fibrinogen: influence of polymer properties*. *J Biomed Mater Res*, 1990. **24**(10): p. 1263-87.
178. Gorbet, M.B., Sefton, M. V., *Leukocyte activation and leukocyte procoagulant activities after blood contact with polystyrene and polyethylene glycol-immobilized polystyrene beads*. *J Lab Clin Med*, 2001. **137**(5): p. 345-55.
179. Bock, P.E., et al., *Protein-protein interactions in contact activation of blood coagulation. Binding of high molecular weight kininogen and the 5-(iodoacetamido) fluorescein-labeled kininogen light chain to prekallikrein, kallikrein, and the separated kallikrein heavy and light chains*. *J Biol Chem*, 1985. **260**(23): p. 12434-43.
180. Warn-Cramer, B.J. and S.P. Bajaj, *Stoichiometry of binding of high molecular weight kininogen to factor XI/XIa*. *Biochem Biophys Res Commun*, 1985. **133**(2): p. 417-22.
181. Dashty, M., et al., *Characterization of coagulation factor synthesis in nine human primary cell types*. *Sci Rep*, 2012. **2**: p. 787.
182. Franz, S., et al., *Immune responses to implants - a review of the implications for the design of immunomodulatory biomaterials*. *Biomaterials*, 2011. **32**(28): p. 6692-709.
183. Griffin, J.H., *Role of surface in surface-dependent activation of Hageman factor (blood coagulation factor XII)*. *Proc Natl Acad Sci U S A*, 1978. **75**(4): p. 1998-2002.
184. Konings, J., et al., *Factor XIIIa regulates the structure of the fibrin clot independently of thrombin generation through direct interaction with fibrin*. *Blood*, 2011. **118**(14): p. 3942-51.
185. Muller, F., et al., *Platelet polyphosphates are proinflammatory and procoagulant mediators in vivo*. *Cell*, 2009. **139**(6): p. 1143-56.
186. Griep, M.A., K. Fujikawa, and G.L. Nelsestuen, *Binding and activation properties of human factor XII, prekallikrein, and derived peptides with acidic lipid vesicles*. *Biochemistry*, 1985. **24**(15): p. 4124-30.
187. Naito, K. and K. Fujikawa, *Activation of human blood coagulation factor XI independent of factor XII. Factor XI is activated by thrombin and factor XIa in the presence of negatively charged surfaces*. *J Biol Chem*, 1991. **266**(12): p. 7353-8.
188. Landry, P., et al., *Existence of a microRNA pathway in anucleate platelets*. *Nat Struct Mol Biol*, 2009. **16**(9): p. 961-6.

189. Stegner, D. and B. Nieswandt, *Platelet receptor signaling in thrombus formation*. J Mol Med (Berl), 2011. **89**(2): p. 109-21.
190. Zhang, G.Y., et al., *Lipopolysaccharide Stimulates Platelet Secretion and Potentiates Platelet Aggregation via TLR4/MyD88 and the cGMP-Dependent Protein Kinase Pathway*. Journal of Immunology, 2009. **182**(12): p. 7997-8004.
191. Jung, F., S. Braune, and A. Lendlein, *Haemocompatibility testing of biomaterials using human platelets*. Clin Hemorheol Microcirc, 2013. **53**(1-2): p. 97-115.
192. Vieira-de-Abreu, A., et al., *Platelets: versatile effector cells in hemostasis, inflammation, and the immune continuum*. Semin Immunopathol, 2012. **34**(1): p. 5-30.
193. Mahaut-Smith, M.P., G. Tolhurst, and R.J. Evans, *Emerging roles for P2X1 receptors in platelet activation*. Platelets, 2004. **15**(3): p. 131-44.
194. Altieri, D.C., W.L. Wiltse, and T.S. Edgington, *Signal transduction initiated by extracellular nucleotides regulates the high affinity ligand recognition of the adhesive receptor CD11b/CD18*. J Immunol, 1990. **145**(2): p. 662-70.
195. Altieri, D.C., J.H. Morrissey, and T.S. Edgington, *Adhesive receptor Mac-1 coordinates the activation of factor X on stimulated cells of monocytic and myeloid differentiation: an alternative initiation of the coagulation protease cascade*. Proc Natl Acad Sci U S A, 1988. **85**(20): p. 7462-6.
196. Wiedmer, T., et al., *Role of calcium and calpain in complement-induced vesiculation of the platelet plasma membrane and in the exposure of the platelet factor Va receptor*. Biochemistry, 1990. **29**(3): p. 623-32.
197. Monkovic, D.D. and P.B. Tracy, *Functional characterization of human platelet-released factor V and its activation by factor Xa and thrombin*. J Biol Chem, 1990. **265**(28): p. 17132-40.
198. May, A.E., P. Seizer, and M. Gawaz, *Platelets: inflammatory firebugs of vascular walls*. Arterioscler Thromb Vasc Biol, 2008. **28**(3): p. s5-10.
199. Hellums, J.D., *1993 Whitaker Lecture: biorheology in thrombosis research*. Ann Biomed Eng, 1994. **22**(5): p. 445-55.
200. Cosemans, J.M., et al., *The effects of arterial flow on platelet activation, thrombus growth, and stabilization*. Cardiovasc Res, 2013. **99**(2): p. 342-52.
201. Jackson, S.P., *The growing complexity of platelet aggregation*. Blood, 2007. **109**(12): p. 5087-95.
202. Shadden, S.C. and S. Hendabadi, *Potential fluid mechanic pathways of platelet activation*. Biomech Model Mechanobiol, 2013. **12**(3): p. 467-74.
203. Suter, S.P., et al., *A programmable, computer-controlled cone-plate viscometer for the application of pulsatile shear stress to platelet suspensions*. Biorheology, 1988. **25**(3): p. 449-59.
204. Jesty, J., et al., *Platelet activation in a circulating flow loop: combined effects of shear stress and exposure time*. Platelets, 2003. **14**(3): p. 143-9.
205. Alemu, Y. and D. Bluestein, *Flow-induced platelet activation and damage accumulation in a mechanical heart valve: numerical studies*. Artif Organs, 2007. **31**(9): p. 677-88.
206. Flamm, M.H., et al., *Multiscale prediction of patient-specific platelet function under flow*. Blood, 2012. **120**(1): p. 190-8.
207. Miyazaki, Y., et al., *High shear stress can initiate both platelet aggregation and shedding of procoagulant containing microparticles*. Blood, 1996. **88**(9): p. 3456-64.
208. Holme, P.A., et al., *Shear-induced platelet activation and platelet microparticle formation at blood flow conditions as in arteries with a severe stenosis*. Arterioscler Thromb Vasc Biol, 1997. **17**(4): p. 646-53.

209. Puddu, P., et al., *The involvement of circulating microparticles in inflammation, coagulation and cardiovascular diseases*. Can J Cardiol, 2010. **26**(4): p. 140-5.
210. Doeuvre, L., et al., *Cell-derived microparticles: a new challenge in neuroscience*. J Neurochem, 2009. **110**(2): p. 457-68.
211. Chu, A.J., *Tissue factor upregulation drives a thrombosis-inflammation circuit in relation to cardiovascular complications*. Cell Biochem Funct, 2006. **24**(2): p. 173-92.
212. Nomura, S., et al., *High-shear-stress-induced activation of platelets and microparticles enhances expression of cell adhesion molecules in THP-1 and endothelial cells*. Atherosclerosis, 2001. **158**(2): p. 277-87.
213. Kuwahara, M., et al., *Platelet shape changes and adhesion under high shear flow*. Arterioscler Thromb Vasc Biol, 2002. **22**(2): p. 329-34.
214. Wu, Y.P., P.G. de Groot, and J.J. Sixma, *Shear-stress-induced detachment of blood platelets from various surfaces*. Arterioscler Thromb Vasc Biol, 1997. **17**(11): p. 3202-7.
215. Jen, C.J., et al., *Flow-induced detachment of adherent platelets from fibrinogen-coated surface*. Am J Physiol, 1996. **270**(1 Pt 2): p. H160-6.
216. Gemmell, C.H., *Activation of platelets by in vitro whole blood contact with materials: increases in microparticle, procoagulant activity, and soluble P-selectin blood levels*. J Biomater Sci Polym Ed, 2001. **12**(8): p. 933-43.
217. Tanaka, Y., et al., *In vitro short-term platelet adhesion on various metals*. J Artif Organs, 2009. **12**(3): p. 182-6.
218. Walkowiak-Przybylo, M., et al., *Adhesion, activation, and aggregation of blood platelets and biofilm formation on the surfaces of titanium alloys Ti6Al4V and Ti6Al7Nb*. J Biomed Mater Res A, 2012. **100**(3): p. 768-75.
219. Floyd, C.N. and A. Ferro, *The platelet fibrinogen receptor: from megakaryocyte to the mortuary*. JRSMB Cardiovasc Dis, 2012. **1**(2).
220. Bai, Z., et al., *Fibrinogen adsorption onto 316L stainless steel, Nitinol and titanium*. Surface Science, 2009. **603**: p. 839-846.
221. Srokowski, E.M. and K.A. Woodhouse, *Evaluation of the bulk platelet response and fibrinogen interaction to elastin-like polypeptide coatings*. J Biomed Mater Res A, 2014. **102**(2): p. 540-51.
222. Wildgoose, P., et al., *The role of phospholipids and the factor VII Gla-domain in the interaction of factor VII with tissue factor*. Thromb Haemost, 1992. **67**(6): p. 679-85.
223. Lisman, T., et al., *Recombinant factor VIIa enhances platelet adhesion and activation under flow conditions at normal and reduced platelet count*. J Thromb Haemost, 2005. **3**(4): p. 742-51.
224. Hoffman, M., H.C. Whinna, and D.M. Monroe, *Circulating tissue factor accumulates in thrombi, but not in hemostatic plugs*. J Thromb Haemost, 2006. **4**(9): p. 2092-3.
225. Hoffman, M., *Some things I thought I knew about tissue factor that turn out to be wrong*. Thromb Res, 2008. **122 Suppl 1**: p. S73-7.
226. Monroe, D.M. and M. Hoffman, *What does it take to make the perfect clot?* Arterioscler Thromb Vasc Biol, 2006. **26**(1): p. 41-8.
227. Dodge, J.T., Jr., et al., *Lumen diameter of normal human coronary arteries. Influence of age, sex, anatomic variation, and left ventricular hypertrophy or dilation*. Circulation, 1992. **86**(1): p. 232-46.
228. Zhu, H., et al., *Cataloguing the geometry of the human coronary arteries: A potential tool for predicting risk of coronary artery disease*. International Journal of Cardiology, 2009. **135**(1): p. 43-52.

229. Nerem, R.M., Seed, W.A., *Coronary artery geometry and its fluid mechanical implications*, in *Fluid Dynamics as a Localizing Factor for Atherosclerosis*, G. Schettler, Nerem, R.M., Schmid-Schönbein, H., Mörl, H., Diehm, C., Editor. 1983, Springer-Verlag: New York. p. 51-59.
230. Zubaid, M., C. Buller, and G.B. Mancini, *Normal angiographic tapering of the coronary arteries*. Can J Cardiol, 2002. **18**(9): p. 973-80.
231. McIntire, L.V., Jiménez, J. M., Eskin, S. G., Davies, P. F., *Rheology and vessel wall stress*, in *Hemostasis and Thrombosis: Basic Principles and Clinical Practice*, V.J. Marder, Aird, W. C., Bennet, J. S., Schulman, S., White, G. C. II., Editor. 2013, Lippincott Williams & Wilkins: New York. p. 516-535.
232. Liepsch, D., Moravic, S., Zimmer, R., *Pulsating Flow in Distensible Models of Vascular Branches*, in *Fluid Dynamics as a Localizing Factor for Atherosclerosis*, G. Schettler, Nerem, R.M., Schmid-Schönbein, H., Mörl, H., Diehm, C., Editor. 1983, Springer-Verlag: New York. p. 46-50.
233. Schlichting, H. and K. Gersten, *Boundary-layer theory*. 8th rev. and enl. ed. 2000, Berlin ; New York: Springer. xxiii, 799 p.
234. Asakura, T. and T. Karino, *Flow patterns and spatial distribution of atherosclerotic lesions in human coronary arteries*. Circ Res, 1990. **66**(4): p. 1045-66.
235. Chesnutt, J.K. and H.C. Han, *Tortuosity triggers platelet activation and thrombus formation in microvessels*. J Biomech Eng, 2011. **133**(12): p. 121004.
236. Niazmand, H. and E. Rajabi Jaghargh, *Bend sweep angle and Reynolds number effects on hemodynamics of s-shaped arteries*. Ann Biomed Eng, 2010. **38**(9): p. 2817-28.
237. Pivkin, I.V., et al., *Combined effects of pulsatile flow and dynamic curvature on wall shear stress in a coronary artery bifurcation model*. Journal of Biomechanics, 2005. **38**(6): p. 1283-1290.
238. He, X. and D.N. Ku, *Pulsatile flow in the human left coronary artery bifurcation: average conditions*. J Biomech Eng, 1996. **118**(1): p. 74-82.
239. Robertson, A.M., Sequeira, A., Owens, R. G., *Rheological models for blood*, in *Cardiovascular Mathematics: Modeling and simulation of the circulatory system*, L. Formaggia, Quarteroni, A., Veneziani, A., Editor. 2009, Springer-Verlag: Milano. p. 211-241.
240. Isfahani, A.H. and J.B. Freund, *Forces on a wall-bound leukocyte in a small vessel due to red cells in the blood stream*. Biophys J, 2012. **103**(7): p. 1604-15.
241. Tokarev, A.A., A.A. Butylin, and F.I. Ataullakhanov, *Platelet adhesion from shear blood flow is controlled by near-wall rebounding collisions with erythrocytes*. Biophys J, 2011. **100**(4): p. 799-808.
242. Naphon, P., Wongwises, S., *A review of flow and heat transfer characteristics in curved tubes*. Renewable and Sustainable Energy Reviews, 2006. **10**: p. 463-490.
243. Jubran, B.A., Hamdan, M.A., Mansour, A.R., *Drag reduction using pure honey, with particular reference to biomedical engineering*. Polym.-Plast. Technol. Eng., 1994. **33**(1): p. 37-53.
244. Khan, M.B., B.J. Briscoe, and S.M. Richardson, *Field-induced phase fractionation in multiphase polymer flow systems: A review*. Polym.-Plast. Technol. Eng., 1994. **33**(3): p. 295-322.
245. Fournier, R.L., *Basic transport phenomena in biomedical engineering*. 3rd ed. 2011, Boca Raton, Fla. ; London: CRC. xxiii, 459 p.
246. Turitto, V.T. and H.R. Baumgartner, *Platelet interaction with subendothelium in flowing rabbit blood: effect of blood shear rate*. Microvasc Res, 1979. **17**(1): p. 38-54.

247. Turitto, V.T., H.J. Weiss, and H.R. Baumgartner, *The effect of shear rate on platelet interaction with subendothelium exposed to citrated human blood*. *Microvasc Res*, 1980. **19**(3): p. 352-65.
248. Tonda, R., et al., *Platelets interact with tissue factor immobilized on surfaces: effects of shear rate*. *Eur J Clin Invest*, 2008. **38**(1): p. 34-42.
249. Shen, F., et al., *Threshold response of initiation of blood coagulation by tissue factor in patterned microfluidic capillaries is controlled by shear rate*. *Arterioscler Thromb Vasc Biol*, 2008. **28**(11): p. 2035-41.
250. Malek, A.M., S.L. Alper, and S. Izumo, *Hemodynamic shear stress and its role in atherosclerosis*. *JAMA*, 1999. **282**(21): p. 2035-42.
251. Oshinski, J.N., J.L. Curtin, and F. Loth, *Mean-average wall shear stress measurements in the common carotid artery*. *J Cardiovasc Magn Reson*, 2006. **8**(5): p. 717-22.
252. Chiu, J.J., S. Usami, and S. Chien, *Vascular endothelial responses to altered shear stress: pathologic implications for atherosclerosis*. *Ann Med*, 2009. **41**(1): p. 19-28.
253. Fung, Y.C., *Biomechanics : mechanical properties of living tissues*. 1981, New York: Springer-Verlag. xii, 433 p.
254. Sardo, M.A., et al., *Tissue factor and monocyte chemoattractant protein-1 expression in hypertensive individuals with normal or increased carotid intima-media wall thickness*. *Clin Chem*, 2008. **54**(5): p. 814-23.
255. Kroll, M.H., et al., *Platelets and shear stress*. *Blood*, 1996. **88**(5): p. 1525-41.
256. Sheriff, J., et al., *High-shear stress sensitizes platelets to subsequent low-shear conditions*. *Ann Biomed Eng*, 2010. **38**(4): p. 1442-50.
257. Papafaklis, M.I., et al., *Relationship of shear stress with in-stent restenosis: bare metal stenting and the effect of brachytherapy*. *Int J Cardiol*, 2009. **134**(1): p. 25-32.
258. Agrawal, S., et al., *Power law fluids in a circular curved tube. Part I. Laminar flow*. *Polym.-Plast. Technol. Eng.*, 1993. **32**(6): p. 595-614.
259. Austin, L.R. and J.D. Seader, *Fully Developed Viscous Flow in Coiled Circular Pipes*. *Aiche Journal*, 1973. **19**(1): p. 85-94.
260. Ward-Smith, A.J., *Pressure losses in ducted flows*. 1971, London: Butterworths. [9], 196 p.
261. Santamarina, A., et al., *Computational analysis of flow in a curved tube model of the coronary arteries: effects of time-varying curvature*. *Ann Biomed Eng*, 1998. **26**(6): p. 944-54.
262. Soeberg, H., *Viscous flow in curved tubes-I. velocity profiles*. *Chemical Engineering Science*, 1988. **43**(4): p. 855-862.
263. Dean, W.R., *The stream-line motion of fluid in a curved pipe. (Second paper.)*. *Philosophical Magazine*, 1928. **5**(30): p. 673-695.
264. Agrawal, S., et al., *Power law fluids in a circular curved tube. Part II. Axial laminar dispersion*. *Polym.-Plast. Technol. Eng.*, 1993. **32**(6): p. 615-634.
265. Teoh, S.H., *Engineering materials for biomedical applications*, in *Biomaterials engineering and processing series ; v. 1*. 2004, World Scientific Pub.: Hackensack, N.J. p. 1 v. (various pagings).
266. Anselme, K.e.a., *Cell/Material Interfaces: Influence of Surface Chemistry and Surface Topography on Cell Adhesion*. *J Adhesion Science and Technology*, 2010. **24**: p. 831-852.
267. MacDonald, D.E., et al., *Thermal and chemical modification of titanium-aluminum-vanadium implant materials: effects on surface properties, glycoprotein adsorption, and MG63 cell attachment*. *Biomaterials*, 2004. **25**(16): p. 3135-46.
268. Shabalovskaya, S., J. Anderegg, and J. Van Humbeeck, *Critical overview of Nitinol surfaces and their modifications for medical applications*. *Acta Biomater*, 2008. **4**(3): p. 447-67.

269. Shabalovskaya, S., et al., *Comparative in vitro performances of bare Nitinol surfaces*. Biomed Mater Eng, 2008. **18**(1): p. 1-14.
270. Löberg, J., Mattisson, I., Hansson, S., Ahlberg, E., *Characterisation of Titanium Dental Implants I: Critical Assessment of Surface Roughness Parameters*. The Open Biomaterials Journal, 2010. **2**: p. 18-35.
271. ASTM, *F2791 Assessment of Surface Texture of Non-Porous Biomaterials in Two Dimensions*. 2009, American National Standards Institute: New York.
272. Davies, J.T., et al., *An in vitro multi-parametric approach to measuring the effect of implant surface characteristics on cell behaviour*. Biomed Mater, 2010. **5**(1): p. 15002.
273. Wirth, C., et al., *Nitinol surface roughness modulates in vitro cell response: a comparison between fibroblasts and osteoblasts*. Mater Sci Eng, 2005. **C25**: p. 51-60.
274. Variola, F., et al., *Tailoring the surface properties of Ti6Al4V by controlled chemical oxidation*. Biomaterials, 2008. **29**(10): p. 1285-98.
275. Clarke, B., et al., *Effect of nitinol wire surface properties on albumin adsorption*. Acta Biomater, 2007. **3**(1): p. 103-11.
276. Song, D.P., et al., *Molecular dynamics study on surface structure and surface energy of rutile TiO<sub>2</sub> (1 1 0)*. Applied Surface Science, 2009. **255**: p. 5702-5708.
277. Gageot, M.P., M. Sprik, and M. Sulpizi, *Oxide/water interfaces: how the surface chemistry modifies interfacial water properties*. J Phys Condens Matter, 2012. **24**(12): p. 124106.
278. Barbosa, J.N., et al., *Adhesion of human leukocytes on mixtures of hydroxyl- and methyl-terminated self-assembled monolayers: effect of blood protein adsorption*. J Biomed Mater Res A, 2010. **93**(1): p. 12-9.
279. Diebold, U., *The surface science of titanium dioxide*. Surface Science Reports, 2003. **48**: p. 53-229.
280. Barteau, M.A., *Organic Reactions at Well-Defined Oxide Surfaces*. Chem Rev, 1996. **96**(4): p. 1413-1430.
281. Henrich, V.E. and P.A. Cox, *The surface science of metal oxides*. 1994, Cambridge ; New York: Cambridge University Press. xiv, 464 p.
282. Wever, D.J., et al., *Electrochemical and surface characterization of a nickel-titanium alloy*. Biomaterials, 1998. **19**(7-9): p. 761-9.
283. McLucas, E., et al., *Analysis of the effects of surface treatments on nickel release from nitinol wires and their impact on candidate gene expression in endothelial cells*. J Mater Sci Mater Med, 2008. **19**(3): p. 975-80.
284. Shabalovskaya, S.A., et al., *Surface conditions of Nitinol wires, tubing, and as-cast alloys. The effect of chemical etching, aging in boiling water, and heat treatment*. J Biomed Mater Res B Appl Biomater, 2003. **65**(1): p. 193-203.
285. Dobson, K.D., et al., *Monitoring hydrous metal oxide surface charge and adsorption by STIRS*. Langmuir, 1997. **13**: p. 2614-2616.
286. MacDonald, D.E., B.E. Rapuano, and H.C. Schniepp, *Surface oxide net charge of a titanium alloy: comparison between effects of treatment with heat or radiofrequency plasma glow discharge*. Colloids Surf B Biointerfaces, 2011. **82**(1): p. 173-81.
287. Zhang, Z., et al., *Ion adsorption at the rutile-water interface: linking molecular and macroscopic properties*. Langmuir, 2004. **20**(12): p. 4954-69.
288. Roddick-Lanzilotta, A.D. and A.J. McQuillan, *An in situ Infrared Spectroscopic Study of Glutamic Acid and of Aspartic Acid Adsorbed on TiO<sub>2</sub>: Implications for the Biocompatibility of Titanium*. J Colloid Interface Sci, 2000. **227**(1): p. 48-54.

289. Yang, Q., et al., *Study of fibrinogen adsorption on hydroxyapatite and TiO<sub>2</sub> surfaces by electrochemical piezoelectric quartz crystal impedance and FTIR-ATR spectroscopy*. Anal Chim Acta, 2007. **597**(1): p. 58-66.
290. Chen, W., et al., *RGD peptide functionalized and reconstituted high-density lipoprotein nanoparticles as a versatile and multimodal tumor targeting molecular imaging probe*. Faseb J, 2010. **24**(6): p. 1689-99.
291. Wu, C., et al., *Peptide-TiO<sub>2</sub> interaction in aqueous solution: conformational dynamics of RGD using different water models*. J Phys Chem B, 2010. **114**(13): p. 4692-701.
292. Vogler, E.A., *How water wets biomaterial surfaces*, in *Water in Biomaterials Surface Science*, M. Morra, Editor. 2001, John Wiley & Sons, Ltd: Chichester. p. 269-290.
293. Eriksson, C. and H. Nygren, *Polymorphonuclear leukocytes in coagulating whole blood recognize hydrophilic and hydrophobic titanium surfaces by different adhesion receptors and show different patterns of receptor expression*. J Lab Clin Med, 2001. **137**(4): p. 296-302.
294. Ratner, B.D., *Surface properties and surface characterization of biomaterials*, in *Biomaterials Science: An Introduction to Materials in Medicine*, 3rd Edition, B.D. Ratner, Hoffman, A. S., Schoen, F. J., Lemons, J. E., Editor. 2013, Elsevier Inc.: London. p. 34-55.
295. Michiardi, A., et al., *The influence of surface energy on competitive protein adsorption on oxidized NiTi surfaces*. Biomaterials, 2007. **28**(4): p. 586-94.
296. Harnett, E.M., J. Alderman, and T. Wood, *The surface energy of various biomaterials coated with adhesion molecules used in cell culture*. Colloids and Surfaces B-Biointerfaces, 2007. **55**(1): p. 90-97.
297. Dillon, P.F., *Load Bearing*, in *Biophysics: A Physiological Approach* 2012, Cambridge University Press: New York.
298. Cho, Y.K., Park, D., Kim, H., Lee, H., Park, H., Kim, H. J., Jung, D., *Bioactive surface modifications on inner walls of poly-tetra-fluoro-ethylene tubes using dielectric barrier discharge*. Applied Surface Science, 2014. **296**: p. 79-85.
299. Ma, W., Ruys, A. J., Zreiqat, H., *Diamond-like carbon (DLC) as a biocompatible coating in in orthopaedic and cardiac medicine*, in *Cellular Response to Biomaterials*, L. Di Silvio, Editor. 2009, CRC Press: Boca Raton. p. 391-426.
300. Han, D.K., et al., *Surface characteristics and blood compatibility of polyurethanes grafted by perfluoroalkyl chains*. J Biomater Sci Polym Ed, 1992. **3**(3): p. 229-41.
301. Ho, T.A., et al., *Liquid water can slip on a hydrophilic surface*. Proc Natl Acad Sci U S A, 2011. **108**(39): p. 16170-5.
302. Tamai, Y. and K. Aratani, *Experimental Study of Relation between Contact Angle and Surface-Roughness*. Journal of Physical Chemistry, 1972. **76**(22): p. 3267-&.
303. Onda, T.e.a., *Super-Water-Repellent Fractal Surfaces*. Langmuir, 1996. **12**(9): p. 2125-2127.
304. Sajadinia, S.H. and F. Sharif, *Thermodynamic analysis of the wetting behavior of dual scale patterned hydrophobic surfaces*. J Colloid Interface Sci, 2010. **344**(2): p. 575-83.
305. Rupp, F., et al., *Enhancing surface free energy and hydrophilicity through chemical modification of microstructured titanium implant surfaces*. J Biomed Mater Res A, 2006. **76**(2): p. 323-34.
306. Lim, Y.J. and Y. Oshida, *Initial contact angle measurements on variously treated dental/medical titanium materials*. Biomed Mater Eng, 2001. **11**(4): p. 325-41.
307. Grodzka, J., Pomianowski, A., *Wettability versus hydrophilicity*. Physicochemical Problems of Mineral Processing, 2006. **40**: p. 5-18.
308. Yeung, K.W., et al., *Surface mechanical properties, corrosion resistance, and cytocompatibility of nitrogen plasma-implanted nickel-titanium alloys: a comparative study with commonly used medical grade materials*. J Biomed Mater Res A, 2007. **82**(2): p. 403-14.

309. Suska, F., et al., *IL-1alpha, IL-1beta and TNF-alpha secretion during in vivo/ex vivo cellular interactions with titanium and copper*. *Biomaterials*, 2003. **24**(3): p. 461-8.
310. Hansi, C., et al., *Differences of platelet adhesion and thrombus activation on amorphous silicon carbide, magnesium alloy, stainless steel, and cobalt chromium stent surfaces*. *Catheter Cardiovasc Interv*, 2009. **73**(4): p. 488-96.
311. Aird, W.C., *Overview of vascular biology*, in *Hemostasis and Thrombosis: Basic Principles and Clinical Practice*, V.J. Marder, Aird, W. C., Bennet, J. S., Schulman, S., White, G. C. II., Editor. 2013, Lippincott Williams & Wilkins: New York. p. 493-497.
312. Detmers, P.A., et al., *Aggregation of complement receptors on human neutrophils in the absence of ligand*. *J Cell Biol*, 1987. **105**(3): p. 1137-45.
313. Bassler, B.L. and R. Losick, *Bacterially speaking*. *Cell*, 2006. **125**(2): p. 237-46.
314. Long, T., et al., *Quantifying the integration of quorum-sensing signals with single-cell resolution*. *PLoS Biol*, 2009. **7**(3): p. e68.
315. Gianchandani, E.P., D.L. Brautigan, and J.A. Papin, *Systems analyses characterize integrated functions of biochemical networks*. *Trends Biochem Sci*, 2006. **31**(5): p. 284-91.
316. Bonneau, R., et al., *A predictive model for transcriptional control of physiology in a free living cell*. *Cell*, 2007. **131**(7): p. 1354-65.
317. Gorbet, M.B., *The importance of platelets and complement in material-induced leukocyte activation in vitro*. 2001. 239 leaves.
318. Baldwin, L. and J.A. Hunt, *The in vivo cytokine release profile following implantation*. *Cytokine*, 2008. **41**(3): p. 217-22.
319. Kuharsky, A.L. and A.L. Fogelson, *Surface-mediated control of blood coagulation: the role of binding site densities and platelet deposition*. *Biophys J*, 2001. **80**(3): p. 1050-74.
320. Braune, S., et al., *Are there sufficient standards for the in vitro hemocompatibility testing of biomaterials?* *Biointerphases*, 2013. **8**(1): p. 30.
321. Waters, S.L., et al., *Theoretical models for coronary vascular biomechanics: progress & challenges*. *Prog Biophys Mol Biol*, 2011. **104**(1-3): p. 49-76.
322. Kim, J.Y., et al., *Comparison of effects of drug-eluting stents versus bare metal stents on plasma C-reactive protein levels*. *Am J Cardiol*, 2005. **96**(10): p. 1384-8.
323. Park, D.W., et al., *C-reactive protein and the risk of stent thrombosis and cardiovascular events after drug-eluting stent implantation*. *Circulation*, 2009. **120**(20): p. 1987-95.
324. Madjid, M. and O. Fatemi, *Components of the complete blood count as risk predictors for coronary heart disease: in-depth review and update*. *Tex Heart Inst J*, 2013. **40**(1): p. 17-29.
325. Dacey, L.J., et al., *Preoperative white blood cell count and mortality and morbidity after coronary artery bypass grafting*. *Ann Thorac Surg*, 2003. **76**(3): p. 760-4.
326. Ruggiero, C., et al., *White blood cell count and mortality in the Baltimore Longitudinal Study of Aging*. *J Am Coll Cardiol*, 2007. **49**(18): p. 1841-50.
327. Cao, L., et al., *Plasma-deposited tetraglyme surfaces greatly reduce total blood protein adsorption, contact activation, platelet adhesion, platelet procoagulant activity, and in vitro thrombus deposition*. *J Biomed Mater Res A*, 2007. **81**(4): p. 827-37.
328. Alp, N., Ali, Z.A., Channon, K.M., *Models for studying coronary artery stenting*. *Drug Discover Today: Disease Models*, 2006. **3**(3).
329. Schnittler, H.J., et al., *Improved in vitro rheological system for studying the effect of fluid shear stress on cultured cells*. *Am J Physiol*, 1993. **265**(1 Pt 1): p. C289-98.
330. Para, A.N. and D.N. Ku, *A low-volume, single pass in-vitro system of high shear thrombosis in a stenosis*. *Thromb Res*, 2013. **131**(5): p. 418-24.
331. Truskey, G.A., F. Yuan, and D.F. Katz, *Transport phenomena in biological systems*. 2nd ed. Pearson Prentice Hall bioengineering. 2009, Boston ; London: Pearson. 886 p.

332. Hinds, M.T., et al., *Local hemodynamics affect monocytic cell adhesion to a three-dimensional flow model coated with E-selectin*. J Biomech, 2001. **34**(1): p. 95-103.
333. van Oeveren, W., I.F. Tielliu, and J. de Hart, *Comparison of modified chandler, roller pump, and ball valve circulation models for in vitro testing in high blood flow conditions: application in thrombogenicity testing of different materials for vascular applications*. Int J Biomater, 2012. **2012**: p. 673163.
334. Rouleau, L., et al., *Neutrophil adhesion on endothelial cells in a novel asymmetric stenosis model: effect of wall shear stress gradients*. Ann Biomed Eng, 2010. **38**(9): p. 2791-804.
335. Chiu, J.J., et al., *Analysis of the effect of disturbed flow on monocytic adhesion to endothelial cells*. J Biomech, 2003. **36**(12): p. 1883-95.
336. Fallon, A.M., et al., *Thrombin formation in vitro in response to shear-induced activation of platelets*. Thromb Res, 2007. **121**(3): p. 397-406.
337. Ekdahl, K.N., et al., *Evaluation of the blood compatibility of materials, cells, and tissues: basic concepts, test models, and practical guidelines*. Adv Exp Med Biol, 2013. **735**: p. 257-70.
338. Cunningham, K.S. and A.I. Gotlieb, *The role of shear stress in the pathogenesis of atherosclerosis*. Lab Invest, 2005. **85**(1): p. 9-23.
339. Aarts, P.A., et al., *Blood platelets are concentrated near the wall and red blood cells, in the center in flowing blood*. Arteriosclerosis, 1988. **8**(6): p. 819-24.
340. Karimo, T., Motomiya, M., Goldsmith, H. L., *Flow Patterns in Model and Natural Branching Vessels*, in *Fluid Dynamics as a Localizing Factor for Atherosclerosis*, G. Schettler, Nerem, R.M., Schmid-Schönbein, H., Mörl, H., Diehm, C., Editor. 1983, Springer-Verlag: New York. p. 60-70.
341. Bark, D.L., Nesbitt, W. S., Wong, A. K. T., Jackson, S. P., *Shear Effects on Platelets and Vessel Wall in the Pathogenesis of Atherothrombosis*, in *Hemostasis and Thrombosis: Basic Principles and Clinical Practice*, V.J. Marder, Aird, W. C., Bennet, J. S., Schulman, S., White, G. C. II., Editor. 2013, Lippincott Williams & Wilkins: New York. p. 410-419.
342. Berne, R.M. and M.N. Levy, *Cardiovascular physiology*. 4th ed. 1981, St. Louis: Mosby. ix, 286 p.
343. Blackman, B.R., K.A. Barbee, and L.E. Thibault, *In vitro cell shearing device to investigate the dynamic response of cells in a controlled hydrodynamic environment*. Ann Biomed Eng, 2000. **28**(4): p. 363-72.
344. Breen, L.T., P.E. McHugh, and B.P. Murphy, *HUVEC ICAM-1 and VCAM-1 synthesis in response to potentially athero-prone and athero-protective mechanical and nicotine chemical stimuli*. Ann Biomed Eng, 2010. **38**(5): p. 1880-92.
345. Leal, L.G., *Laminar flow and convective transport processes : scaling principles and asymptotic analysis*. Butterworth-Heinemann series in chemical engineering. 1992, Boston: Butterworth-Heinemann. xviii, 740 p.
346. Fung, Y.C., *Biodynamics : circulation*. 1984, New York: Springer-Verlag. xi, 404 p.
347. Robbie, L.A., et al., *Thrombi formed in a Chandler loop mimic human arterial thrombi in structure and RAI-1 content and distribution*. Thromb Haemost, 1997. **77**(3): p. 510-5.
348. McClung, W.G., D.E. Babcock, and J.L. Brash, *Fibrinolytic properties of lysine-derivatized polyethylene in contact with flowing whole blood (Chandler loop model)*. J Biomed Mater Res A, 2007. **81**(3): p. 644-51.
349. Christensen, K., et al., *Coagulation and complement activation*. Biomaterials, 2001. **22**(4): p. 349-55.
350. Tepe, G., et al., *Reduced thrombogenicity of nitinol stents--in vitro evaluation of different surface modifications and coatings*. Biomaterials, 2006. **27**(4): p. 643-50.

351. Skilbeck, C., et al., *Dependence of adhesive behavior of neutrophils on local fluid dynamics in a region with recirculating flow*. *Biorheology*, 2001. **38**(2-3): p. 213-27.
352. Skilbeck, C.A., et al., *Disturbed flow promotes deposition of leucocytes from flowing whole blood in a model of a damaged vessel wall*. *Br J Haematol*, 2004. **126**(3): p. 418-27.
353. Mazzolai, L., et al., *Tissue factor activity is upregulated in human endothelial cells exposed to oscillatory shear stress*. *Thromb Haemost*, 2002. **87**(6): p. 1062-8.
354. Gardner, R.A., *An examination of the fluid mechanics and thrombus formation time parameters in a Chandler rotating loop system*. *J Lab Clin Med*, 1974. **84**(4): p. 494-508.
355. ISO, *ISO 10993-4:2002 Biological evaluation of medical devices - Part 4: Selection of tests for interactions with blood*. 2002, International Standards Organization: Geneva.
356. Kolandaivelu, K. and E.R. Edelman, *Low background, pulsatile, in vitro flow circuit for modeling coronary implant thrombosis*. *J Biomech Eng*, 2002. **124**(6): p. 662-8.
357. Whitmore, R.L., *Rheology of the circulation*. 1st ed. 1968, Oxford: Pergamon Press. 196p.
358. Weydahl, E.S. and J.E. Moore, *Dynamic curvature strongly affects wall shear rates in a coronary artery bifurcation model*. *J Biomech*, 2001. **34**(9): p. 1189-96.
359. Mark, F.F., et al., *Nonquasi-steady character of pulsatile flow in human coronary arteries*. *J Biomech Eng*, 1985. **107**(1): p. 24-8.
360. Braddock, M., et al., *Fluid Shear Stress Modulation of Gene Expression in Endothelial Cells*. *News Physiol Sci*, 1998. **13**: p. 241-246.
361. Ghista, D.N. and F. Kabinejadian, *Coronary artery bypass grafting hemodynamics and anastomosis design: a biomedical engineering review*. *Biomed Eng Online*, 2013. **12**: p. 129.
362. Schott, U. and P.I. Johansson, *II. Bringing flow into haemostasis diagnostics*. *Br J Anaesth*, 2013. **111**(6): p. 864-7.
363. Sumida, M., *Pulsatile entrance flow in curved pipes: effect of various parameters*. *Experiments in Fluids*, 2007. **43**: p. 949-958.
364. Chang, L.J. and J.M. Tarbell, *A numerical study of flow in curved tubes simulating coronary arteries*. *J Biomech*, 1988. **21**(11): p. 927-37.
365. Caro, C.G., *The mechanics of the circulation*. 2nd ed. 2012, Cambridge, UK ; New York: Cambridge University Press. xxvi, 523 p.
366. Ishikawa, T., *Fluid Dynamics*, in *Handbook of Physics in Medicine and Biology*, R. Splinter, Editor. 2010, CRC Press: Boca Raton. p. 17.1-17.12.
367. Genic, S., Arandjelovic, I., Kolendic, P., Jaric, M., Budimir, N., Genic, V., *A review of explicit approximations of colebrook's equation*. *FME Transactions*, 2011. **39**: p. 67-71.
368. Yang, Z., Zhao, Z., Liu, Y., Chang, Y., Cao, Z., *Convective heat transfer characteristics of high-pressure gas in heat exchanger with membrane helical coils and membrane serpentine tubes*. *Experimental Thermal and Fluid Science*, 2011. **35**: p. 1427-1434.
369. Jani, J.M., Wessling, M., Lammertink, R. G. H., *Geometric influence on mixing in helical porous membrane microcontactors*. *Journal of Membrane Science*, 2011. **378**: p. 351-358.
370. Kaufhold, D., Kopf, F., Wolff, C., Beutel, S., Hilterhaus, L., Hoffmann, M., Scheper, T., Schlüter, M., Liese, A., *Generation of Dean vortices and enhancement of oxygen transfer rates in membrane contactors for different hollow fiber geometries*. *Journal of Membrane Science*, 2012. **423-424**: p. 342-347.
371. Ishigaki, H., *Laminar flow in rotating curved pipes*. *J. Fluid Mech.*, 1996. **329**: p. 373-388.
372. Li, W., Webb, R. L., *Fouling characteristics of internal helical-rib roughness tubes using low-velocity cooling tower water*. *Internal Journal of Heat and Mass Transfer*, 2002. **45**: p. 1685-1691.
373. Fujisawa, N., et al., *Fluid dynamics of a textured blood-contacting surface*. *J Biomech Eng*, 2001. **123**(1): p. 97-105.

374. Jimenez, J.M. and P.F. Davies, *Hemodynamically driven stent strut design*. Ann Biomed Eng, 2009. **37**(8): p. 1483-94.
375. LaDisa, J.F., Jr., et al., *Three-dimensional computational fluid dynamics modeling of alterations in coronary wall shear stress produced by stent implantation*. Ann Biomed Eng, 2003. **31**(8): p. 972-80.
376. Pant, S., et al., *The influence of strut-connectors in stented vessels: a comparison of pulsatile flow through five coronary stents*. Ann Biomed Eng, 2010. **38**(5): p. 1893-907.
377. Neutrium. *Friction factor for flow in coils and curved pipe*. [cited 2013 December 15]; Available from: [http://neutrium.net/fluid\\_flow/friction-factor-for-flow-in-coils-and-curved-pipe/](http://neutrium.net/fluid_flow/friction-factor-for-flow-in-coils-and-curved-pipe/).
378. Wilkes, J.O., *Fluid mechanics for chemical engineers with Microfluidics and CFD*. 2nd ed. Prentice-Hall international series in the physical and chemical engineering sciences. 2006, Upper Saddle River, NJ: Prentice Hall Professional Technical Reference. xvii, 755 p.
379. Charonko, J., et al., *In vitro, time-resolved PIV comparison of the effect of stent design on wall shear stress*. Ann Biomed Eng, 2009. **37**(7): p. 1310-21.
380. Rikhtegar, F., et al., *Hemodynamics in coronary arteries with overlapping stents*. J Biomech, 2014. **47**(2): p. 505-11.
381. Charonko, J., et al., *In vitro comparison of the effect of stent configuration on wall shear stress using time-resolved particle image velocimetry*. Ann Biomed Eng, 2010. **38**(3): p. 889-902.
382. Choi, I.J., et al., *Impact of the stent length on long-term clinical outcomes following newer-generation drug-eluting stent implantation*. Am J Cardiol, 2014. **113**(3): p. 457-64.
383. Papafaklis, M.I., et al., *Drug-eluting stent restenosis: effect of drug type, release kinetics, hemodynamics and coating strategy*. Pharmacol Ther, 2012. **134**(1): p. 43-53.
384. Neyt, M., et al., *Cost-effectiveness analyses of drug eluting stents versus bare metal stents: a systematic review of the literature*. Health Policy, 2009. **91**(2): p. 107-20.
385. Semiatin, S.L., Knisley, S. L., Fagin, P. N., Zhang, F., Barker, D. R., *Microstructure Evolution during Alpha-Beta Heat Treatment of Ti-6Al-4V*. Metallurgical and Materials Transactions A, 2003. **34A**: p. 2377-2386.
386. Smith, W.F., *Structure and properties of engineering alloys*. 2nd ed. McGraw-Hill series in materials science and engineering. 1993, New York: McGraw-Hill. xviii, 630 p.
387. Ryffel, H.H., ed. *Machinery's Handbook*. 22nd Revised Edition ed. 1984, Industrial Press Inc.: New York.
388. Wieland, M., et al., *Wavelength-dependent roughness: A quantitative approach to characterizing the topography of rough titanium surfaces*. International Journal of Oral & Maxillofacial Implants, 2001. **16**(2): p. 163-181.
389. Rupp, F., et al., *Adsorption/desorption phenomena on pure and Teflon((R)) AF-coated titania surfaces studied by dynamic contact angle analysis*. J Biomed Mater Res A, 2002. **62**(4): p. 567-578.
390. Dee, K.C., D.A. Puleo, and R. Bizios, *An introduction to tissue-biomaterial interactions*. 2002, Hoboken, N.J.: Wiley-Liss. xx, 228 p.
391. ASTM, *F2129 Standard Test Method for Conducting Cyclic Potentiodynamic Polarization Measurements to Determine the Corrosion Susceptibility of Small Implant Devices*. 2008, ASTM International: West Conshohocken, PA.
392. Oyane, A., et al., *Preparation and assessment of revised simulated body fluids*. J Biomed Mater Res A, 2003. **65**(2): p. 188-95.
393. Rupp, F., et al., *Roughness induced dynamic changes of wettability of acid etched titanium implant modifications*. Biomaterials, 2004. **25**(7-8): p. 1429-38.

394. Vogler, E.A., *Structure and reactivity of water at biomaterial surfaces*. Adv Colloid Interface Sci, 1998. **74**: p. 69-117.
395. Mattisson, I., Gretzer, C., Ahlberg, E., *Surface characterization, electrochemical properties and in vitro testing of hierarchically structured titanium surfaces*. Materials Research Bulletin, 2013. **48**: p. 389-398.
396. Zhao, X.M., Wu, Y. P., Cai, H. X., Wei, R., Lisman, T., Han, J. J., Xia, Z. L., de Groot, P. G., *The influence of the pulsatility of the blood flow on the extent of platelet adhesion*. Thrombosis Research, 2008. **121**: p. 821-825.
397. Abe, R., et al., *Varying effects of hemodynamic forces on tissue factor RNA expression in human endothelial cells*. J Surg Res, 2011. **170**(1): p. 150-6.
398. Hamad, O.A., et al., *Platelets, complement, and contact activation: partners in inflammation and thrombosis*. Adv Exp Med Biol, 2012. **946**: p. 185-205.
399. Shapiro, S., Laffan, M., *Making contact with microparticles*. J Thromb Haemost, 2012. **10**: p. 1352-4.
400. Diamant, M., et al., *Cellular microparticles: new players in the field of vascular disease?* Eur J Clin Invest, 2004. **34**(6): p. 392-401.
401. Forlow, S.B., R.P. McEver, and M.U. Nollert, *Leukocyte-leukocyte interactions mediated by platelet microparticles under flow*. Blood, 2000. **95**(4): p. 1317-23.
402. Hugel, B., Martínez, M. C., Kunzelmann, C., Freyssinet, J., *Membrane Microparticles: Two Sides of the Coin*. Physiology, 2005. **20**: p. 22-27.
403. Simak, J., Gelderman, P., *Cell Membrane Microparticles in Blood and Blood Products- Potentially Pathogenic Agents and Diagnostic Markers*. Transfusion Medicine Reviews, 2006. **20**(1).
404. Tans, G., et al., *Comparison of anticoagulant and procoagulant activities of stimulated platelets and platelet-derived microparticles*. Blood, 1991. **77**(12): p. 2641-8.
405. Gyongyosi, M., et al., *Platelet activation and high tissue factor level predict acute stent thrombosis in pig coronary arteries: prothrombotic response of drug-eluting or bare stent implantation within the first 24 hours*. Thromb Haemost, 2006. **96**(2): p. 202-9.
406. Malarstig, A., Siegbahn, A., *The intersubject variability of tissue factor mRNA production in human monocytes- relation with the toll-like receptor 4*. Thromb Res, 2007. **120**(3): p. 407-13.
407. Settmacher, B., et al., *Modulation of C3a activity: internalization of the human C3a receptor and its inhibition by C5a*. J Immunol, 1999. **162**(12): p. 7409-16.
408. Pajarinen, J., et al., *Titanium particles modulate expression of Toll-like receptor proteins*. J Biomed Mater Res A, 2010. **92**(4): p. 1528-37.
409. Elsenberg, E.H., et al., *Toll-Like Receptor induced CD11b and L-selectin response in patients with coronary artery disease*. PLoS One, 2013. **8**(4): p. e60467.
410. Fukuda, S., et al., *Mechanisms for regulation of fluid shear stress response in circulating leukocytes*. Circ Res, 2000. **86**(1): p. E13-8.
411. Touma, H., et al., *Numerical investigation of fluid flow in a chandler loop*. ASME J Biomech Eng, 2014. **136**(7).
412. Harding, S.A., et al., *Flow cytometric analysis of circulating platelet-monocyte aggregates in whole blood: methodological considerations*. Thromb Haemost, 2007. **98**(2): p. 451-6.
413. Jaroszeski, M.J. and G. Radcliff, *Fundamentals of flow cytometry*. Mol Biotechnol, 1999. **11**(1): p. 37-53.
414. Hulspas, R., et al., *Considerations for the control of background fluorescence in clinical flow cytometry*. Cytometry B Clin Cytom, 2009. **76**(6): p. 355-64.

415. Sakariassen, K.S., et al., *Shear-induced platelet activation and platelet microparticle formation in native human blood*. *Thromb Res*, 1998. **92**(6 Suppl 2): p. S33-41.
416. Li, M., D.N. Ku, and C.R. Forest, *Microfluidic system for simultaneous optical measurement of platelet aggregation at multiple shear rates in whole blood*. *Lab Chip*, 2012. **12**(7): p. 1355-62.
417. Thor, A., et al., *The role of whole blood in thrombin generation in contact with various titanium surfaces*. *Biomaterials*, 2007. **28**(6): p. 966-74.
418. Chang, X. and M. Gorbet, *The effect of shear on in vitro platelet and leukocyte material-induced activation*. *J Biomater Appl*, 2012.
419. Lawrence, M.B. and T.A. Springer, *Leukocytes roll on a selectin at physiologic flow rates: distinction from and prerequisite for adhesion through integrins*. *Cell*, 1991. **65**(5): p. 859-73.
420. Ikeda, Y., Handa, M., Kawano, K., Kamata, T., Murata, M., Araki, Y., Anbo, H., Kawai, Y., Watanabe, K., Itagaki, I., Sakai, K., Ruggeri, Z. M., *The Role of von Willebrand Factor and Fibrinogen in Platelet Aggregation under Varying Shear Stress*. *J. Clin. Invest.*, 1991. **87**: p. 1234-1240.
421. Gitz, E., et al., *Platelet interaction with von Willebrand factor is enhanced by shear-induced clustering of glycoprotein Ibalpha*. *Haematologica*, 2013. **98**(11): p. 1810-8.
422. Sanders, Y.V., et al., *Reduced prevalence of arterial thrombosis in von Willebrand disease*. *J Thromb Haemost*, 2013. **11**(5): p. 845-54.
423. Yin, W., S.K. Shanmugavelayudam, and D.A. Rubenstein, *The effect of physiologically relevant dynamic shear stress on platelet and endothelial cell activation*. *Thromb Res*, 2011. **127**(3): p. 235-41.
424. Michelson, A.D., et al., *Circulating monocyte-platelet aggregates are a more sensitive marker of in vivo platelet activation than platelet surface P-selectin: studies in baboons, human coronary intervention, and human acute myocardial infarction*. *Circulation*, 2001. **104**(13): p. 1533-7.
425. Malarstig, A., et al., *Genetic variations in the tissue factor gene are associated with clinical outcome in acute coronary syndrome and expression levels in human monocytes*. *Arterioscler Thromb Vasc Biol*, 2005. **25**(12): p. 2667-72.
426. Lin, M.C., et al., *Shear stress induction of the tissue factor gene*. *J Clin Invest*, 1997. **99**(4): p. 737-44.
427. Rochier, A., et al., *Laminar shear, but not orbital shear, has a synergistic effect with thrombin stimulation on tissue factor expression in human umbilical vein endothelial cells*. *J Vasc Surg*, 2011. **54**(2): p. 480-8.
428. Zhang, X., D. Zhan, and H.Y. Shin, *Integrin subtype-dependent CD18 cleavage under shear and its influence on leukocyte-platelet binding*. *J Leukoc Biol*, 2013. **93**(2): p. 251-8.
429. Shin, H.Y., S.I. Simon, and G.W. Schmid-Schonbein, *Fluid shear-induced activation and cleavage of CD18 during pseudopod retraction by human neutrophils*. *J Cell Physiol*, 2008. **214**(2): p. 528-36.
430. Diamond, M.S. and T.A. Springer, *A subpopulation of Mac-1 (CD11b/CD18) molecules mediates neutrophil adhesion to ICAM-1 and fibrinogen*. *J Cell Biol*, 1993. **120**(2): p. 545-56.
431. Bao, L., et al., *Distinct roles for C3a and C5a in complement-induced tubulointerstitial injury*. *Kidney Int*, 2011. **80**(5): p. 524-34.
432. Rogers, T.H. and J.E. Babensee, *Altered adherent leukocyte profile on biomaterials in Toll-like receptor 4 deficient mice*. *Biomaterials*, 2010. **31**(4): p. 594-601.
433. Bechtel, J.F., et al., *Leukocyte depletion during cardiopulmonary bypass in routine adult cardiac surgery*. *Interact Cardiovasc Thorac Surg*, 2011. **12**(2): p. 207-12.

434. Yin, W., Rubenstein, DA., *Dose Effect of Shear Stress on Platelet Complement Activation in a Cone and Plate Shearing Device*. Cellular and Molecular Bioengineering, 2009. **2**(2): p. 274-280.
435. Ando, B., et al., *Complement proteins C5b-9 initiate secretion of platelet storage granules without increased binding of fibrinogen or von Willebrand factor to newly expressed cell surface GPIIb-IIIa*. J Biol Chem, 1988. **263**(24): p. 11907-14.
436. Harrison, P., Michelson, A. D., *Laboratory markers of platelet activation*, in *Hemostasis and Thrombosis: Basic Principles and Clinical Practice*, V.J. Marder, Aird, W. C., Bennet, J. S., Schulman, S., White, G. C. II., Editor. 2013, Lippincott Williams & Wilkins: Baltimore. p. 829-839.
437. Connor, D.E., et al., *The majority of circulating platelet-derived microparticles fail to bind annexin V, lack phospholipid-dependent procoagulant activity and demonstrate greater expression of glycoprotein Ib*. Thromb Haemost, 2010. **103**(5): p. 1044-52.
438. Zhang, Y., et al., *Contact- and agonist-regulated microvesiculation of human platelets*. Thromb Haemost, 2013. **110**(2): p. 331-9.
439. Rullo, J., et al., *Actin polymerization stabilizes alpha4beta1 integrin anchors that mediate monocyte adhesion*. J Cell Biol, 2012. **197**(1): p. 115-29.
440. Lee, R.G. and S.W. Kim, *Adsorption of proteins onto hydrophobic polymer surfaces: adsorption isotherms and kinetics*. J Biomed Mater Res, 1974. **8**(5): p. 251-9.
441. Pfeiffer, N., et al., *Effects of secondary flow caused by a curved channel on plasma protein adsorption to artificial surfaces*. Biotechnol Prog, 1998. **14**(2): p. 338-42.
442. Kopp, R., K. Mottaghy, and M. Kirschfink, *Mechanism of complement activation during extracorporeal blood-biomaterial interaction: effects of heparin coated and uncoated surfaces*. ASAIO J, 2002. **48**(6): p. 598-605.
443. Kourtzelis, I., et al., *Complement anaphylatoxin C5a contributes to hemodialysis-associated thrombosis*. Blood, 2010. **116**(4): p. 631-9.
444. Takano, M., et al., *Serial long-term evaluation of neointimal stent coverage and thrombus after sirolimus-eluting stent implantation by use of coronary angiography*. Heart, 2007. **93**(12): p. 1533-6.
445. Ligthart, S., et al., *The cost-effectiveness of drug-eluting stents: a systematic review*. CMAJ, 2007. **176**(2): p. 199-205.
446. Philpott, A.C., et al., *Long-term outcomes of patients receiving drug-eluting stents*. CMAJ, 2009. **180**(2): p. 167-74.
447. Gaamangwe, T., Gorbet, M., *Model Stent Roughness Influences Complement C3a Receptor Expression*, in *9th World Biomaterials Congress*. June 1-5, 2012: Chengdu, China.
448. Del Conde, I., et al., *Platelet activation leads to activation and propagation of the complement system*. J Exp Med, 2005. **201**(6): p. 871-9.
449. Peerschke, E.I., et al., *Blood platelets activate the classical pathway of human complement*. J Thromb Haemost, 2006. **4**(9): p. 2035-42.
450. Huber-Lang, M., et al., *Generation of C5a in the absence of C3: a new complement activation pathway*. Nat Med, 2006. **12**(6): p. 682-7.
451. Mollnes, T.E. and M. Kirschfink, *Strategies of therapeutic complement inhibition*. Mol Immunol, 2006. **43**(1-2): p. 107-21.
452. Woodruff, T.M., K.S. Nandakumar, and F. Tedesco, *Inhibiting the C5-C5a receptor axis*. Mol Immunol, 2011. **48**(14): p. 1631-42.
453. Larsson, R., et al., *Inhibition of complement activation by soluble recombinant CR1 under conditions resembling those in a cardiopulmonary circuit: reduced up-regulation of CD11b*

- and complete abrogation of binding of PMNs to the biomaterial surface. *Immunopharmacology*, 1997. **38**(1-2): p. 119-27.
454. Ricklin, D. and J.D. Lambris, *Compstatin: a complement inhibitor on its way to clinical application*. *Adv Exp Med Biol*, 2008. **632**: p. 273-92.
455. Nilsson, B., et al., *Compstatin inhibits complement and cellular activation in whole blood in two models of extracorporeal circulation*. *Blood*, 1998. **92**(5): p. 1661-7.
456. DeAngelis, R.A., et al., *Targeted complement inhibition as a promising strategy for preventing inflammatory complications in hemodialysis*. *Immunobiology*, 2012. **217**(11): p. 1097-105.
457. Takahashi, H., et al., *Combined treatment with nafamostat mesilate and aspirin prevents heparin-induced thrombocytopenia in a hemodialysis patient*. *Clin Nephrol*, 2003. **59**(6): p. 458-62.
458. Issekutz, A.C., D.M. Roland, and R.A. Patrick, *The effect of FUT-175 (Nafamstat Mesilate) on C3a, C4a and C5a generation in vitro and inflammatory reactions in vivo*. *Int J Immunopharmacol*, 1990. **12**(1): p. 1-9.
459. Morimoto, N., et al., *Cardiopulmonary bypass strategy with low-dose heparin and nafamostat mesilate in cardiac surgery: a safe option for patients with acute stroke*. *J Thorac Cardiovasc Surg*, 2012. **144**(3): p. 726-8.
460. Gal, P., et al., *Inhibition of the serine proteases of the complement system*. *Adv Exp Med Biol*, 2013. **735**: p. 23-40.
461. Gupta, S. and I. Reviakine, *Platelet activation profiles on TiO<sub>2</sub>: effect of Ca<sup>2+</sup> binding to the surface*. *Biointerphases*, 2012. **7**(1-4): p. 28.
462. Fuse, I., et al., *Inhibitory mechanism of human platelet aggregation by nafamostat mesilate*. *Platelets*, 1999. **10**(4): p. 212-8.
463. Ugawa, S., et al., *Nafamostat mesilate reversibly blocks acid-sensing ion channel currents*. *Biochem Biophys Res Commun*, 2007. **363**(1): p. 203-8.
464. Chen, X., et al., *An anti-coagulation agent Futhan preferentially targets GABA(A) receptors in lung epithelia: implication in treating asthma*. *Int J Physiol Pathophysiol Pharmacol*, 2011. **3**(4): p. 249-56.
465. Miyata, M., et al., *Effects of nafamostat mesilate on ADP-induced platelet aggregation and disaggregation in hemodialysis patients*. *ASAIO J*, 2006. **52**(3): p. 272-5.
466. Hiramatsu, Y., et al., *Nafamostat preserves neutrophil deformability and reduces microaggregate formation during simulated extracorporeal circulation*. *Ann Thorac Surg*, 2005. **79**(4): p. 1326-32.
467. Kourtzelis, I., et al., *Inhibition of biomaterial-induced complement activation attenuates the inflammatory host response to implantation*. *FASEB J*, 2013. **27**(7): p. 2768-76.
468. Hamad, O.A., et al., *Complement activation triggered by chondroitin sulfate released by thrombin receptor-activated platelets*. *J Thromb Haemost*, 2008. **6**(8): p. 1413-21.
469. Hamad, O.A., et al., *Contribution of chondroitin sulfate A to the binding of complement proteins to activated platelets*. *PLoS One*, 2010. **5**(9): p. e12889.
470. Uchiba, M., et al., *Effect of nafamostat mesilate, a synthetic protease inhibitor, on tissue factor-factor VIIa complex activity*. *Thromb Res*, 1994. **74**(2): p. 155-61.
471. Niccoli, G., et al., *The evolving role of inflammatory biomarkers in risk assessment after stent implantation*. *J Am Coll Cardiol*, 2010. **56**(22): p. 1783-93.
472. Lausmaa, J., *Surface spectroscopic characterization of titanium implant materials*. *Journal of Electron Spectroscopy and Related Phenomena*, 1996. **81**(3): p. 343-361.

473. Zhang, K., et al., *Surface modification of implanted cardiovascular metal stents: from antithrombosis and antirestenosis to endothelialization*. J Biomed Mater Res A, 2014. **102**(2): p. 588-609.
474. Martinez, A.W. and E.L. Chaikof, *Microfabrication and nanotechnology in stent design*. Wiley Interdiscip Rev Nanomed Nanobiotechnol, 2011. **3**(3): p. 256-68.
475. Ponsonnet, L., Comte, V., Othmane, A., Lagneau, C., Charbonnier, M., Lissac, M., Jaffrezic, N., *Effect of surface topography and chemistry on adhesion, orientation and growth of fibroblasts on nickel–titanium substrates*. Material Science and Engineering C, 2002. **21**: p. 157-165.
476. Choudhary, S., et al., *Increased endothelial and vascular smooth muscle cell adhesion on nanostructured titanium and CoCrMo*. Int J Nanomedicine, 2006. **1**(1): p. 41-9.
477. Lu, J., D. Khang, and T.J. Webster, *Greater endothelial cell responses on submicron and nanometer rough titanium surfaces*. J Biomed Mater Res A, 2010. **94**(4): p. 1042-9.
478. Lu, J., et al., *Improved endothelial cell adhesion and proliferation on patterned titanium surfaces with rationally designed, micrometer to nanometer features*. Acta Biomater, 2008. **4**(1): p. 192-201.
479. Scully, C.C., et al., *Selective hexapeptide agonists and antagonists for human complement C3a receptor*. J Med Chem, 2010. **53**(13): p. 4938-48.
480. Nygren, H., C. Eriksson, and J. Lausmaa, *Adhesion and activation of platelets and polymorphonuclear granulocyte cells at TiO<sub>2</sub> surfaces*. J Lab Clin Med, 1997. **129**(1): p. 35-46.
481. Koh, L.B., I. Rodriguez, and S.S. Venkatraman, *The effect of topography of polymer surfaces on platelet adhesion*. Biomaterials, 2010. **31**(7): p. 1533-45.
482. Linneweber, J., et al., *The effect of surface roughness on activation of the coagulation system and platelet adhesion in rotary blood pumps*. Artif Organs, 2007. **31**(5): p. 345-51.
483. Park, J.Y., C.H. Gemmell, and J.E. Davies, *Platelet interactions with titanium: modulation of platelet activity by surface topography*. Biomaterials, 2001. **22**(19): p. 2671-82.
484. Liistro, F. and A. Colombo, *Late acute thrombosis after paclitaxel eluting stent implantation*. Heart, 2001. **86**(3): p. 262-4.
485. Wessely, R., A. Kastrati, and A. Schomig, *Late restenosis in patients receiving a polymer-coated sirolimus-eluting stent*. Annals of internal medicine, 2005. **143**(5): p. 392-4.
486. King, L., et al., *Five-year clinical outcomes of a polymer-free sirolimus-eluting stent versus a permanent polymer paclitaxel-eluting stent: final results of the intracoronary stenting and angiographic restenosis - test equivalence between two drug-eluting stents (ISAR-TEST) trial*. Catheter Cardiovasc Interv, 2013. **81**(1): p. E23-8.
487. Stiermaier, T., et al., *Five-year clinical follow-up of a randomized comparison of a polymer-free sirolimus-eluting stent versus a polymer-based paclitaxel-eluting stent in patients with diabetes mellitus (LIPSIA Yukon trial)*. Catheter Cardiovasc Interv, 2014. **83**(3): p. 418-24.
488. Golas, A., et al., *Surface-energy dependent contact activation of blood factor XII*. Biomaterials, 2010. **31**(6): p. 1068-79.
489. Vermesse, E., Mabru, C., Arurault, L., *Surface integrity after pickling and anodization of Ti–6Al–4V titanium alloy*. Applied Surface Science, 2013. **285P**: p. 629-637.
490. Palsson, B. and S. Bhatia, *Tissue engineering*. 2004, Upper Saddle River, N.J.: Pearson Prentice Hall. xviii, 407 p.
491. Anselme, K., Brigerelle, M., *Role of materials surface topography on mammalian cell response*. Internal Materials Review, 2011. **56**(4): p. 243-266.

492. Ferguson, S.J., et al., *Biomechanical evaluation of the interfacial strength of a chemically modified sandblasted and acid-etched titanium surface*. J Biomed Mater Res A, 2006. **78**(2): p. 291-7.
493. Lancaster, S., S. Kakade, and G. Mani, *Microrough cobalt-chromium alloy surfaces for paclitaxel delivery: preparation, characterization, and in vitro drug release studies*. Langmuir, 2012. **28**(31): p. 11511-26.
494. Hong, J., S. Kurt, and A. Thor, *A hydrophilic dental implant surface exhibits thrombogenic properties in vitro*. Clin Implant Dent Relat Res, 2013. **15**(1): p. 105-12.
495. Gaamangwe, T., Peterson, S. D., Gorbet, M. B., *Investigating the effect of blood sample volume in the Chandler loop model: Theoretical and experimental analysis*. Cardiovascular Engineering and Technology, 2014(In press).
496. Duraiswamy, N., et al., *Effects of stent geometry on local flow dynamics and resulting platelet deposition in an in vitro model*. Biorheology, 2008. **45**(5): p. 547-61.
497. Scharnweber, D., et al., *How is wettability of titanium surfaces influenced by their preparation and storage conditions?* J Mater Sci Mater Med, 2010. **21**(2): p. 525-32.
498. Jirouskova, M., J.K. Jaiswal, and B.S. Collier, *Ligand density dramatically affects integrin alpha IIb beta 3-mediated platelet signaling and spreading*. Blood, 2007. **109**(12): p. 5260-9.
499. Silva-Bermudez, P., Muhl, S., Rodil, S. E., *A comparative study of fibrinogen adsorption onto metal oxide thin films*. Applied Surface Science, 2013. **282**: p. 351-362.
500. Sprague, E.A. and J.C. Palmaz, *A model system to assess key vascular responses to biomaterials*. J Endovasc Ther, 2005. **12**(5): p. 594-604.
501. Thevenot, P., W. Hu, and L. Tang, *Surface chemistry influences implant biocompatibility*. Curr Top Med Chem, 2008. **8**(4): p. 270-80.
502. Fojt, L., Klapetek, P., Strašák, L., Vetterl, V., *Fibrinogen and cellular adherability on differently treated titanium as implants*. Central European Journal of Physics, 2011. **10**(1): p. 232-238.
503. Wendorf, J.R., C.J. Radke, and H.W. Blanch, *The role of electrolytes on protein adsorption at a hydrophilic solid-water interface*. Colloids Surf B Biointerfaces, 2010. **75**(1): p. 100-6.
504. Versteeg, H.H., et al., *New fundamentals in hemostasis*. Physiol Rev, 2013. **93**(1): p. 327-58.
505. Yahyapour, N., et al., *Thrombin, kallikrein and complement C5b-9 adsorption on hydrophilic and hydrophobic titanium and glass after short time exposure to whole blood*. Biomaterials, 2004. **25**(16): p. 3171-6.
506. Ding, Y., et al., *Effects of microtopographic patterns on platelet adhesion and activation on titanium oxide surfaces*. J Biomed Mater Res A, 2013. **101**(3): p. 622-32.
507. Deng, Z.J., et al., *Nanoparticle-induced unfolding of fibrinogen promotes Mac-1 receptor activation and inflammation*. Nat Nanotechnol, 2011. **6**(1): p. 39-44.
508. Sitrin, R.G., et al., *Fibrinogen activates NF-kappa B transcription factors in mononuclear phagocytes*. J Immunol, 1998. **161**(3): p. 1462-70.
509. Dibra, A., et al., *Influence of stent surface topography on the outcomes of patients undergoing coronary stenting: a randomized double-blind controlled trial*. Catheter Cardiovasc Interv, 2005. **65**(3): p. 374-80.
510. Yang, H., et al., *Fibrinogen and von Willebrand factor-independent platelet aggregation in vitro and in vivo*. J Thromb Haemost, 2006. **4**(10): p. 2230-7.
511. Gaamangwe, T., Pye, J. Gorbet, M., *The effect of roughness on platelet and tissue factor expression*, in *28th Canadian Biomaterials Society Conference*. 2011: Vancouver, BC.
512. Han, Y.L., et al., *Cell adhesion on zein films under shear stress field*. Colloids Surf B Biointerfaces, 2013. **111C**: p. 479-485.

513. Zorlutuna, P., et al., *Influence of nanopatterns on endothelial cell adhesion: Enhanced cell retention under shear stress*. Acta Biomater, 2009. **5**(7): p. 2451-9.
514. *Fort Wayne Metals*. Ti 6Al-4V ELI [cited 2013 December 9]; Available from: [http://www.fwmetals.com/assets/files/TI6Al-4V\\_ELI.pdf](http://www.fwmetals.com/assets/files/TI6Al-4V_ELI.pdf).
515. *The Engineering ToolBox*. Density of dry air, water vapour and moist humid air [cited 2013 December 15]; Available from: [http://www.engineeringtoolbox.com/density-air-d\\_680.html](http://www.engineeringtoolbox.com/density-air-d_680.html).
516. *Holsoft educational software and solutions*. Physical properties of air [cited 2013 December 15]; Available from: <http://physics.holsoft.nl/physics/tpair.htm>.

## Appendix A

### Material Composition and Properties

Ti-6Al-4V ELI (extra low interstitial), Table A-1, is a higher purity alloy with lower iron, carbon and oxygen elements compared to the standard Ti-6Al-4V. Since it has both alpha (Al) and beta (V) stabilizers, it can be heat treated and transformed to stabilize between the alpha (hexagonal) and beta (cube) phase. Ti-6Al-4V has the advantage of toughness and corrosion resistance.

**Table A-1. Properties and specifications of Ti-6Al-4V ELI. Adapted from [514].**

		Ti-6Al-4V ELI (max ave. Wt %)
Bulk chemical composition	Ti	89.7082
	Al	6.06
	V	3.97
	Fe	0.12
	O	0.11
	C	0.015
	N	0.011
	H	0.0058
Physical/Mechanical properties	Density	0.160 lbs/in <sup>2</sup>
	Ultimate tensile strength	1000-1172 MPa
	Modulus of elasticity	16.5x10 <sup>6</sup> psi
	Thermal conductivity	6.6-6.8 W/m K
Electrical properties	Electrical resistivity	1.71 μohms-m
Thermal properties	Melting point	1604-1660 °C

## Appendix B

### Application of Blasius Correlation

Substituting average velocity from Table 3-4 into the Blasius correlation,

$$\tau = \frac{f\rho v^2}{2}$$

Gives,

$$\tau = \frac{f\rho}{2} \cdot \frac{\pi R_0 \omega}{30} \cdot \frac{\pi R_0 \omega}{30}$$

Grouping terms and multiplying by  $R/R$  and  $\mu/\mu$  terms gives,

$$\tau = \frac{f}{2 \times 2 \times 4} \left( \frac{\pi \rho \omega R_0 R}{15 \mu} \right) \left( \frac{2 \pi R_0 \omega \mu}{15 R} \right)$$

The first bracket can be recognized as  $R_e$  from Table 3-4 and the second bracket can also be recognized as wall shear stress  $\tau_w$  from equation (19). Therefore, the equation can be written as,

$$\tau = f \left( \frac{R_e}{16} \right) \tau_w$$

## Appendix C

### Determination of Density, Viscosity and Wall Shear Stress Effect of Humid Air

The density of humid air can be determined from basic gas principles, as briefly describe below [515]. The following constants are known:

Atmospheric air pressure,  $p_a = 760 \text{ mmHg} = 101.325 \text{ kPa}$  .

Gas constants:

$$R_{air} = 286.9 \text{ J/kgK}$$

$$R_{w.vapor} = 461.5 \text{ J/kgK}$$

The saturated vapor pressure at the actual temperature (T in Kelvin) is expressed as,

$$p_{ws} = \left( e^{77.3450 + 0.0057T - 7235/T} \right) / T^{8.2}$$

At 37°C, the temperature in Kelvin is given by  $T = 37 + 273.16 = 310.16 \text{ K}$  . Substituting gives,

$$p_{ws} = 6261.142 \text{ pascal} .$$

The specific humidity at saturation is given by the equation,

$$x_s = 0.62198 \frac{p_{ws}}{(p_a - p_{ws})}$$

The density of dry air from ideal gas law is  $\rho_a = 0.0035 p_a / T = 1.1434 \text{ kg/m}^3$  at 37°C. The density of moist air is expressed as,

$$\rho_w = \rho_a \frac{1 + x_s}{(1 + 1.609 x_s)}$$

After substitution, the density of moist air in the loop at 37°C is  $\rho_w = 1.1166 \text{ kg/m}^3$ .

The viscosity of humid air at 37°C is given by the equation [516],

$$\eta_a = (17.1 + 0.067T - 0.0004T^2) \times 10^{-6}$$

where T is in °C. After substituting 37°C,  $\eta = 19.03 \times 10^{-6} \text{ Pa.s}$ .

With density and viscosity determined, the contribution of humid air to the shear stress can be determined. The second terms of equation (42) and (43) representing air contribution to time-averaged wall shear stress are expressed separately below as equation (42air) and (43air) in the presence and absence of model stent, respectively.

$$\tau = \frac{\rho_a V^2}{2} [\beta f_{cra} + (1 - \lambda - \beta) f_{csa}] \quad (42\text{air})$$

$$\tau = \frac{\rho_a V^2}{2} (1 - \lambda) f_{csa} \quad (43\text{air})$$

Equation (42air) and (43air) are plotted on Figure C-1. Similar to shear stress due to blood sample volume, the effect of air sample volume shows clustering of the plots around the two volume samples. The results suggest that air sample volume does not have a significant effect on the overall wall shear stress as all the time-averaged wall shear stress values are below 0.04 dyn/cm<sup>2</sup>.

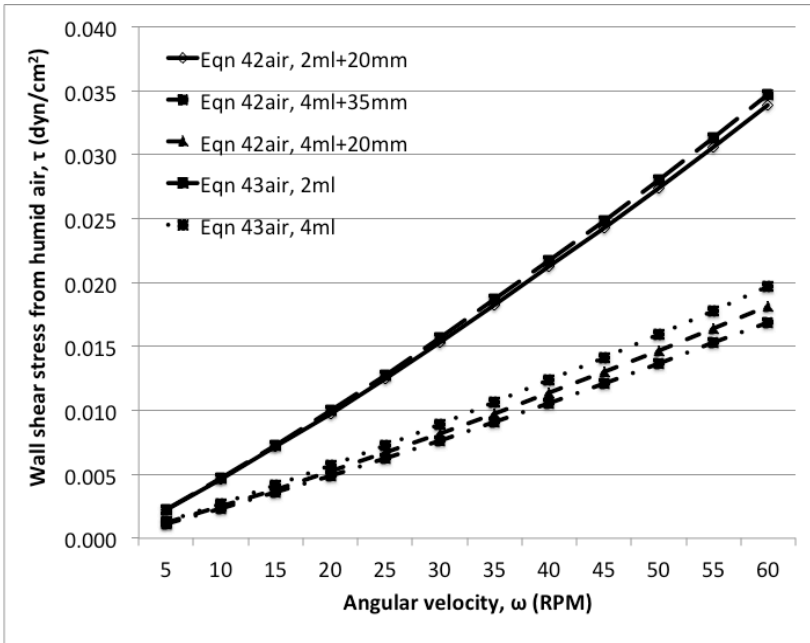


Figure C-1. Time-averaged wall shear stress due to moist air in the loop

## Appendix D

### Rotor Calibration

The Roto-Torque™, model RT50 (Cole-Palmer Instrument Co., Illinois, USA) was specified to have electronic speed control from about 3 to about 80 RPM. The disk was specified to rotate as high as 60 RPM. However, it was necessary to calibrate the rotor because the markings on the speed control knob were not related to any quantitative rotational speed values.

**Calibration setup:** The rotor calibration was done with a Digital Stroboscope Tachometer, model 461831 (Extech Instruments, Melrose, MA, USA). The stroboscope specifications are as presented on Table D-1. The stroboscope was mounted on a mini-tripod stand and positioned at about 25 cm from the rotor disc, in line with the center of the rotating disc, Figure D-1. Since the lower limit of the measurement range of the stroboscope (100 RPM) was above the maximum rotational speed of the rotor, the measurements were based on harmonics, i.e. there was no 1:1 measurements, only 2:1, 3:1 or higher ratios were possible. This meant that, if there was one marker on the rotor disk, and it showed as four stationary marks when rotating under the stroboscope light, then the strobe flash rate to disk speed was 4:1. In this case, since the rotor maximum speed was far below the minimum strobe measurement range limit, a ratio of 10:1 was necessary, i.e. the rotor speed was 1/10 of the stroboscope reading.

**Table D-1. Stroboscope specifications**

<b>Measuring range</b>	100 to 10000 RPM/FPM (FPM – flashes per minute)
<b>Resolution</b>	0.1 (<1000 RPM/FPM) 1 (1000 to 9999 RPM/FPM) 10 (10000 RPM/FPM)
<b>Accuracy</b>	± (0.05%+1 digits)
<b>Sampling time</b>	1 second
<b>Strobe flash adjustment range</b>	LOW: 100 to 1000 RPM/FPM HIGH: 1000 to 10000 RPM/FPM



**Figure D-1. Rotor calibration setup**

**Results:** Using the LOW range setting on the stroboscope, the results of the calibration are presented on Table D-2.

**Table D-2. Calibrated rotor rotation speed**

Marker setting on rotor	Stroboscope reading (RPM/FPM)	Disk speed (RPM)
1	N/A	N/A
2	106.0	10.6
3	178.1	17.8
4	239.4	23.9*
5	308.0	30.8
6	370.6	37.1
7	447.8	44.8*
8	558.6	55.9
9	565.7	56.6
10	569.6	57.0

N/A – it was not possible to measure very low speeds. \*Angular velocities used in the experiments.

## Appendix E

### Determining AFM Scanning Area

The atomic force microscopy (AFM) scanning area is usually easy to determine on a flat surface. For a curved surface, curvature error may occur if the scan area is too large. Since the model stent wire has a circular cross-section and has a small diameter, its curvature imposes a limit on the maximum AFM scan area, without curvature error. Scanning along the length of the wire does not pose any problems except in the case where the wire is in the form of a coil, in which case the coil radius of curvature should be taken into account. For this configuration, the coil radius of curvature ( $4.775 \text{ mm}/2 = 2.388 \text{ mm}$ ) is much larger than the radius of the wire ( $0.0635 \text{ mm}$ ). Therefore, it is sufficient to calculate scan area based on the radius of the wire. A cross section of the wire is presented on Figure E-1.

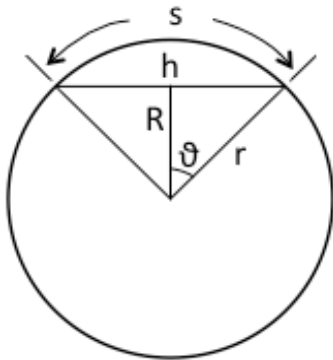


**Figure E-1. Schematic cross-section of stent wire**

$s$  = arc length

$h$  = straight line across curvature = scan length

$r$  = radius of wire

$R$  = length from center to  $h$  (perpendicular to  $h$  and divides  $h$  in half)

Diameter of wire =  $0.127 \text{ mm}$

$\therefore r = 0.0635 \text{ mm}$

$$s = (2\theta)r$$

where  $\theta$  is in degrees. But,

$$2\theta = 2 \sin^{-1}\left(\frac{h/2}{r}\right)$$

$$\therefore s = 2r \sin^{-1}\left(\frac{h/2}{r}\right)$$

Converting  $\theta$  to radians,

$$s = 2r \left(\frac{2\pi}{360}\right) \sin^{-1}\left(\frac{h/2}{r}\right)$$

$$s = \left(\frac{\pi r}{90}\right) \sin^{-1}\left(\frac{h/2}{r}\right)$$

In order to scan without curvature error, ideally  $h \approx s$ . Typical values of  $s$  for possible scan areas are presented on Table E-1. Hence, scan area less than 15  $\mu\text{m}$  may be acceptable. The maximum scan area selected for this study was 10x10  $\mu\text{m}^2$ .

**Table E-1. AFM scan area determination**

Scan length, $h$ ( $\mu\text{m}$ )	Arc length, $s$ ( $\mu\text{m}$ )	Relative error
10	10.01	0.1%
15	15.04	0.2%
20	20.08	0.4%
25	25.16	0.7%

## Appendix F

### Dynamic Contact Angle Analysis

The Wilhelmy dynamic contact angle method is based on the force equation [389],

$$F = mg + \gamma L \cos \vartheta - F_b$$

where  $F$  is total force,  $m$  is mass of the solid sample (e.g. wire),  $g$  is gravitational constant,  $\gamma$  is the surface tension of the liquid,  $L$  is wetted perimeter (wetted length) of the solid sample,  $\theta$  is the contact angle between the solid and the liquid and  $F_b$  is the buoyancy force. In performing the measurement, the electro-balance was reset to zero with autocal so that the gravity force  $mg$  did not contribute to the recorded force. For the measurement, the surface tension of water and the wetted length are known. Thus, force can be accurately measure with a high precision instrument. The instrument uses linear regression to eliminate the buoyance force so that the equation resembles the Young's equation, from which the contact angle can be determined.

The setup consists of an electro-balance, an immersion liquid and sample, Figure F-1. The electro-balance was the auto-calibrating Sigma 700 (KSV Instruments, Helsinki, Finland) and the working liquid used was MilliQ water. Six immersion and emersion loops were carried out continuously at a velocity of 10 mm/min, giving six successive time-dependent hysteresis loops (force loops). Advancing and receding contact angle measurements were obtained from each loop.

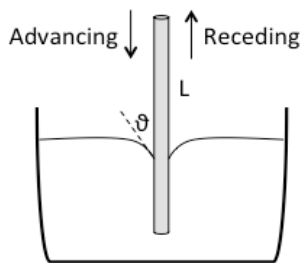


Figure F-1. Schematic illustration of the Wilhelmy method

## Appendix G

### Physiological Solution Preparation

The physiological solution was prepared with reagents as listed on Table G-1, as per procedure described by Oyane et al [392]. Before preparing the solution, HEPES was dissolved in 10 ml of ultrapure water and 1.0 M NaOH was prepared by dissolving 0.4 g NaOH in 10 ml of ultrapure water. To prepare the solution, 70 ml of ultrapure water was poured in a beaker and kept at 35°C. The reagents were then dissolved sequentially as listed on Table G-1, with the aid of a magnetic stirrer. The solution volume was adjusted to 100 ml by adding ultrapure water. The solution was then filtered into 50 ml conical tubes and stored at 4°C. The solution was used within two days of preparation.

**Table G-1. Reagents for 100 ml simulated body fluid**

Reagent Common Name	Reagent	Quantity
Sodium Chloride	NaCl	0.5403 g
Sodium Bicarbonate	NaHCO <sub>3</sub>	0.0740 g
Sodium Carbonate	Na <sub>2</sub> CO <sub>3</sub>	0.2046 g
Potassium Chloride	KCl	0.0225 g
Potassium Phosphate	K <sub>2</sub> HPO <sub>4</sub>	0.0230 g
Magnesium Chloride	MgCl <sub>2</sub>	0.0311 g
HEPES	C <sub>8</sub> H <sub>18</sub> N <sub>2</sub> O <sub>4</sub> S	1.1928 g
Calcium Chloride	CaCl <sub>2</sub>	0.0293 g
Sodium Sulfate	Na <sub>2</sub> SO <sub>4</sub>	0.0072 g
Sodium Hydroxide	1.0 M NaOH	0.08 ml

### **Results**

The ionic concentration of the prepared physiological solution was not measured but has been found to have similar ionic concentration to blood plasma, Table G-2.

**Table G-2. Simulated body fluid ion concentration (mM). Adapted from [392].**

<b>Ions</b>	<b>Total Blood Plasma</b>	<b>Expected Simulated Body Fluid</b>
Na <sup>+</sup>	142.0	142.0
K <sup>+</sup>	5.0	5.0
Mg <sup>2+</sup>	1.5	1.5
Ca <sup>2+</sup>	2.5	2.5
Cl <sup>-</sup>	103.0	103.0
HCO <sub>3</sub> <sup>-</sup>	27.0	27.0
HPO <sub>4</sub> <sup>2-</sup>	1.0	1.0
SO <sub>4</sub> <sup>2-</sup>	0.5	0.5